Eastern Illinois University
The Keep

Masters Theses | Student Theses & Publications

1-1-2004

Electron Transfer In Phosphido-Bridged Complexes

Pradeep N. Perera
Eastern Illinois University

This research is a product of the graduate program in Chemistry at Eastern Illinois University. Find out more about the program.

Recommended Citation
Perera, Pradeep N., "Electron Transfer In Phosphido-Bridged Complexes" (2004). *Masters Theses*. 1105.
http://thekeep.eiu.edu/theses/1105

This Thesis is brought to you for free and open access by the Student Theses & Publications at The Keep. It has been accepted for inclusion in Masters Theses by an authorized administrator of The Keep. For more information, please contact tabruns@eiu.edu.

*****US Copyright Notice*****

No further reproduction or distribution of this copy is permitted by electronic transmission or any other means.

The user should review the copyright notice on the following scanned image(s) contained in the original work from which this electronic copy was made.

Section 108: United States Copyright Law

The copyright law of the United States [Title 17, United States Code] governs the making of photocopies or other reproductions of copyrighted materials.

Under certain conditions specified in the law, libraries and archives are authorized to furnish a photocopy or other reproduction. One of these specified conditions is that the reproduction is not to be used for any purpose other than private study, scholarship, or research. If a user makes a request for, or later uses, a photocopy or reproduction for purposes in excess of "fair use," that use may be liable for copyright infringement.

This institution reserves the right to refuse to accept a copying order if, in its judgment, fulfillment of the order would involve violation of copyright law. No further reproduction and distribution of this copy is permitted by transmission or any other means.

THESIS REPRODUCTION CERTIFICATE

TO: Graduate Degree Candidates (who have written formal theses)

SUBJECT: Permission to Reproduce Theses

The University Library is receiving a number of request from other institutions asking permission to reproduce dissertations for inclusion in their library holdings. Although no copyright laws are involved, we feel that professional courtesy demands that permission be obtained from the author before we allow these to be copied.

PLEASE SIGN ONE OF THE FOLLOWING STATEMENTS:

Booth Library of Eastern Illinois University has my permission to lend my thesis to a reputable college or university for the purpose of copying it for inclusion in that institution's library or research holdings.

06/15/04.

Author's Signature Date

I respectfully request Booth Library of Eastern Illinois University **NOT** allow my thesis to be reproduced because:

_____

_____

_____

Author's Signature Date

This form must be submitted in duplicate.

Electron Transfer in Phosphido-Bridged Complexes

(TITLE)

BY

Pradeep N. Perera

THESIS

SUBMITTED IN PARTIAL FULFILLMENT OF THE REQUIREMENTS
FOR THE DEGREE OF

Master of Science in Chemistry

IN THE GRADUATE SCHOOL, EASTERN ILLINOIS UNIVERSITY
CHARLESTON, ILLINOIS

2004

YEAR

I HEREBY RECOMMEND THAT THIS THESIS BE ACCEPTED AS FULFILLING
THIS PART OF THE GRADUATE DEGREE CITED ABOVE

6/15/04
DATE

THESIS DIRECTOR

6/15/04
DATE

DEPARTMENT/SCHOOL HEAD

Electron Communication in Phosphido-Bridged Complexes

By: Pradeep N. Perera

Advisor: Prof. Richard L. Keiter

Submitted date: June 15, 2004

Approved by the thesis committee

Richard L. Keiter 6/15/04

Dr. Richard L. Keiter Date

Ellen A. Keiter 6/15/04

Dr. Ellen A. Keiter Date

Mark E. McGuire 6/15/04

Dr. Mark E. McGuire Date

6/15/04

Dr. Daniel J. Sheeran Date

Acknowledgments

I would like to thank Professor Richard L. Keiter for the guidance and the support given to me during my two-year stay at EIU. I also appreciate the patience he showed for another two years while I finished writing the thesis. I am grateful to Dr. Ellen A. Keiter for her research advice and for NMR data and to Dr. Mark E. McGuire for helpful discussions on and for assistance with cyclic voltammetry.

Special appreciation is due to my parents and brother whose love, support and encouragement have always catalyzed me to achieve more than I thought possible of myself.

Finally, I would like to remember my friends at EIU and Purdue University who always encouraged me to complete the degree.

Table of Contents

List of Tables

Abstract

Diphenylphosphido-bridged complexes, $(OC)_4M[\mu\text{-}P(Ph_2]_2M(CO)_4$ (M = Mo, W) were synthesized in 56% yield from the reaction of $(OC)_5MPPh_2H$ with BuLi in THF followed by air oxidation. Reactions of these complexes in refluxing toluene with $Ph_2PC{\equiv}CPPh_2$ or *trans*-$Ph_2PCH{=}CHPPh_2$ led to CO loss and formation of a mixture of tetrametallic and dimetallic complexes that were separated by thick layer chromatography. Isolated were the four tetrametallic complexes, $(OC)_4M[\mu\text{-}PPh_2]_2M(CO)_3(\mu\text{-}PPh_2C{\equiv}CPPh_2)(OC)_3M[\mu\text{-}PPh_2]_2M(CO)_4$ and $(OC)_4M[\mu\text{-}PPh_2]_2M(CO)_3(\mu\text{-}$*trans*-$PPh_2CH{=}CHPPh_2)(OC)_3M[\mu\text{-}PPh_2]_2M(CO)_4$, and the four dimetallic complexes, $(OC)_4M[\mu\text{-}PPh_2]_2M(CO)_3(PPh_2C{\equiv}CPPh_2)$ and $(OC)_4M[\mu\text{-}PPh_2]_2M(CO)_3($*trans*-$PPh_2CH{=}CHPPh_2)$. In the dimetallic complexes, $Ph_2PC{\equiv}CPPh_2$ and *trans*-$Ph_2PCH{=}CHPPh_2$ are coordinated as monodentate ligands. The complexes, which may be thought of as precursors for molecular wires, were characterized by IR, $^{31}P\{^1H\}$ NMR, and cyclic voltammetry.

Oxidation of the tetrametallic complexes occurs in two one-electron steps indicating that electronic communication between the the dimetallic units and through the ditertiary phosphine bridging ligand takes place. The differences in potential between the two steps for the tungsten and molybdenum complexes of $Ph_2PC{\equiv}CPPh_2$ were 115 mv and 100 mV, respectively. Analogous complexes of *trans*-$PPh_2CH{=}CHPPh_2$ gave differences of 100 mV and 95 mV, respectively. We can conclude from these results that

the tendency for electron transfer is slightly better for the tungsten complexes as compared to those of molybdenum, and that electron transfer is slightly better for the acetylenic ligand than for the olefinic one.

Oxidation of each of the dimetallic complexes occurs in a one-electron step. The tungsten complexes are easier to oxidize than those of molybdenum, and olefinic complexes are easier to oxidize than acetylenic complexes..

Efforts to prepare a tetramolybdenum complex in which $Ph_2PCH_2CH_2PPh_2$ bridges two dimolybdenum units were unsuccessful. No reaction occurred when hydrogen gas in the presence of a palladium catalyst was used in an attempt to reduce the double bond in $(OC)_4Mo[\mu\text{-}PPh_2]_2Mo(CO)_3(\mu\text{-}\textit{trans}\text{-}PPh_2CH{=}CHPPh_2)(OC)_3Mo[\mu\text{-}PPh_2]_2Mo(CO)_4$.

Introduction

Since the mid-twentieth century synthetic organic polymers have revolutionized the world and been used for many applications in a wide range of fields such as structural materials, films, compact discs and fibers for clothing. However, the inclusion of inorganic elements in organic polymers, called coordination polymers, has introduced a new set of properties and new applications in many areas. Unlike the organic counterpart, coordination polymers are believed to provide a combination of the best properties of both organic (e.g. flexibility) and inorganic (e.g. thermal stability) components[1]. Among the many other properties, a considerable amount of attention has been focused on the electronic properties of conjugated organometallic systems with multiple electroactive centers joined by organic bridges. These types of organometallic polymers are known to show semi-conducting properties in many cases. Two basic requirements must be met in order to attain conductivity[2]. There should be a strong interaction between redox active metal centers and it should be possible to partially oxidize or reduce the polymer to permit free charge transfer along the chain. Polymers with the above qualities are assumed to be useful for fabricating "molecular electronic circuits".

As the feature size of electronic equipment grows smaller, there is a necessity to store thousands of micro-integrated circuits in a few cubic centimeters that are capable of executing millions of instructions per second. However, several limitations exist in the design of ultra small electronic devices. These include high electric fields, quantum effects, the difficulty in connecting micro-elements and the release of large amounts of heat. It is expected that "molecular circuits" can be designed to overcome these problems and some positive results have already been reported[3]. Motivated by those expectations a

significant number of research groups around the world are working with transition metal-based polymers.

Transition metal-based polymers can be divided into two categories. In the first group, transition metals are incorporated in the side group of the main organic chain, e.g. poly(vinylferrocene):

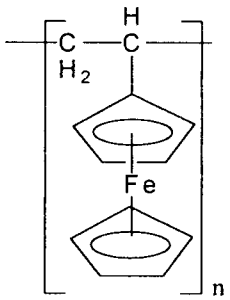

Often, the synthesis of this type of polymers can be achieved by conventional organic synthetic routes. In the second group metal atoms are attached to the backbone of the polymer and require more advanced synthetic routes especially when the metal centers are at close proximity. One of the early successful methods for synthesizing this type of polymer was based on condensation (step-growth) technique. This method was successfully used to synthesize polymers containing ferrocene and silicon. In addition, a polyaromatic complex was first synthesized in Japan in 1970.[1]

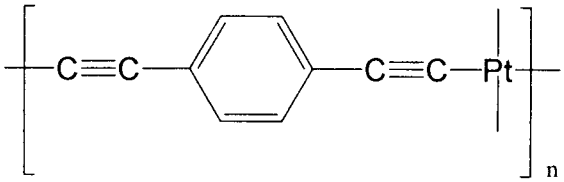

This polymer has been shown to have application as an optical material and an electrical conductor. However, today scientists are looking for developing better methods of

obtaining well-defined high molecular weight polymers. One such successful method is based on a ring-opening technique that converts cyclic molecules into linear chains via a chain growth process. The first ring-opening polymer containing metallacenes was reported in Germany in 1989.[1]

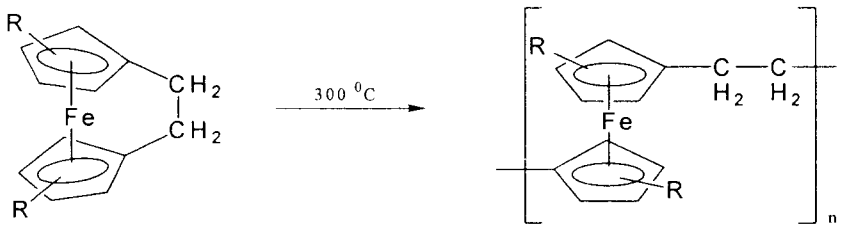

The investigation of the potential bimetallic complexes for their electrochemical behavior is one of the key starting steps for developing molecular wires. Unfortunately, reported electrochemical work on hetero and homonuclear bimetallic complexes (with or without metal-metal bond) bridged by organic or inorganic linkage is very limited.

Researchers from University of Miami, Florida[4] have done some electrochemical work with diruthinium complexes recently. They synthesized a complex

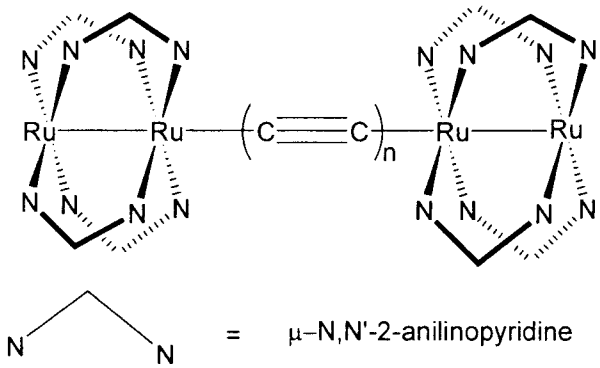

with butadiynediyl (n = 2) or ethynediyl (n = 1) bridges and compared their electrochemical properties to unbridged complexs,

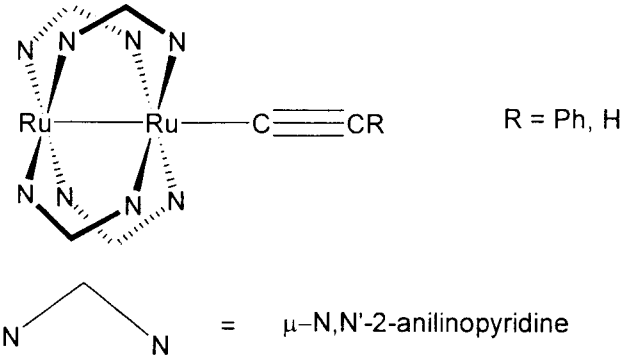

R = Ph, H

Electrochemical studies of the unbridged complex showed two reversible redox processes, one oxidation at 462 mV [$Ru_2 \rightarrow Ru_2^+$] and one reduction at -873 mV [$Ru_2 \rightarrow Ru_2^-$]. The bridged tetrameric compound showed four reversible one-electron redox processes: two oxidations and two reductions between -1600 mV- 1200 mV. They assigned the four redox processes as follows.

$$[Ru]_2^{-}\sim\sim[Ru]_2^{-} \overset{I}{\rightleftharpoons} [Ru]_2^{-}\sim\sim[Ru]_2 \overset{II}{\rightleftharpoons} [Ru]_2\sim\sim[Ru]_2$$

$$[Ru]_2^{+}\sim\sim[Ru]_2^{+} \overset{IV}{\rightleftharpoons} [Ru]_2^{+}\sim\sim[Ru]_2 \overset{III}{\rightleftharpoons}$$

Processes I and II correspond to the reduction process of the dangling compound and processes III and IV correspond to the oxidation. Based on the $\Delta E_{1/2}$ differences, 389 mV (n = 1) and 667 mV (n = 2) for processes I/II, 157 mV (n = 1) and 285 mV (n = 2) for processes III/IV, they have concluded that there is significant interaction between the two dimeric centers. It is also evident that highly conjugated linkages are more capable of facilitating electronic communication between two centers.

In another front, there is some reported work on transition metal complexes with metal centers in close proximity, but with no metal-metal bonds, that shows electrical

communication between metal centers. Researchers of the University of Texas-Austin[2] in 1994 synthesized a series of Ni (II), Pd (II) and Pt (II) polymers.

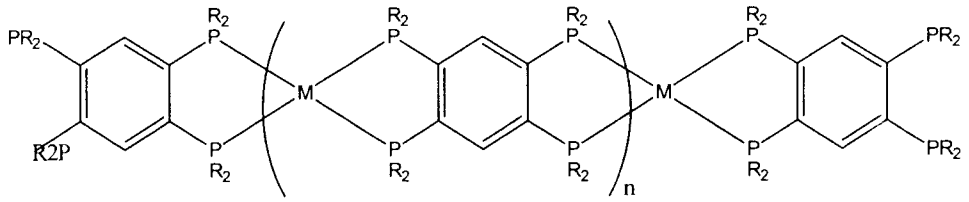

M = Ni(II), Pd(II), Pt(II)

In order to assess the electronic communication between two metal centers of the polymer, they also synthesized a series of model monometallic and bimetallic complexes.

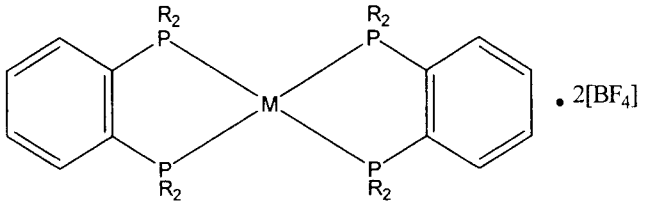

M = Ni(II), Pd(II), Pt(II)

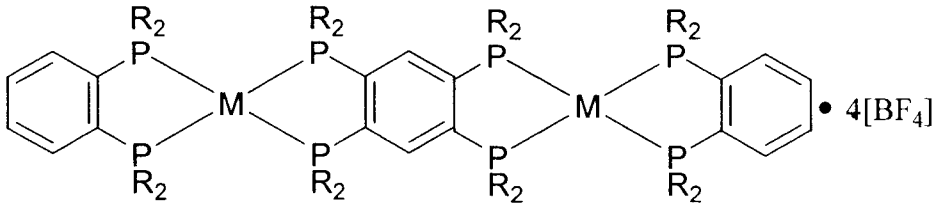

M = Ni(II), Pd(II), Pt(II)

The electrochemical data for the monometallic compound of Ni(II) showed two reversible one electron reductions at -0.20 V [Ni(II/I)] and -0.60 V [Ni(I/0)] while both

Pd(II) and Pt(II) mononuclear complexes showed one reversible two-electron reduction at -0.68 V [Pd(II/0)] and -0.78 V [Pt(II/0)], respectively. The bimetallic $[Ni(II)]_2$ compound showed one two-electron reduction [Ni(II/II)→Ni(I/I)] at -0.20 V and two other one-electron reductions at -0.47 V [Ni(I/I) →Ni(I/0)] and -0. 56 V [Ni(I/0) →Ni(0/0)]. The direct reduction of [Ni(II/II)→Ni(I/I)] at the same potential as the monometallic complex indicated no significant interaction between the two Ni centers. Bimetallic Pd(II) and Pt(II) showed two reversible two-electron reductions at -0.56 V [Pd(II/II) →Pd(II/0)] and -0.67 V [Pd(II/0) →Pd(0/0)], and -0.65 V [Pt(II/II) →Pt(II/0)] and -0.77 V [Pt(0/II) → Pt(0/0)], revealing 120 mV and 130 mV peak shifts for the first two-electron reductions (II/0) for Pd and Pt respectively, compared to the monometallic complexes. They also demonstrated that changing the diphenylphosphinobenzene ligand to diphenylphosphinopropane shifted the reduction of the Pd(II)→Pd(0) for both the monometallic and bimetallic complexes by about 50 mV.

Phosphido bridged metal complexes were first prepared in the early 1960s. The first group 6 binuclear carbonyl complex was synthesized by pyrolyzing two moles of metal-carbonyl complex with one mole of Ph_2PPPh_2 in a Carius tube.[5] Since then phosphido-bridged bimetallic carbonyl complexes of group 6 metals have been thoroughly investigated. Convenient routes for synthesizing these complexes have been developed. Keiter *et al* synthesized a series of unsubstituted and substituted binuclear tungsten and molybdenum carbonyl complexes by reacting $M(CO)_6$ (M = Mo, W) with PPh_2H and $NaBH_4$ in refluxing ethanol, 1-butanol or 1-hexanol.[6]

$$M(CO)_6 + PPh_2H \xrightarrow[\text{reflux}]{NaBH_4} (CO)_4M(\mu\text{–}PPh_2)_2M(CO)_4 + \text{other pdts}$$

M = Mo, W

(1)

Earlier the same group reported that refluxing an equimolar solution of $(CO)_5WPPh_2H$ and KO-t-Bu in THF followed by oxidation in air gives $(CO)_8(\mu\text{-}PPh_2)_2W_2$.[7]

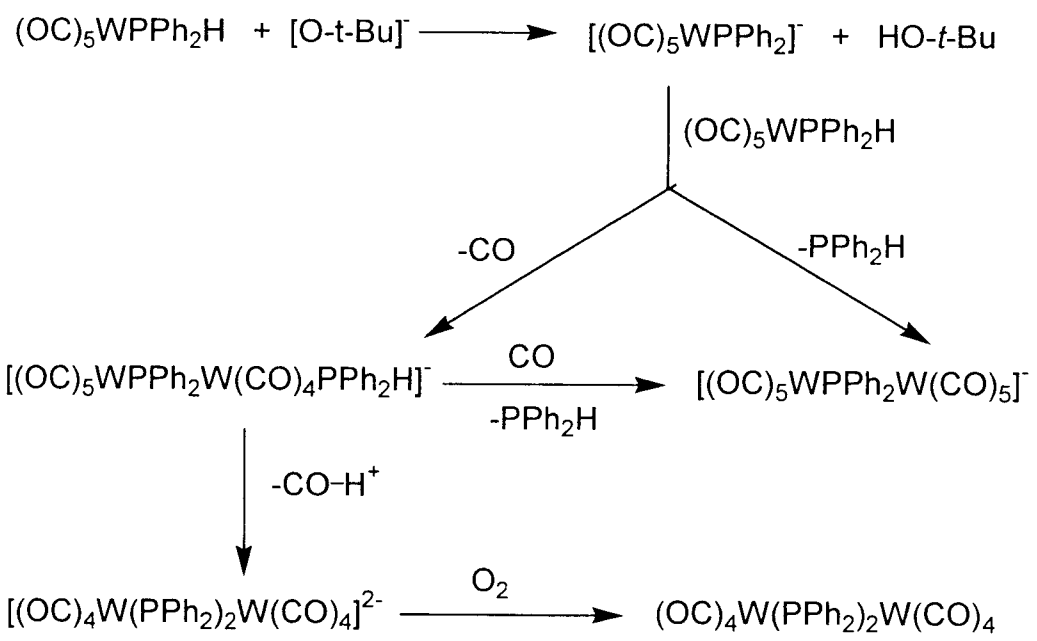

Treichel and Dean *et al* [8] have shown that irradiation of a sample of $W(CO)_5PPh_2H$ in THF gives a mixture of $(CO)_8(\mu\text{-}PPh_2)_2W_2$ and $(CO)_7(\mu\text{-}PPh_2)_2W_2PPh_2H$. Generally, the percentage yield of these bridging complexes was relatively poor or high yields could not be easily achieved on the gram scale. Recently Planinic and Calogovic[9] reported a high yield procedure for synthesizing $(CO)_8(\mu\text{-}PPh_2)_2W_2$ (57 %) and $(CO)_8(\mu\text{-}PPh_2)_2Mo_2$ (81 %). They pyrolyzed $M(CO)_6$ and 1,4,8,11-

tetrakis(diphenylphosphinomethyl)- 1,4,8,11-tetraazacyclotetradecane (TPTA) 4:1 molar ratio in a Carius tube.

The role of phosphorus in transition metal chemistry is well documented.[6,7,10,11] Phosphines are known to be very good substitution ligands for group 6 metal carbonyl complexes under mild conditions. Much work has been reported in this area including a number of reactions from our research group.[6,7,8,9,23] Also there is evidence that bidentate phosphorus ligands may bind to the same metal atom or bridge two atoms.[12,13]

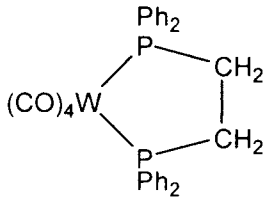

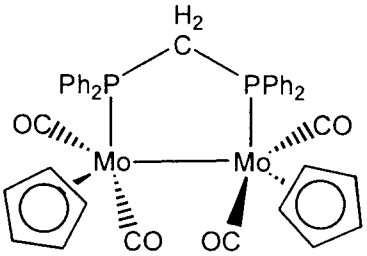

Metal complexes with more than one metal center that are linked by ligands containing nitrogen donor atoms and have unsaturated bonds have shown electronic communication between adjacent centers. The classic example for this is the Creutz-Taube ion[14].

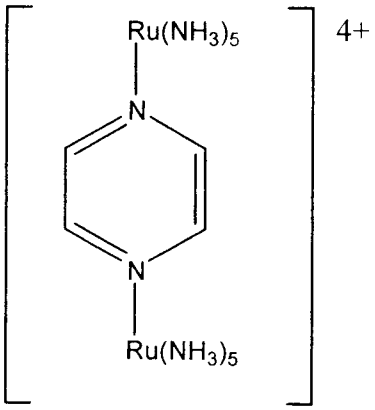

Previously our research group established that $W_2(CO)_8(\mu\text{-}PPh_2)_2$ could be oxidized reversibly both chemically and mechanically. This led us to consider linking phosphido-bridged metal centers with unsaturated diphosphines. Our purpose was to determine if oxidation of one bimetallic center can influence the oxidation of the second center, i.e. will there be electronic communication between two centers. In this work, we used bis(diphenylphosphinoacetylene), $Ph_2PC{\equiv}CPPh_2$ (DPPA) and *trans*-diphenylphosphinoethylene, *trans*-$Ph_2PCH{=}CHPPh_2$ to bridge the metal centers. To determine if the unsaturation in the bridge enhances communication between the metal centers, we also wanted to prepare complexes in which the bridge is saturated. With that in mind we wanted to use $Ph_2PCH_2CH_2PPh_2$ (DPPE) as a linkage between metal centers. Our plan for synthesizing the target compounds was as follows.

$$M(CO)_5PPh_2H \xrightarrow{(1)\ BuLi\ (2)\ O_2} (CO)_4M(PPh_2)_2M(CO)_4 \qquad (2)$$

$$2\ M(CO)_8(\mu\text{–}PPh_2)_2 + Ph_2PC{\equiv}CPPh_2 \xrightarrow{\Delta} 2\ CO +$$

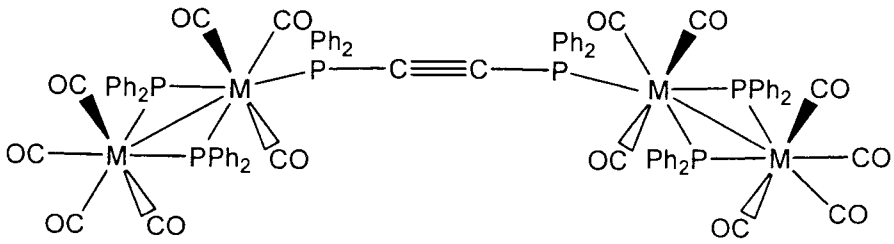

M = W, Mo

(3)

$$2\ M(CO)_8(\mu\text{–}PPh_2)_2 \ + \ \textit{trans}\text{-}\ Ph_2PCH{=}{=}HCPPh_2 \xrightarrow{\Delta} 2\ CO \ +$$

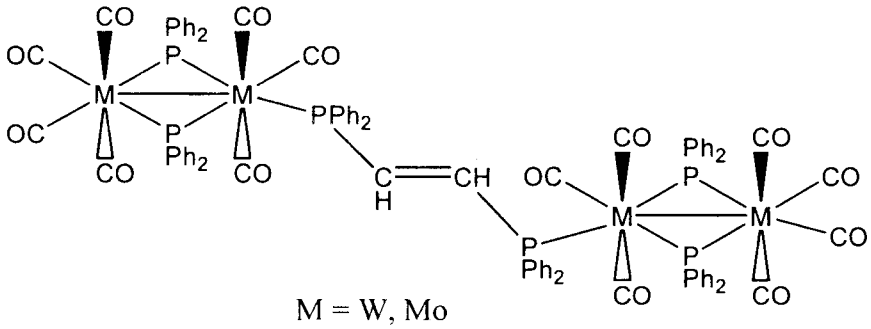

M = W, Mo

(4)

Attempts to synthesize the $Ph_2PCH_2CH_2PPh_2$ bridged complex by thermal methods would not be expected to be successful because previous work in the group showed that chelation occurs.[15]

$$M(CO)_8(\mu\text{–}PPh_2)_2 \ + \ Ph_2PCH_2\ CH_2PPh_2 \xrightarrow{\Delta} 2\ CO \ +$$

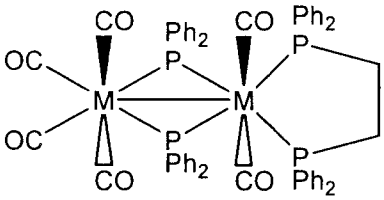

M = W, Mo (5)

One route for obtaining the phosphinoethane bridged complex would be to hydrogenate either the acetylene-bridged or ethylene-bridged complex. Methods for hydrogenation of unsaturated phosphine ligands have been reported. Louis D. Quin *et al*[16] demonstrated that unsaturated cyclic phosphines could be catalytically hydrogenated.

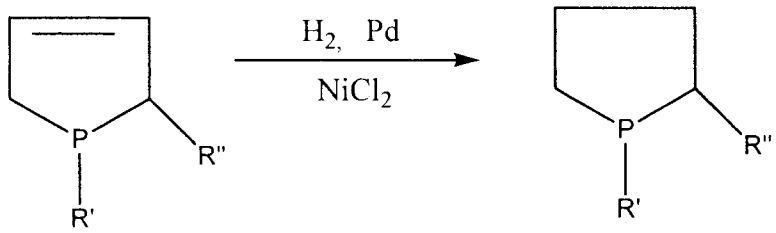

(6)

They converted the free ligand to its nickel complex in order to avoid the interaction between the catalyst and the lone pair of electrons on the phosphorus atom that would lead to inactivation of the Pd catalyst.

An alternative approach is to use Me_3NO as a method of assistance in the removal of CO at low temperatures and thus avoid chelation.

$$(CO)_4M(PPh_2)_2M(CO)_4 \;+\; PPh_2CH_2CH_2PPh_2 \xrightarrow{2\,Me_3NO} (CO)_4M(PPh_2)_2M(CO)_3\,PPh_2CH_2CH_2PPh_2\,(CO)_3M(PPh_2)_2M(CO)_4 \quad (7)$$

Cyclic voltammetry is a common but excellent technique to investigate the electronic communication between adjacent metal centers.[18,19] Often oxidation and reduction of those bridging complexes is reversible. Therefore, it is possible to measure the ease of oxidation or reduction of these complexes. If oxidation of one of the metal center does not have an effect on the oxidation of the second metal center, it can be concluded that there is no communication between metal centers.

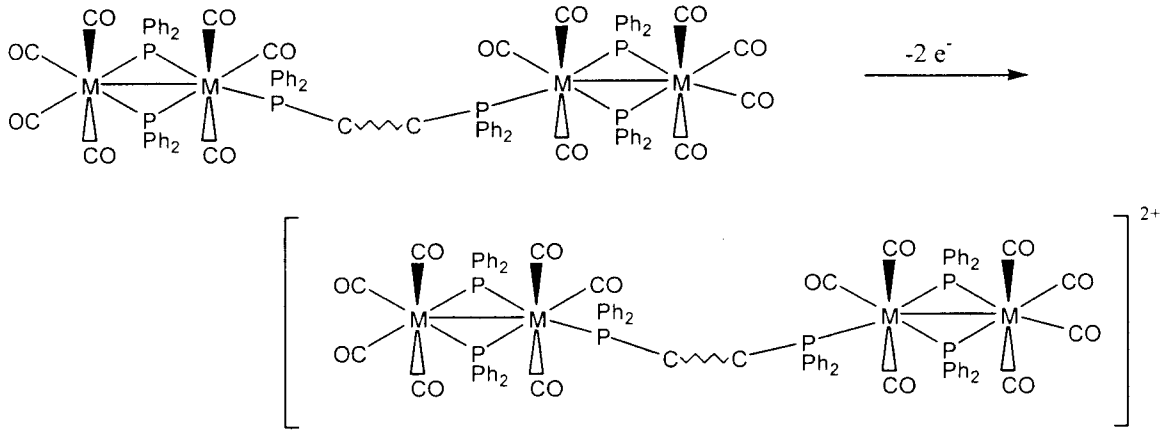

(8)

If, however, oxidation of the first metal center affects the oxidation of the second, it may indicate communication through the bridge.

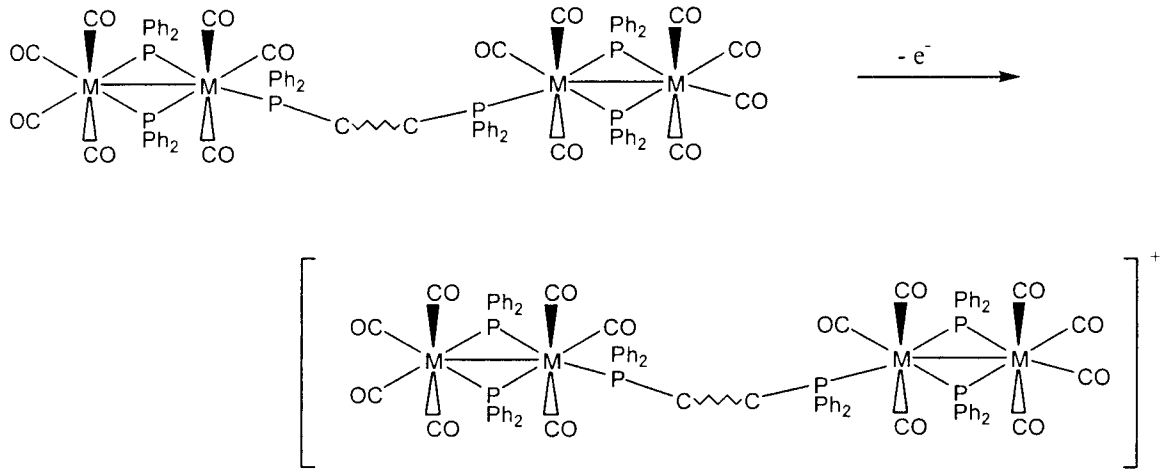

(9)

The magnitude of ΔE_p, where ΔE_p is defined as the separation of the peak potentials, is important. Bard[30] has shown that the maximum ΔE_p that can result from simple electronic "coulombic" effect is 36 mV for noncommunicating ferrocene centers and that the

electrostatic effect is a function of $1/d^2$ where d is the distance between the centers. Assuming that similar reasoning can be applied to our system, it might be expected that ΔE_p values substantially larger than 36 mV can be interpreted as communication through the bridge.

Experimental

All the reactions were carried out in an inert nitrogen atmosphere unless otherwise stated. Tungsten hexacarbonyl, molybdenum hexacarbonyl, diphenylphosphine and diphenylphosphinoacetylene were received from Aldrich chemicals. Tetrahydrofuran (THF) was distilled from a sodium/benzophenone mixture. Prior to use toluene and monoglyme were deoxygenated with a nitrogen gas flow. All the other solvents were commercial grade and were used without further purification. A 5 inch 450 Watt UV lamp and quartz immersion well were used for photolysis. Thick layer chromatographic plates were received from Analtech and were used to separate and purify the bridging and dangling products. Nicolet Avatar 360 FT-IR E.S.P. and Bio-Rad Excalibur Series FTS 30000MX FT-IR spectrophotometers were used to obtain infrared (IR) spectra of CO vibrational modes. A General Electric QE 300 NMR spectrometer was used for $^{31}P\ \{^1H\}$ NMR spectra. A Shimadzu UV-3100 UV-Vis near IR spectrophotometer was used to obtain UV-Visible spectra.

All the samples for the IR spectroscopy were dissolved in CH_2Cl_2. Samples for $^{31}P\ \{^1H\}$ NMR were dissolved in CD_2Cl_2. UV/Vis spectra were obtained in CH_2Cl_2 solutions.

A. Electrochemistry.

Cyclic voltammetry was carried out with an EG & G Princeton applied research Potentiostat/Galvanostat model 263 A. A small portion of each sample (approximately 2 mg) was dissolved in ~ 2 mL of 0.1 M tetrabutylammonium hexaflurophosphate (TBAH) in CH_2Cl_2. Approximately 3 mL of TBAH was added to a custom made container in which a working electrode (platinum disk), an auxiliary electrode (platinum wire) and a reference electrode silver wire were arranged in a triangular position. A miniscule amount of ferrocene was used as an internal standard. Voltammograms were recorded at two different scanning rates, 50 mV/sec and 100 mV/sec.

B. Separation of dangling and bridging complexes.

Silica gel plates (silica gel GF, 2 mm, and 20 cm x 20 cm, 2000 microns) were employed. Samples were dissolved in CH_2Cl_2 and put on the plates with capillary tubes made for thin layer chromatography. Between 40 – 60 mg was input per plate. A mixture of hexanes and CH_2Cl_2 (2:1) was used as the solvent system. The silica gel portions that contained products were scratched off immediately and put into separate columns. The products in the columns were eluted with CH_2Cl_2 and the solvent was removed from the solutions collected by vacuum. The purified product was tested for purity using TLC and/or $^{31}P\ \{^1H\}$ NMR spectroscopy. The

purification procedure was repeated if required. The purified product was recrystallized from CH_2Cl_2/CH_3OH. Samples were kept in the refrigerator.

C. Synthesis of *trans*-$PPh_2CH{=}CHPPh_2$ (DPPEthylene) (c). [17]

Diphenylphosphine (10 mL, 0.058 mol) and n-butyllithium (36 mL of 1.6 M, 0.058 mol) were transferred via syringes into a 500 mL 3-necked round bottom flask containing 100 mL of dry THF. The resulting dark red solution was transferred to a solution of *trans*-ClCH=CHCl (2.22 mL, 0.0262 mol) with a syringe. The solution turned brown and was stirred for six hours. Saturated NH_4Cl (50 mL) was added and the dark color of the solution disappeared as two layers developed. The top organic layer was separated and the solvent was removed under vacuum to leave behind a light yellow residue. Recrystallization from CH_3OH/CH_2Cl_2 gave a colorless product (10.59 g, 50.9 %, m.p. 125-126 °C). A $^{31}P\{^1H\}$ NMR spectrum of the product is shown in the Figure 01 and NMR data is given in Table 02 (page 42).

D. Synthesis of tungsten compounds

1. Synthesis of $W(CO)_5NH_2Ph$ (D-1).[18]

Tungsten hexacarbonyl (10.0 g, 0.0280 mol) and 10.1 mL of aniline (0.0280 mol) were added to 300 mL of distilled THF. The mixture was irradiated with UV light for 10 h and constantly stirred with a magnetic

stirring bar. The solution turned to light yellow from colorless. The solvent was removed using a vacuum line leaving behind a yellow oily sediment. Distilled water (about 75 mL) was added to the oil followed by 6 M HCl until coagulation occurred. The green/yellow solid was recovered by filtration. The solid was sublimed at 50 °C for 24 h to remove the unreacted $W(CO)_6$. The product remained unsublimed (8.20 g, 70.6 %). See Figure 02 and Table 01 (page 41) for IR data.

2. Synthesis of $W(CO)_5PPh_2H$ (D-2).[6]

Deoxygenated toluene (about 250 mL) was added to a 500 mL round bottom flask and $W(CO)_5NH_2Ph$ (10.9 g, 0.0260 mol) was transferred to it. After a nitrogen flow was established, diphenylphosphine (6.00 mL, 0.0260 mol) was added via a syringe. The mixture was stirred at room temperature for 24 h. The color of the sample changed to dark green from light green. The solvent was removed using a vacuum line to leave behind a yellow/green sediment. This sediment was recrystallized with CH_2Cl_2/CH_3OH to obtain a colorless solid (8.90 g, 67.2 %). See Figure 03 and Table 01 for IR data.

3. Synthesis of $[(CO)_4W(\mu\text{-}PPh_2)_2W(CO)_4]$ (D-3).[20]

Deoxygenated THF (about 250 mL) was transferred to 500 mL round bottom flask and $W(CO)_5PPh_2H$ (8.00 g, 0.0160 mol) was added to it. The solution was treated with n-butyllithium (10 mL of 1.6 M, 0.016 mol)

slowly via a syringe. The color of the solution turned to orange red from colorless. The mixture was refluxed and stirred for 10 h under a continuous flow of nitrogen. The color of the solution turned dark red and a dark red solid appeared. The red solid was collected by filtration and the filtrate evaporated to dryness. The two solids were combined. The solid was washed with 50 mL of pentane. Recrystallization from CH_2Cl_2/CH_3OH gave the product (4.25 g, 56.3 %). See Figure 04 and Table 01 for IR data. See Figure 05a,b and Table 02 for $^{31}P\ \{^1H\}$ NMR data.

4. Synthesis of $[(CO)_4W(\mu\text{-}PPh_2)_2W(CO)_3PPh_2C{\equiv}CPPh_2]$ (D-4-A) and $[(CO)_4W(\mu\text{-}PPh_2)_2W(CO)_3(\mu\text{-}PPh_2C{\equiv}CPPh_2)\text{-}(CO)_3W(\mu\text{-}PPh_2)_2W(CO)_4]$ (D-4-B).

Two equivalents of $(CO)_4W(\mu\text{-}PPh_2)_2W(CO)_4$ (1.99 g, 2.07 x 10^{-3} mol) and one equivalent of $PPh_2C{\equiv}CPPh_2$, (DPPA) (0.410 g, 1.03 x 10^{-3} mol) were added to deoxygenated toluene and refluxed for 18 h under a continuous nitrogen flow. The solvent was removed by vacuum and the resulting red solid was recrystallized from CH_2Cl_2/CH_3OH. Analysis of the product by TLC plates showed the presence of four major compounds. The starting material $(CO)_4W(\mu\text{-}PPh_2)_2W(CO)_4$ eluted followed by the free ligand $PPh_2C{\equiv}CPPh_2$. The two major products D-4-A and D-4-B eluted third and fourth respectively. Thick layer chromatography plates

were used for the separation of the products. An IR spectrum of D-4-A is shown in Figure 06 and data is given in Table 01. $^{31}P\ \{^{1}H\}$ NMR spectra of D-4-A and D-4-B are shown in Figure 07a,b,c,d,e and 08a,b,c,d and $^{31}P\ \{^{1}H\}$ NMR data for both compounds are given in Table 02. The UV/Vis spectrum of D-4-B is shown in Figure 10 and data given in Table 03 (page 56).

5. Synthesis of $(CO)_4W(\mu\text{-}PPh_2)_2W(CO)_3$(*trans*-$PPh_2CH{=}CHPPh_2$) (D-5-A) and [$(CO)_4W(\mu\text{-}PPh_2)_2W(CO)_3(\mu\text{-}$*trans*-$PPh_2CH{=}CHPPh_2)(CO)_3W(\mu\text{-}PPh_2)_2W(CO)_4$] (D-5-B).

Two equivalents of $(CO)_4W(\mu\text{-}PPh_2)_2W(CO)_4$ (2.10 g, 2.18 x 10^{-3} mol) and one equivalent of *trans*-$PPh_2CH{=}CHPPh_2$ (DPPEthylene) (0.432 g, 1.09 x 10^{-3} mol) were added to deoxygenated toluene and refluxed for 18 h under a continuous nitrogen flow. The solvent was removed by vacuum. The resulting red solid was recrystallized from CH_2Cl_2/CH_3OH. Analysis of the product by TLC plates showed the presence of four major compounds. The sequence of elution of the compounds was same as for reaction 4. Thick layer chromatography plates were used for the separation of the products. IR spectra of D-5-A and D-5-B are shown in Figures 11 and 13 and IR data are given in Table 01. $^{31}P\ \{^{1}H\}$ NMR spectra of both complexes are shown in Figures 12a,b,c,d,e and 14a,b,c,d and $^{31}P\ \{^{1}H\}$

NMR data are given in Table 02. A UV/Vis spectrum of D-5-B is shown in Figure 16 and data is given in Table 03.

E. Synthesis of molybdenum compounds.

1. Synthesis of $Mo(CO)_5PPh_2H$ (E-1).[6]

Deoxygenated monoglyme (250 mL) was added to a two-necked round bottom flask and heated for 30 minutes under a continuous flow of nitrogen. $Mo(CO)_6$ (10.0 g, 0.038 mol) and PPh_2H (2.60 mL, 0.038 mol) were added to the above solution, the latter via syringe, and refluxed for 8 h. The solvent was removed by vacuum. The resulting yellow oily residue was recrystallized from CH_2Cl_2/CH_3OH. The product was sublimed at 52 °C for 24 h to remove unreacted $Mo(CO)_6$. Colorless crystalline product remained unsublimed (8.20 g, 51.3 %). An IR spectrum is shown in Figure 17 and IR data are given in Table 01.

2. Synthesis of $[(CO)_4Mo(\mu\text{-}PPh_2)_2Mo(CO)_4]$ (E-2).[19]

In deoxygenated THF, $Mo(CO)_5PPh_2H$ (8.0 g, 0.019 mol) and n-butyllithium (12 mL of 1.6 mol; 0.019 mol) were refluxed under a continuous nitrogen flow for 15 h. The color of the solution changed to orange from colorless immediately upon addition of n-butyllithium. The solution was stirred in an open atmosphere with a magnetic stirring bar for

24 h at room temperature. The color changed to red from orange and a red colored solid appeared. The solvent was removed by vacuum and red solid was collected by filtration. The product was recrystallized from CH_2Cl_2/CH_3OH (4.25 g, 55.7 %). An IR spectrum is shown in Figure 18 and IR data are given in Table 01.

3. Synthesis of $[(CO)_4Mo(\mu\text{-}PPh_2)_2Mo(CO)_3(PPh_2C{\equiv}CPPh_2)]$ (E-3-A) and $[(CO)_4Mo(\mu\text{-}PPh_2)_2Mo(CO)_3\text{-}(\mu\text{-}PPh_2C{\equiv}CPPh_2)(CO)_3Mo(\mu\text{-}PPh_2)_2Mo(CO)_4]$ (E-3-B).

Two equivalents of $(CO)_4Mo(\mu\text{-}PPh_2)_2Mo(CO)_4$ (4.21 g, 5.36 x 10^{-3} mol) and one equivalent of $PPh_2C{\equiv}CPPh_2$ (DPPA) (1.06 g, 2.68 x 10^{-3} mol) were refluxed in deoxygenated THF for 24 h under a continuous nitrogen flow. The solvent was removed by vacuum and the resulting red solid was recrystallized from CH_2Cl_2/CH_3OH. Analysis of the product by TLC plates showed the presence of four major compounds. The sequence of the elution of compounds was the same as similar reactions of tungsten described above. Thick layer chromatography plates were used for the separation of the products. IR spectra of E-3-A and E-3-B are shown in Figures 19 and 22 and IR data for both compounds are given in Table 01. $^{31}P\ \{^1H\}$ NMR spectra of both complexes are shown in Figures 20a,b,c,d,e and 23a,b,c,d, and the data is given in Table 02. An UV/Vis spectrum of E-3-A is shown in Figure 21 and data is given in Table 03.

4. Synthesis of $[(CO)_4Mo(\mu\text{-}PPh_2)_2Mo(CO)_3(trans\text{-}PPh_2CH{=}CHPPh_2)$ (E-4-A) and $[(CO)_4Mo(\mu\text{-}PPh_2)_2Mo(CO)_3\text{-}(\mu\text{-}trans\text{-}PPh_2CH{=}CHPPh_2)(CO)_3Mo(\mu\text{-}PPh_2)_2Mo(CO)_4]$ (E-4-B).

Two equivalents of $(CO)_4Mo(\mu\text{-}PPh_2)_2Mo(CO)_4$ (2.00 g, 2.55 x 10^{-3} mol) and one equivalent of *trans*-$PPh_2CH{=}CHPPh_2$ (DPPEthylene) (0.504 g, 1.28 x 10^{-3} mol) were refluxed in deoxygenated THF for 20 h under a continuous nitrogen flow. The red color of the solution became darker. The solvent was removed by vacuum and the resulting red solid was recrystallized from CH_2Cl_2/CH_3OH. Analysis of the product by TLC plates showed the presence of four major compounds. The sequence of elution of the compounds was same as in reaction 3. Thick layer chromatography plates were used for the separation of the products. An IR spectrum of E-4-A is shown in Figure 24 and data is given in Table 01. $^{31}P\{^1H\}$ NMR spectra of both complexes are shown in Figures 25a,b,c,d,e and 26a,b,c,d and $^{31}P\{^1H\}$ NMR data is given in Table 02. UV/Vis spectrum of E-4-B is shown in Figure 28 and data is given in Table 03.

5. Attempted synthesis of $[(CO)_4Mo(\mu\text{-}PPh_2)_2Mo(CO)_3\text{-}(PPh_2CH_2CH_2PPh_2)$ and $[(CO)_4Mo(\mu\text{-}PPh_2)_2Mo(CO)_3\text{-}(PPh_2CH_2CH_2PPh_2)(CO)_3Mo(\mu\text{-}PPh_2)_2Mo(CO)_4]$ (E-5).

Two equivalents of $(CO)_4Mo(\mu\text{-}PPh_2)_2Mo(CO)_4$ (2.00 g, 2.54 x 10^{-3} mol) and two equivalents of $(CH_3)_3NO{\cdot}2H_2O$ (0.283 g, 2.54 x 10^{-3} mol) were added to deoxygenated THF. The temperature was brought to near zero with ice and stirred with a magnetic stirring bar. One equivalent of $Ph_2PCH_2CH_2PPh_2$ (0.506 g, 1.27 x 10^{-3} mol) was added to the above solution and stirring was continued for 36 h in the ice bath. The color changed from red to reddish brown. The precipitated solid was collected by filtration and redissolved in CH_2Cl_2. Analysis of the crude product using TLC showed that presence of four major different compounds. The starting materials, $(CO)_4Mo(\mu\text{-}PPh_2)_2Mo(CO)_4$ and $Ph_2PCH_2CH_2PPh_2$ came off first followed by two unknown compounds. A substantial amount of the first unknown complex was collected and an IR spectrum (Figure 30).

F. Attempted hydrogenation of unsaturated compounds.

1. Hydrogenation of *trans*-$Ph_2PCH{=}CHPPh_2$.[15]

To *trans*-$Ph_2PCH{=}CHPPh_2$ (100 mg) dissolved in 100 ml of CH_2Cl_2, was added palladium metal (5 mg) as a catalyst for hydrogenation. This

mixture was exposed to H_2 at 40 PSI at room temperature for 1 h. The solvent was removed by vacuum and palladium metal was removed by filtration. The analysis of the product with TLC (hexane methylene chloride 2 :1 solvent system) against reference compounds *trans*-$Ph_2PCH{=}CHPPh_2$ and $Ph_2PCH_2CH_2PPh_2$ suggested that no reaction had occurred. The same procedure was carried out with 20 mg of palladium metal and the result was no different than on the previous occasion.

2. Hydrogenation of $[(CO)_4Mo(\mu\text{-}PPh_2)_2Mo(CO)_3(\mu\text{-}trans\text{-}PPh_2CH{=}CHPPh_2)(CO)_3Mo(\mu\text{-}PPh_2)_2Mo(CO)_4]$

A small portion of $[(CO)_4Mo(\mu\text{-}PPh_2)_2Mo(CO)_3\text{-}(\mu\text{-}trans\text{-}PPh_2CH{=}CHPPh_2)(CO)_3Mo(\mu\text{-}PPh_2)_2Mo(CO)_4]$ (100 mg) was dissolved in 100 mL of CH_2Cl_2 and palladium metal (100 mg) was added as the catalyst for hydrogenation. The mixture was exposed to H_2 at 40 PSI and room temperature for 1 h. The solvent was removed by vacuum and palladium metal was removed by filtration. The analysis of the residue did not show a TLC profile different from the unhydrogenated compound. It was concluded that no reaction occurred.

G. Oxidation and UV/Vis of bridging complexes.

1. Chemical oxidation of $[(CO)_4Mo(\mu\text{-}PPh_2)_2Mo(CO)_3\text{-}(\mu\text{-}\textit{trans}\text{-}PPh_2CH{=}CHPPh_2)(CO)_3Mo(\mu\text{-}PPh_2)_2Mo(CO)_4]$.

a. $AgBF_6$.

A diluted solution of the above compound (0.25 mM, 5.00 mL) in CH_2Cl_2 was prepared. A 3.00 mL aliquot of this solution was used to obtain the UV/Vis spectrum of the neutral complex (Figure 28). A 0.10 ml portion of 7.5 mM $AgBF_6$ (7.5 mg, 5.00 mL of CH_2Cl_2) was added to the above solution. The color of the sample turned from red to orange-green. Attempt to obtain a UV/Vis spectrum of the resulting solution was unsuccessful because of the formation of a grey-solid layer inside the cell wall. The resulting solution started fuming after few minutes upon the addition of $AgBF_6$.

b. AgCl.

AgCl was gradually added to a fresh solution of the above solution. The solution turned orange-green after addition of few crystals of AgCl and turned completely green after the addition of excess AgCl. Figure 29a shows a UV/Vis spectrum of the resulting solution after addition of few crystals of AgCl and Figure 29b shows UV/Vis spectrum of the resulting solution after addition of excess AgCl.

Results and Discussion

The synthesis of the target compounds was done by a series of stepwise reactions starting from hexacarbonyl complexes of molybdenum and tungsten. The product of each step was analyzed by $^{31}P\ \{^{1}H\}$ NMR and/or IR techniques or both as was necessary.

It is possible to obtain $Mo(CO)_5PPh_2H$ directly from $Mo(CO)_6$ because it loses CO at relatively low temperatures.

$$Mo(CO)_6 + PPh_2H \xrightarrow{\text{monoglyme}} Mo(CO)_5PPh_2H + CO \qquad (10)$$

The analogous reaction for $W(CO)_6$ requires a much higher temperature and a mixture of products is obtained. Therefore an indirect approach was used in which $W(CO)_5NH_2Ph$ was prepared.

$$W(CO)_6 + NH_2Ph \xrightarrow{\text{THF / UV}} W(CO)_5NH_2Ph + CO \qquad (11)$$

The product in this reaction, $W(CO)_5NH_2Ph$ (D-1) showed two IR absorptions at 1931 cm^{-1} (strong) and 2074 cm^{-1} (weak) (Figure 02). This data is consistent with C_{4v} symmetry for the complex. IR data is also useful in the purification step as unreacted hexacarbonyl starting material gives rise to strong signal at 1977 cm^{-1}. During the sublimation step in which $W(CO)_6$ is removed, the residue can be monitored to determine how much of the starting material remains. The color of $W(CO)_5NH_2Ph$ was mostly dependent upon the amount of the HCl added in the work-up to remove unreacted aniline and varied from the yellowish green to dark green. The percentage yield of the product varied from 42 to 92 % and may be due to the several factors

such as quality of aniline used and technical errors. The product was kept in the refrigerator in closed containers but it was stable at room temperature and open air for a couple of weeks. Our spectroscopic data was in agreement with previous work.[21]

Aniline is a good leaving group and its reaction with PPh_2H is selective for the production of $W(CO)_5PPh_2H$. In the second step we converted the aniline derivative to the diphenylphosphine derivative.

$$W(CO)_5NH_2Ph + PPh_2H \longrightarrow W(CO)_5PPh_2H + NH_2Ph \qquad (12)$$

The $Mo(CO)_5PPh_2H$ and $W(CO)_5PPh_2H$ products both showed IR spectra for C_{4v} symmetry. The $W(CO)_5PPh_2H$ (D-2) showed one strong peak at 1941 cm^{-1} and one medium peak at 2074 cm^{-1} (Figure 03) while $Mo(CO)_5PPh_2H$ gave a medium signal at 2075 cm^{-1} and a strong signal at 1949 cm^{-1} (Figure 17). The results are consistent with literature assignments.[22]

Recrystallization was used to purify the complexes. The shifting of the peak at 1931 cm^{-1} in $W(CO)_5NH_2Ph$ to 1943 cm^{-1} in $W(CO)_5PPh_2H$ can be attributed to the difference of the two ligands involved. Aniline is a better σ-donor than diphenylphosphine and causes an increase in the electron density at the metal center. This extra electron density increases the π-back bonding ability of the metal and hence weakens the CO bond strength and lowers the IR frequency when electrons are received in the π^* orbitals of CO. On the other hand PPh_2H is a weaker σ-donor and a better π-acceptor. Both these qualities reduce the electron density on the metal hence the π-back donation to the π^* orbitals of CO is decreased. That results in a stronger CO bond that shows a higher stretching frequency.

The percentage yield for the reaction was increased from 45 to 80 % over time.

The following reaction was used to synthesize the tungsten and molybdenum dimers.

$$M(CO)_5PPh_2H \xrightarrow[M = Mo, W]{BuLi} (CO)_4M(PPh_2)_2M(CO)_4 \qquad (13)$$

The tungsten dimer showed two strong IR peaks at 2031 cm^{-1} and 1959 cm^{-1} (Figure 04). The molybdenum dimer showed two strong IR peaks at 2033 cm^{-1} and 1965 cm^{-1} (Figure 18). These values are well in agreement with the literature values of 2032 cm^{-1} (s) and 1958 cm^{-1} (vs) for tungsten and 2034 (s) cm^{-1} and 1967 (vs) cm^{-1} for molybdenum.[23] According to the literature both tungsten and molybdenum dimers have D_{2h} symmetry. Our calculation of the number of symmetry allowed IR modes resulted in three IR bands, B_{1u}, B_{2u} and B_{3u}. Braterman[31] reported that $(CO)_4Mo(PPh_2)_2Mo(CO)_4$ had been shown to have three IR signals at 2025 cm^{-1},1957 cm^{-1} and 1970 cm^{-1} (shoulder peak).

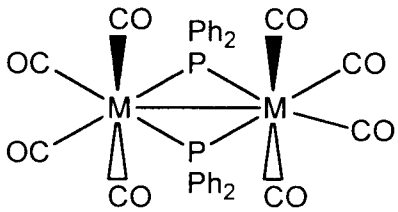

M = W, Mo

Probably two of those three symmetry allowed IR signals overlapped to give rise to only two peaks in CH_2Cl_2 as we saw in the experimental data. This is supported by the broad asymmetric peaks at 1959 cm^{-1} for tungsten and at 1965 cm^{-1} for molybdenum which is a signature for overlapped bands. The $^{31}P\{^1H\}$ NMR spectrum of tungsten compound showed a strong signal at 181.4 ppm (Figure 05). The presence

of just one signal confirms that the product only contained one type of phosphorus atom. Satellite signals show that the phosphorus atoms are directly connected to the tungsten metal center (J_{PW} = 162.4 Hz). NMR data is in agreement with the literature values of 180.0 ppm and 162.0 Hz for tungsten.[6] Although, the percentage yield was relatively poor, the IR and NMR spectra suggest that the final product was not contaminated with other by-products. The maximum yield obtained was 48 % for the tungsten dimer and was 52 % for molybdenum. Purity of products is the main advantage of the stepwise procedure unlike other routes for synthesizing the dimers. For example, a one step reaction of $W(CO)_6$ with PPh_2H and $NaBH_4$ yields a mixture of seven different compounds.[6] The relatively high purity of the product mixture in our reaction made recrystallisation adequate for final purification.

Thin layer chromatography was useful for monitoring the number of products present in the product mixture and typically we saw at least two compounds, one red and one pale yellow. The pale yellow compound did not contain either CO or phosphorus as shown by IR and ^{31}P spectroscopy. Therefore, it was assumed that the second compound was a Li salt. When the product was washed with water as required by our procedure, salts were removed leaving the red-colored dimer. The percentage yield was relatively poor in tetrahydrofuran (THF). Different solvents (toluene and decalin) were tried in order to enhance the product formation but improvement did not result. Working with decalin was especially tedious as it was difficult to remove the high-boiling solvent from the product. The dimer was stable for months in the refrigerator in a closed container. Spectroscopic results for molybdenum and tungsten complexes are found in Tables 01 and 02.

Synthesis of the first two target compounds was accomplished via the following reaction:

$$2\,(CO)_4M(\mu\text{-}PPh_2)_2M(CO)_4 + Ph_2PC{\equiv}CPPh_2 \xrightarrow{\text{toluene / reflux}}$$

$$[(CO)_4M(\mu\text{-}PPh_2)_2M(CO)_3PPh_2C{\equiv}CPPh_2] +$$

$$[(CO)_4M(\mu\text{-}PPh_2)_2M(CO)_3(\mu\text{-}PPh_2C{\equiv}CPPh_2)(CO)_3M(\mu\text{-}PPh_2)_2M(CO)_4]$$

$$M = Mo, W \qquad (14)$$

It was a difficult process because most of the time we ended up getting a mixture of five to eight compounds in the product mixture. Given that all of these were red in color and contained CO groups and phosphorus atoms it was very difficult to infer the nature of all the products in a mixture. Different solvents were tried (THF and decalin) for the procedure but improvement was not achieved. There was no reaction when THF was used as the solvent. A possible reason is that the refluxing conditions provided by THF did not give a temperature high enough to overcome the reaction barrier. Although the introduction of decalin as the solvent made it possible to go to a much higher refluxing temperature, the product mixture did not show improvement and only made the removal of the solvent very difficult. Therefore we tried to modify the given synthetic procedure or use new methods.

In the first method we tried to use UV irradiation to weaken the metal-carbonyl bonds of the starting dimer, thus facilitating the removal of a CO group.

$$(CO)_4W(PPh_2)_2W(CO)_4 + Ph_2PC{\equiv}CPPh_2 \xrightarrow{\text{UV / THF}} \text{Products} \qquad (15)$$

By monitoring the reaction with IR spectroscopy, it was found out that no reaction had taken place after 8 h. This is surprising because UV light is well-known to break

M-CO bonds. Perhaps the UV light frequency used was not sufficient to break the metal-carbonyl bond for this complex.

The second method we used can be described as nucleophilic assistance of ligand substitution.

$$(CO)_4W(PPh_2)_2W(CO)_4 + Ph_2PC{\equiv}CPPh_2 \xrightarrow{Me_3NO.2H_2O\,/\,THF} \text{products} \quad (16)$$

It is well known that $Me_3NO.2H_2O$ can assist the leaving of a carbonyl group from a metal and convert it into CO_2 according to the following reaction.[25]

$$\text{M-CO} + Me_3NO \longrightarrow \text{M-}NMe_3 + CO_2 \quad (17)$$

This would inhibit the following equilibrium and thus minimize the competition between CO and DPPA for the vacant coordination site.

$$(CO)_4W(PPh_2)_2W(CO)_4 \rightleftharpoons (CO)_4W(PPh_2)_2W(CO)_3 + CO \quad (18)$$

From our experience and that of others we know that removal of NMe_3 by a phosphine is much easier than direct substitution of CO. However the TLC profile of the product mixture suggested that the conditions we used for this experiment did not yield the desired products. Infrared spectroscopy was used to monitor the reaction.

The failure of the irradiation procedures and of the Me_3NO route led us to return to thermal substitution as described on the previous page. Although many products were obtained, it was decided that they could be separated by thick layer chromatography. Most of the product mixtures contained five to six different compounds according to the thin layer chromatography plates but separation was great enough for isolation of important products. Given below is a TLC (thin layer chromatography) sketch of the crude product mixture.

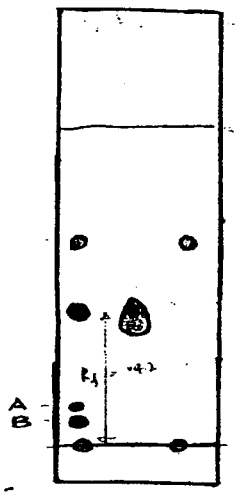

X Y Z (see Experimental)

X = sample, Y = DPPA, Z = W- dimmer.

Spot X is the crude product of the reaction D-4, Y is DPPA and Z is the starting material-tungsten dimer. Comparison with the starting materials suggested that the top two spots belonged to the starting materials, $Ph_2PC{\equiv}CPPh_2$ and $(CO)_4W(PPh_2)_2W(CO)_4$. The size of the tungsten dimer spot also suggested that a large amount of starting material was left unreacted even after long reaction times. Spots A and B were relatively intense and separated using thick layer chromatographic plates.

Prior to using thick layer plates we tried to use a Chromatron to achieve separation. About 0.65 g of crude product was introduced to a 2 mm thick plate and the elution bands were collected. TLC showed that separation was not achieved. It is possible that we failed because of heavy loading of the plate. The difficulty of making plates for Chromatotron and poor separation made this method of no value. The selection of the thick layer chromatography with 2 mm thick plates proved to be a better option. The efficiency of this method was also dependent upon the amount of

the material input to the plate but most of the time two consecutive separations gave enough pure products for most applications. The major problem associated with this method was that most of the products deteriorated on silica. Therefore it was necessary to minimize the time that compounds spent on the silica. In order to improve separations different ratios of hexanes to methylene chloride were tried. Ratios of, 2:1, 1:1 and 3:1 gave approximately the same separation of the compounds of interest. Given below is a comparison of different solvent systems for the crude product of reaction D-4.

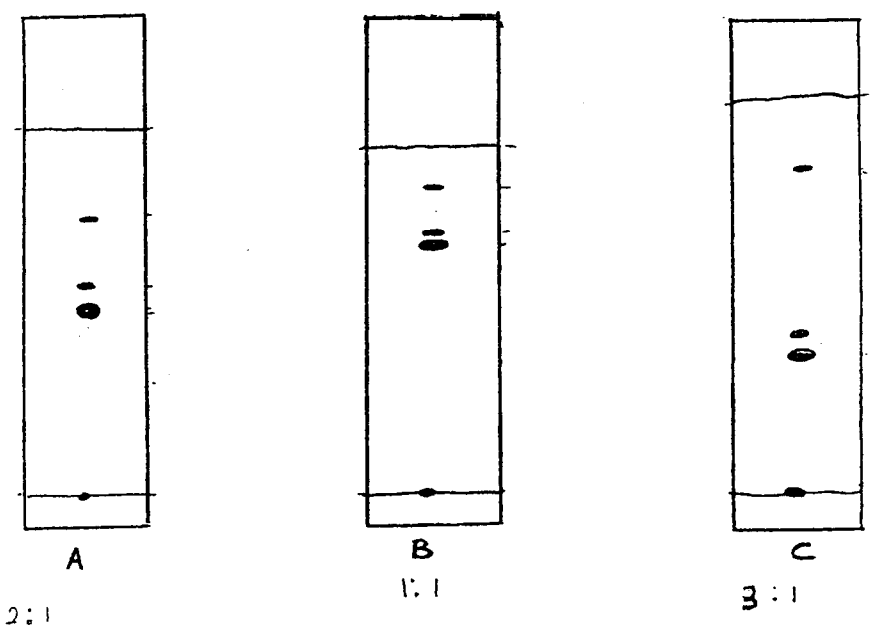

Plate A represents solvent system 2:1, B represents 1:1 and C represents 3:1.

After the separation, each new compound was analyzed with $^{31}P\{^{1}H\}$ NMR and IR spectroscopy. The IR spectra of the complexes were very similar and did not help in identification.

Spot A labeled as D-4-A showed four $^{31}P\ \{^{1}H\}$ NMR signals at 175.0 (dd) ppm, 151.6 (dd) ppm, -12.3 (m) ppm and -31.7 (d) ppm (Figure 07). The chemical shifts of the phosphorus atoms cannot be simply explained by considering electron density about the nucleus as in the case of hydrogen. In hydrogen the diamagnetic effect is dominant and the paramagnetic effect is negligible. Therefore, changes in chemical shifts results from different chemical environments can be understood by looking at the changes in electron density around the atom. In phosphorus both diamagnetic and paramagnetic effects make significant contributions to shielding and influence the chemical shift values. A change of the substituents on phosphorus can greatly alter the paramagnetic contribution and therefore the simple electron density explanation does not work when comparing different compounds but does have some applicability when comparing similar compounds.

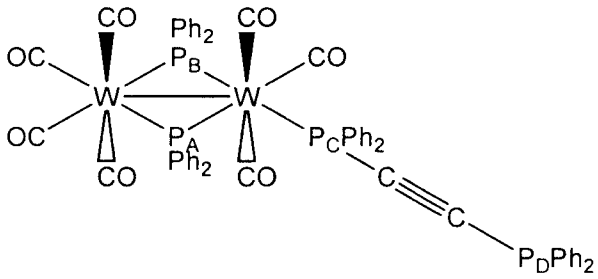

Structure I (D-4-A)

Bearing that in mind, the signals at 175.0 ppm and 151.6 ppm were thought to arise from the two bridging phosphorus atoms, P_A and P_B because their chemical shifts are the closest to those of the starting material which has a chemical shift of 181.3 ppm. Furthermore it is reasonable to assume that the bridging P trans to CO

(P_A) can be assigned to the signal at 175.0 ppm because the changes in the trans position will have a larger effect on the chemical shift than changes in the cis position. The presence of tungsten satellites for both signals further supported the assignment.

The tungsten-phosphorus satellites are of particular interest because the two tungsten atoms are nonequivalent. For P_A, the values of J_{WP} are so similar that they cannot be resolved, and only an average value can be reported (172.8 Hz). In the case of P_B, the J_{WP} values are sufficiently different that they can be determined. Although all sixteen satellite lines are not observed, we do see twelve of them and the outer and inner lines could be used to obtain accurate coupling constants (197.6 Hz and 135.9 Hz).

The signal at chemical shift 151.6 ppm (P_B) shows two P-P couplings of 29.5 Hz and 16.4 Hz while the other (P_A) shows couplings of 34.4 Hz and 16.3 Hz. The smaller coupling corresponds to coupling between the two bridging phosphorus atoms. The coupling of 34.4 Hz belongs to that of P_A-P_C (cis coupling) and 29.5 Hz belongs to P_B-P_C (trans coupling).

The third and fourth chemical shifts arise from the phosphorous atoms in the non-bridging ligand, $Ph_2PC{\equiv}CPPh_2$. Free $Ph_2PC{\equiv}CPPh_2$ has a chemical shift of -32.9 ppm and when one end binds to a metal center, the bonded end experiences a large downfield chemical shift change, while the unbound end changes only slightly. Based on this argument we can assign the chemical shift of -12.3 ppm to P_C which also shows tungsten satellite signals and the dangling end, P_D, to -31.7 ppm. The

resolution was poor at -12.3 ppm and only an average J_{WP} value was obtained (268.7 Hz).

It is also possible to conclude that P_C is trans to one of the bridging P atoms because if $Ph_2PC{\equiv}CPPh_2$ had attached to tungsten in a cis position to both P_A and P_B then both P_A and P_B would be equivalent and that would contradict the NMR data. Considering all the facts, we rejected structure II as a possibility for D-4-A.

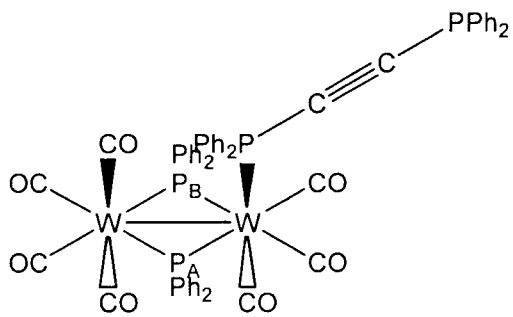

Structure II

Structure I (C_s symmetry) showed four signals at 2041 cm^{-1}(m), 2002 cm^{-1}(m), 1935 cm^{-1}(vs) and 1888 cm^{-1}(w) (Figure 06). The signal at 1888 cm^{-1} probably arises from natural abundance ^{13}CO. The IR pattern could not be described by simple symmetry for IR spectroscopy. Our calculation of number of symmetry allowed IR transitions yielded only two bands, 5A′ and A″.

As D-4-A is a new compound, there were no NMR or IR data in the literature to provide confirmation. Similar compounds such as $(CO)_4W(PPh_2)_2W(CO)_3PPh_2H$ are in agreement with these assignments, however.[6] A complete analysis of IR and NMR data is given in Tables 01 and 02.

The presence of three sets of $^{31}P\ \{^{1}H\}$ NMR signals for D-4-B, all of which showed tungsten satellites, suggested that all the phosphorus atoms are bound to tungsten atoms (Figure 08). This led us to conclude that D-4-B contained a bridging $Ph_2PC{\equiv}CPPh_2$ unit. The three sets of NMR signals were found at 175.1 ppm, 149.9 ppm and -8.1 ppm. Using the argument we built in the previous case we were able to assign the 175.1 ppm peak to P_A and 149.9 ppm to P_B. The third peak belongs to P_C from $Ph_2PC{\equiv}CPPh_2$. Analysis of the second order effect in a simulated $^{31}P\ \{^{1}H\}$ NMR spectrum of D-4-B revealed that (Figure 09) coupling between two phosphorus atoms is negligible and therefore two halves of the molecule behave independently. NMR data was in agreement with the following structure for D-4-B.

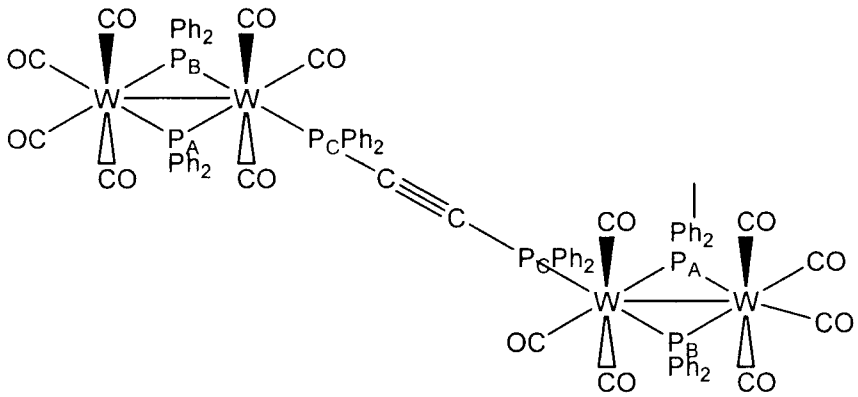

D-4-B

Relevant chemical shifts and coupling constants are found in Table 02. The infrared spectrum showed three signals at 1935 (s) cm^{-1}, 2001 (m) cm^{-1} and 2042 (m) cm^{-1}.

The molybdenum analog (E-3-A) of the tungsten complex D-4-A showed four $^{31}P\ \{^{1}H\}$ NMR signals at 229.6 (dd), 197.3 (dd), 21.1 (m) and -31.4 (d) ppm. The P-P

splitting pattern was identical to that of D-4-A (Figure 20). Therefore using previous knowledge we assigned 229.6 ppm to P_A, 197.3 ppm to P_B, 21.1 ppm to P_C and -31.4 ppm to P_D. A complete analysis of NMR data is given in Table 02. NMR data is consistent with the following structure.

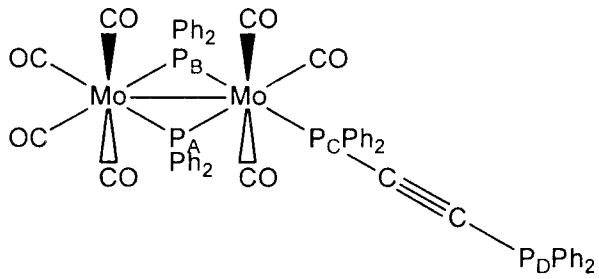

E-3-A

Infrared spectroscopy of E-3-A showed three signals at 2043 (w) cm^{-1}, 2006 (w) cm^{-1} and 1943 (s) cm^{-1} (Figure 19) and as in the previous example the number of signals could not be accounted for with simple symmetry consideration.

Complex E-3-B showed three $^{31}P\ \{^1H\}$ NMR peaks at 229.9(dd), 195.0(dd), 24.8(dd,) ppm (Figure 23). The P-P splitting pattern was similar to that of the tungsten complex D-4-B except there were no metal-phosphorus satellites. Based on the argument built earlier in the case of D-4-B, we were able to assign peak 229.9 ppm to P_A, 195.0 ppm to P_B and 24.8 ppm to P_C. The small coupling (3.6 Hz) between phosphorus atoms in $Ph_2PCH{\equiv}CHPPh_2$ in complex E-3-A suggested that the system could be treated as a first order spectrum. The NMR data was used to elucidate the following structure.

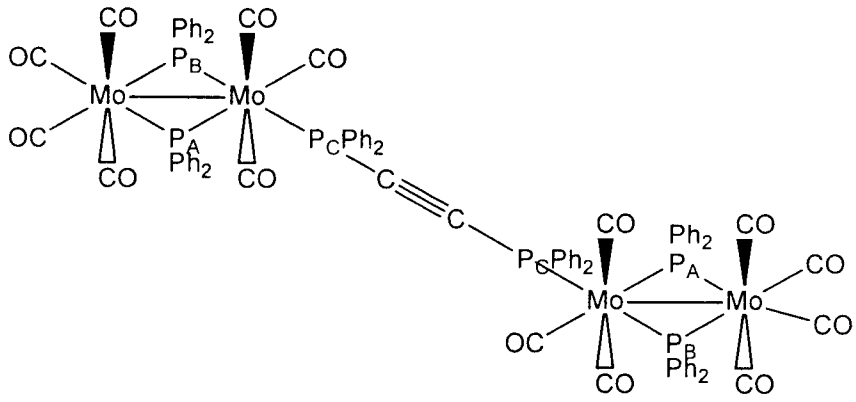

E-3-B

A complete analysis of NMR data is given in Table 02.

The IR spectrum of E-3-B showed three signals found at 2043(w), 2006(w), 1944(s) (Figure 22).

Complex D-5-A showed four $^{31}P\ \{^{1}H\}$ NMR signals at 175.0 ppm (dd), 147.1 ppm (dd), 6.9 ppm (m) and -7.5 ppm (d) (Figure 12). Peaks at 175.0 ppm and 147.1 ppm were assigned to bridging P_A and P_B. The peaks at 6.9 ppm and -7.5 ppm came from the two phosphorus atoms in $Ph_2PCH{=}CHPPh_2$. The coupling of P_A-P_C and P_B-P_C were 31.8 Hz and 27.3, slightly smaller than corresponding coupling constants of D-4-A (34.4 Hz and 29.5 Hz). The coupling of P_A-P_B (16.6 Hz) was close to that of D-4-A (16.5 Hz) but the coupling between P_C-P_D was 16.7 Hz and much larger than the P-P coupling for $PPh_2{\equiv}CCPP_2$ (4.2 Hz). The following structure is consistent with the $^{31}P\ \{^{1}H\}$ NMR data.

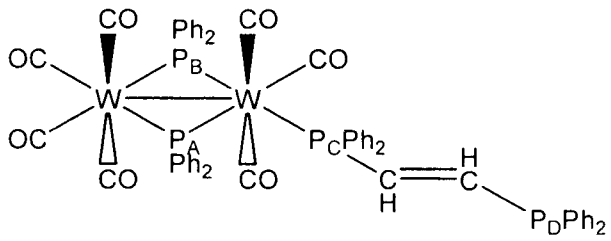

D-5-A

A complete listing of NMR data is given in Table 02.

Complex D-5-B showed three $^{31}P\{^{1}H)$ NMR signals at 175.3 ppm (m) (P_A), 147.3 ppm (m) (P_B) and 7.5 ppm (m) (P_C) (Figure 14). The couplings of the two phosphorus atoms of *trans*-$PPh_2CH{=}CHPPh_2$ were significant and therefore the system displayed a second order effect. The simulated spectrum of D-5-B (Figure 15) revealed a coupling of 17.2 Hz. The following structure is consistent with the NMR data and complete analysis of NMR data is given in Table 02.

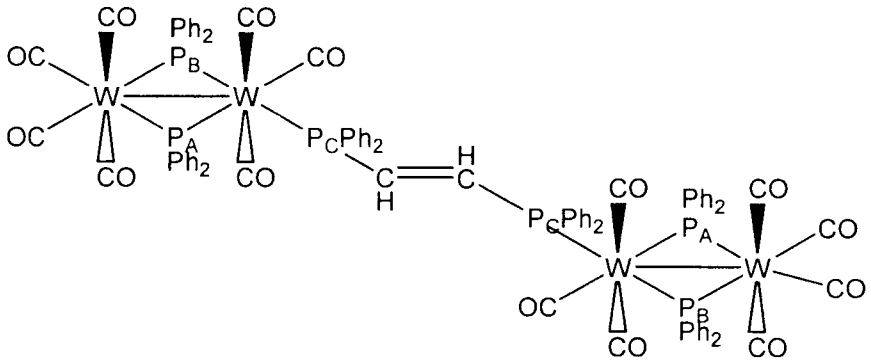

D-5-B

The IR spectrum showed three signals at 2040(m), 1998(m), 1935(s) (Figure 13).

The molybdenum analog (E-4-A) of the tungsten complex D-5-A showed four signals at 229.4(dd,P_A) ppm, 191.1(dd,P_B) ppm, 37.3(m,P_C) ppm, 7.8(d,P_D) ppm

(Figure 25) . The coupling of the two phosphorus atoms of $PPh_2CH{=}CHPPh_2$, (15.3 Hz) was significantly larger than that of D-4-A (3.6 Hz). The following structure is consistent with NMR data.

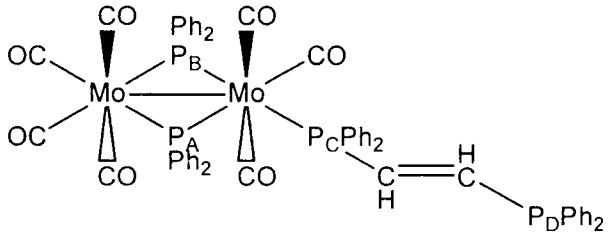

E-4-A

A complete listing of NMR data is given in Table 02.

The IR spectrum showed three signals at 2041 cm^{-1}(w), 2003 cm^{-1}(w) and 1942 cm^{-1} (s) (Figure 24).

Complex E-4-B showed three $^{31}P\ \{^1H\}$ NMR signals at 230.0 (dd, P_A), 191.6 (dd, P_B), 38.2 (m, P_C) (figure 26). The P-P coupling of *trans*-$PPh_2CH{=}CHPPh_2$ was significantly large and therefore the system was investigated for a second order effect. The simulated spectrum suggested a P-P coupling of 14.8 Hz.

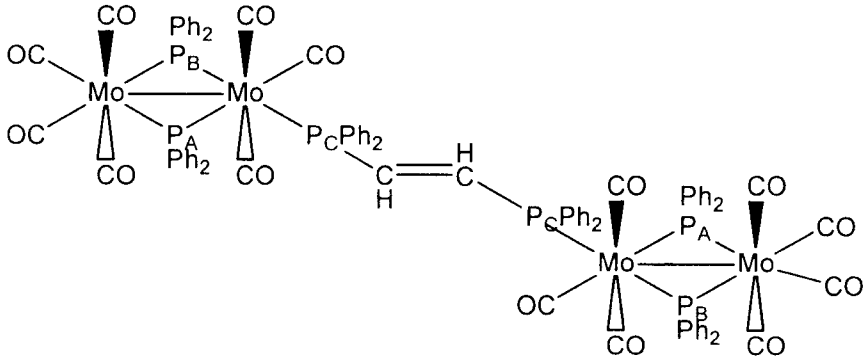

E-4-B

A complete analysis of the NMR data is given in Table 02.

The following Tables summarize IR data and $^{31}P\ \{^{1}H\}$ NMR data.

Table 01 – IR data.

Complex	IR data (cm^{-1})
D-1	1975 (m), 1930 (s)
D-2	2074 (m), 1941 (s)
D-3	2031 (s), 1959 (s)
D-4-A	2041 (m), 2002 (m), 1934 (s), 1888 (m)
D-4-B	2042 (m), 2002(m), 1935 (s)
D-5-A	2040(m), 1999(m), 1934 (s), 1885 (m)
D-5-B	2040(m), 1998(m), 1935(s), 1884 (m)
E-1	2075 (w), 1949(s)
E-2	2033 (w), 1965(s)
E-3-A	2043(w), 2006(w), 1943(s)
E-3-B	2043(w), 2006(w), 1944(s)
E-4-A	2041(w), 2003(w),1942(s)
E-4-B	Not Available

Table 02 - $^{31}P\{^{1}H\}$ NMR data for selected complexes

Comp	$^{31}P\{^{1}H\}$ NMR data	
	δ (ppm)	Coupling constants (Hz)
C	-7.1	--
D-3	181.4	162.5 (W,P)
D-4-A	175.0 (dd,P_A), 151.6(dd,P_B) -12.3 (m, P_C), -31.7 (d,P_D)	34.4 (P_A,P_C) , 29.5 (P_B,P_C), 16.5 (P_A,P_B), 4.2 (P_D,P_C), 268.7 (W,P_C), 134.7 (W,P_B), 173.0 (W,P_A)
D-4-B	175.1 (dd,P_A), 149.9 (dd,P_B) -8.1 (dd, P_C)	33.6 (P_A,P_C) , 28.7 (P_B,P_C), 16.0 (P_A,P_B), 267.8 (W,P_C), 107.7 (W,P_B), 173.8 (W,P_A)
D-5-A	175.0 (dd,P_A),147.1(dd,P_B) ,6.9(m,P_C), -7.5(d,P_D)	31.8 (P_A,P_B),27.3(P_B,P_C), 16.6(P_A,P_B),16.7(P_C,P_D),196(P,W)
D-5-B	175.3 (m,P_A),147.3(m,P_B) 7.5(m,P_C)	31.3(P_A,P_B), 27.2(P_B,P_C), 15.6 (P_A,P_B), 175.2(P,W)
E-3-A	229.6 (dd,P_A),197.3 (dd,P_B), 21.1 (m,P_C), -31.4 (d,P_D)	36.0 (P_A,P_C) , 31.1 (P_B,P_C), 10.1 (P_A,P_B), 3.6 (P_D,P_C),
E-3-B	229.9(dd,P_A),195.0(dd,P_B), 24.8(dd,P_C)	36.7 (P_A,P_C) , 30.8 (P_B,P_C), 9.8 (P_A,P_B)
E-4-A	229.4(dd,P_A),191.1(dd,P_B), 37.3(m,P_C),7.8(d,P_D)	10.0(P_A,P_B), 33.4(P_A,P_C), 28.9(P_B,P_C),15.3(P_C,P_D)

E-4-B	230.0 (dd,P_A), 191.6 (dd,P_B), 38.2 (m,P_C)	8.9 (P_A,P_B), 33.3 (P_A,P_C), 27.5 (P_B,P_C)

The synthesis of $PPh_2CH_2CH_2PPh_2$ complexes analogous to the above complexes were not straight forward and could not be done with the same procedure described in the experimental section. This is because chelation instead of bridging occurs under the conditions we used for the other complexes.

$$(CO)_4Mo(\mu\text{-}PPh_2)_2Mo(CO)_4 + PPh_2CH_2CH_2PPh_2 \xrightarrow{\Delta\ /\ \text{toluene}}$$

$$(CO)_4Mo(\mu\text{-}PPh_2)_2Mo(CO)_2(\eta^2\text{-}PPh_2CH_2CH_2PPh_2) \qquad (10)$$

Therefore we tried a new procedure which is described in the Experimental section. Although the TLC profile for this reaction looked promising and showed four spots (two starting materials and two new compounds) we were able to recover only one compound (**E-5**). A $^{31}P\ \{^1H\}$ NMR spectrum of this complex was obtained. The NMR spectrum suggested that the sample was not pure enough and low concentration caused large signal to noise ratio and hence the spectrum was not very useful. The IR spectrum of the crude product showed five signals at 2041(m) cm^{-1}, 2033(m) cm^{-1}, 2002 (m) cm^{-1}, 1939 (s) cm^{-1} and 1886 (m) cm^{-1} (Figure 30). The literature IR data of $(CO)_4Mo(\mu\text{-}PPh_2)_2Mo(CO)_2(\eta^2\text{-}PPh_2CH_2CH_2PPh_2)$ showed three signals at 2021 cm^{-1}, 1916 cm^{-1} and 1844 cm^{-1}. There were not matching IR signals of this complex and our crude product does not appear to contain the chelated complex. It is also possible to assign the peak at 2033 cm^{-1} as one of the starting material

$(CO)_4Mo(\mu\text{-}PPh_2)_2Mo(CO)_4$ (the other signal arising from this compound is probably hidden under the signal at 1939 cm^{-1}). Then the rest of the peaks fit to the pattern of the IR spectrum of the other dangling complexes (D-4-A, D-5-A, E-3-A and E-4-A) by number and the intensity. So it is possible that we may have synthesized the $(CO)_4Mo(\mu\text{-}PPh_2)_2Mo(CO)_3(PPh_2CH_2CH_2PPh_2)$ but without NMR data of this complex it cannot be verified. There was no evidence for the bridged complex, $(CO)_4Mo(\mu\text{-}PPh_2)_2Mo(CO)_2(\mu\text{-}PPh_2CH_2CH_2PPh_2)(CO)_3Mo(\mu\text{-}PPh_2)_2Mo(CO)_4$.

Electrochemistry

The bridging and dangling compounds were examined with cyclic voltammetry as described in the experimental section. The insolubility of these complexes in aqueous medium prevented us from using universally accepted reference electrodes such as the standard hydrogen electrode (SHE) and the standard calomel electrodes (SCE). There is no universally accepted reference electrode for non-aqueous solvents such as methylene chloride.[25] Therefore, we used ferrocene as an internal standard. Ferrocene undergoes a one-electron oxidation-reduction in methylene chloride, the ferrocinium/ferrocene couple.[27] The formal potential for this couple was calculated using the following equation.

$$E^\circ = [E_{p(anode)} + E_{p(cathode)}] / 2$$

In our system, the formal potential for ferrocene couple was 0.36 V in methylene chloride with 0.1 M TBAH. Cooper reported that $E^\circ = +0.15$ volts for the above couple in methylene chloride with 0.1 molar TBAH.[26] For the same redox system,

Hershberger[28] and Bond[29] measured E° values to be +0.31 volts against saturated NaCl/SCE and +0.50 volts against Ag/AgCl reference electrodes. These values suggest that E° depends on the type of the electrode and the experimental conditions used. Therefore, recorded formal potentials may be different for each experiment for ferrocene as well as our complexes. The use of an internal standard allows the difference between the formal potential, $E°(Fe/Fe^+)$ couple and that of the complex of interest to be measured. So our compounds are all measured with respect to the ferrocene couple. This method should provide reproducible formal potentials because parameters such as peak potential, liquid junction potentials and reference electrode degradation will be eliminated.[27] Ferrocene is an excellent choice as an internal standard because the formal potential of the ferrocene couple does not depend on the solvent used and because the Fe center is well protected by the large cyclopentadienyl rings.[30]

There are few factors that can be used to evaluate the reversibility of a redox system.[27] If the ratio of $i_{p,c}/i_{p,a}$ is unity for a redox system where $i_{p,c}$ is the peak current of the reduction and $i_{p,a}$ is the peak current of the oxidation, that system is considered as a reversible system. Also peak potential E_p should be independent of the scanning rate and the peak current, i_p should be dependent on $v^{-1/2}$ where v is the scan rate. Since our primary concern in this research was to characterize the electron communication between two bridging dimers, we did not go into details of the above factors. However, they will be discussed depending on the availability of the data.

We carried out cyclic voltammetric experiments for our complexes at two different scanning rates, 50 mV/s and 100 mV/s. The following table summarizes the electrochemical data for ferrocene and the dangling complexes.

Table 03 – electrochemical data for ferrocene and dangling complexes.

Complex	Scan Rate (mV/S^{-1})	Ferrocene				Complex			
		E^0 (V)	$i_{p,c}$ (μA)	$i_{p,a}$ (μA)	$i_{p,a}/i_{p,c}$	E^0 (V)	$i_{p,c}$ (μA)	$i_{p,a}$ (μA)	$i_{p,a}/i_{p,c}$
D-4-A	50	0.464	2.07	2.76	1.33	0.776	18.44	18.28	0.99
	100	0.463	2.24	3.10	1.50	0.772	17.93	19.31	1.08
D-5-A	50	0.492	13.79	13.45	0.98	0.764	15.17	12.41	0.82
	100	0.481	12.41	13.28	1.07	0.751	11.55	10.34	0.90
E-3-A	50	0.446	23.45	20.40	0.87	0.785	9.51	8.84	0.93
	100	0.420	20.69	17.93	0.87	0.775	8.62	7.93	0.92
E-4-A	50	0.440	8.97	10.34	1.15	0.748	17.93	20.00	1.12
	100	0.428	7.24	9.31	1.29	0.741	17.93	17.59	0.98

E^0 average peak potential, $i_{p,c}$ cathodic peak current and $i_{p,a}$ anodic peak current.

There are a few important factors to notice in Table 03. The internal standard ferrocene showed its $i_{p,a}/i_{p,c}$ ratio significantly deviated from unity most of the time suggesting a pseudo type reversibility in these scanning rates. It is reported that ferrocene undergoes reversible redox processes only below 50 mV/s^{-1}.[27] Contrary to ferrocene all dangling complexes showed $i_{p,a}/i_{p,c}$ ratios much closer to unity suggesting a reversible redox processes. We could not compare the peak current ratios of ferrocene and the complex because we didn't measure the concentration of ferrocene during these experiments. Hence we cannot use peak current comparison to find the number of electrons involved in the redox process for the complexes. Therefore the use of the ferrocene in this work was limited to electrode potential comparison.

The following table shows the formal potential data of the dangling complexes and the ferrocene.

Table 04 – Formal potential data for dangling complexes and ferrocene.

Complex	Scan Rate (mV/S^{-1})	$E^0_{(Ferrocene)}$ (V)	$E^0_{(Complex)}$ (V)	$E^0_{(Comp)}$- $E^0_{(Ferro)}$ (V)	*Average* $\{E^0_{(Comp)} - E^0_{(Ferro)}\}$ (V)
D-4-A	50	0.464	0.776	0.312	0.310
	100	0.463	0.772	0.309	
D-5-A	50	0.492	0.764	0.272	0.270
	100	0.481	0.751	0.269	
E-3-A	50	0.446	0.785	0.339	0.346
	100	0.420	0.775	0.354	
E-4-A	50	0.440	0.748	0.308	0.310
	100	0.428	0.741	0.312	

Average $\{E^0_{(Comp)} - E^0_{(Ferro)}\}$ shows the average for both scanning rates for a given compound.

From these data it is evident that formal potentials of these complexes are independent of the scanning rate which is a quality of a chemically reversible system. Tungsten complexes were easier to oxidize than similar molybdenum complexes

(0.310 V (D-4-A) vs 0.346 V (E-3-A) and 0.270 V (D-5-A) vs 0.310 V (E-4-A)). The formal potential difference between $(CO)_4W(\mu\text{-}PPh_2)_2W(CO)_3PPh_2C{\equiv}CPPh_2$ (D-4-A) and $(CO)_4Mo(\mu\text{-}PPh_2)_2Mo(CO)_3PPh_2C{\equiv}CPPh_2$ (E-3-A) was -0.036 V. The difference between $(CO)_4W(\mu\text{-}PPh_2)_2W(CO)_3$(*trans*-$PPh_2CH{=}CHPPh_2$) (D-5-A) and $(CO)_4Mo(\mu\text{-}PPh_2)_2Mo(CO)_3$(*trans*-$PPh_2CH{=}CHPPh_2$) (E-4-A) was -0.040 V. Although we did not find electrochemistry data of the same dimeric compounds of tungsten and molybdenum in the literature with which to compare our results, we can assume that the higher electron density of the tungsten atom when compared to the less electron dense molybdenum atom led to that result. The other noticeable trend was difference in the difficulty of oxidizing $(CO)_4W(\mu\text{-}PPh_2)_2W(CO)_3PPh_2C{\equiv}CPPh_2$ (D-4-A) by 0.040 V in comparison to $(CO)_4W(\mu\text{-}PPh_2)_2W(CO)_3$(*trans*-$PPh_2CH{=}CHPPh_2$) (D-5-A), and $(CO)_4Mo(\mu\text{-}PPh_2)_2Mo(CO)_3PPh_2C{\equiv}CPPh_2$ (E-3-A) by 0.036 V in comparison to $(CO)_4Mo(\mu\text{-}PPh_2)_2Mo(CO)_3$(*trans*-$PPh_2CH{=}CHPPh_2$) (E-4-A). Although it is difficult to see the reason for this, Ren *et al*[4] have shown that electron transfer was strongly dependent on the nature of the ligands.

Previous work in our group has shown that similar dimeric complexes of tungsten and molybdenum undergo one reversible one-electron transfer and one irreversible one-electron transfer below 1.2 V.[22] It has also been shown that for some systems electrons are removed from the metal-metal bond leaving zero bond order between metal centers.

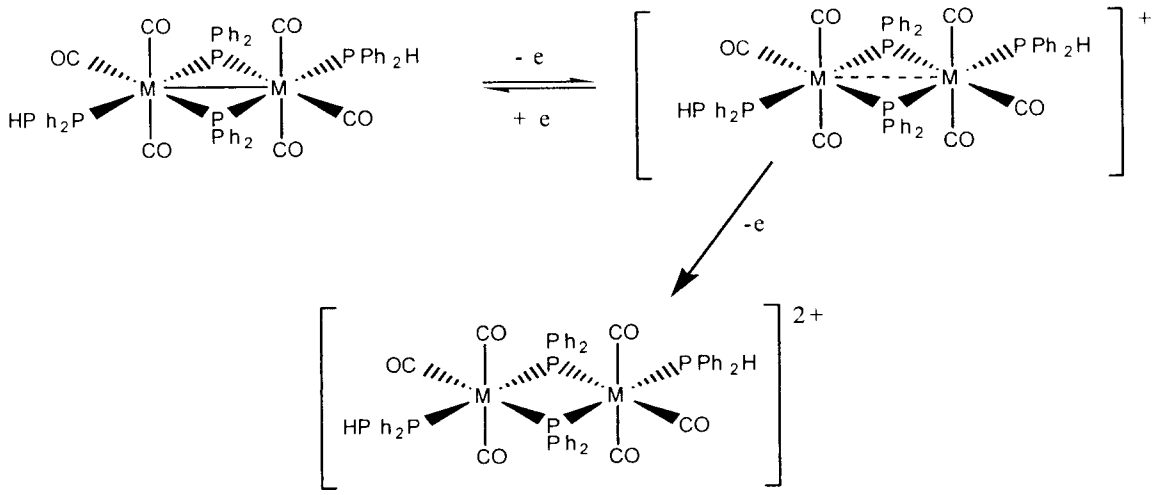

M = W, Mo

The loss of the electron in the reversible step occurred at 0.19 V for tungsten complex and only was 0.04 V more positive that of the ferrocene couple. The second electron is lost at 0.72 V irreversibly, against $Ag/AgNO_3$ reference electrode. The important factor to remember is that the two waves were approximately 530 mV apart.

It is worth noticing that our complexes do not undergo irreversible transfer below 1.2 V as was observed for $HPh_2P(CO)_3(\mu\text{-}PPh_2)_2W(CO)_3PPh_2H$. Also the reversible oxidations for our systems occurred at more positive potential than the above system. They were approximately 0.30 V more positive than the ferrocene couple.

The following table summarizes selected electrochemical data for all important bridging complexes.

Table 05 – Formal potential data for bridging complexes.

Complex	Rate (mV/S^{-1})	$i_{p,a}/i_{p,c}$	E_1^0 (Comp)– E^0 (Fe/Fe+) (V)	{E_2^0 (Comp)– E^0 (Fe/Fe+)} (V)	ΔE (mV)	*Average* {E_1^0 (Comp) – E^0 (Fe/Fe+)} (V)	*Average* {E_2^0 (Comp)– E^0 (Fe/Fe+)} (V)	Ave. ΔE (mV)
D-4-B	50	0.89	0.340	0.450	110	0.335	.450	115
	100	0.97	0.330	0.450	120			
D-5-B	50	0.90	0.310	0.410	100	0.315	.415	100
	100	0.92	0.320	0420	100			
E-3-B	50	0.88	0.375	0.475	100	.375	0.475	100
	100	0.88	0.375	0.475	100			
E-4-B	50	0.77	0.330	0.420	90	0.330	0.425	95
	100	0.92	0.330	0.430	100			

The data in the Table 5 also confirmed the tendencies we saw for the dangling complexes. Here also among similar complexes, it was easier to oxidize tungsten than its molybdenum partner. For the same metal the $PPh_2C{\equiv}CPPh_2$ complex was harder to oxidize than the *trans*-$PPh_2CH{=}CHPPh_2$ complex. We can assume that both redox steps behave reversibly because the formal potentials for both redox steps are independent of the scanning rate

The formal potential difference of two waves of most of the bridging complexes was approximately 100 mV. Since earlier our group had shown that loss of the second electron of a dimeric complex, $(CO)_4W(\mu\text{-}PPh_2)_2W(CO)_3PPh_2H$, occurs about 530 mV from the first electron transfer, both electrons couldn't come from the same dimeric center[23]. Therefore the second electron comes from the second dimeric unit. There is a precedent for these kinds of complexes and some of them were discussed in the Introduction.

According to our results there is no significant difference of the two ligands in their capacity of electron coupling. The DPPA bridge a showed a 15 mV difference over DPPEthylene in the tungsten complexes, while it was only 5 mV for molybdenum complexes. Within the experimental error and the method we used to calculate the formal potentials it is difficult to reach a firm conclusion on electron communication ability of these complexes. This results was somewhat unexpected because the C≡C bond of DPPA has better electron delocalization compared to the C=C bond of DPPEthylene and therefore should have shown better communication through the bridge. The insignificant difference tells us that there should be something else other than the C-C bonds governing the electronic coupling through

the bridge. One of the factors to consider is, the M(W,Mo)-P bond. If the metal-phosphorus bond controls the coupling then it should be dependent on the overlapping between the *d* orbital (metal) and the $\sigma*$ orbital of the phosphorus. Since the *5d* orbital of tungsten is more extended and available for bonding with $\sigma*$ orbital in comparison to the *4d* orbital of molybdenum, we should have seen better electronic communication for tungsten complexes. In fact tungsten complexes are better by 15 mV and 5 mV over molybdenum complexes. We could have drawn a much firmer conclusion on this aspect if we could synthesize analogous chromium complexes because the differences berween 3*d* and 4*d* orbitals are more prominent than between 4*d* and 5*d* orbitals. Also we could have had a better understanding about the bridge if we were able to synthesize the complexes of $PPh_2CH_2CH_2PPh_2$, which does not have C-C π bonds. The failure of attempts to synthesize $PPh_2CH_2CH_2PPh_2$ analogs of these complexes bars us from reaching a firm conclusion on the nature of relative electron communication between metal centers and the factors that control it.

The attempt to hydrogenate *trans*-$PPh_2CH{=}CHPPh_2$ failed even though there was a literature example of hydrogenation of well hindered double bonds as described in Introduction. It is possible that lone pairs of the phosphorus atoms react with palladium and inactivate it as suggested in the literature[16]. There are no lone pairs of electrons available in $[(CO)_4Mo(\mu\text{-}PPh_2)_2Mo(CO)_3(\mu\text{-}$*trans*-$PPh_2CH{=}CHPPh_2)(CO)_3Mo(\mu\text{-}PPh_2)_2Mo(CO)_4]$. Even so, hydrogenation failed. Therefore, it might be possible that the double bond in this complex is well hindered and was not able to undergo hydrogenation.

The UV/Vis spectra of bridging complexes and their oxidized partners were sought in an attempt to investigate the optical intervalence charge transfer bands of these complexes.

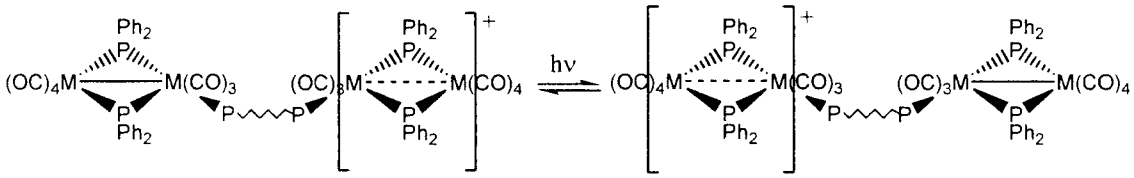

M = W, Mo

Chemical oxidation was intended to oxidize bridging complexes to their first oxidation state (+1). The first choice as the oxidizing agent was $AgPF_6$ because it has been used in our group for the oxidation of tungsten and molybdenum dimers.[22]

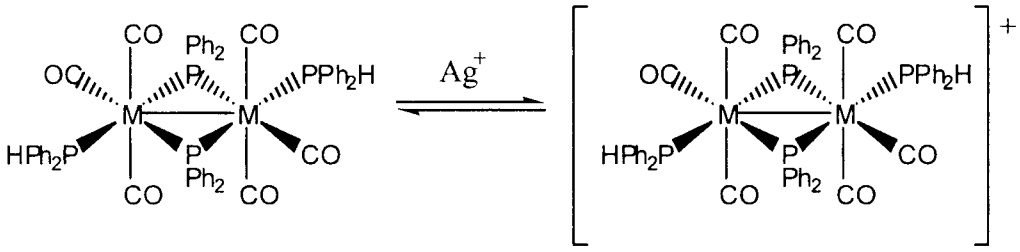

M = W, Mo

The addition of $AgPF_6$ to a solution of E-4-B as described in experimental section formed a grey layer inside the cell wall preventing a UV/Vis spectrum of resulting solution from being obtained. Deposition of Ag(0) is the probable explanation for the grey layer inside. Failure of a quantified oxidation by $AgPF_6$ and absence of enough purified bridging complexes forced us to abandon this work.

It has also been shown qualitatively that other oxidizing reagents could be used to oxidize our bridging complexes. In such an attempt we used AgCl as the oxidizing agent. The UV/Vis spectrum of E-4-B showed three peaks at 352 nm (vs) and 542 nm

(m) and 723 nm (w) (figure 29). Gradual addition of AgCl showed two strong peaks at 534 nm and 796 nm and excess addition of AgCl showed a peak at 805 nm (vs) and peak at 530 nm (figure 30).

The following table is summarized the UV/Vis data of selected compounds.

Table 03 – UV/Vis data of selected compounds.

Complex	UV/Vis data (nm)
D-4-B (unoxidized)	349 (vs), 541 (m)
D-5-B (unoxidized)	336 (vs), 542 (m)
E-3-A (unoxidized)	354 (vs), 539 (m), 744 (w,broad)
E-4-B (unoxidized)	352 (s), 539 (m), 725 (w, broad)
(oxidized)	530 (w), 805 (m)

In conclusion, we have successfully synthesized and characterized ten new complexes. Although electron coupling was not significantly large, bridging complexes have shown definite electronic coupling through the bridge.

Reference:

1. Chen, C-T; Suslick, K.S ; *Coord. Chem. Rev.* 128 (**1993**), 293.
2. Wang, P.W.; Fox, M.A. *Inorg. Chem.*, **1994**,*33*,2938.
3. Tour, J.M.; *Acc. Chem. Res.*, **2000**, *33*, 791.
4. Tong, R.; Gang, Z.; Alvarez, J.C. *Chem. Commun.*, **2000**, 1197.
5. Chatt, J.; Thronton,D.A. *J. Chem. Soc.* **1964**,1005
6. Keiter, R.L.; Keiter, E.A.; Mittleberg, K.N; Martin, J.S, Meyers, V.M; Wang, J.G; *Organometallics*, **1989**, *8*, 1399.
7. Keiter, R.L.; Madigan, M.J.; *Organometallics*,**1982**,1, 410.
8. Treichel, P.M.;Dean, W, K. *et al*, *J. Organomet. Chem.*, **1972**, *42*, 145.
9. Planinic, P; Matcovic-Calogovic, D; *Structural chemistry*, **2001**, 12(6), 439.
10. Nakazawa, H; *J. Organomet. chem.* **2000**, 611 (1,2), 349.
11. Scherer, Otto; *Acc. Chem. Res.* **1999**, 32(9), 751.
12. Connor,J.A; Day,S.P; Jones,E.M; McEwen,G.K; *J.Chem. Soc*, *Dalton trans.*, (1972-1999), (3),347-54.
13. Riera,V; Ruiz, M.A; Villafane, F; *Organomettalics.* **1992**, 11(8), 2854-63.
14. Karim, W; Klein, A; Gloeckle, M; *Acc. Chem. Res.* **2000**,33(11),755.
15. Rogers, T; Unpublished Research.
16. Quin, L.D; Somers, J.H; Prince, R.H; *J. Org. Chemistry.* **1969**, 34(11), 3700.
17. Gosser, D.K; ***Cyclic Voltammtry**: Stimulation and analysis of reaction mechanisms.* **1993**, 154 pp.
18. Aguiar, A.M; Daigle, D; *J. Am Chem. Soc.* **1964**, 86(23), 5354.
19. Taylor R.C; Keiter, R.L; Cary,L.W; *Inorganic Chem.* **1974**, 13(8), 1928-32.

20. Treichel, P.M; Dean, W.K; Douglas, W.M; *J. organomet. Chem.* **1972**, 42, 145.

21. Robert, J.A; Sr. Malone, M.D; *Inorg. Chem.* **1976**, 6(9), 1731.

22. Smith, J.G; Thompson, D.T; *J. Cheml soc A*, **1967**, 10, 1694

23. Keiter, R.L, Ellen, E.A; Merle, S.R; Miller, D.R; Sherman, E.O; Cooper, W.E; *Organometallics.* **1992**, 11(1), 487.

24. Brateman, P.S, Thompson, D.T; *J. Chem. Soc.* **1968**, 1454.

25. Huheey,J.E; Keiter, E.A; Keiter,R.L; **Inorganic Chemistry,** *4th Ed.*, p217

26. Willard, H.H; Merritt, L.L; Dean, J.A; Settle, F.A; "Instrumental Methods of Analysis" D.VanNostrand, New york, (**1981**) pp. 634-638

27. Cooper, D.W; M.Sc Thesis: *Electrochemical Studies of Transition Metal Carbonyls*; 1986.

28. Bond, A.M; Coltan, R; McGregor, K; *Inorganic Chemistry.* **1986**, 25, 2378.

29. Alexander, R; Parker, A.J; Sharp, S.H; Waghorne, W.E; *J. Am. Chem. Soc.* **1972**, 94, 1148.

30. Flanagan, J.B; Margel S; Bard A.J; Anson F.C; *J. Am. Chem. Soc.*1978, 100(13), 4248-53

31. Bratermann, P.S; Song, J.I; Kohlmann,S; Volger,C; Kaim, W; *J. Organomet. Chem.* 1991, 411(1-2),207-13.

Appendix

List of Figures.

14. $^{31}P\ \{^1H\}$ NMR spectrum of $[(CO)_4W(\mu\text{-}PPh_2)_2W(CO)_3(\mu\text{-}trans\text{-}PPh_2CH{=}CHPPh_2)(CO)_3W(\mu\text{-}PPh_2)_2W(CO)_4]$ (**D-5-B**).

15. Simulated $^{31}P\ \{^1H\}$ NMR spectrum of $[(CO)_4W(\mu\text{-}PPh_2)_2W(CO)_3(\mu\text{-}trans\text{-}PPh_2CH{=}CHPPh_2)(CO)_3W(\mu\text{-}PPh_2)_2W(CO)_4]$ (**D-5-B**).

16. UV/Vis spectrum of $[(CO)_4W(\mu\text{-}PPh_2)_2W(CO)_3(\mu\text{-}trans\text{-}PPh_2CH{=}CHPPh_2)(CO)_3W(\mu\text{-}PPh_2)_2W(CO)_4]$ (**D-5-B**).

17. IR spectrum of $Mo(CO)_5PPh_2H$ (**E-1**).

18. IR spectrum of $[(CO)_4Mo(\mu\text{-}PPh_2)_2Mo(CO)_4]$ (**E-2**).

19. IR spectrum of $[(CO)_4Mo(\mu\text{-}PPh_2)_2Mo(CO)_3(PPh_2C{\equiv}CPPh_2)]$ (**E-3-A**).

20. $^{31}P\ \{^1H\}$ NMR spectrum of $[(CO)_4Mo(\mu\text{-}PPh_2)_2Mo(CO)_3(PPh_2C{\equiv}CPPh_2)]$ (**E-3-A**).

21. UV/Vis spectrum of $[(CO)_4Mo(\mu\text{-}PPh_2)_2Mo(CO)_3(PPh_2C{\equiv}CPPh_2)]$ (**E-3-A**)

22. IR spectrum of $[(CO)_4Mo(\mu\text{-}PPh_2)_2Mo(CO)_3\ (\mu\text{-}PPh_2C{\equiv}CPPh_2)\ (CO)_3Mo(\mu\text{-}PPh_2)_2Mo(CO)_4]$ (**E-3-B**).

23. $^{31}P\ \{^1H\}$ NMR spectrum of $[(CO)_4Mo(\mu\text{-}PPh_2)_2Mo(CO)_3\ (\mu\text{-}PPh_2C{\equiv}CPPh_2)\ (CO)_3Mo(\mu\text{-}PPh_2)_2Mo(CO)_4]$ (**E-3-B**).

24. IR spectrum of $[(CO)_4Mo(\mu\text{-}PPh_2)_2Mo(CO)_3(trans\text{-}PPh_2CH{=}CHPPh_2)$ (**E-4-A**).

25. $^{31}P\ \{^1H\}$ NMR spectrum of $[(CO)_4Mo(\mu\text{-}PPh_2)_2Mo(CO)_3(trans\text{-}PPh_2CH{=}CHPPh_2)$ (**E-4-A**).

26. $^{31}P\{^{1}H\}$ NMR spectrum of $[(CO)_4Mo(\mu\text{-}PPh_2)_2Mo(CO)_3\text{-}(\mu\text{-}trans\text{-}PPh_2CH{=}CHPPh_2)(CO)_3Mo(\mu\text{-}PPh_2)_2Mo(CO)_4]$ (**E-4-B**).

27. Simulated $^{31}P\{^{1}H\}$ NMR spectrum of $[(CO)_4Mo(\mu\text{-}PPh_2)_2Mo(CO)_3\text{-}(\mu\text{-}trans\text{-}PPh_2CH{=}CHPPh_2)(CO)_3Mo(\mu\text{-}PPh_2)_2Mo(CO)_4]$ (**E-4-B**).

28. UV/Vis spectrum of $[(CO)_4Mo(\mu\text{-}PPh_2)_2Mo(CO)_3\text{-}(\mu\text{-}trans\text{-}PPh_2CH{=}CHPPh_2)(CO)_3Mo(\mu\text{-}PPh_2)_2Mo(CO)_4]$ (**E-4-B**).

29. UV/Vis spectrum of oxidation of $[(CO)_4Mo(\mu\text{-}PPh_2)_2Mo(CO)_3\text{-}(\mu\text{-}trans\text{-}PPh_2CH{=}CHPPh_2)(CO)_3Mo(\mu\text{-}PPh_2)_2Mo(CO)_4]$ (**E-4-B**) with AgCl.

30. IR spectrum of the crude product of reaction E-5.

31. A. Voltammogram of $[(CO)_4W(\mu\text{-}PPh_2)_2W(CO)_3(PPh_2C{\equiv}CPPh_2)$ at 50 mV/sec.

    B. Voltammogram of $[(CO)_4W(\mu\text{-}PPh_2)_2W(CO)_3(\mu\text{-}PPh_2C{\equiv}CPPh_2)$ at 100 mV/sec.

32. A. Voltammogram of $[(CO)_4W(\mu\text{-}PPh_2)_2W(CO)_3(\mu\text{-}PPh_2C{\equiv}CPPh_2)(CO)_3W(\mu\text{-}PPh_2)_2W(CO)_4]$ at 50 mV/sec.

    B. Voltammogram of $[(CO)_4W(\mu\text{-}PPh_2)_2W(CO)_3(\mu\text{-}PPh_2C{\equiv}CPPh_2)(CO)_3W(\mu\text{-}PPh_2)_2W(CO)_4]$ at 100 mV/sec.

33. A. Voltammogram of $[(CO)_4W(\mu\text{-}PPh_2)_2W(CO)_3(trans\text{-}PPh_2CH{=}CHPPh_2)$ at 50 mV/sec.

    B. Voltammogram of $[(CO)_4W(\mu\text{-}PPh_2)_2W(CO)_3(trans\text{-}PPh_2CH{=}CHPPh_2)$ at 100 mV/sec.

34. A. Voltammogram of $[(CO)_4W(\mu\text{-}PPh_2)_2W(CO)_3$ (μ-*trans*-$PPh_2CH{=}CHPPh_2)(CO)_3W(\mu\text{-}PPh_2)_2W(CO)_4]$ at 50 mV/sec.

B. Voltammogram of $[(CO)_4W(\mu\text{-}PPh_2)_2W(CO)_3$ (μ-*trans*-$PPh_2CH{=}CHPPh_2)(CO)_3W(\mu\text{-}PPh_2)_2W(CO)_4]$ at 100 mV/sec.

35. A. Voltammogram of $[(CO)_4Mo(\mu\text{-}PPh_2)_2Mo(CO)_3$ $(PPh_2C{\equiv}CPPh_2)$ at 50 mV/sec.

B. Voltammogram of $[(CO)_4W(\mu\text{-}PPh_2)_2W(CO)_3(Ph_2C{\equiv}CPPh_2)$ at 100 mV/sec.

36. A. A. Voltammogram of $[(CO)_4Mo(\mu\text{-}PPh_2)_2Mo(CO)_3$ (μ-$PPh_2C{\equiv}CPPh_2)(CO)_3Mo(\mu\text{-}PPh_2)_2Mo(CO)_4]$ at 50 mV/sec.

B. Voltammogram of $[(CO)_4Mo(\mu\text{-}PPh_2)_2Mo(CO)_3(\mu$-$PPh_2C{\equiv}CPPh_2)(CO)_3Mo(\mu\text{-}PPh_2)_2Mo(CO)_4]$ at 100 mV/sec.

37. A. Voltammogram of $[(CO)_4Mo(\mu\text{-}PPh_2)_2Mo(CO)_3$ (*trans*-$PPh_2CH{=}CHPPh_2)$ at 50 mV/sec.

B. Voltammogram of $[(CO)_4Mo(\mu\text{-}PPh_2)_2Mo(CO)_3$(*trans*-$PPh_2CH{=}CHPPh_2)$ at 100 mV/sec.

38. A. Voltammogram of $[(CO)_4Mo(\mu\text{-}PPh_2)_2Mo(CO)_3$ (μ-*trans*-$PPh_2CH{=}CHPPh_2)(CO)_3Mo(\mu\text{-}PPh_2)_2Mo(CO)_4]$ at 50 mV/sec.

B. Voltammogram of $[(CO)_4Mo(\mu\text{-}PPh_2)_2Mo(CO)_3$ (μ-*trans*-$PPh_2CH{=}CHPPh_2)(CO)_3Mo(\mu\text{-}PPh_2)_2Mo(CO)_4]$ at 100 mV/sec.

Figure 01

$^{31}P\ \{^{1}H\}$ NMR spectrum of *trans*-$PPh_2CH{=}CHPPh_2$ (DPPEthylene).

01

GE NMR
QE-300

PF 16.000
12 JUN97

TRANS-(PH2P)Pt-N(Et)Et2

OPERATOR, [illegible]

ONE PULSE SEQUENCE

PULSE WIDTH = [illegible]
= [illegible]
ACQ. TIME = [illegible]
RECYCLE TIME = [illegible]

NO. OF ACQS. = [illegible]
DATA SIZE = [illegible]
LINE BROADNG = [illegible] HZ
SPIN RATE = [illegible] RPS

OBSERVE,
FREQUENCY = 121.70722
SPEC WIDTH = 17241 HZ
GAIN = [illegible]

DECOUPLER, STANDARD 64 MOD
FREQUENCY = 4.000 PPM
POWER = 29.07 [illegible]
HIGH POWER ON
HIGH POWER OUTPUT = [illegible]

PLOT SCALE,
[illegible] HZ/CM
7.[illegible] PPM/CM
FROM [illegible]
TO -7.[illegible] PPM

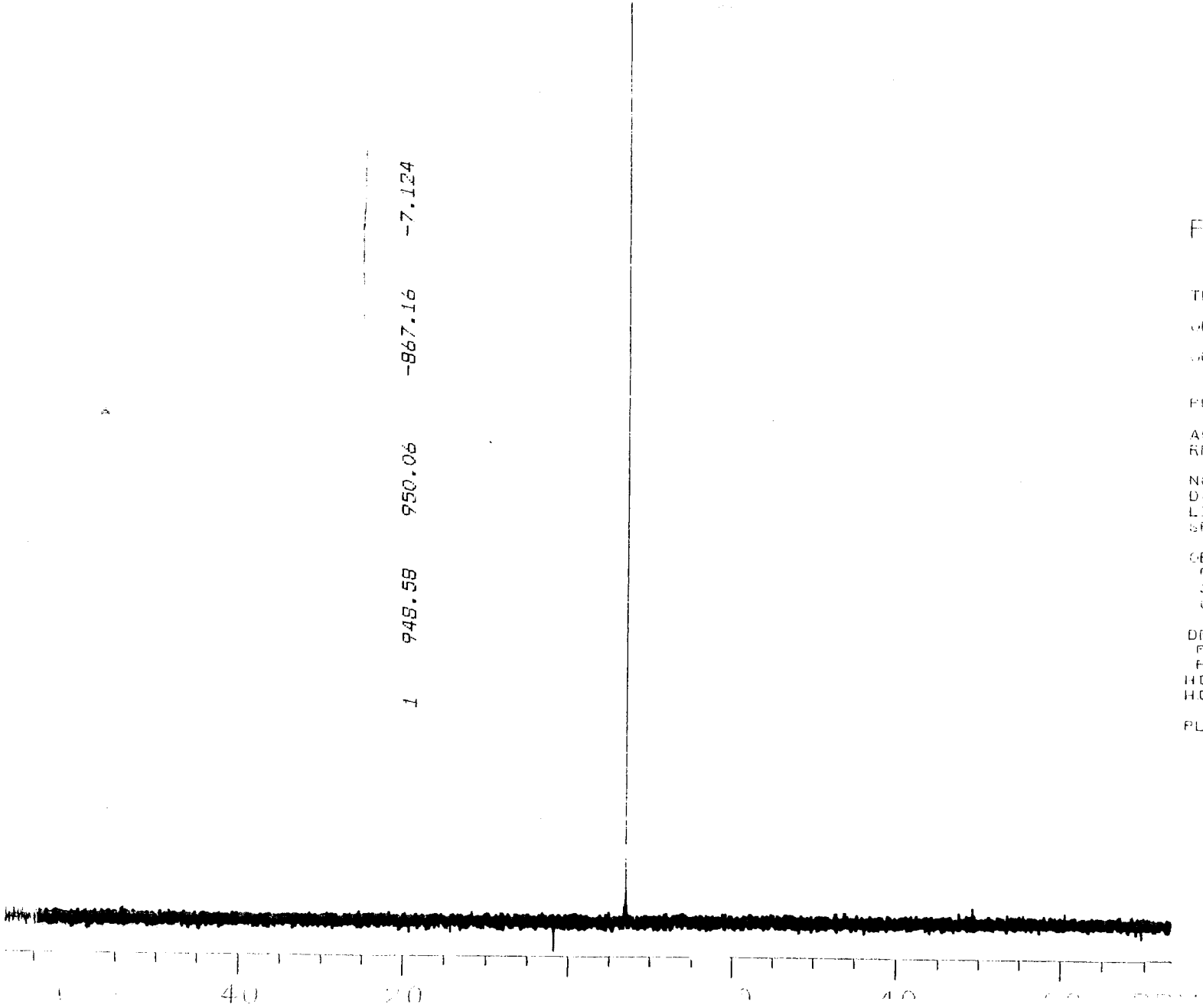

Figure 02

IR spectrum of $W(CO)_5NH_2Ph_2$ (D-1).

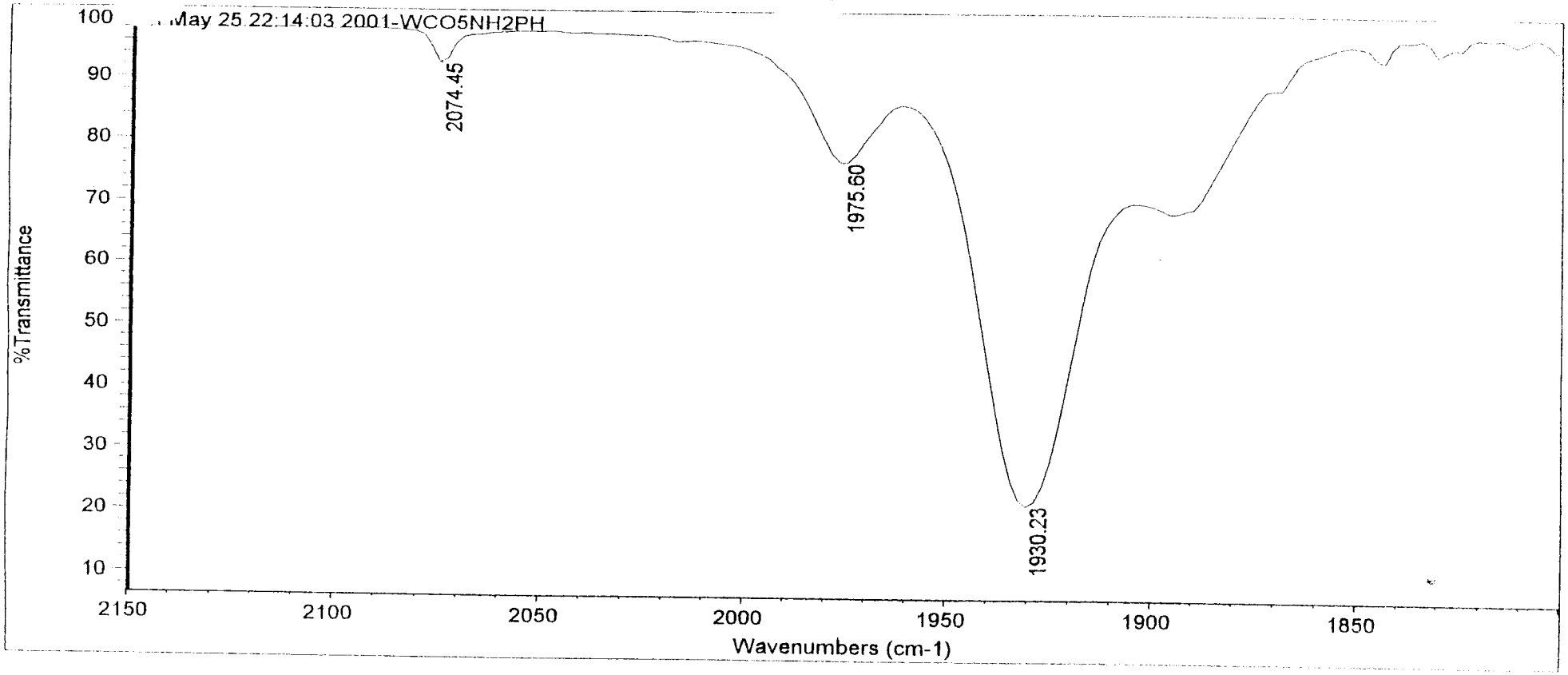

Fri May 25 22:19:57 2001
FIND PEAKS:

Spectrum:	Fri May 25 22:14:03 2001-WCO5NH2PH
Region:	2150.00 1800.00
Absolute threshold:	95.062
Sensitivity:	50
Peak list:	

Position:	1930.23	Intensity:	21.634
Position:	1975.60	Intensity:	76.814
Position:	2074.45	Intensity:	92.508

Figure 03

IR spectrum of $W(CO)_5PPh_2H$ (D-2).

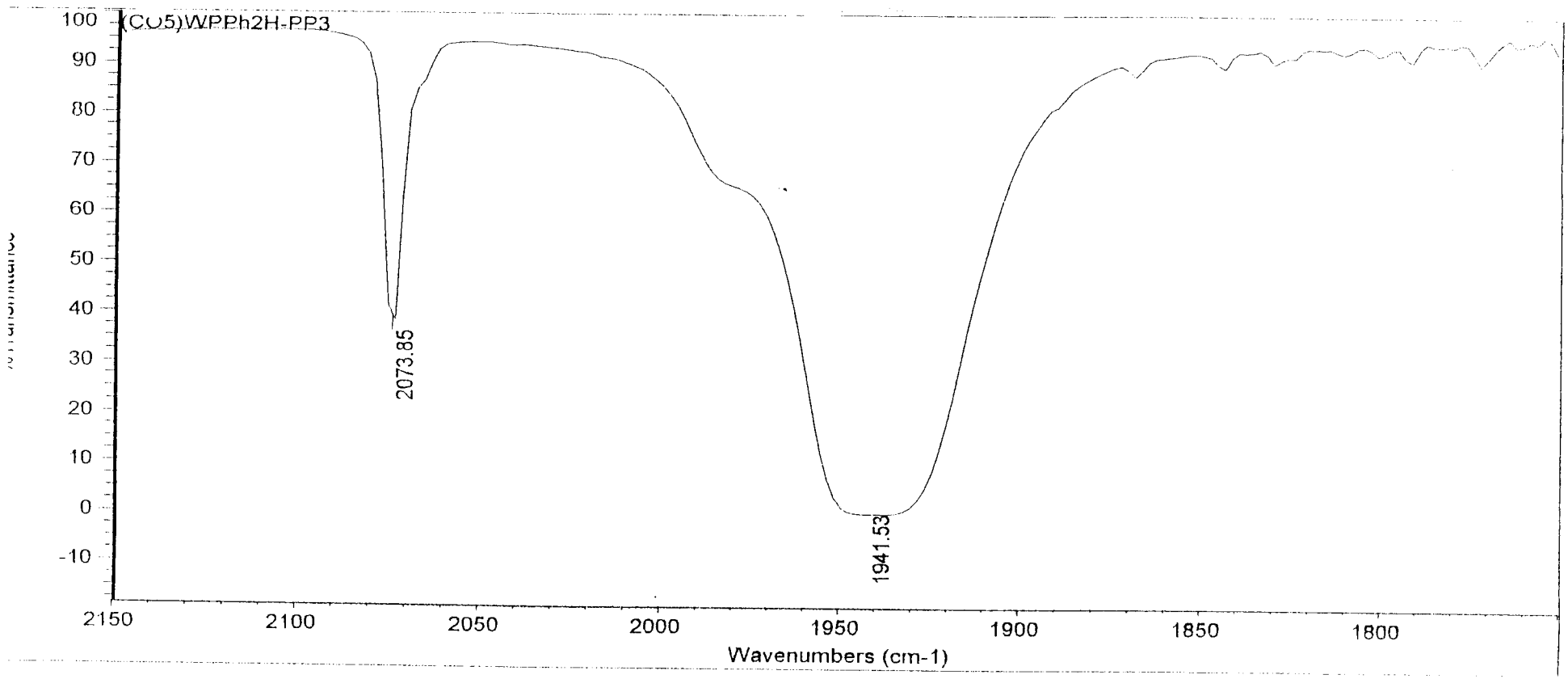

ıu Feb 08 18:14:54 2001
ND PEAKS:

Spectrum:	(CO5)WPPh2H-PP3	
Region:	2150.00	1750.00
Absolute threshold:	48.529	
Sensitivity:	50	
Peak list:		

Position:	1941.53	Intensity:	0.256
Position:	2073.85	Intensity:	36.372

Figure 04

IR spectrum of $[(CO)_4W(\mu\text{-}PPh_2)_2W(CO)_4]$ (D-3).

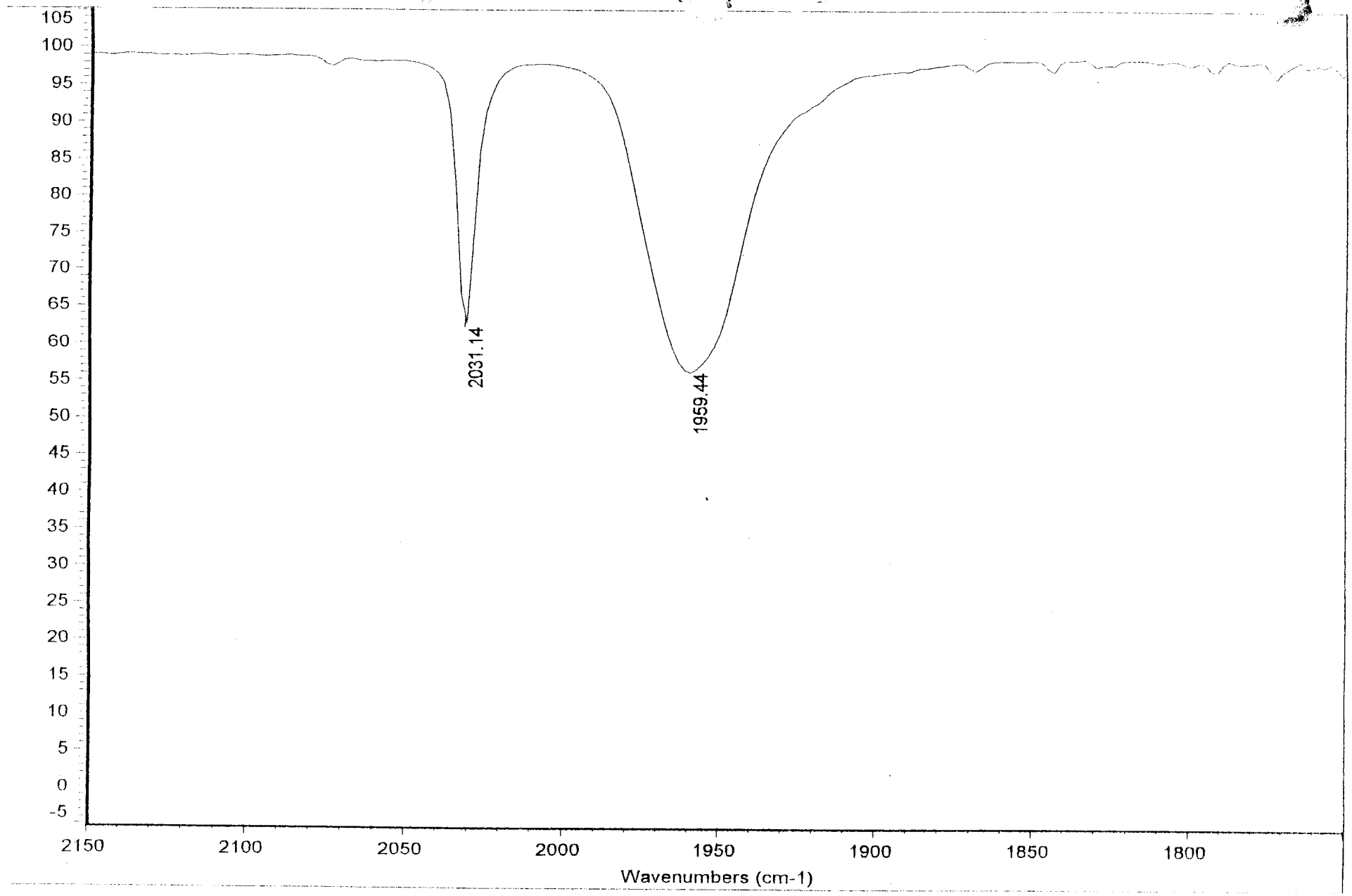
2031.14
1959.44
105
100
95
90
85
80
75
70
65
60
55
50
45
40
35
30
25
20
15
10
5
0
-5
2150
2100
2050
2000
1950
1900
1850
1800
Wavenumbers (cm-1)

Figure 05

$^{31}P\ \{^{1}H\}$ NMR spectrum of $[(CO)_4W(\mu\text{-}PPh_2)_2W(CO)_4]$ (D-3).

GE NMR
GE -

EAK, 200
16-MAY 97

PROJECT

HEATER, EAK

ONE PULSE SEQUENCE

PULSE WIDTH =
=
ACQ. TIME =
RECYCLE TIME =

NO. OF ACQS. =
DATA SIZE =
LINE BROADENING =
SPIN RATE =

OBSERVE:
FREQUENCY =
SPECT WIDTH =
GAIN =

DECOUPLER: STANDARD = 4 MHz
FREQUENCY =
POWER =
HIGH POWER ON
HIGH POWER OUTPUT =

PLOT SCALE:
HZ/CM
PPM/CM
FROM
TO

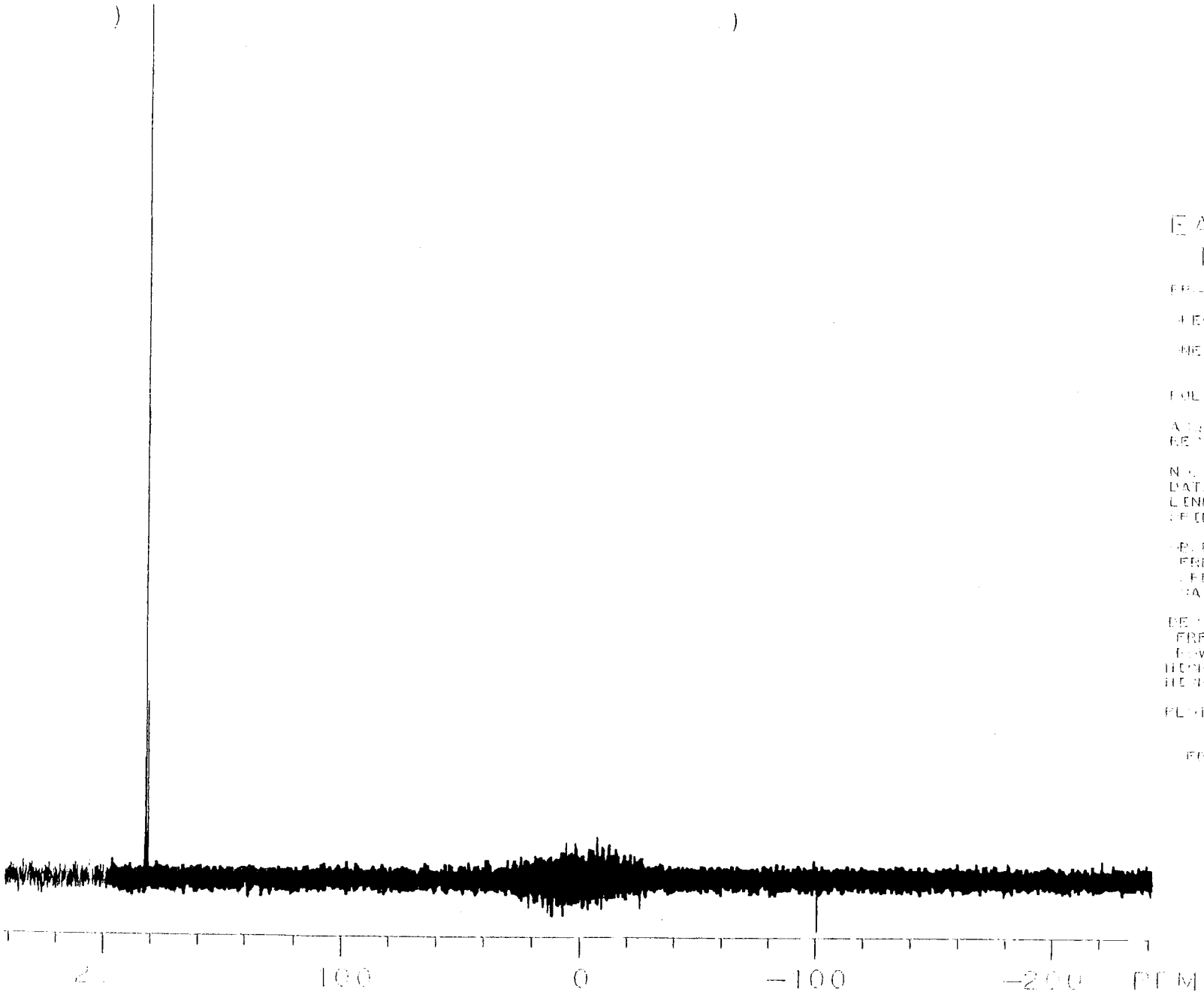

GE NI
QE-3

EAK.200
16MAY97

PP-05

OPERATOR: EAK

LINE#	HEIGHT	HEIGHT(L)	FREQ(HZ)	PPM
1	125.75	148.98	22000.57	180.765
2	620.84	1217.13	22082.50	181.439
3	85.54	------	22162.94	182.100

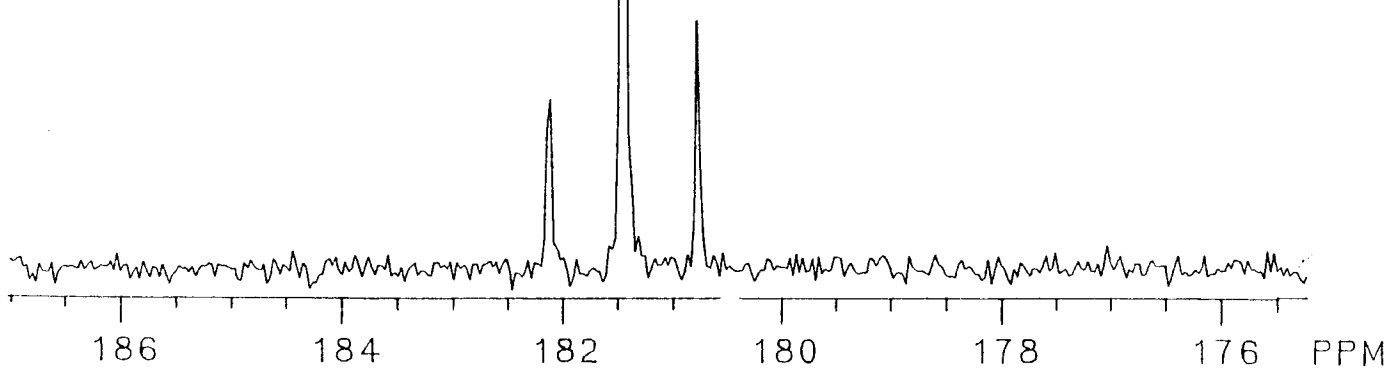

Figure 06

IR spectrum of $[(CO)_4W(\mu\text{-}PPh_2)_2W(CO)_3PPh_2C{\equiv}CPPh_2]$ (D-4-A).

06

o-Rad Win-IR Pro

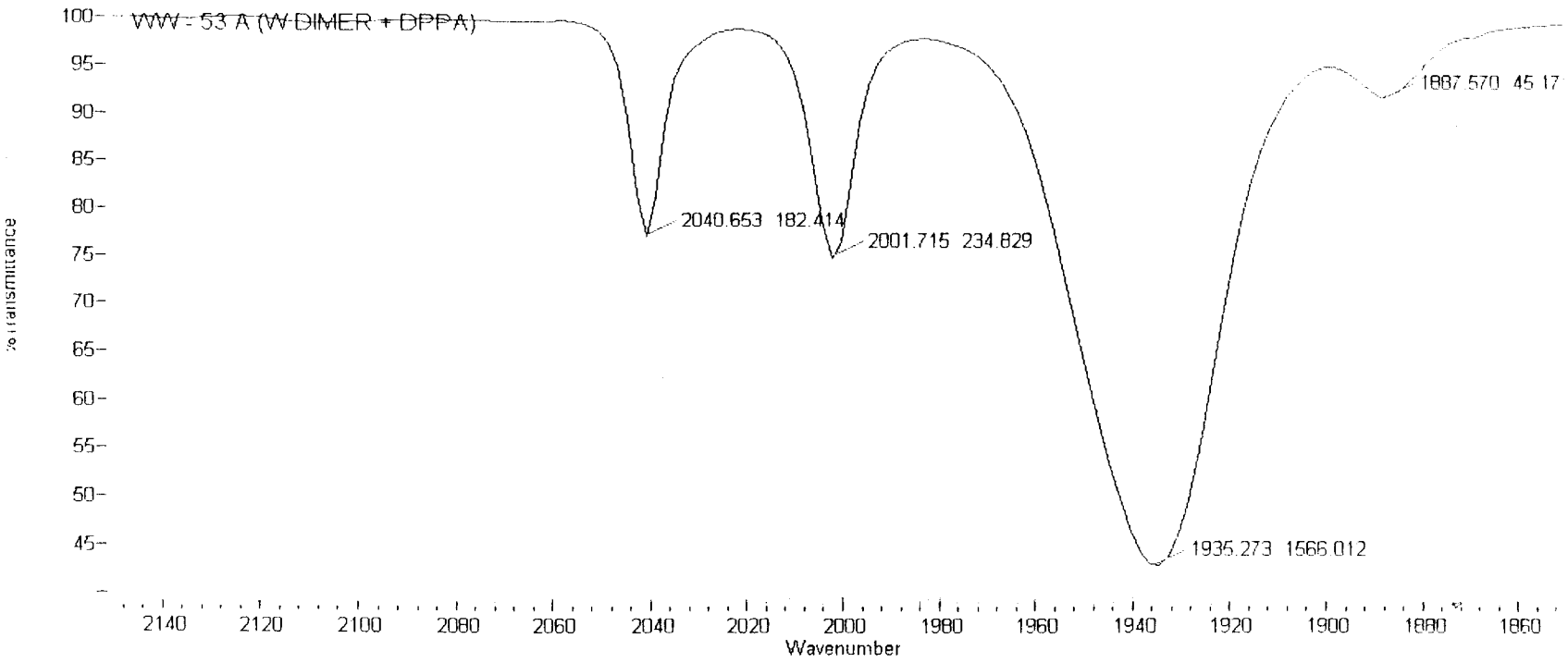

	Name	Spectrum									
Spectrum1	WW - 53 A (W DIMER +										
Spectrum2	WW - 53 A (W DIMER +										
Spectrum3											

Figure 07

$^{31}P\ \{^{1}H\}$ NMR spectrum of $[(CO)_4W(\mu\text{-}PPh_2)_2W(CO)_3PPh_2C{\equiv}CPPh_2]$

(D-4-A).

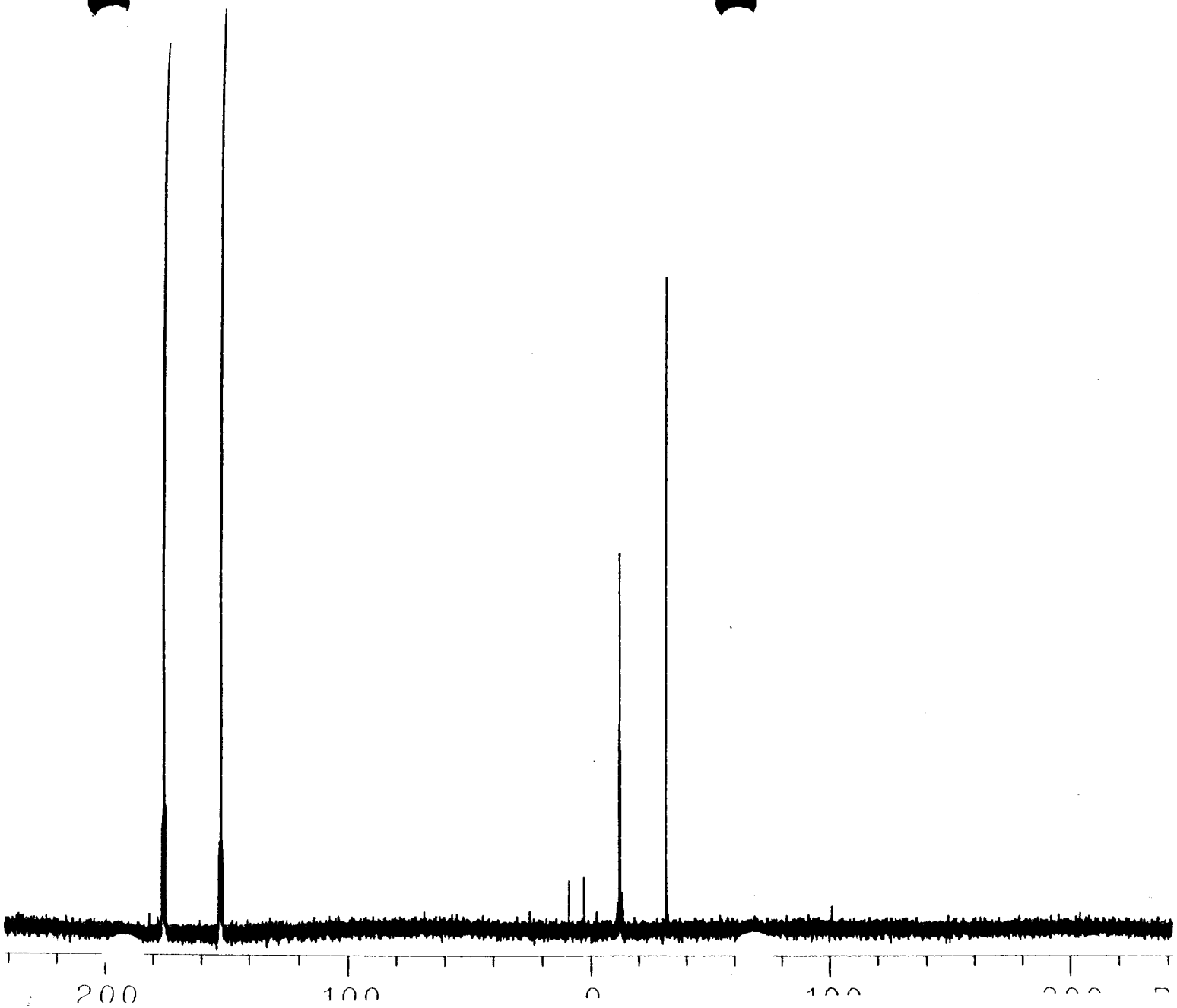

GE NMR
QE-300

EAK.207
02JUL97

PP-23

OPERATOR: EAK

ONE PULSE SEQUENCE

PULSE WIDTH - 7.00 USEC
- 36 DEGREE
ACQ. TIME - 278.53 MSEC
RECYCLE TIME - 1.55 SEC

NO. OF ACQS. - 3007
DATA SIZE - 65536
LINE BROADNG - .20 HZ
SPIN RATE - 22 RPS

OBSERVE:
FREQUENCY - 121.707505 MHZ
SPEC WIDTH- 58823 HZ
GAIN - 50 *1

DECOUPLER: STANDARD-64 MODULAT
FREQUENCY - 4.000 PPM
POWER - 3040/ 3000
HIGH POWER ON
HIGH POWER OUTPUT - 63 DB

PLOT SCALE:
2941.17 HZ/CM
24.1659 PPM/CM
FROM 241.33
TO -241.96 PPM

GE NMR
QE-300

EAK.207
02JUL97

PP-23

OPERATOR: EAK

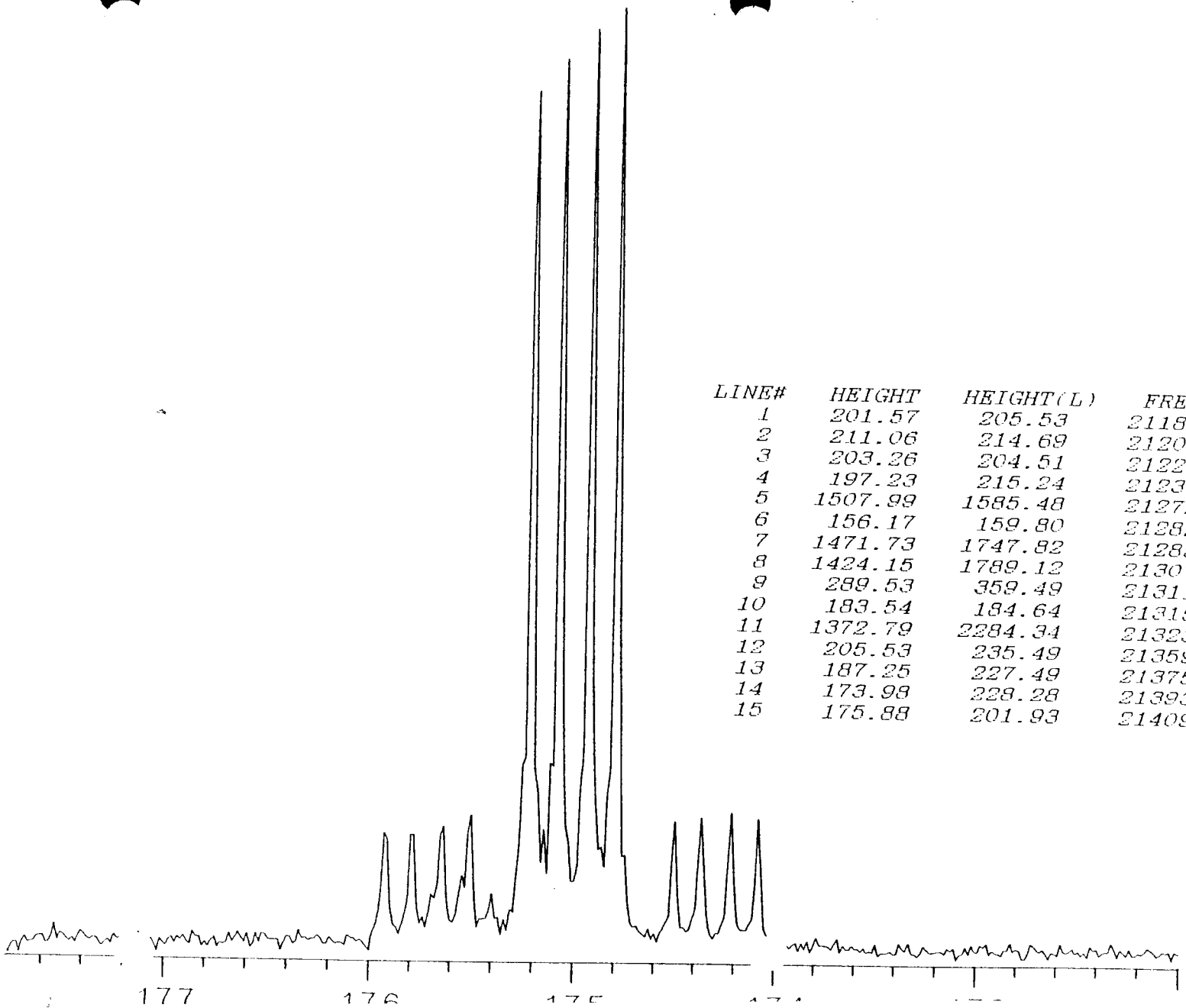

LINE#	HEIGHT	HEIGHT(L)	FREQ(HZ)	PPM
1	201.57	205.53	21186.11	174.074
2	211.06	214.69	21202.78	174.210
3	203.26	204.51	21220.66	174.357
4	197.23	215.24	21237.15	174.493
5	1507.99	1585.48	21272.87	174.786
6	156.17	159.80	21282.19	174.863
7	1471.73	1747.82	21289.25	174.921
8	1424.15	1789.12	21307.30	175.069
9	289.53	359.49	21311.16	175.101
10	183.54	184.64	21315.81	175.139
11	1372.79	2284.34	21323.58	175.203
12	205.53	235.49	21359.43	175.498
13	187.25	227.49	21375.68	175.631
14	173.98	228.28	21393.71	175.779
15	175.88	201.93	21409.96	175.913

GE NMR
QE-300

EAK.207
02JUL97

PP-23

OPERATOR: EAK

LINE#	HEIGHT	HEIGHT(L)	FREQ(HZ)	PPM
1	111.81	175.96	18327.34	150.585
2	123.69	177.39	18343.46	150.717
3	135.92	140.00	18358.40	150.840
4	152.83	157.96	18374.64	150.973
5	110.66	202.35	18388.69	151.089
6	115.60	127.26	18405.05	151.223
7	197.18	345.32	18422.54	151.367
8	1475.75	1674.60	18426.73	151.401
9	164.82	172.46	18433.78	151.459
10	239.25	254.35	18438.46	151.498
11	1566.34	1618.95	18443.11	151.536
12	212.32	212.73	18450.35	151.595
13	1556.10	1611.92	18456.22	151.644
14	176.38	177.26	18464.35	151.710
15	1552.95	1786.38	18472.61	151.778
16	151.45	151.57	18493.73	151.952
17	149.23	166.89	18510.44	152.089
18	149.70	153.53	18524.83	152.207
19	134.01	141.32	18541.21	152.342
20	108.46	128.53	18555.87	152.462
21	124.42	131.02	18572.28	152.597

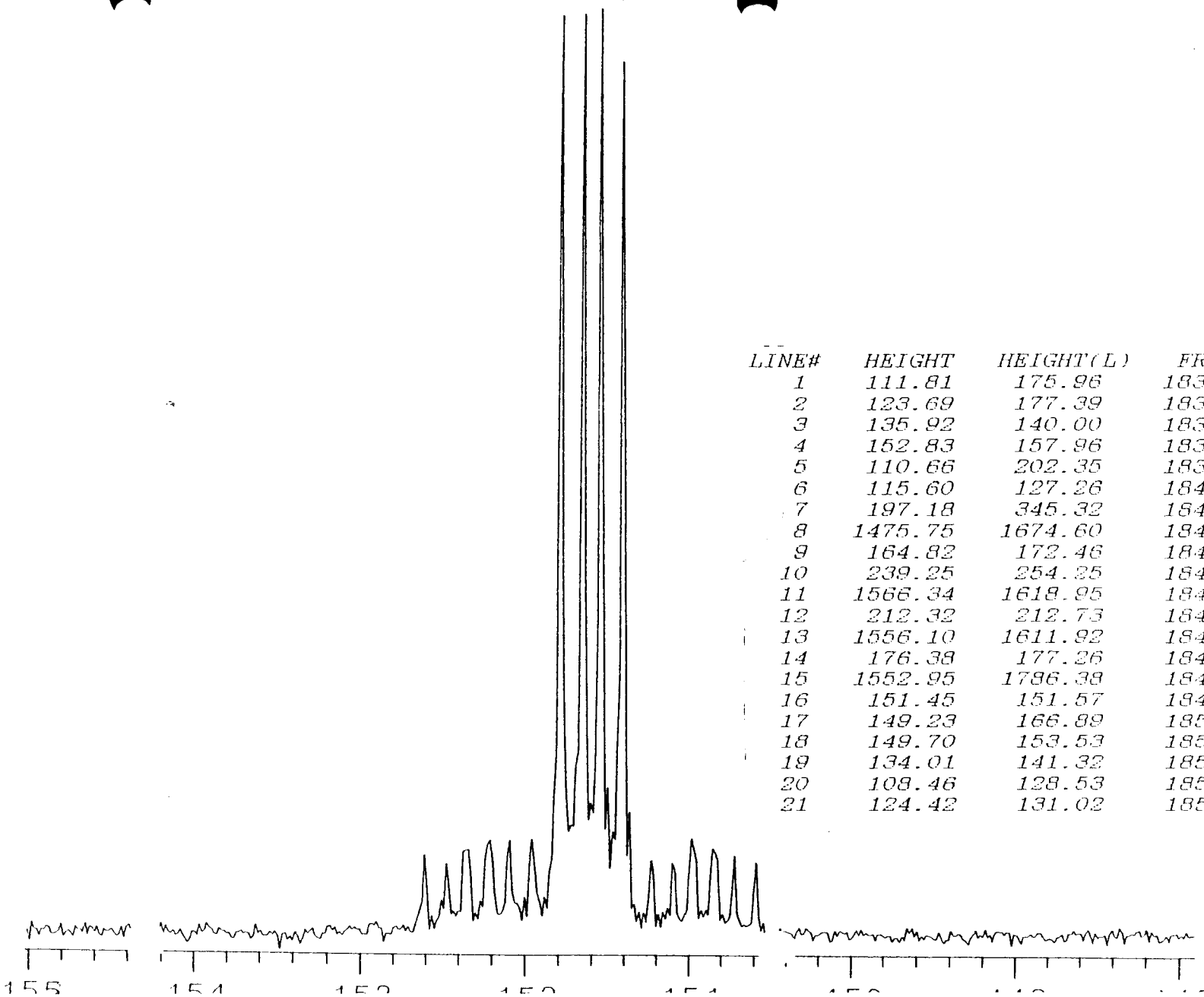

GE NMR
QE-300

EAK.207
02JUL97

PP-23

OPERATOR: EAK

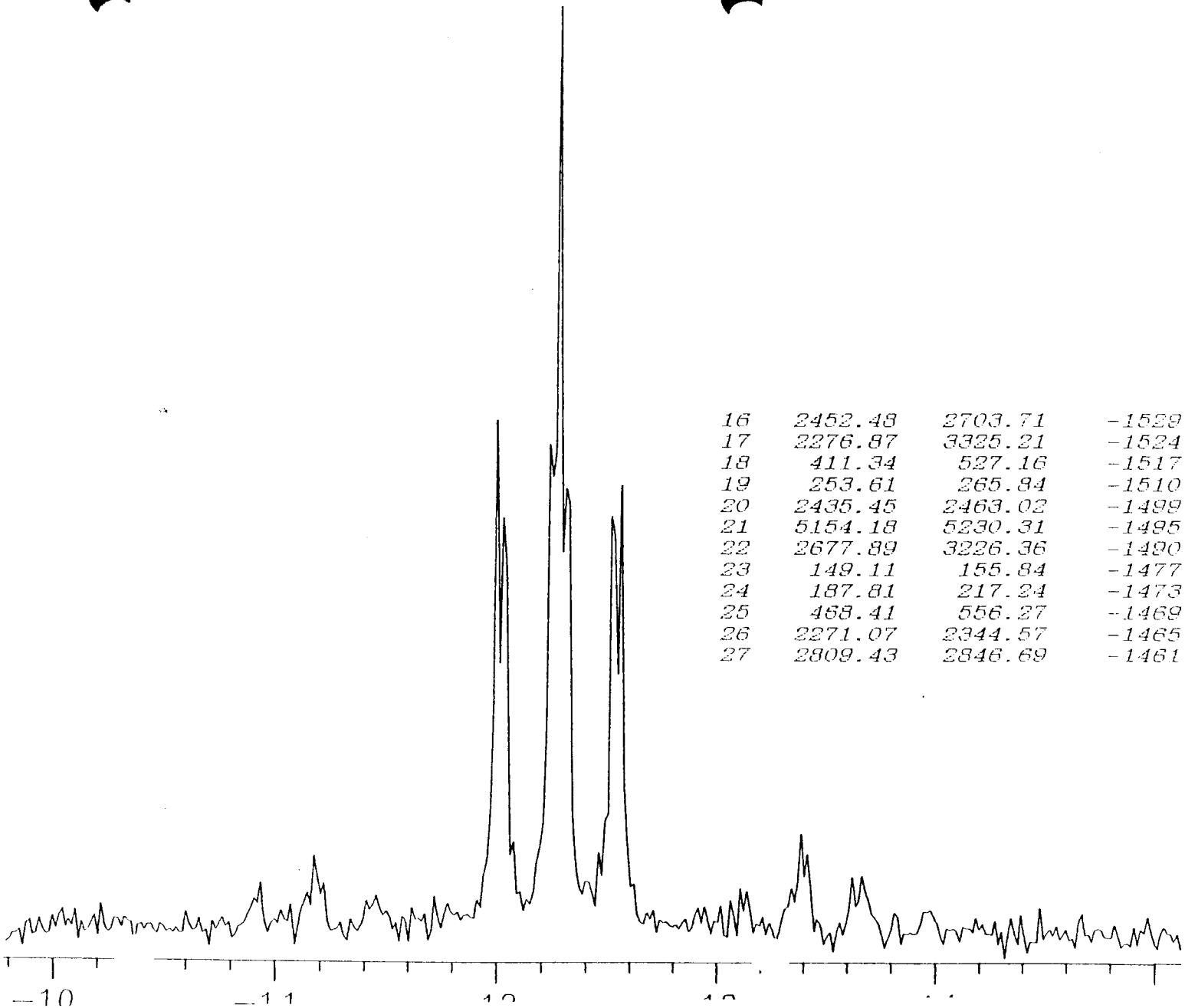

16	2452.48	2703.71	-1529.02	-12.663
17	2276.87	3325.21	-1524.94	-12.529
18	411.34	527.16	-1517.54	-12.468
19	253.61	265.84	-1510.44	-12.410
20	2435.45	2463.02	-1499.53	-12.320
21	5154.18	5230.31	-1495.16	-12.284
22	2677.89	3226.36	-1490.79	-12.248
23	149.11	155.84	-1477.90	-12.143
24	187.81	217.24	-1473.05	-12.103
25	468.41	556.27	-1469.50	-12.074
26	2271.07	2344.57	-1465.38	-12.040
27	2809.43	2846.69	-1461.44	-12.007

GE NMR
QE-300

EAK.207
02JUL97

PP-23

OPERATOR: EAK

LINE#	HEIGHT	HEIGHT(L)	FREQ(HZ)	PPM
1	539.41	654.30	-3858.19	-31.700
2	556.01	749.92	-3853.68	-31.663

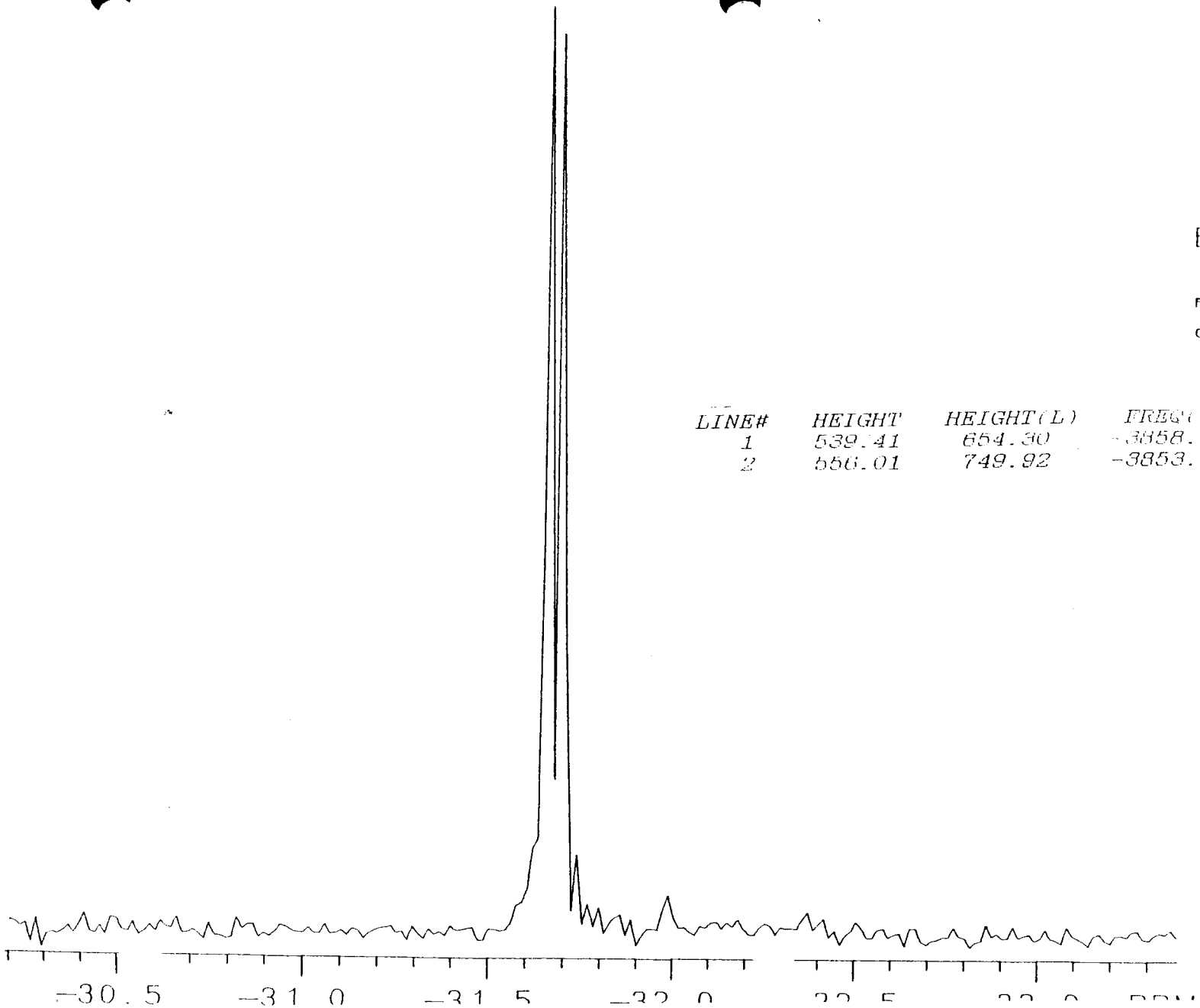

Figure 08

$^{31}P\ \{^{1}H\}$ NMR spectrum of

$[(CO)_4W(\mu\text{-}PPh_2)_2W(CO)_3(\mu\text{-}PPh_2C{\equiv}CPPh_2)(CO)_3W(\mu\text{-}PPh_2)_2W(CO)_4]$ (D-4-B).

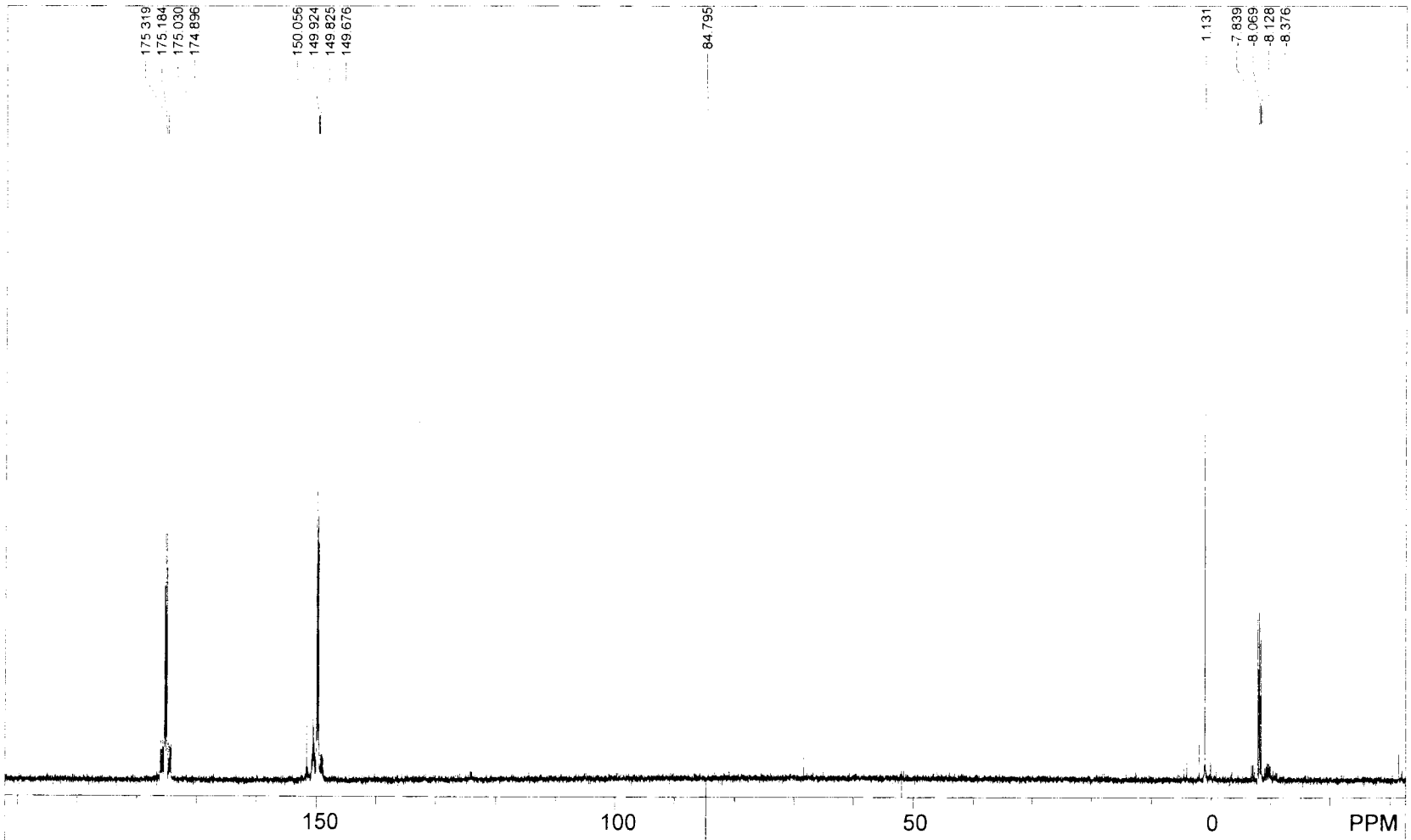

PP-63B1[PROD OF W DIMER + DPPA[3/16/02 USER: EAK -- DATE: 17MAR1997

F1: 121.718	F2: 1.000	SW1: 28571		OF1: 10321.9		PTS1d: 16384
EX: 1PULSE		PW: 7.0 usec	PD: 1.0 sec	NA: 3730	LB: 0.0	WinNuts - $EAK253

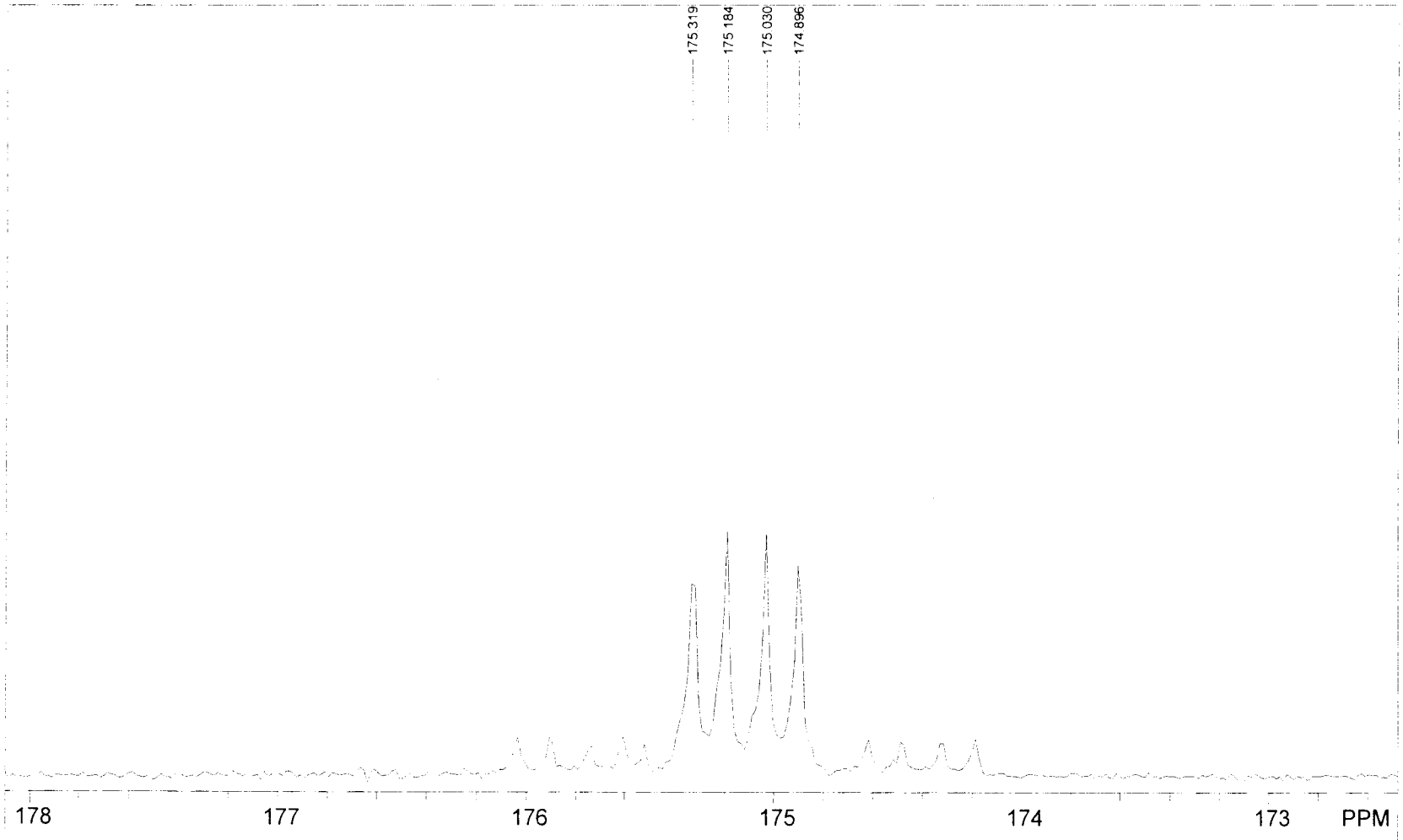

PP-63B1[PROD OF W DIMER + DPPA[3/16/02 USER: EAK -- DATE: 17MAR1997

F1: 121.718	F2: 1.000	SW1: 28571		OF1: 10321.9		PTS1d: 16384
EX: 1PULSE		PW: 7.0 usec	PD: 1.0 sec	NA: 3730	LB: 0.0	WinNuts - $EAK253

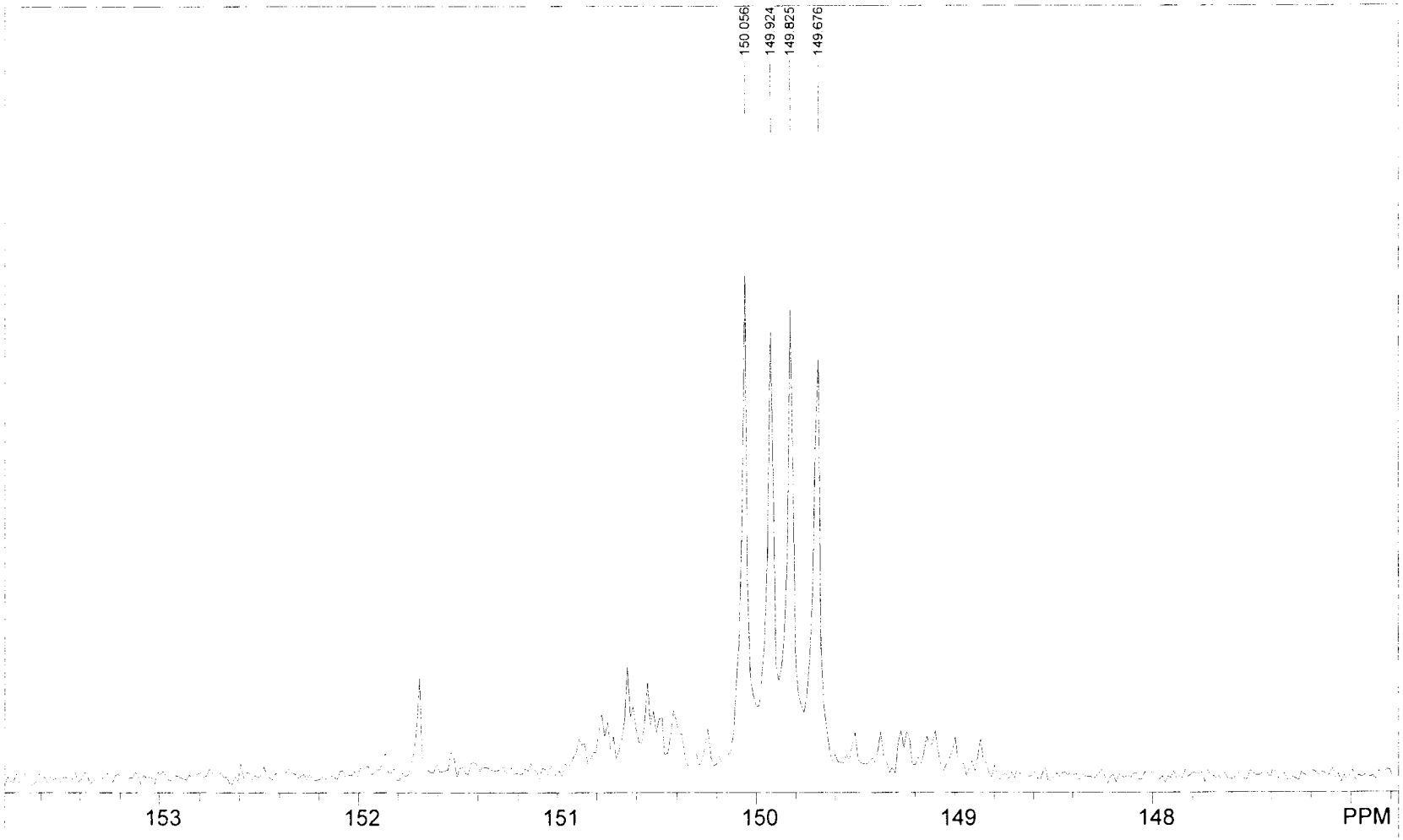

PP-63B1[PROD OF W DIMER + DPPA[3/16/02 USER: EAK -- DATE: 17MAR1997

F1: 121.718	F2: 1.000	SW1: 28571		OF1: 10321.9		PTS1d: 16384
EX: 1PULSE		PW: 7.0 usec	PD: 1.0 sec	NA: 3730	LB: 0.0	WinNuts - $EAK253

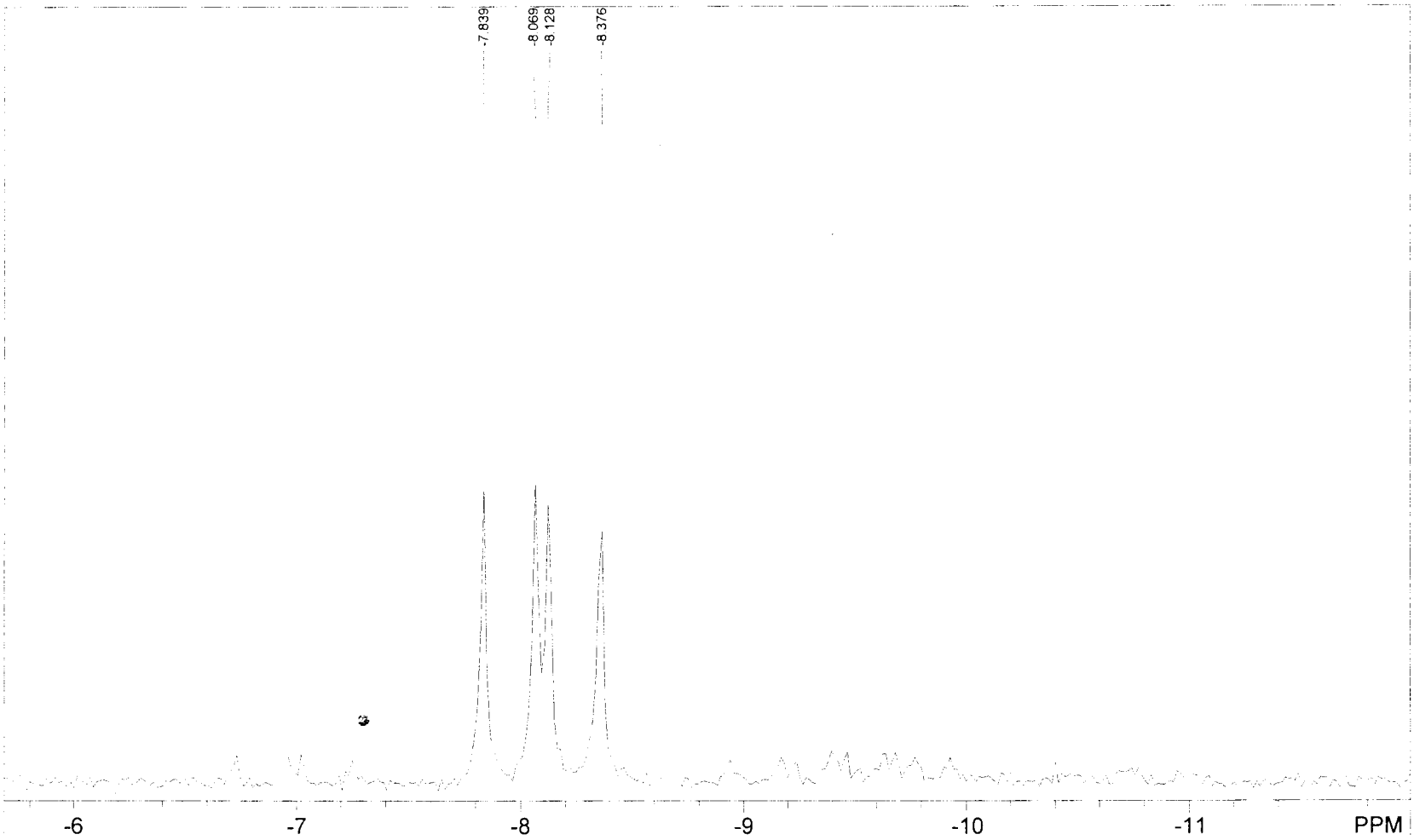

PP-63B1[PROD OF W DIMER + DPPA[3/16/02 USER: EAK -- DATE: 17MAR1997

F1: 121.718	F2: 1.000	SW1: 28571		OF1: 10321.9		PTS1d: 16384
EX: 1PULSE		PW: 7.0 usec	PD: 1.0 sec	NA: 3730	LB: 0.0	WinNuts - $EAK253

Figure 09

Simulated $^{31}P\{^{1}H\}$ NMR spectrum of

$[(CO)_4W(\mu\text{-}PPh_2)_2W(CO)_3(\mu\text{-}PPh_2C{\equiv}CPPh_2)(CO)_3W(\mu\text{-}PPh_2)_2W(CO)_4]$ (D-4-B).

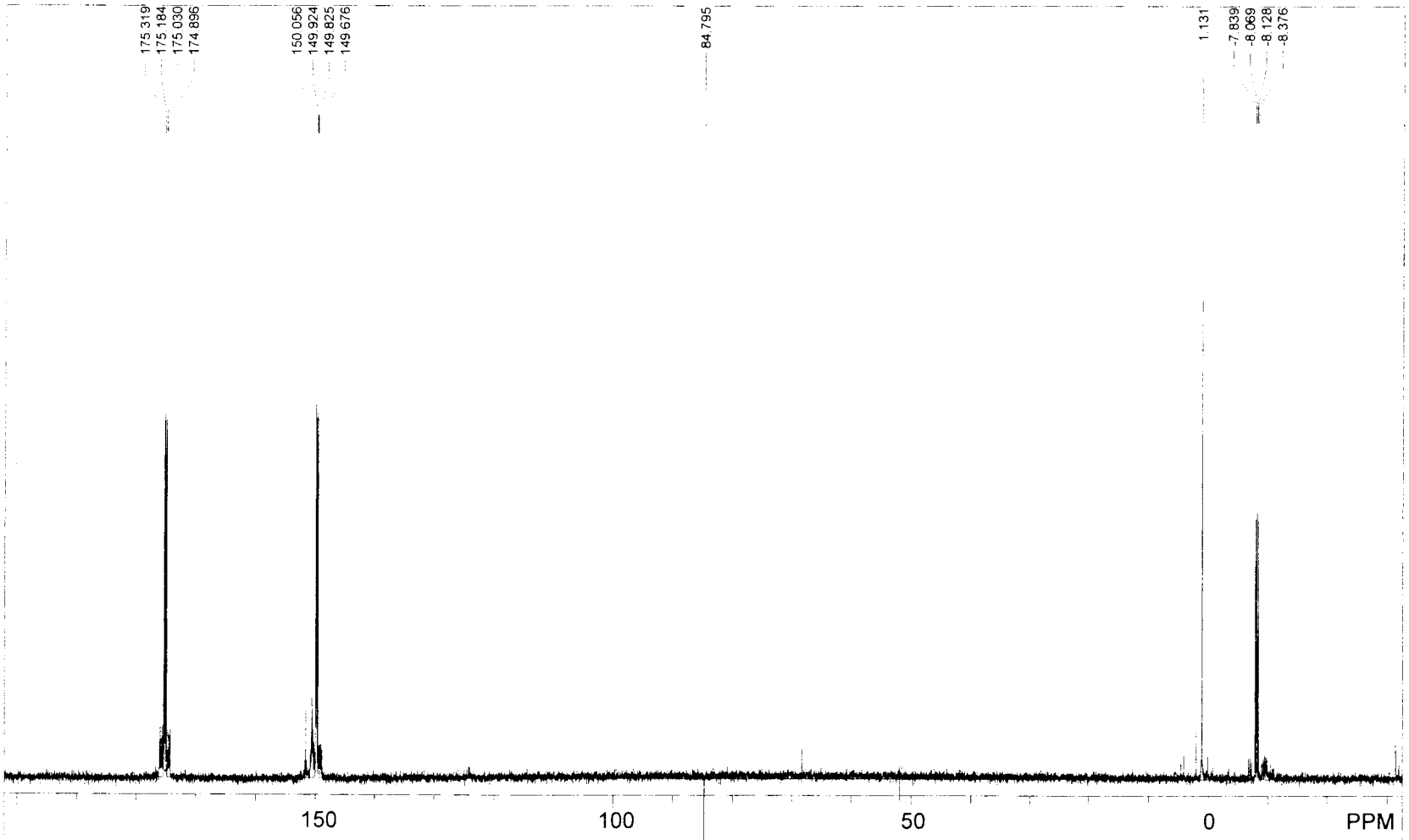

PP-63B1[PROD OF W DIMER + DPPA[3/16/02 USER: EAK -- DATE: 17MAR1997

F1: 121.718	F2: 1.000	SW1: 28571		OF1: 10321.9		PTS1d: 16384
EX: 1PULSE		PW: 7.0 usec	PD: 1.0 sec	NA: 3730	LB: 0.0	WinNuts - $EAK253

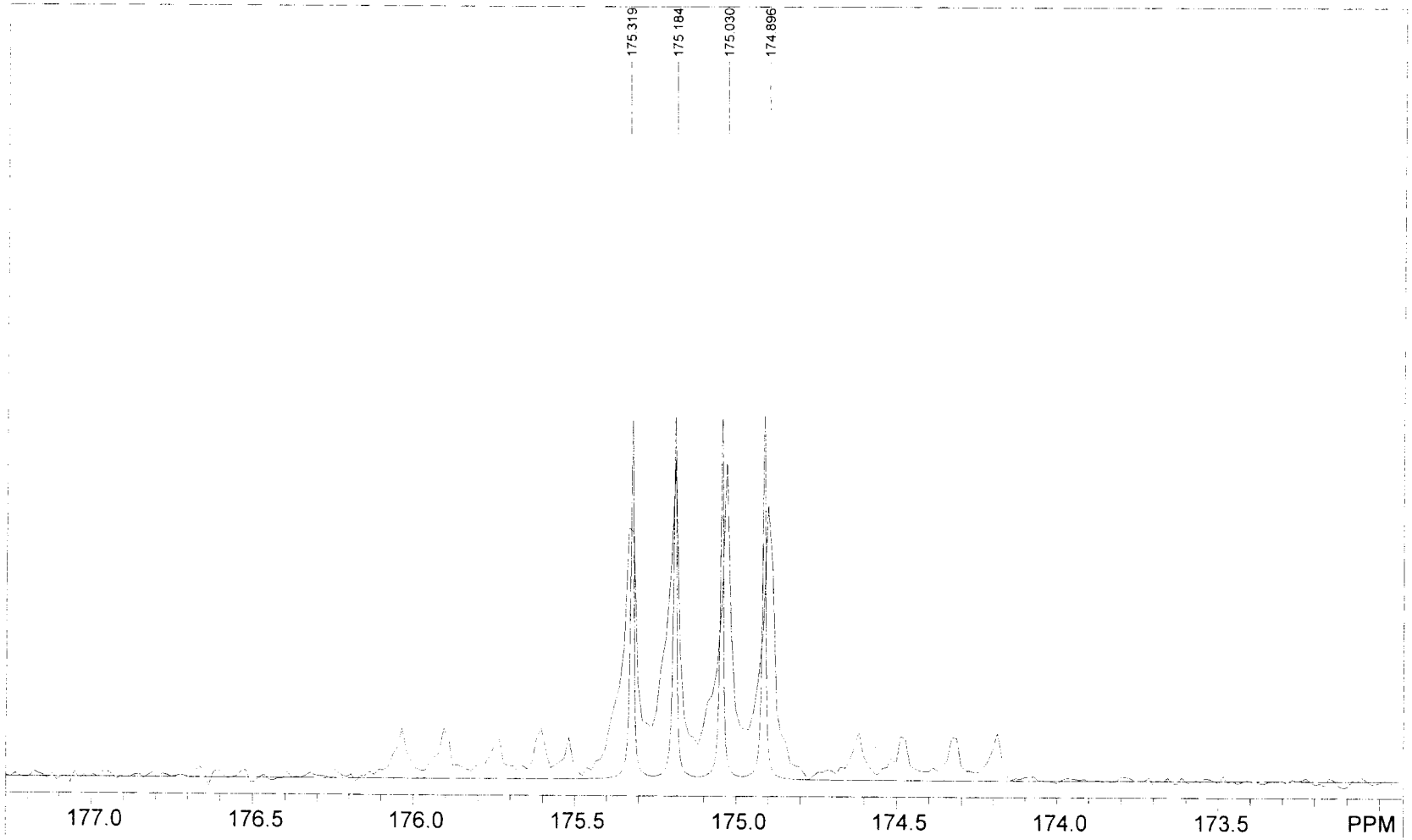

PP-63B1[PROD OF W DIMER + DPPA[3/16/02 USER: EAK -- DATE: 17MAR1997

F1: 121.718	F2: 1.000	SW1: 28571		OF1: 10321.9		PTS1d: 16384
EX: 1PULSE		PW: 7.0 usec	PD: 1.0 sec	NA: 3730	LB: 0.0	WinNuts - $EAK253

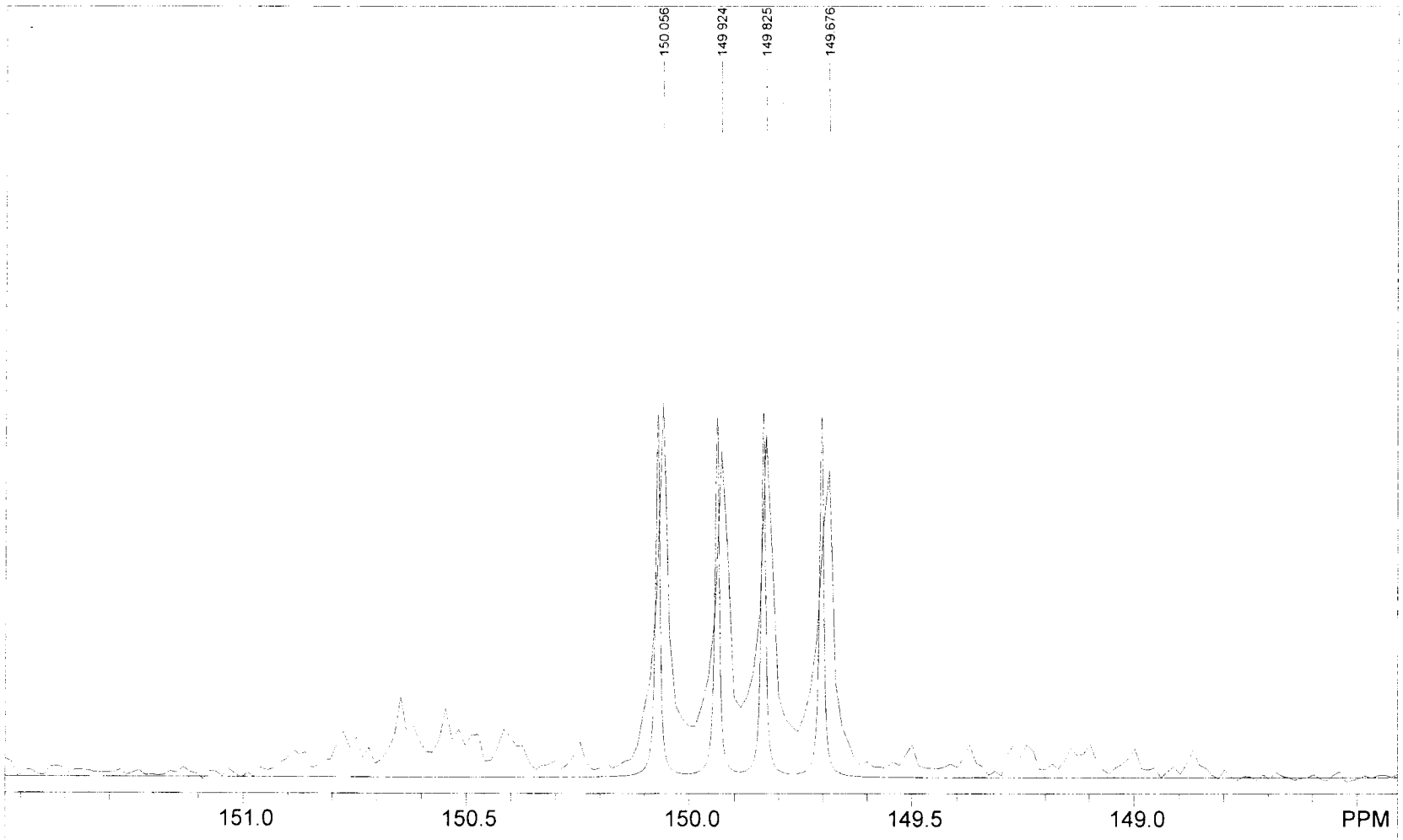

PP-63B1[PROD OF W DIMER + DPPA[3/16/02 USER: EAK -- DATE: 17MAR1997

F1: 121.718	F2: 1.000	SW1: 28571		OF1: 10321.9		PTS1d: 16384
EX: 1PULSE		PW: 7.0 usec	PD: 1.0 sec	NA: 3730	LB: 0.0	WinNuts - $EAK253

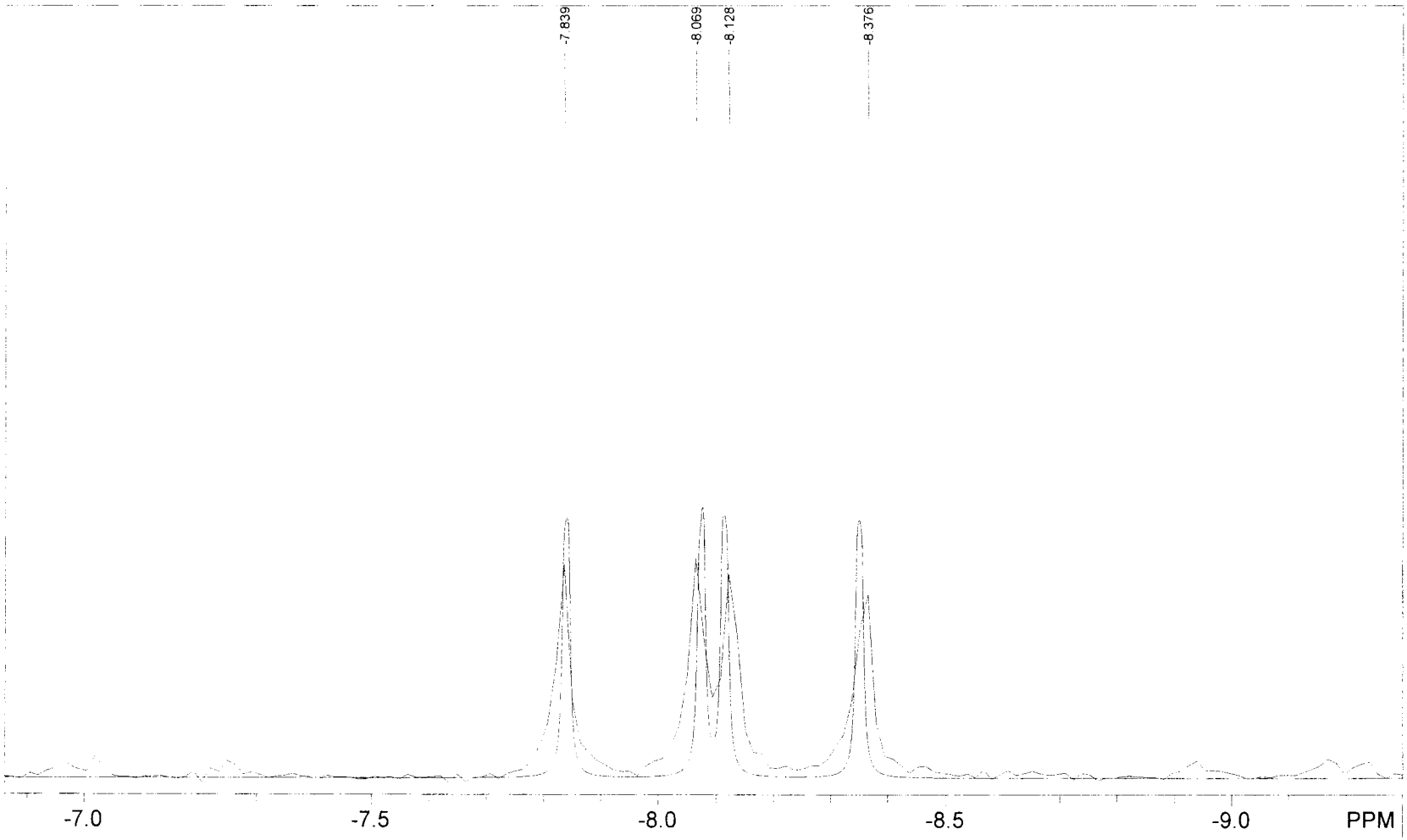

PP-63B1[PROD OF W DIMER + DPPA[3/16/02 USER: EAK -- DATE: 17MAR1997

F1: 121.718	F2: 1.000	SW1: 28571		OF1: 10321.9		PTS1d: 16384
EX: 1PULSE		PW: 7.0 usec	PD: 1.0 sec	NA: 3730	LB: 0.0	WinNuts - $EAK253

Figure 10

UV/Vis spectrum of

$[(CO)_4W(\mu\text{-}PPh_2)_2W(CO)_3(\mu\text{-}PPh_2C{\equiv}CPPh_2)(CO)_3W(\mu\text{-}PPh_2)_2W(CO)_4]$ (D-4-B).

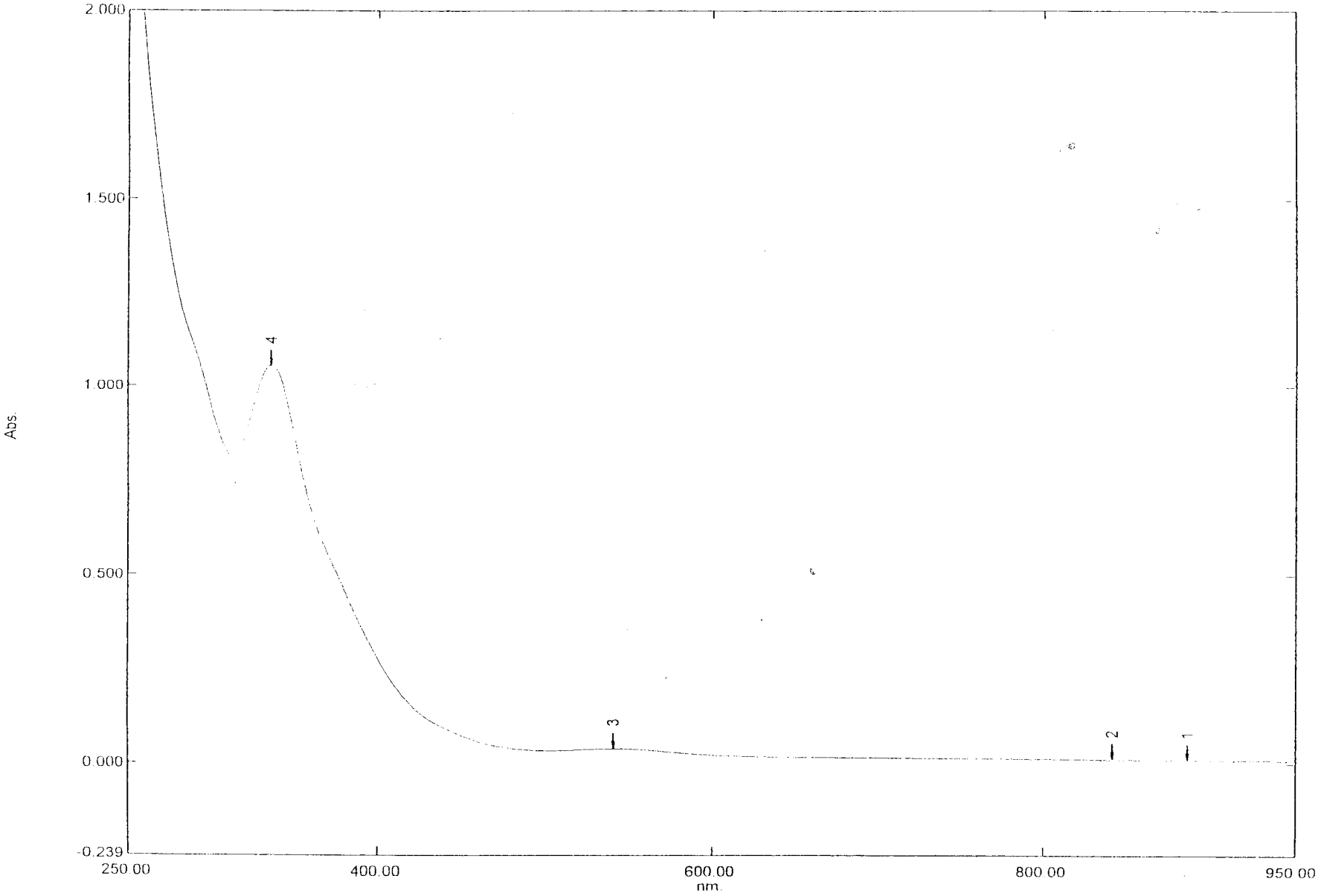
2.000
1.500
1.000
0.500
0.000
-0.239
Abs.
250.00
400.00
600.00
800.00
950.00
nm.
4
3
2
1

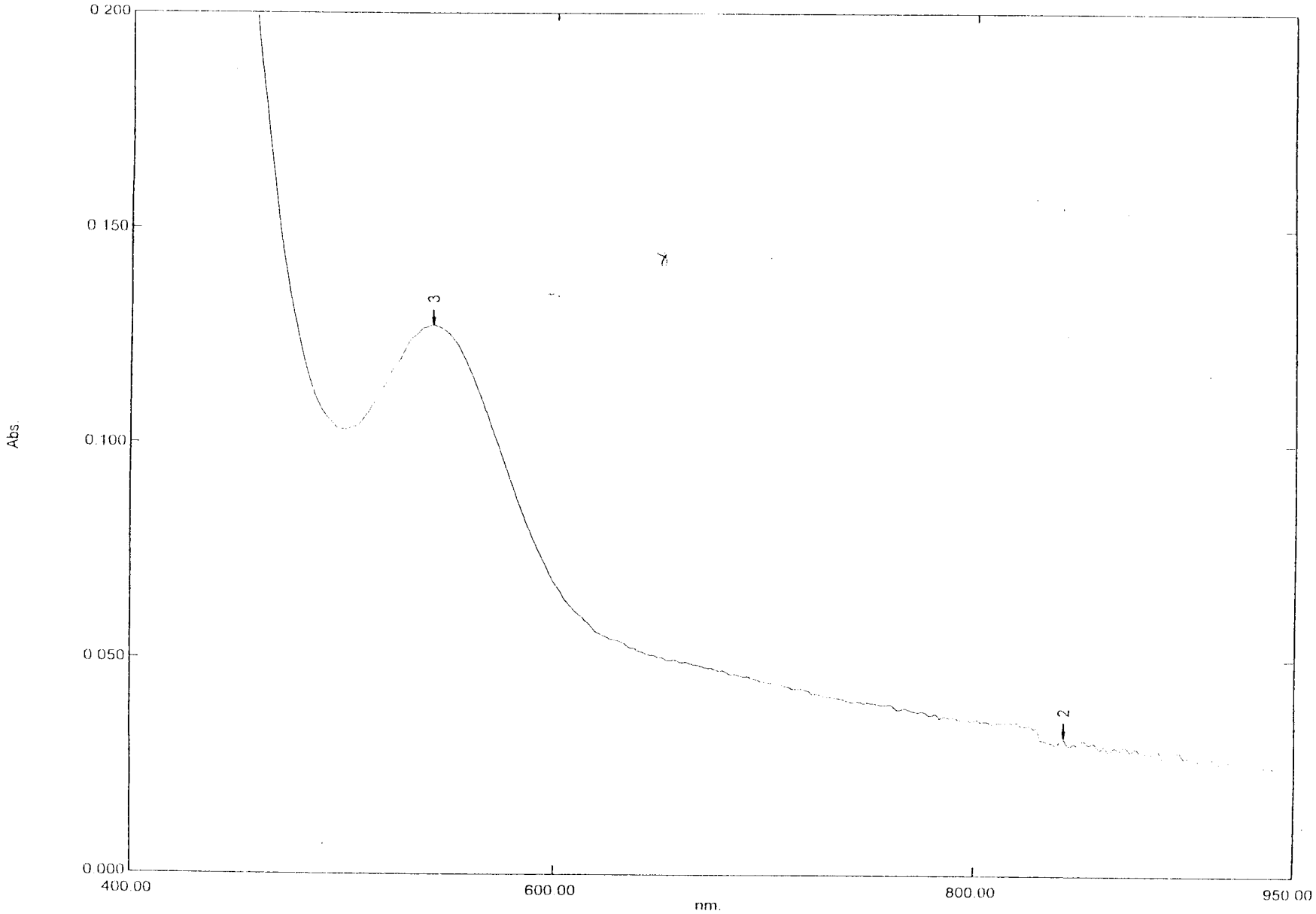
0 200
0 150
0.100
0 050
0 000
Abs
3
2
400.00
600.00
800.00
950 00
nm.

Figure 11

IR spectrum of $(CO)_4W(\mu\text{-}PPh_2)_2W(CO)_3(\textit{trans}\text{-}PPh_2CH{=}CHPPh_2)$ (D-5-A).

Bio-Rad Win-IR Pro

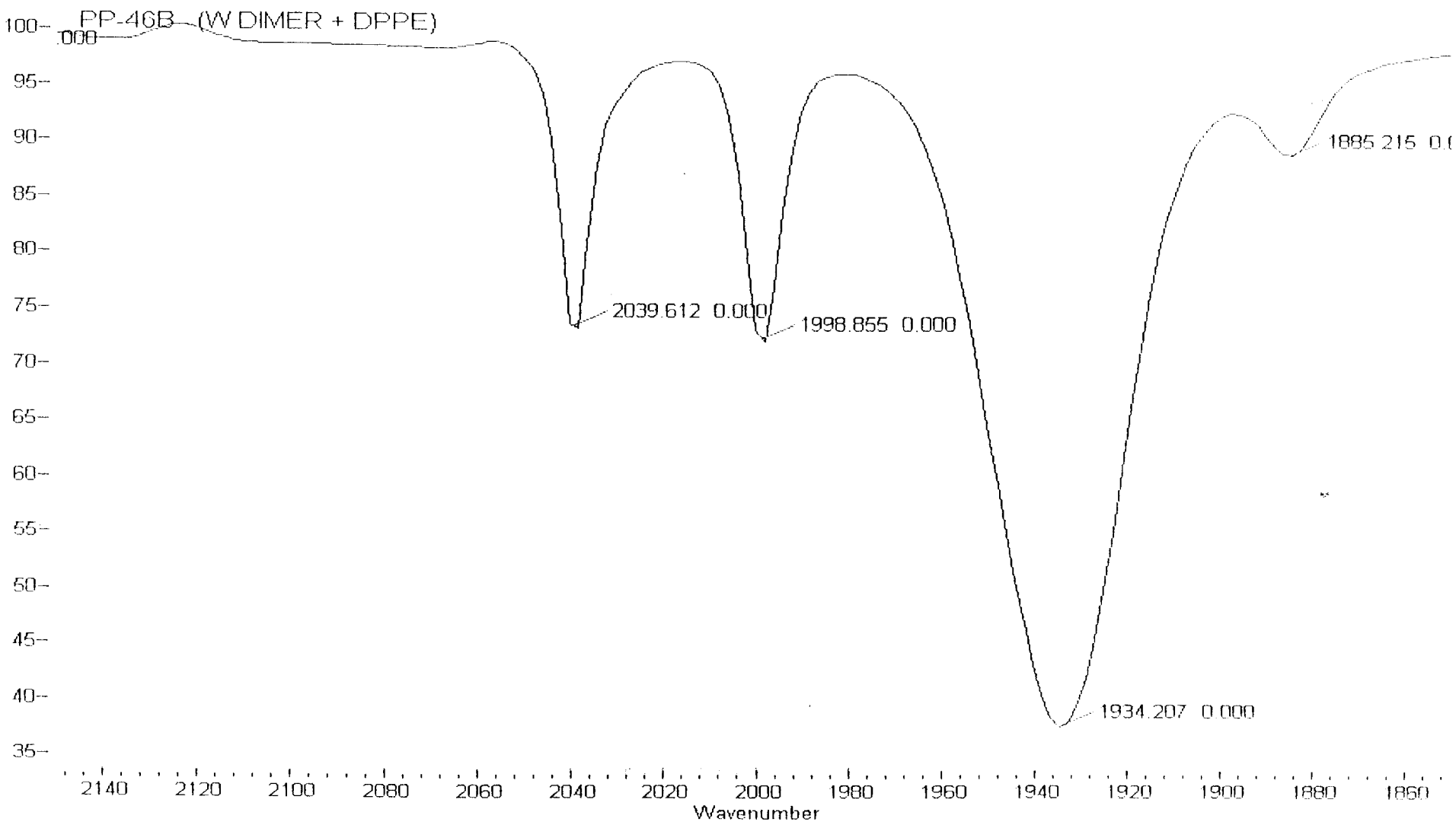

Figure 12

$^{31}P\{^{1}H\}$ NMR spectrum of

$(CO)_4W(\mu\text{-}PPh_2)_2W(CO)_3(\textit{trans}\text{-}PPh_2CH{=}CHPPh_2)$ (D-5-A).

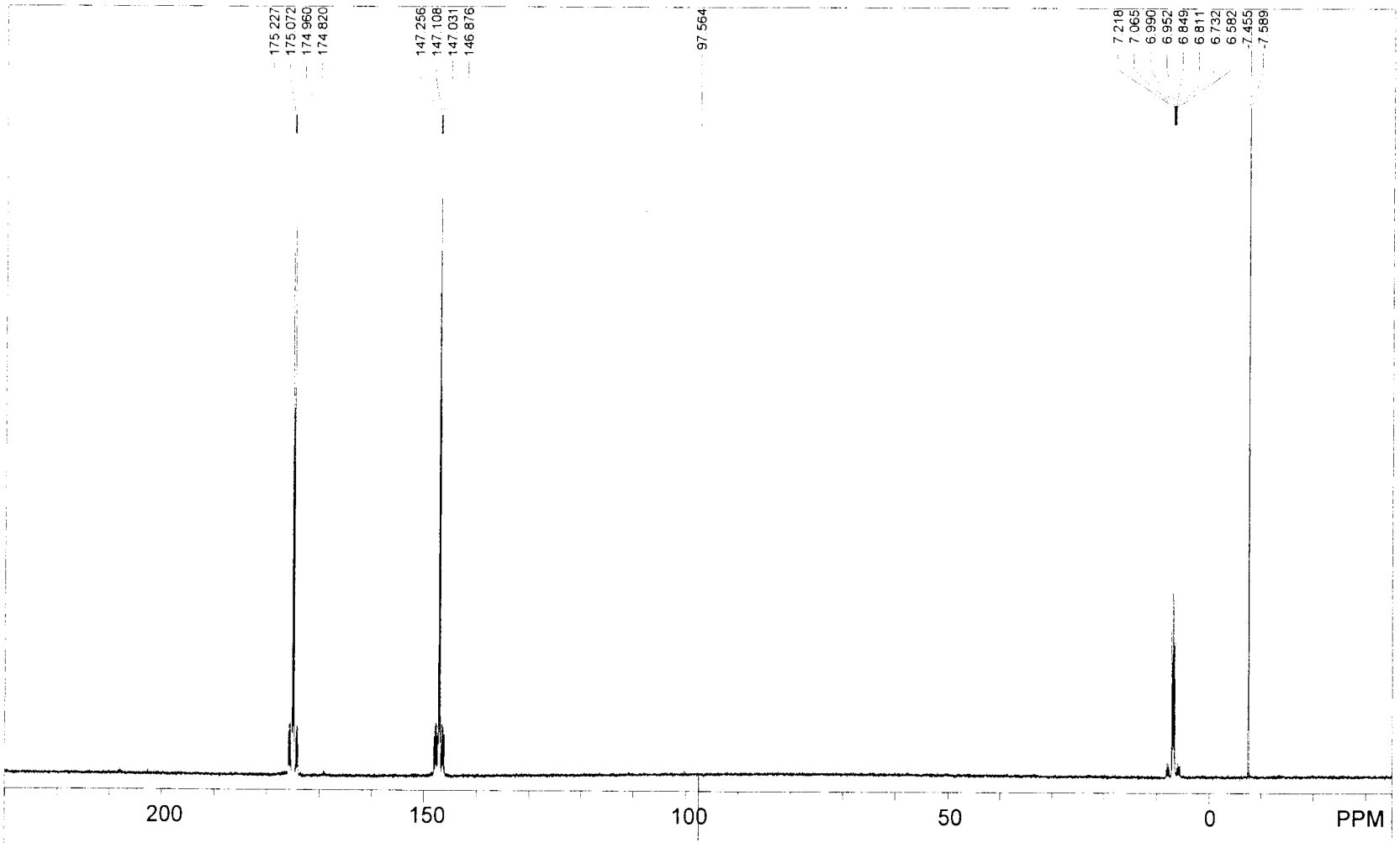

PP-46B1[PROD OF W + DPP ETHYLENE[2/23/02

USER: EAK -- DATE: 24FEB1997

F1: 121.719	F2: 1.000	SW1: 32258		OF1: 11876.4		PTS1d: 16384
EX: 1PULSE		PW: 7.0 usec	PD: 1.0 sec	NA: 1683	LB: 0.0	WinNuts - $EAK.245

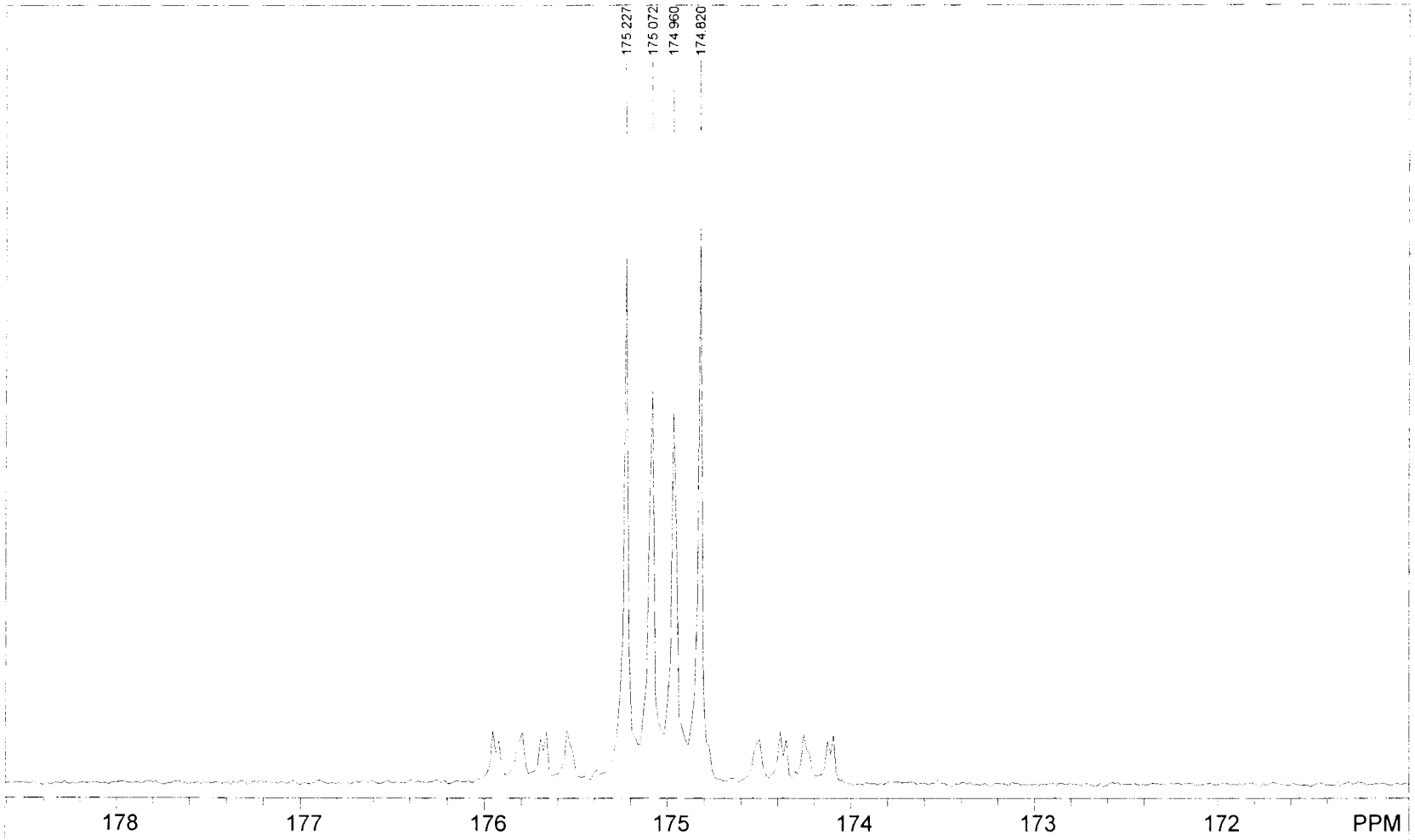

PP-46B1[PROD OF W + DPP ETHYLENE[2/23/02 USER: EAK -- DATE: 24FEB1997

F1: 121.719	F2: 1.000	SW1: 32258		OF1: 11876.4		PTS1d: 16384
EX: 1PULSE		PW: 7.0 usec	PD: 1.0 sec	NA: 1683	LB: 0.0	WinNuts - $EAK.245

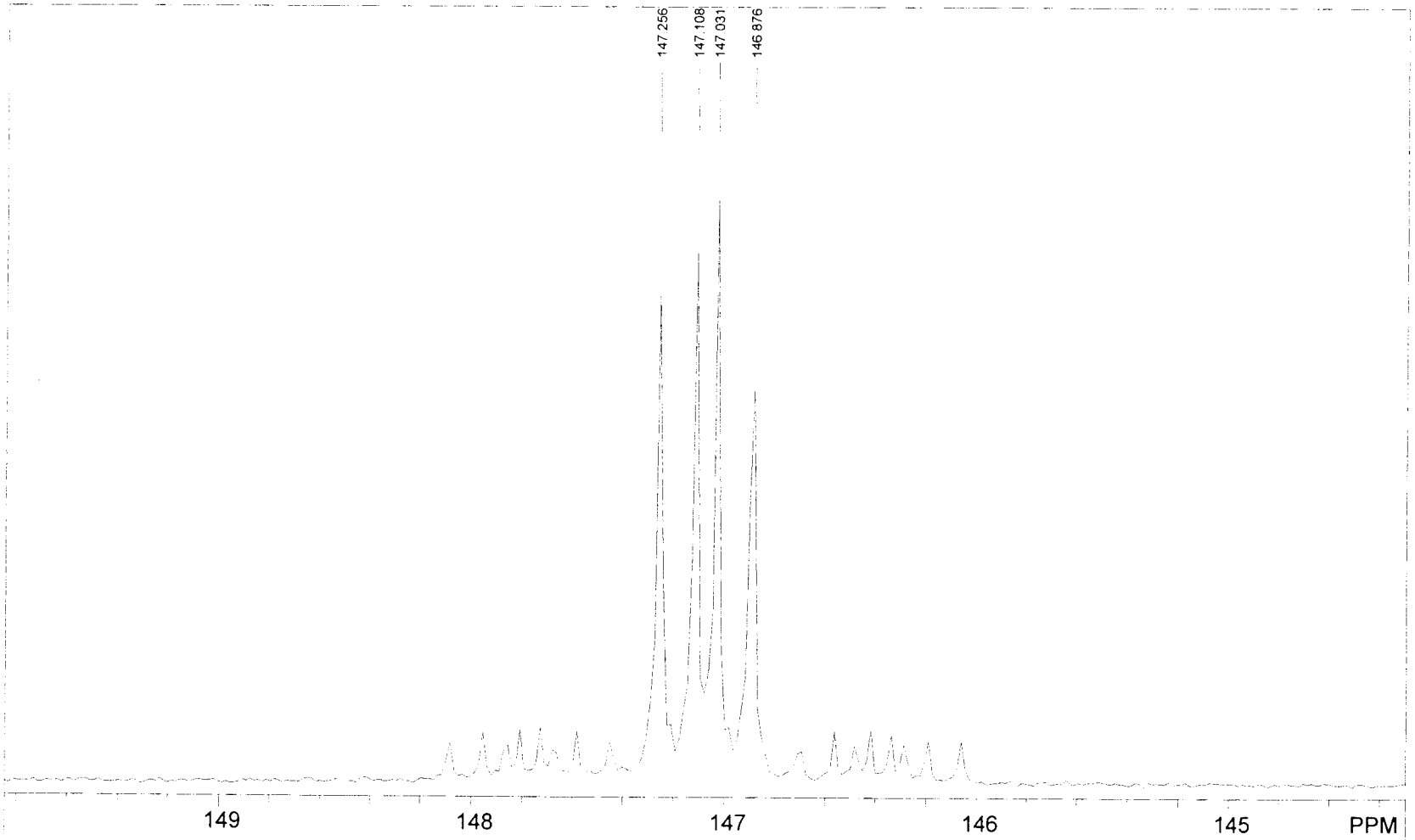

PP-46B1[PROD OF W + DPP ETHYLENE[2/23/02 USER: EAK -- DATE: 24FEB1997

F1: 121.719	F2: 1.000	SW1: 32258		OF1: 11876.4		PTS1d: 16384
EX: 1PULSE		PW: 7.0 usec	PD: 1.0 sec	NA: 1683	LB: 0.0	WinNuts - $EAK.245

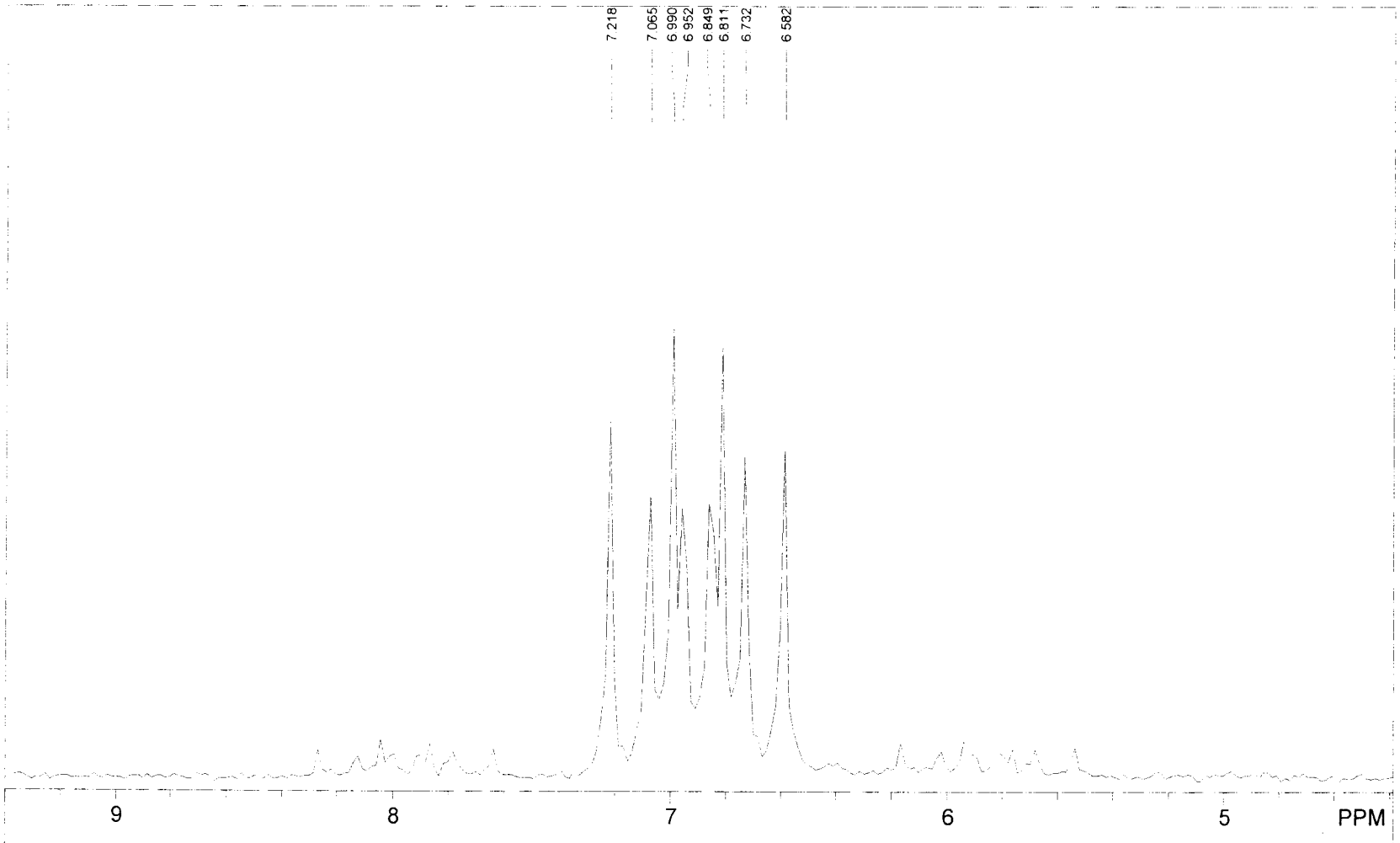

PP-46B1[PROD OF W + DPP ETHYLENE[2/23/02 USER: EAK -- DATE: 24FEB1997

F1: 121.719	F2: 1.000	SW1: 32258		OF1: 11876.4		PTS1d: 16384
EX: 1PULSE		PW: 7.0 usec	PD: 1.0 sec	NA: 1683	LB: 0.0	WinNuts - $EAK.245

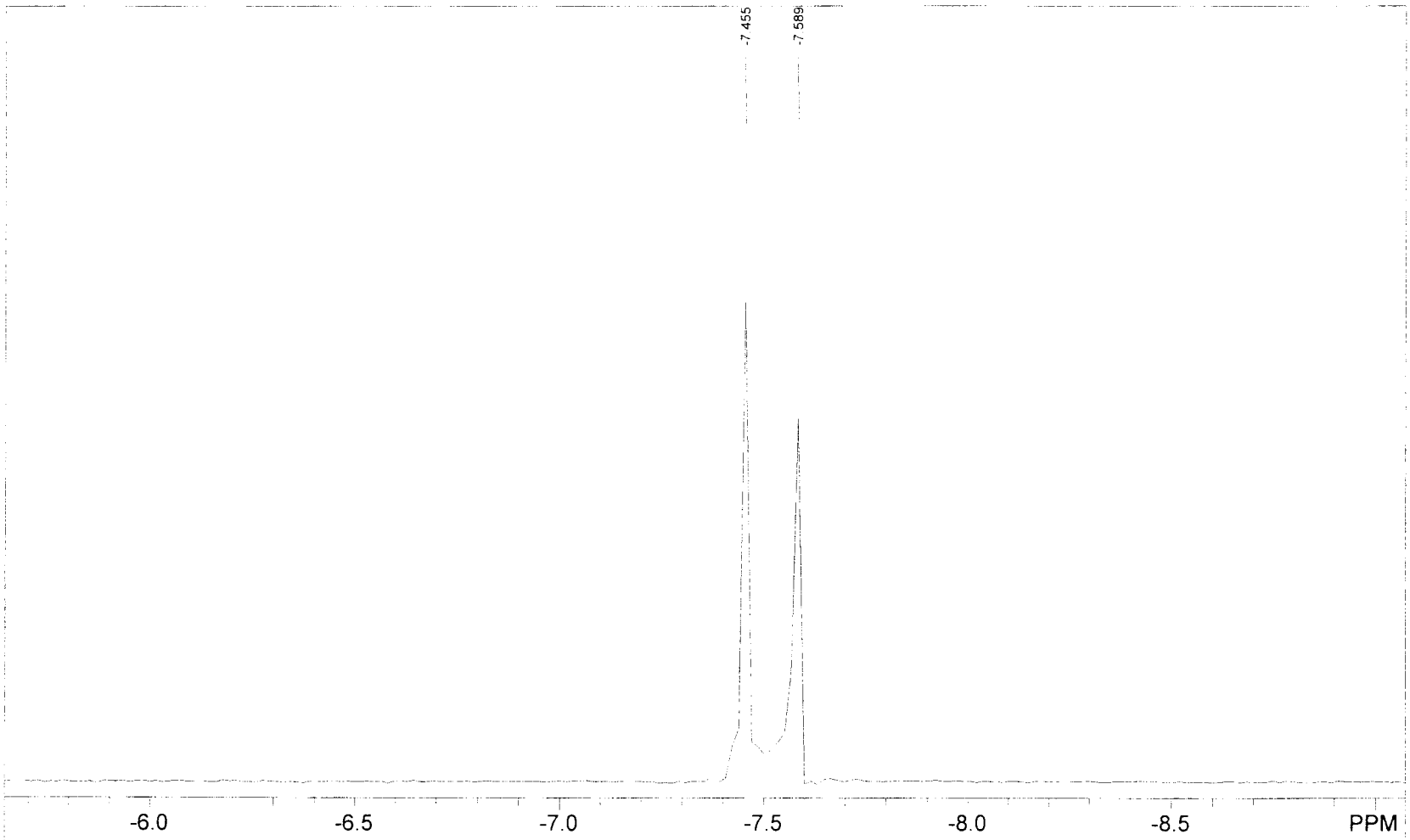

PP-46B1[PROD OF W + DPP ETHYLENE[2/23/02 USER: EAK -- DATE: 24FEB1997

F1: 121.719	F2: 1.000	SW1: 32258		OF1: 11876.4		PTS1d: 16384
EX: 1PULSE		PW: 7.0 usec	PD: 1.0 sec	NA: 1683	LB: 0.0	WinNuts - $EAK.245

Figure 13

IR spectrum of

$[(CO)_4W(\mu\text{-}PPh_2)_2W(CO)_3(\mu\text{-}\textit{trans}\text{-}PPh_2CH{=}CHPPh_2)(CO)_3W(\mu\text{-}PPh_2)_2W(CO)_4]$

(D-5-B).

o-Rad Win-IR Pro

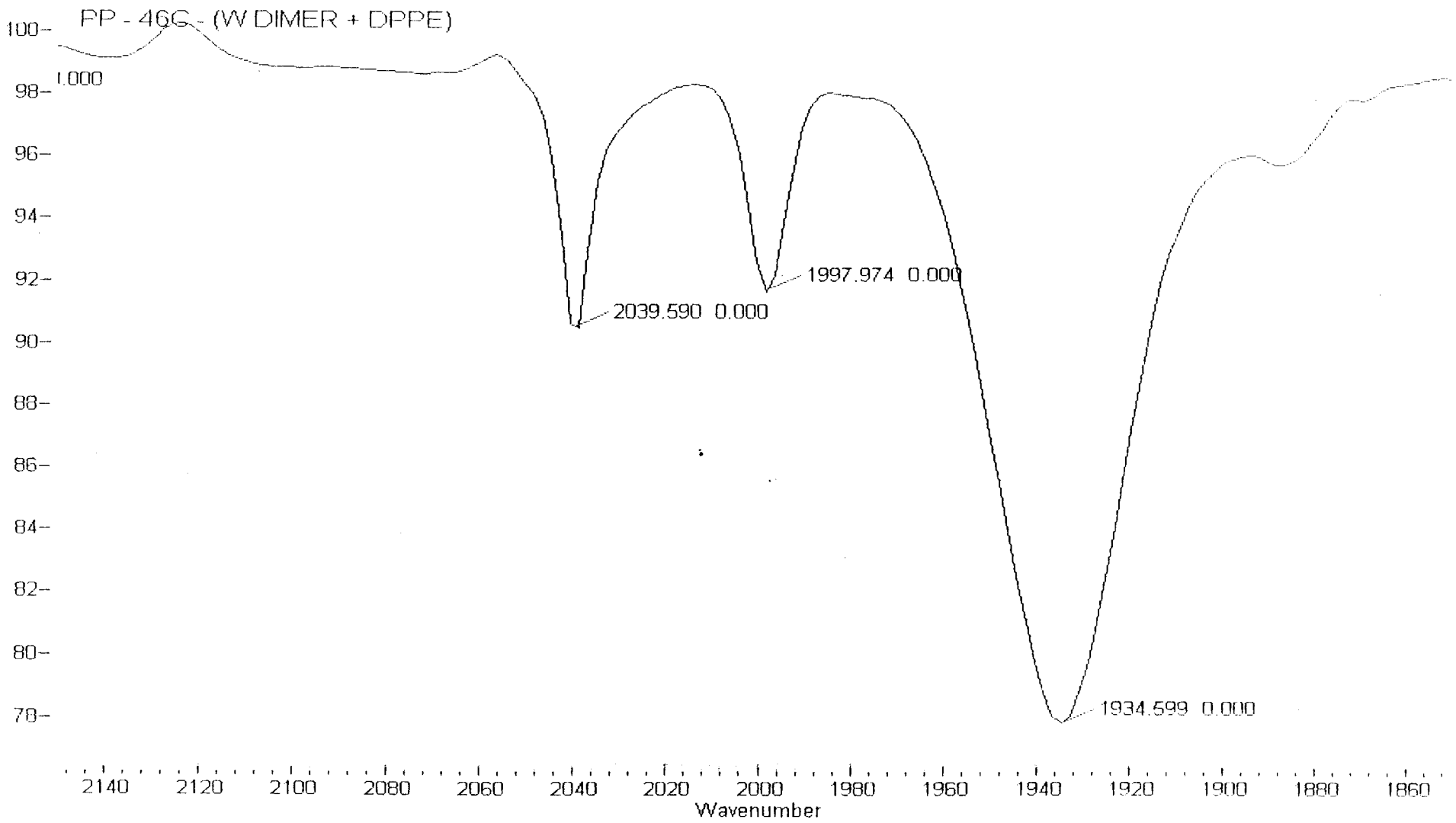

Figure 14

$^{31}P\{^{1}H\}$ NMR spectrum of

$[(CO)_4W(\mu\text{-}PPh_2)_2W(CO)_3(\mu\text{-}trans\text{-}PPh_2CH{=}CHPPh_2)(CO)_3W(\mu\text{-}PPh_2)_2W(CO)_4]$

(D-5-B).

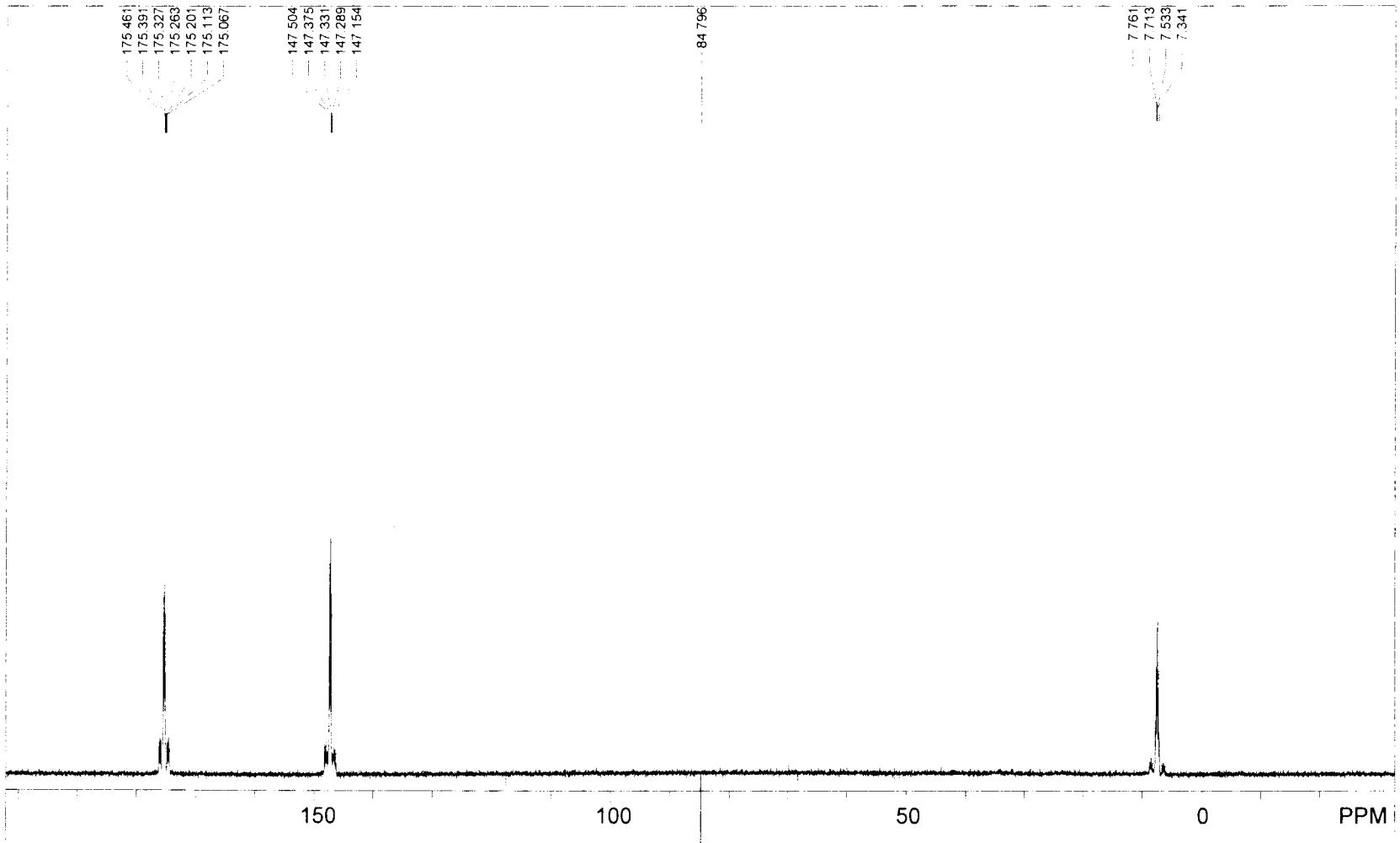

PP-46C[PROD OF W DIMER + DPPE[3/15/02 USER: EAK -- DATE: 16MAR1997

F1: 121.718	F2: 1.000	SW1: 28571		OF1: 10322.0		PTS1d: 16384
EX: 1PULSE		PW: 7.0 usec	PD: 1.0 sec	NA: 2486	LB: 0.0	WinNuts - $EAK252

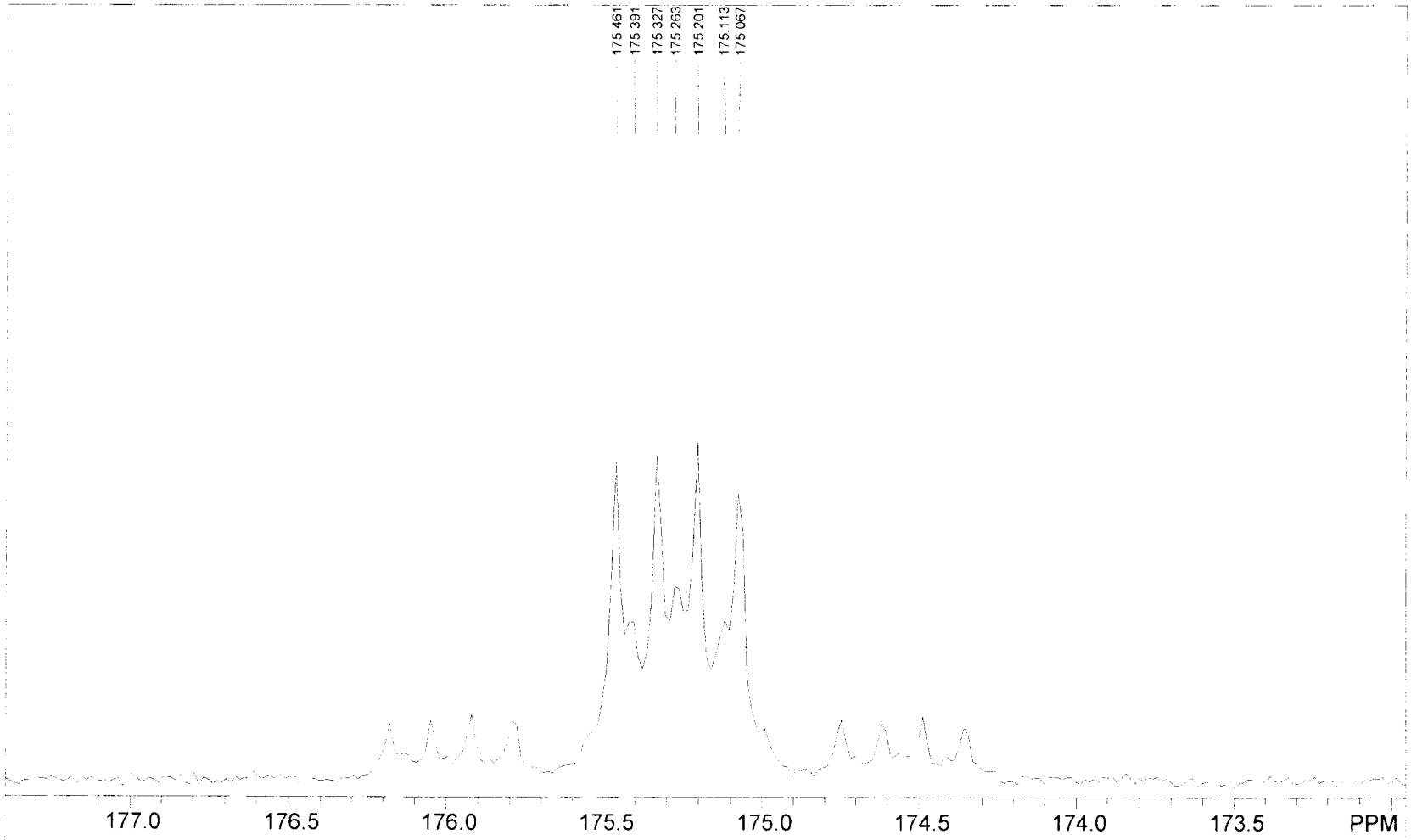

PP-46C[PROD OF W DIMER + DPPE[3/15/02 USER: EAK -- DATE: 16MAR1997

F1: 121.718	F2: 1.000	SW1: 28571		OF1: 10322.0		PTS1d: 16384	
EX: 1PULSE		PW: 7.0 usec	PD: 1.0 sec	NA: 2486	LB: 0.0		WinNuts - $EAK252

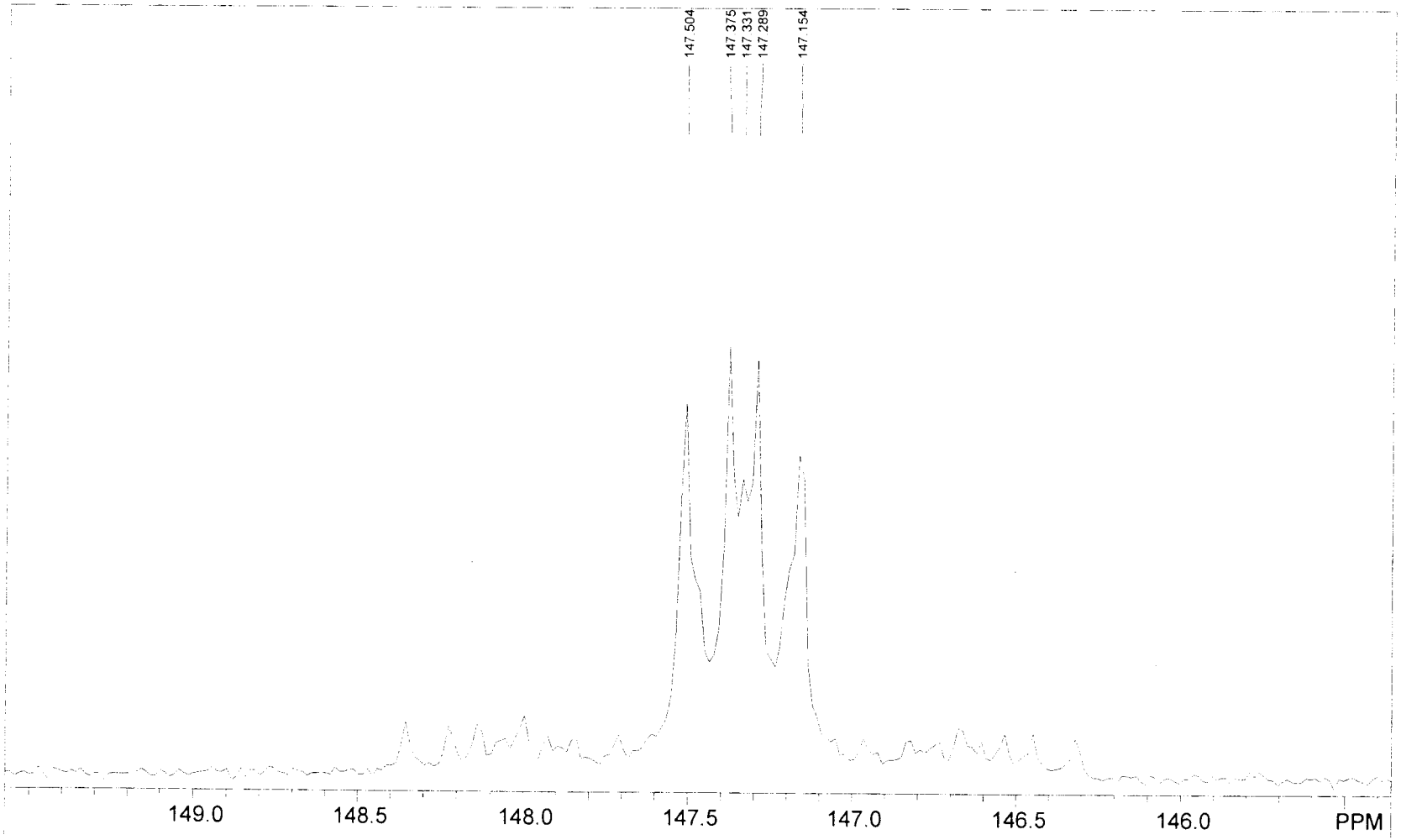

PP-46C[PROD OF W DIMER + DPPE[3/15/02 USER: EAK -- DATE: 16MAR1997

F1: 121.718	F2: 1.000	SW1: 28571		OF1: 10322.0		PTS1d: 16384
EX: 1PULSE		PW: 7.0 usec	PD: 1.0 sec	NA: 2486	LB: 0.0	WinNuts - $EAK252

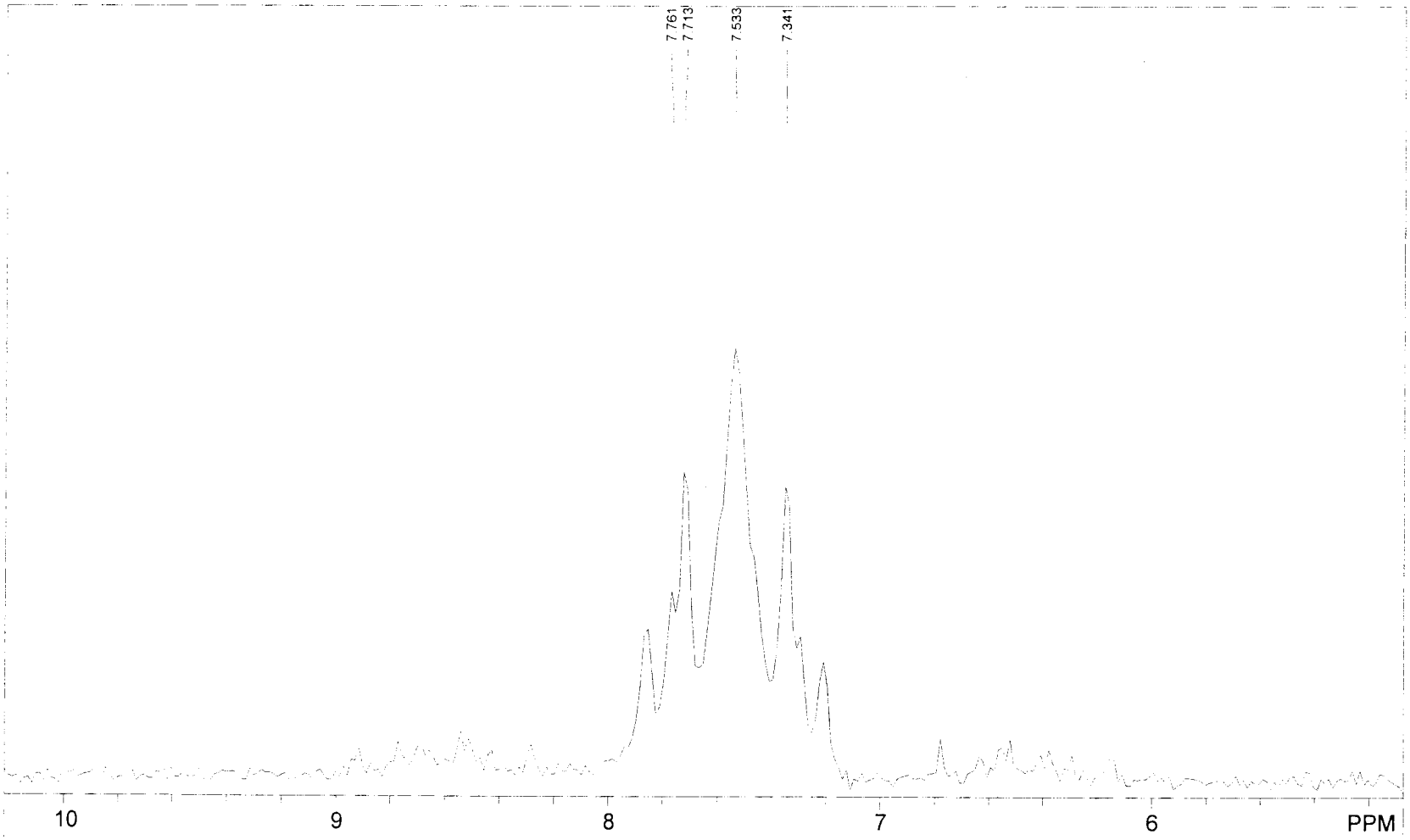

PP-46C[PROD OF W DIMER + DPPE[3/15/02 USER: EAK -- DATE: 16MAR1997

F1: 121.718	F2: 1.000	SW1: 28571		OF1: 10322.0		PTS1d: 16384	
EX: 1PULSE		PW: 7.0 usec	PD: 1.0 sec	NA: 2486	LB: 0.0		WinNuts - $EAK252

Figure 15

Simulated $^{31}P\{^{1}H\}$ NMR spectrum of

$[(CO)_4W(\mu\text{-}PPh_2)_2W(CO)_3(\mu\text{-}\textit{trans}\text{-}PPh_2CH{=}CHPPh_2)(CO)_3W(\mu\text{-}PPh_2)_2W(CO)_4]$

(D-5-B).

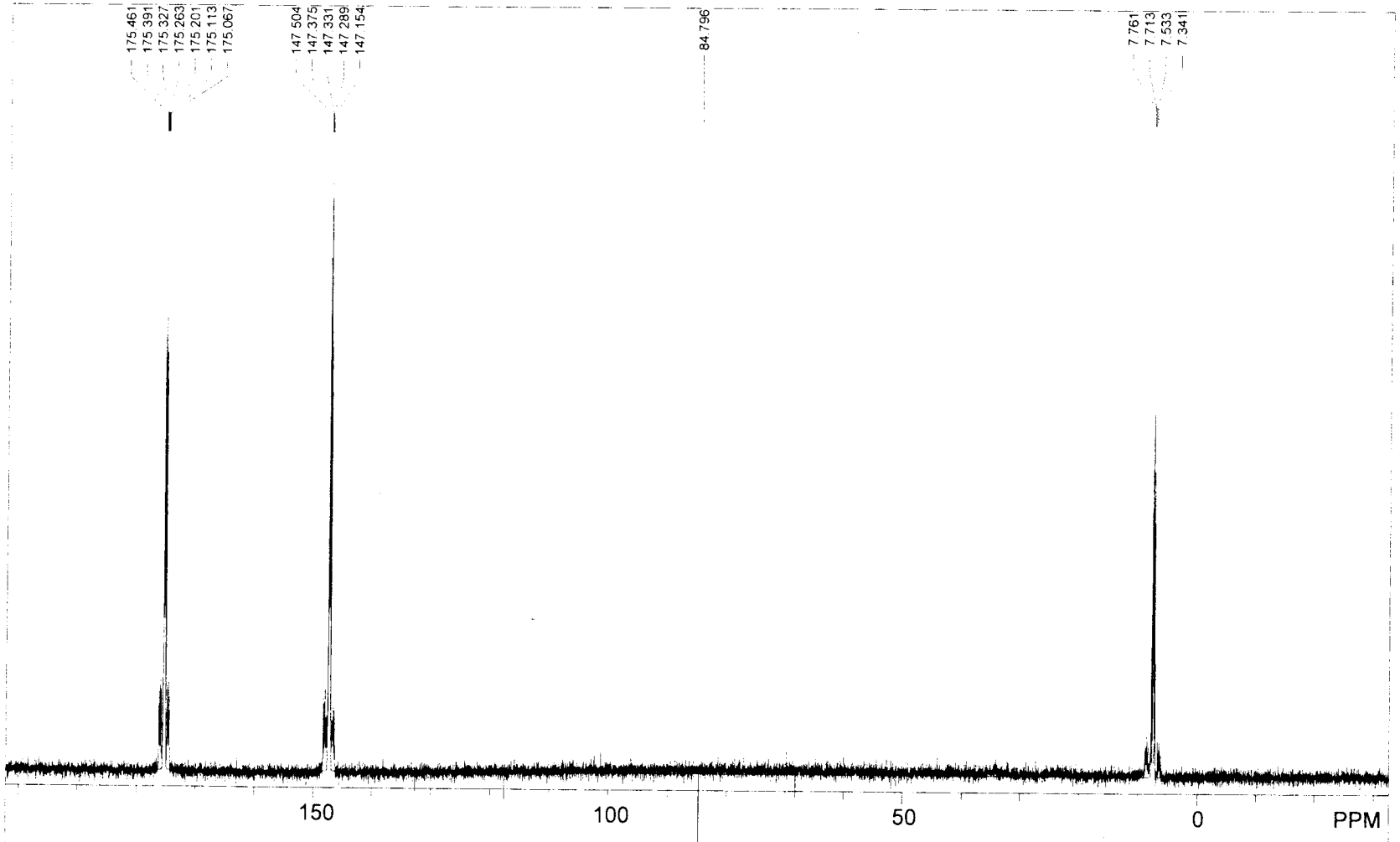

PP-46C[PROD OF W DIMER + DPPE[3/15/02

USER: EAK -- DATE: 16MAR1997

F1: 121.718	F2: 1.000	SW1: 28571		OF1: 10322.0		PTS1d: 16384
EX: 1PULSE		PW: 7.0 usec	PD: 1.0 sec	NA: 2486	LB: 0.0	WinNuts - $EAK252

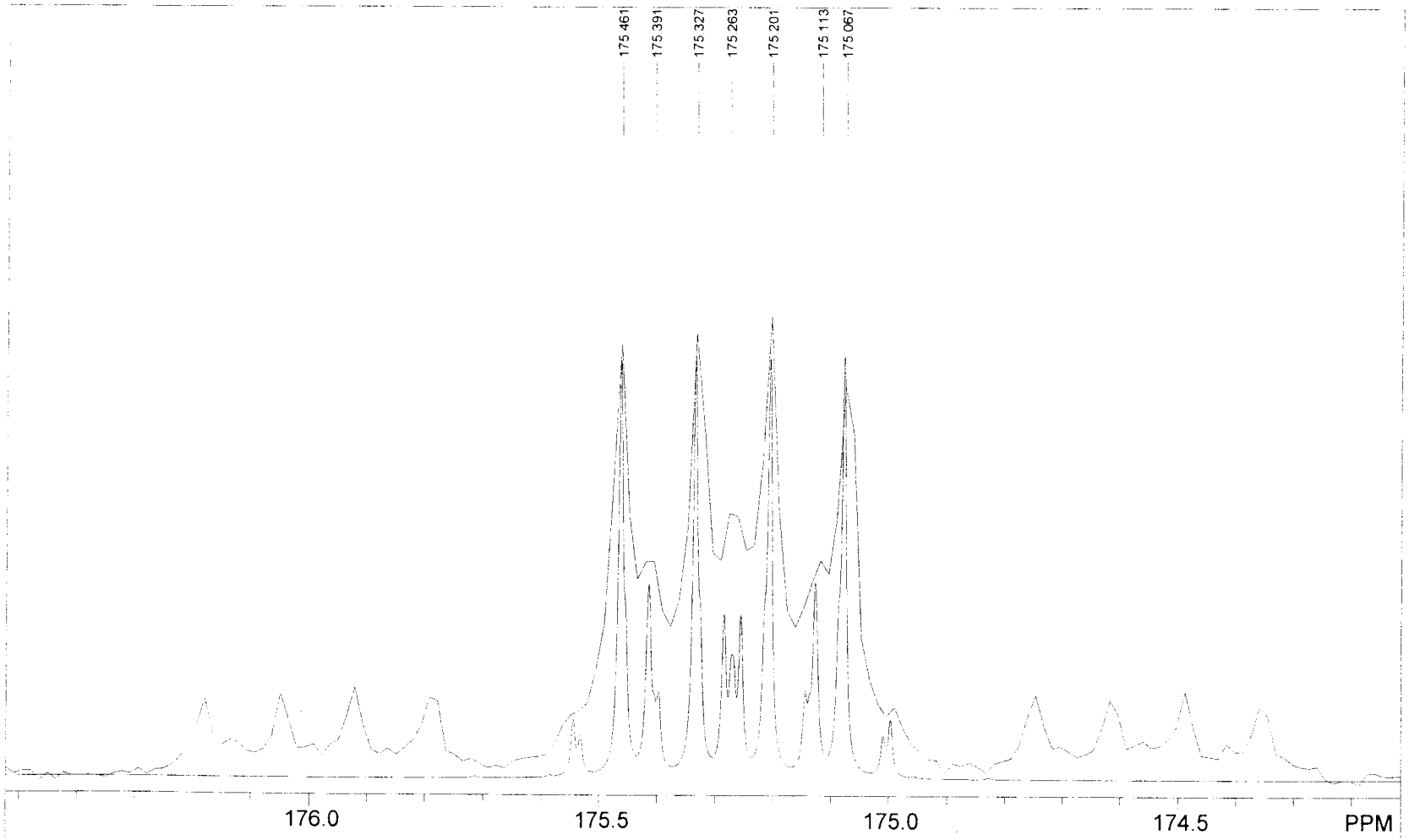

PP-46C[PROD OF W DIMER + DPPE[3/15/02 USER: EAK -- DATE: 16MAR1997

F1: 121.718	F2: 1.000	SW1: 28571		OF1: 10322.0		PTS1d: 16384
EX: 1PULSE		PW: 7.0 usec	PD: 1.0 sec	NA: 2486	LB: 0.0	WinNuts - $EAK252

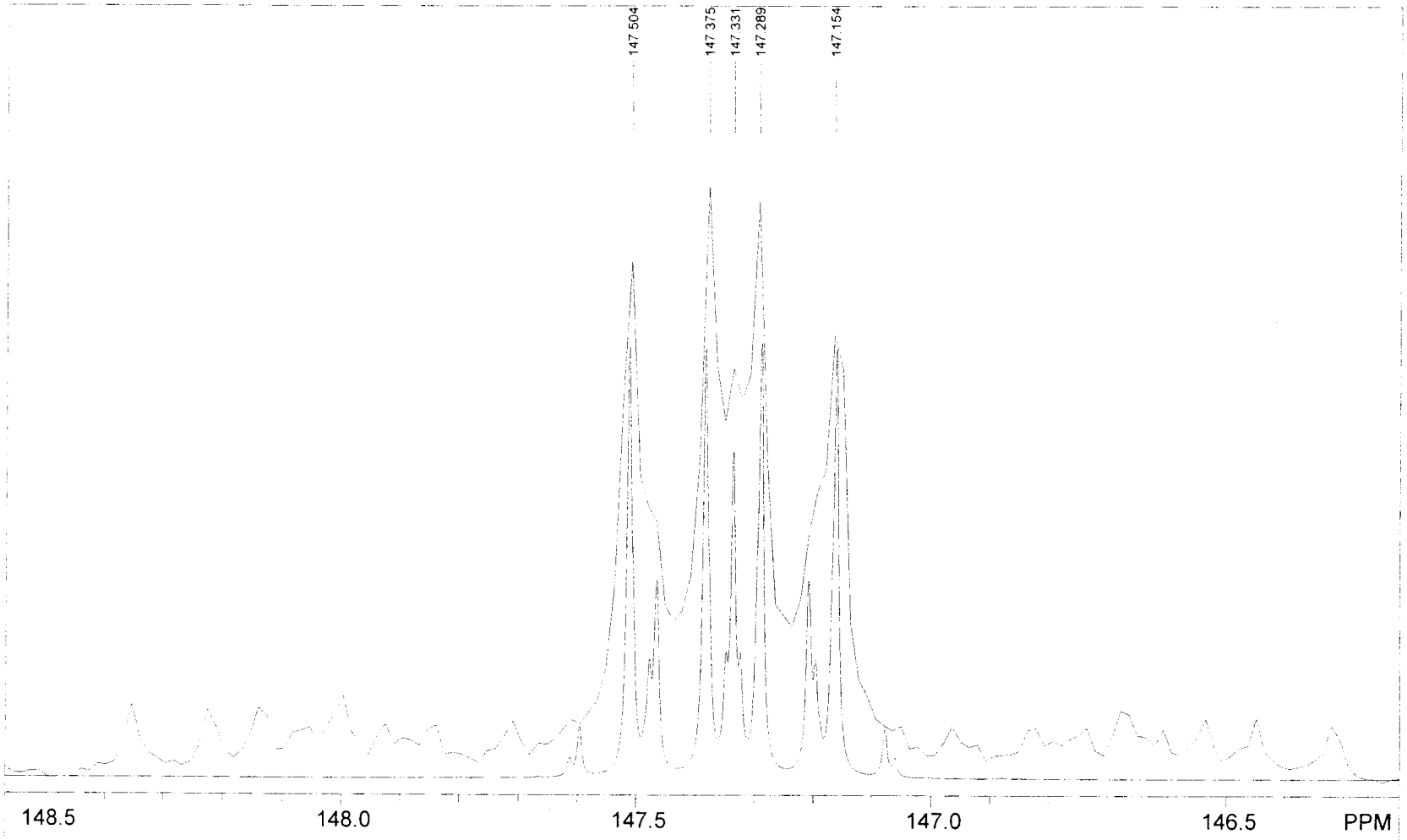

PP-46C[PROD OF W DIMER + DPPE[3/15/02 USER: EAK -- DATE: 16MAR1997

F1: 121.718	F2: 1.000	SW1: 28571		OF1: 10322.0		PTS1d: 16384
EX: 1PULSE		PW: 7.0 usec	PD: 1.0 sec	NA: 2486	LB: 0.0	WinNuts - $EAK252

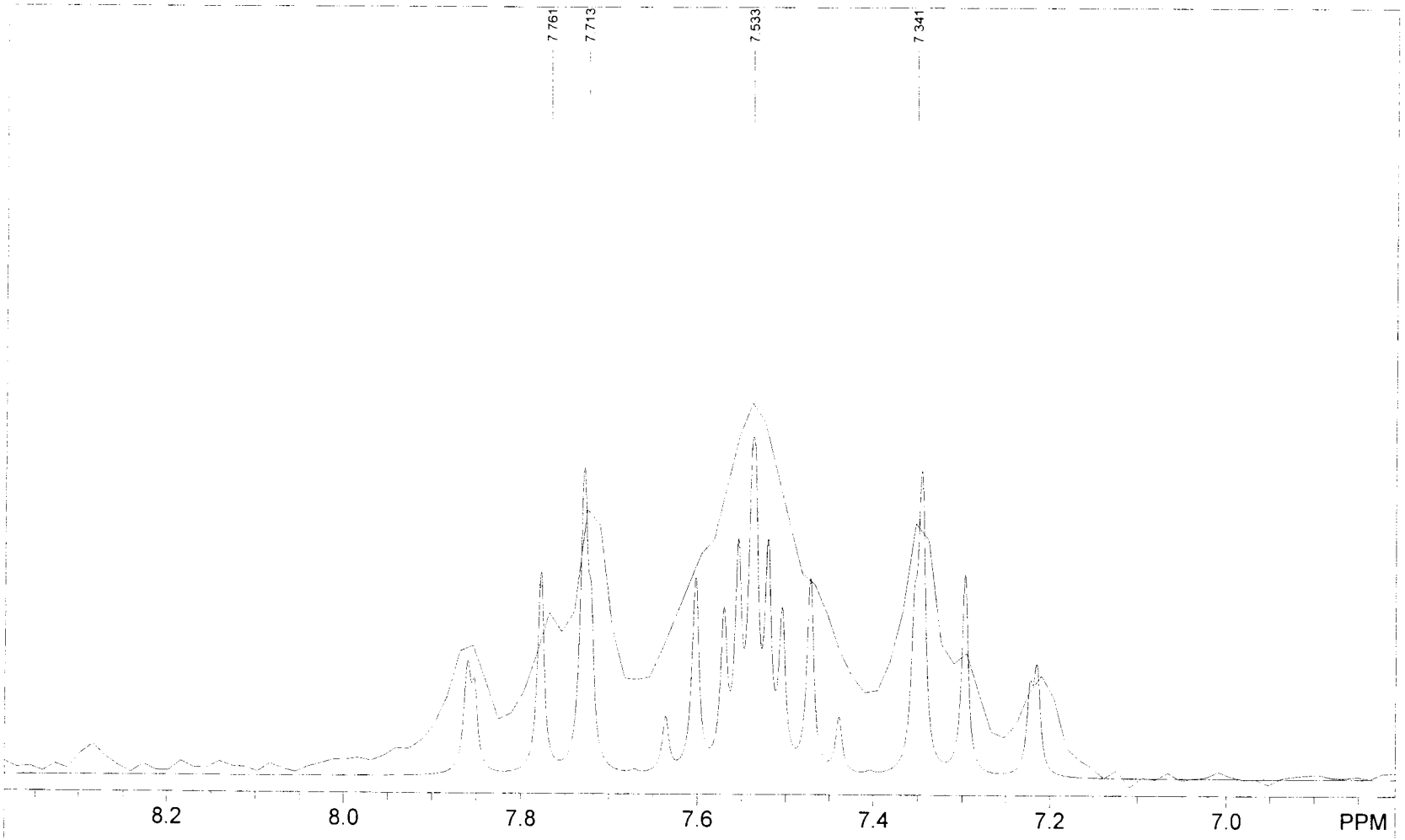

PP-46C[PROD OF W DIMER + DPPE[3/15/02 USER: EAK -- DATE: 16MAR1997

F1: 121.718	F2: 1.000	SW1: 28571		OF1: 10322.0		PTS1d: 16384
EX: 1PULSE		PW: 7.0 usec	PD: 1.0 sec	NA: 2486	LB: 0.0	WinNuts - $EAK252

Figure 16

UV/Vis spectrum of

$[(CO)_4W(\mu\text{-}PPh_2)_2W(CO)_3(\mu\text{-}\textit{trans}\text{-}PPh_2CH{=}CHPPh_2)(CO)_3W(\mu\text{-}PPh_2)_2W(CO)_4]$

(D-5- B).

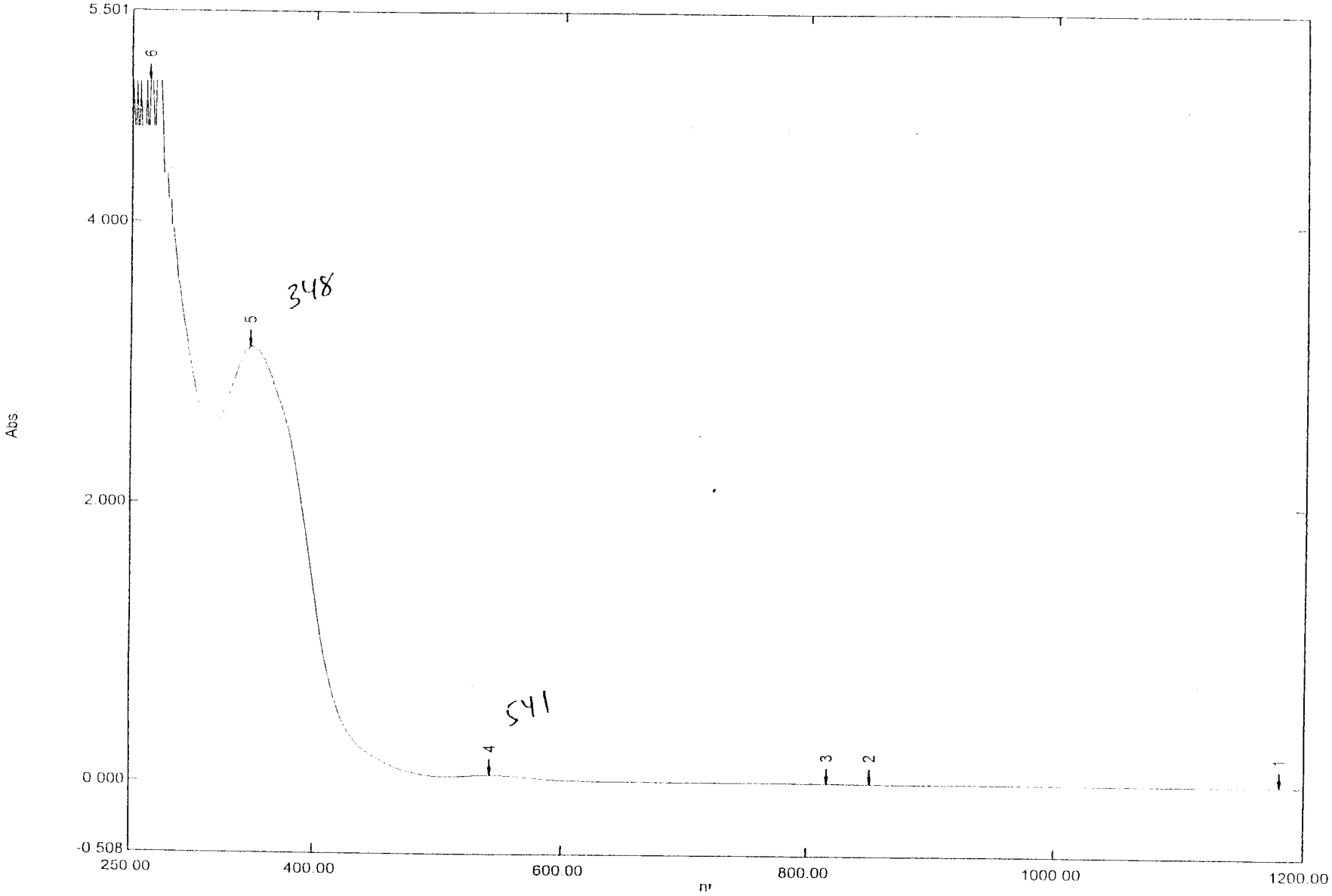
5.501
4.000
2.000
0.000
-0.508
Abs
250.00
400.00
600.00
800.00
1000.00
1200.00
nm
6
5
4
3
2
1
348
541

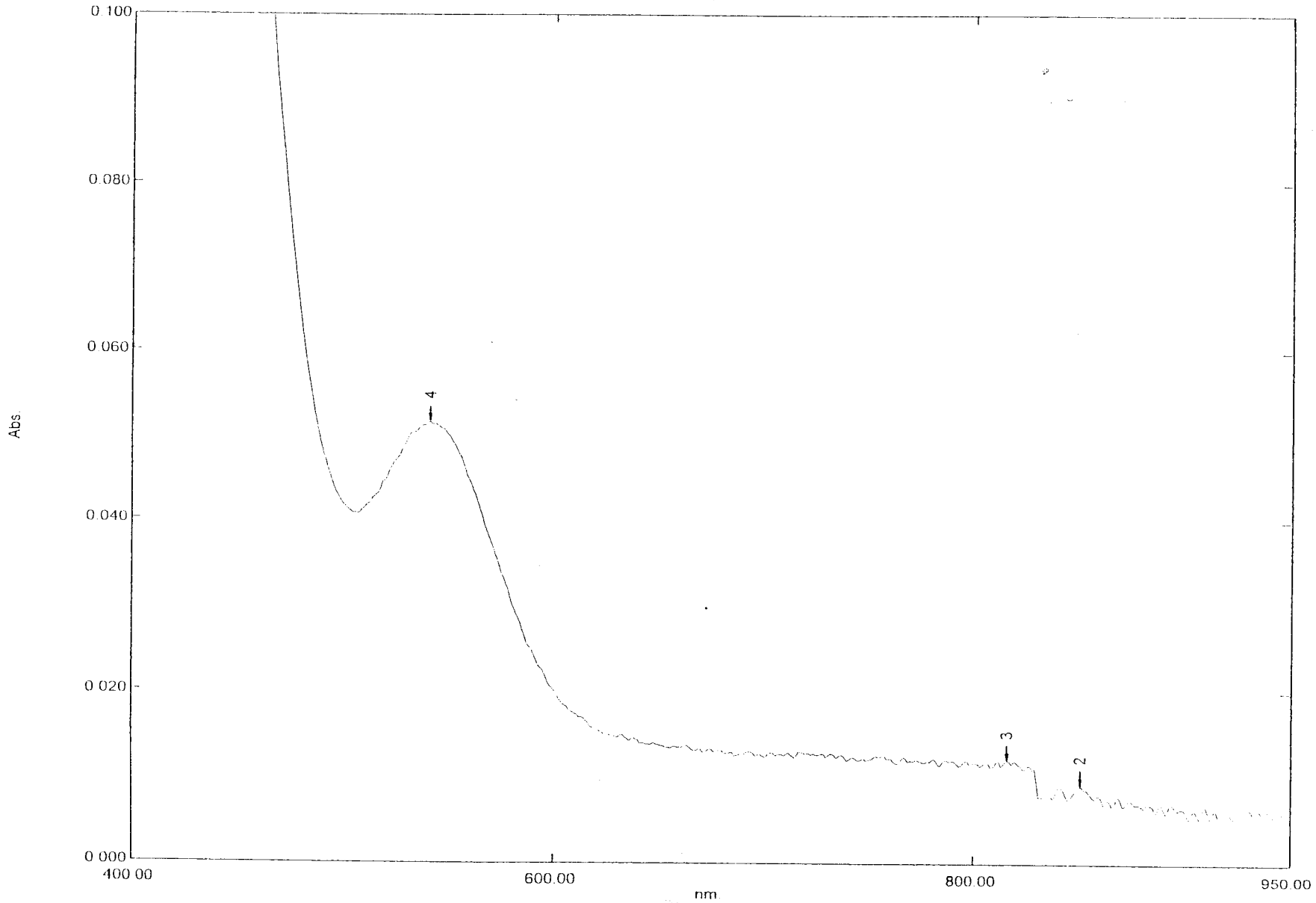
0.100
0.080
0.060
0.040
0.020
0.000
Abs.
400.00
600.00
800.00
950.00
nm.
4
3
2

Figure 17

IR spectrum of $Mo(CO)_5PPh_2H$ (E-1).

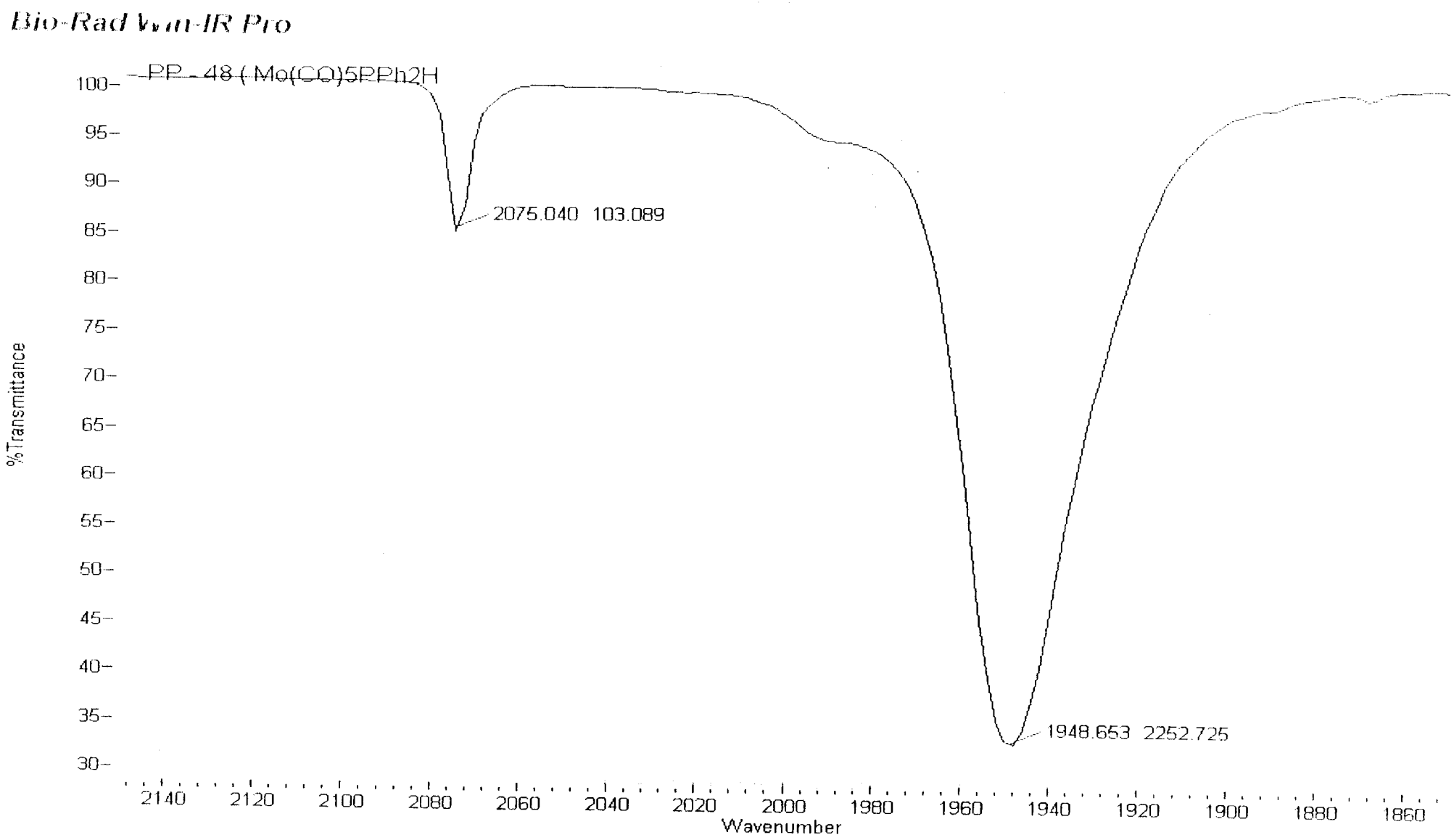
Bio-Rad Varian-IR Pro
PP-48 (Mo(CO)5PPh2H
2075.040 103.089
1948.653 2252.725
%Transmittance
100
95
90
85
80
75
70
65
60
55
50
45
40
35
30
2140
2120
2100
2080
2060
2040
2020
2000
1980
1960
1940
1920
1900
1880
1860
Wavenumber

Figure 18

IR spectrum of $[(CO)_4Mo(\mu\text{-}PPh_2)_2Mo(CO)_4]$ (E-2).

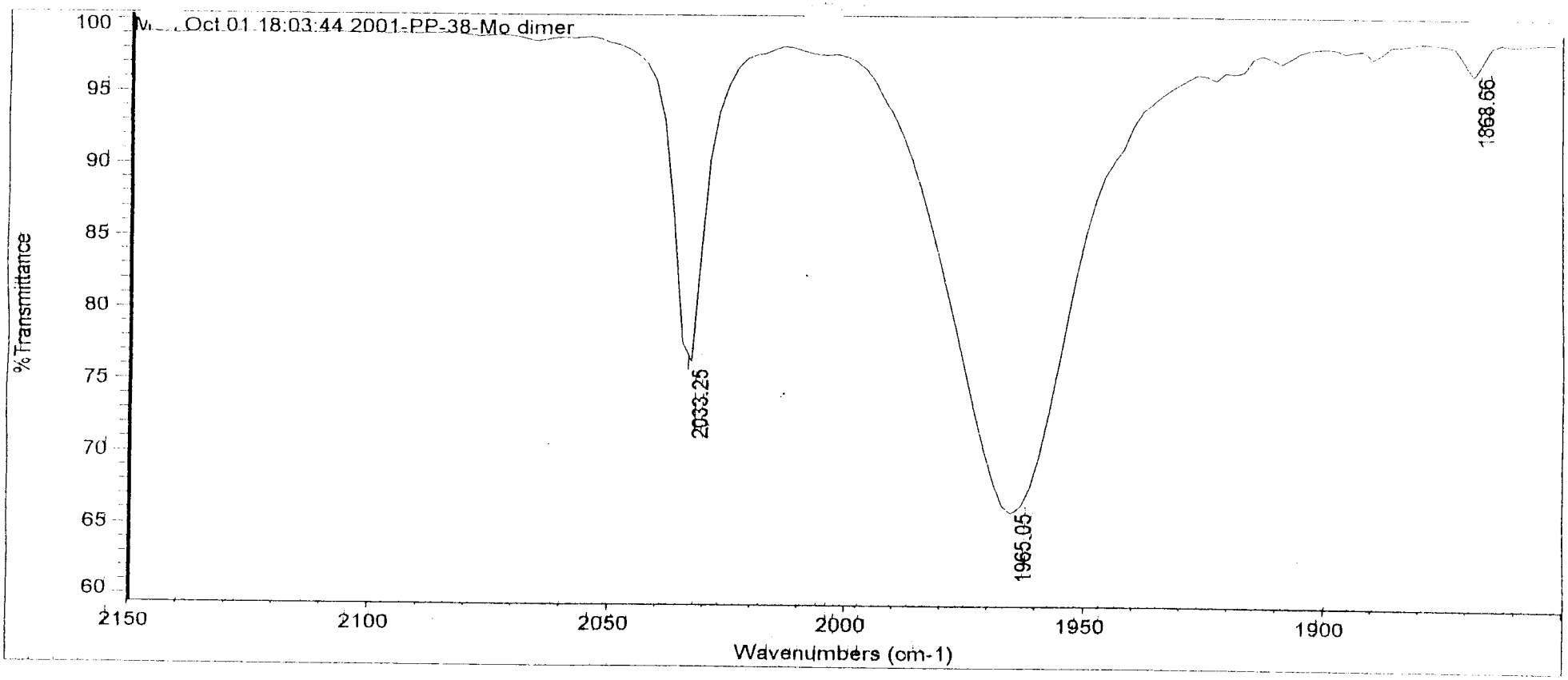

Tue Nov 27 12:48:36 2001
FIND PEAKS:

Spectrum:	Mon Oct 01 18:03:44 2001-PP-38-Mo dimer			
Region:	2150.00	1850.00		
Absolute threshold:	98.862			
Sensitivity:	50			
Peak list:				
	Position:	1965.05	Intensity:	65.972
	Position:	2033.25	Intensity:	75.829
	Position:	1868.66	Intensity:	96.447

Figure 19

IR spectrum of $[(CO)_4Mo(\mu\text{-}PPh_2)_2Mo(CO)_3(PPh_2C{\equiv}CPPh_2)]$ (E-3-A).

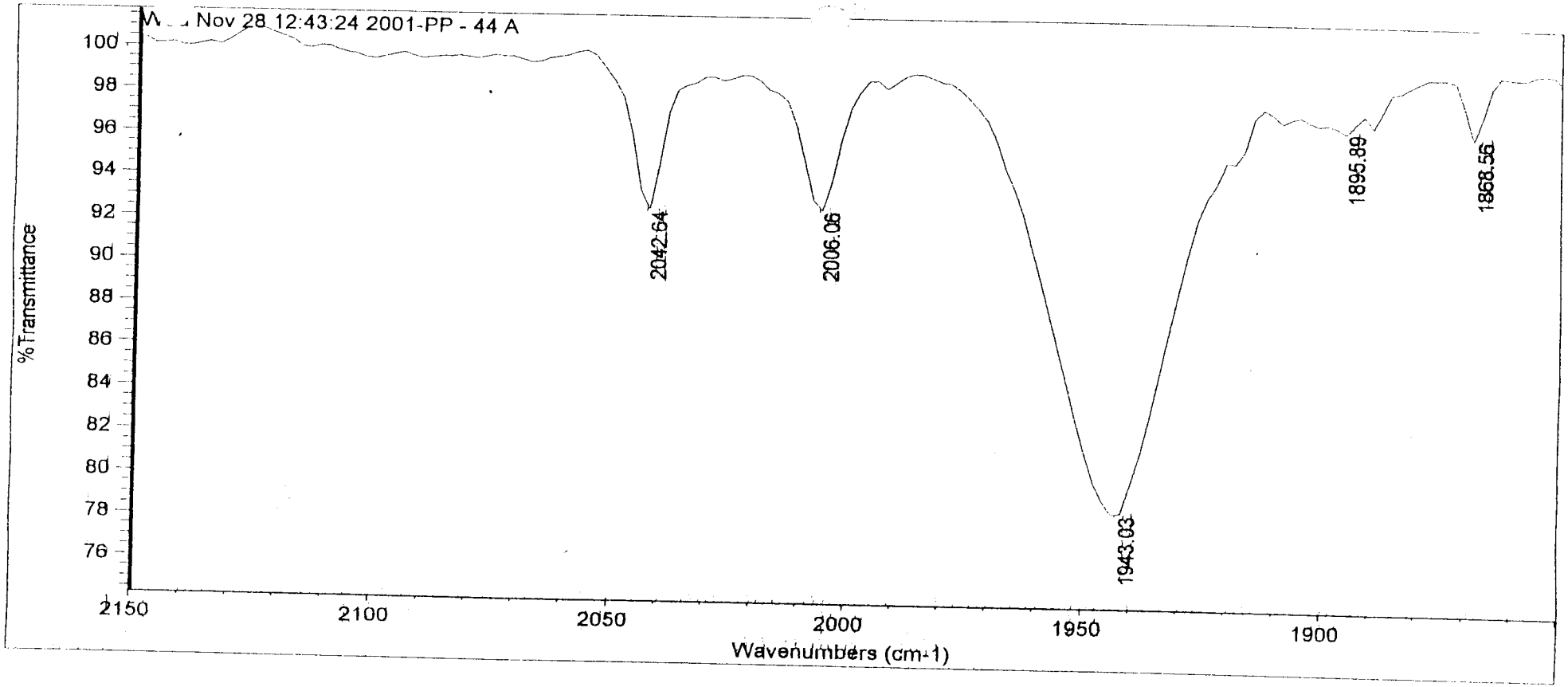

Wed Nov 28 12:49:16 2001
FIND PEAKS:

Spectrum: Wed Nov 28 12:43:24 2001-PP - 44 A
Region: 2150.00 1850.00
Absolute threshold: 99.422
Sensitivity: 50
Peak list:

Position:	1943.03	Intensity:	78.611
Position:	2042.64	Intensity:	92.589
Position:	2006.06	Intensity:	92.649
Position:	1868.56	Intensity:	96.506
Position:	1895.89	Intensity:	96.719

Figure 20

$^{31}P\{^{1}H\}$ NMR spectrum of $[(CO)_4Mo(\mu\text{-}PPh_2)_2Mo(CO)_3(PPh_2C{\equiv}CPPh_2)]$ (E-3-A).

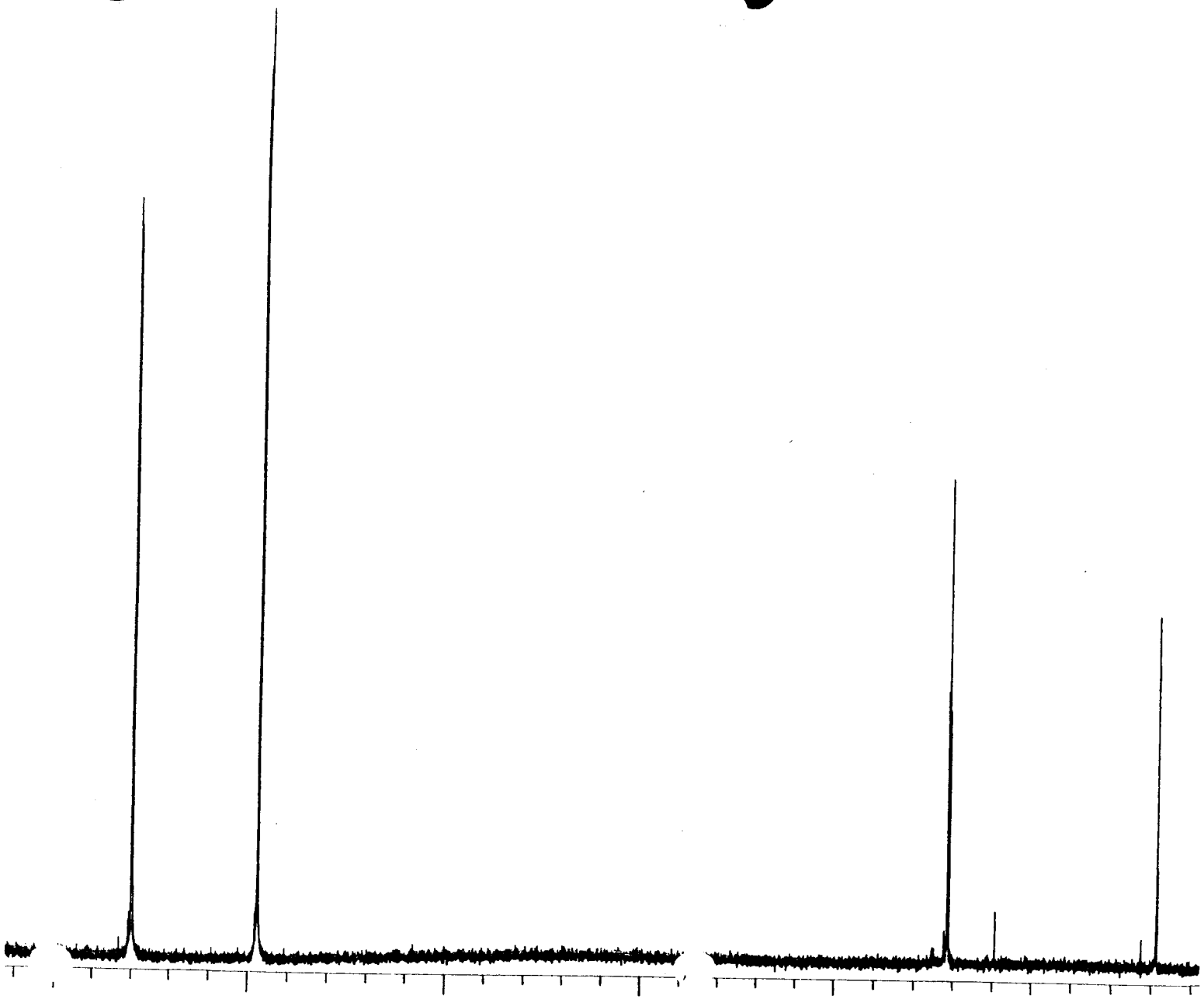

GE NMR
QE-300

EAK.231
10DEC97

PP-44A
(CO)4MO(PPH2)2MO(CO)3D

OPERATOR: EAK

ONE PULSE SEQUENCE

PULSE WIDTH	=	7
	=	3
ACQ. TIME	=	442
RECYCLE TIME	=	1
NO. OF ACQS.	=	27193
DATA SIZE	=	65536
LINE BROADNG	=	.20
SPIN RATE	=	19

OBSERVE:
FREQUENCY = 121.72(
SPEC WIDTH= 37037 HZ
GAIN = 52 +1

DECOUPLER: STANDARD-64
FREQUENCY = 4.000 PPM
POWER = 3040/ 3000
HIGH POWER ON
HIGH POWER OUTPUT =

PLOT SCALE:
1851.85 HZ/CM
15.2139 PPM/CM
FROM 281.98
TO -42.30 PPM

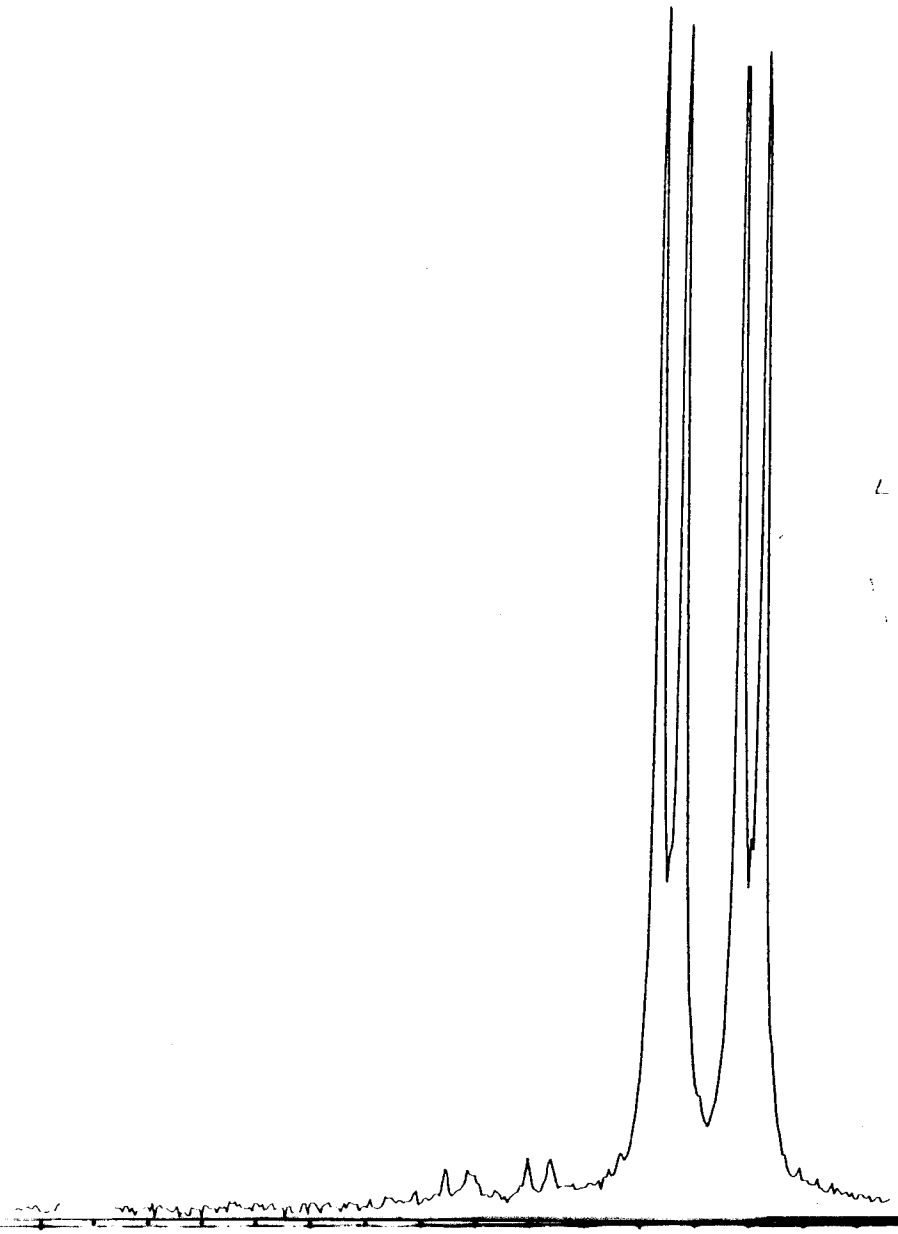

GE NMR
QE-300

EAK.231
10DEC97

PP-44A
(CO)4MO(PPH2)2MO(CO)3DPP

OPERATOR: EAK

LINE#	HEIGHT	HEIGHT(L)	FREQ(HZ)	PPM
1	144.01	146.68	27900.30	229.215
2	3068.75	3302.35	27918.74	229.366
3	1024.56	1033.73	27923.39	229.405
4	3030.57	3386.06	27928.82	229.449
5	3139.28	3414.29	27954.70	229.662
6	3185.67	3334.87	27964.77	229.745
7	185.06	189.50	27979.80	229.868
8	139.25	139.26	27984.79	229.909
9	167.02	168.99	28011.08	230.125
10	170.62	171.16	28021.04	230.207
11	131.96	134.27	28047.79	230.427
12	135.31	143.11	28057.80	230.509

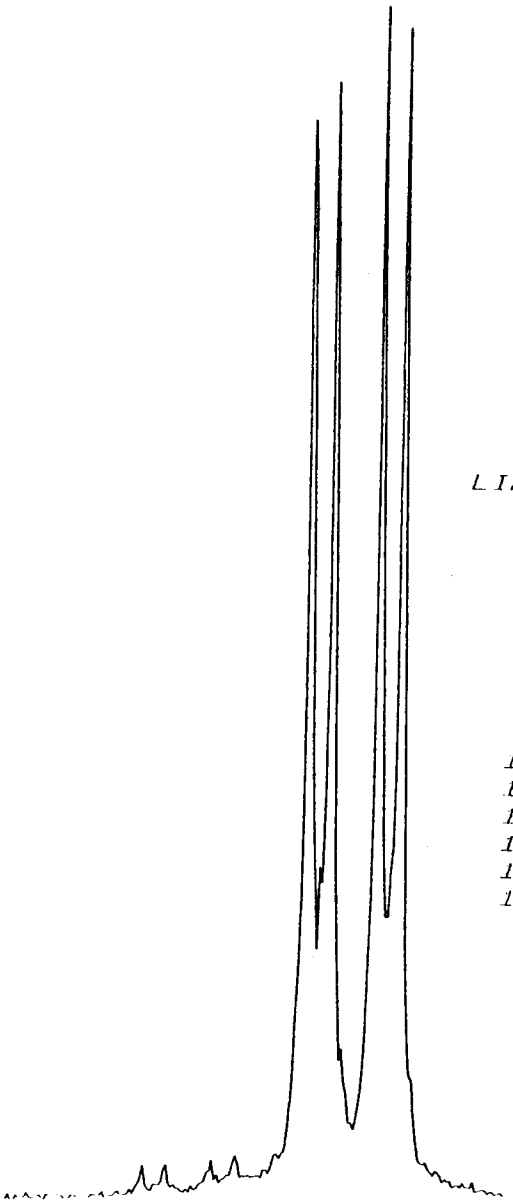

GE NMR
QE-300

EAK.231
10DEC97

PP-44A
(CO)4MO(PPH2)2MO(CO)3DPPA

OPERATOR: EAK

LINE#	HEIGHT	HEIGHT(L)	FREQ(HZ)	PPM
1	160.98	161.59	23975.48	196.971
2	197.08	198.48	23980.43	197.011
3	3919.18	3966.93	23992.77	197.113
4	3992.30	3995.03	24002.83	197.196
5	335.73	338.63	24014.64	197.292
6	586.87	592.58	24018.90	197.327
7	3738.76	3990.08	24023.89	197.368
8	1177.98	1204.39	24028.38	197.405
9	3614.97	4065.57	24033.93	197.451
10	227.75	228.94	24047.17	197.560
11	156.62	161.73	24052.01	197.599
12	216.68	217.41	24064.81	197.704
13	199.56	204.57	24075.37	197.791
14	177.00	186.43	24095.84	197.959
15	172.73	180.57	24105.93	198.042

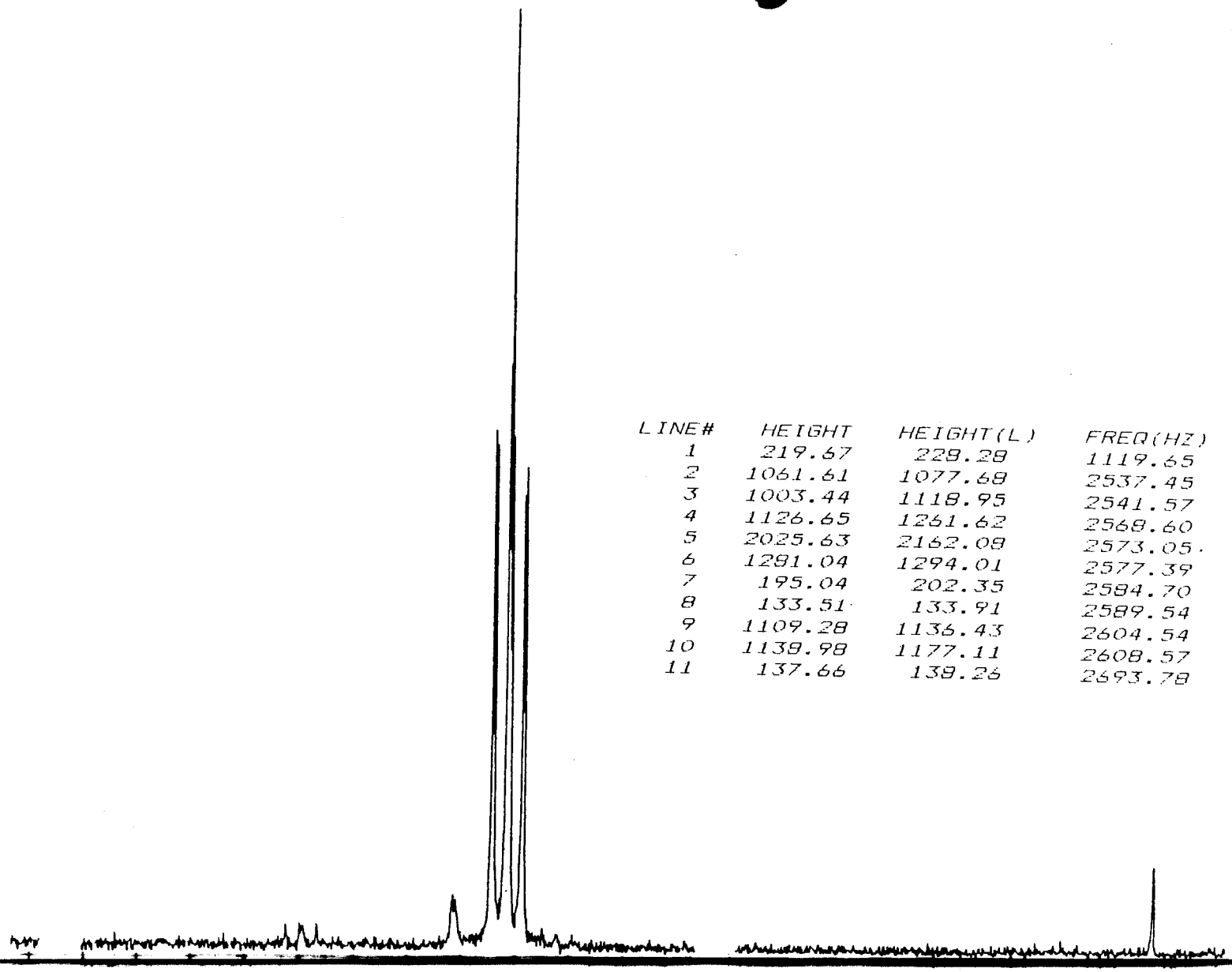

GE NMR
QE-300

EAK.231
10DEC97

PP-44A
(CO)4MO(PPH2)2MO(CO)3DP

OPERATOR: EAK

LINE#	HEIGHT	HEIGHT(L)	FREQ(HZ)	PPM
1	219.67	228.28	1119.65	9.198
2	1061.61	1077.68	2537.45	20.846
3	1003.44	1118.95	2541.57	20.880
4	1126.65	1261.62	2568.60	21.102
5	2025.63	2162.08	2573.05	21.138
6	1291.04	1294.01	2577.39	21.174
7	195.04	202.35	2584.70	21.234
8	133.51	133.91	2589.54	21.274
9	1109.28	1136.43	2604.54	21.397
10	1138.98	1177.11	2608.57	21.430
11	137.66	138.26	2693.78	22.130

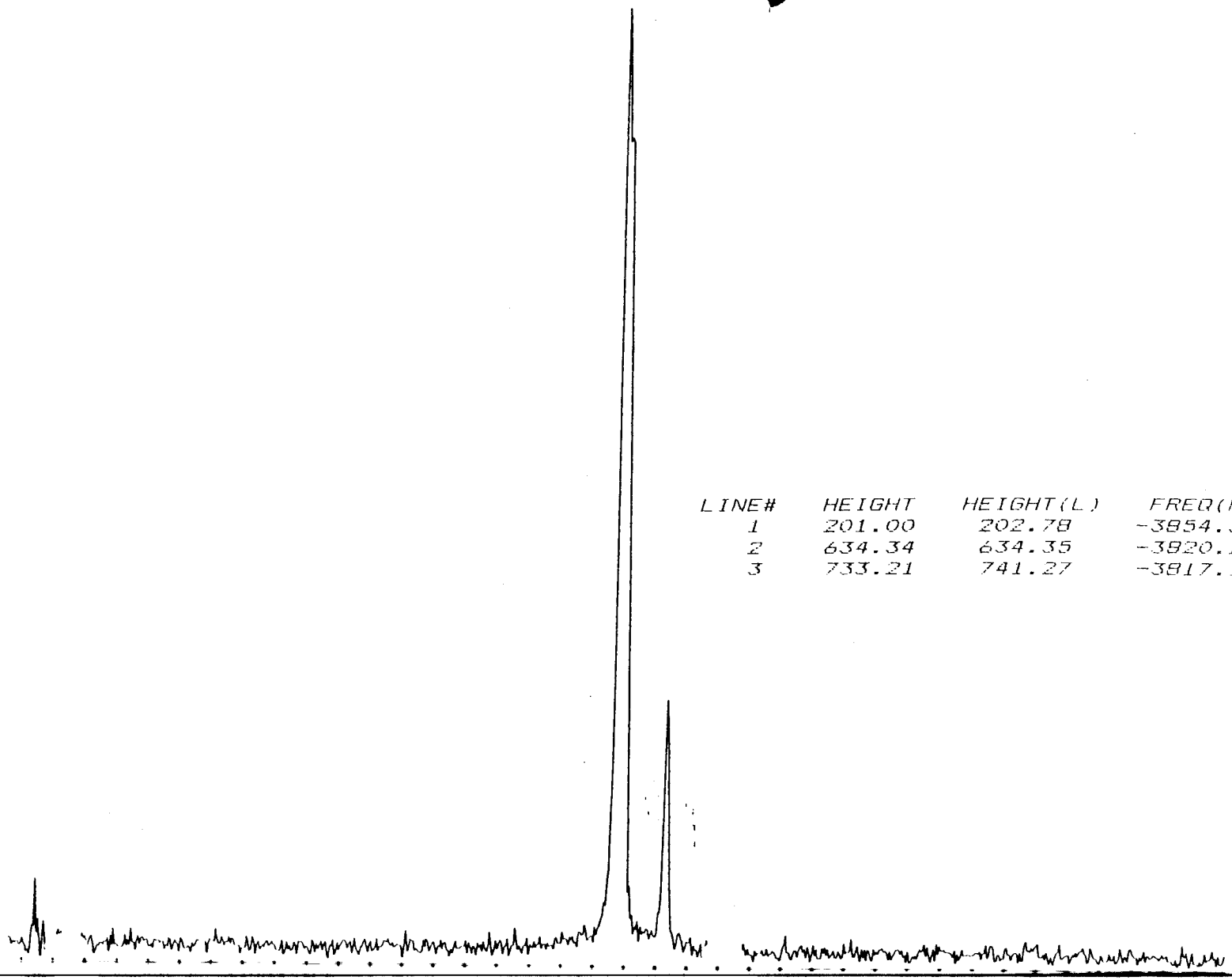

GE NMR
QE-300

EAK.231
10DEC97

PP-44A
(CO)4MO(PPH2)2MO(CO)3DPP

OPERATOR: EAK

LINE#	HEIGHT	HEIGHT(L)	FREQ(HZ)	PPM
1	201.00	202.78	-3854.30	-31.665
2	634.34	634.35	-3820.22	-31.385
3	733.21	741.27	-3817.11	-31.359

Figure 21

UV/Vis spectrum of $[(CO)_4Mo(\mu\text{-}PPh_2)_2Mo(CO)_3(PPh_2C{\equiv}CPPh_2)]$

(E-3-A)

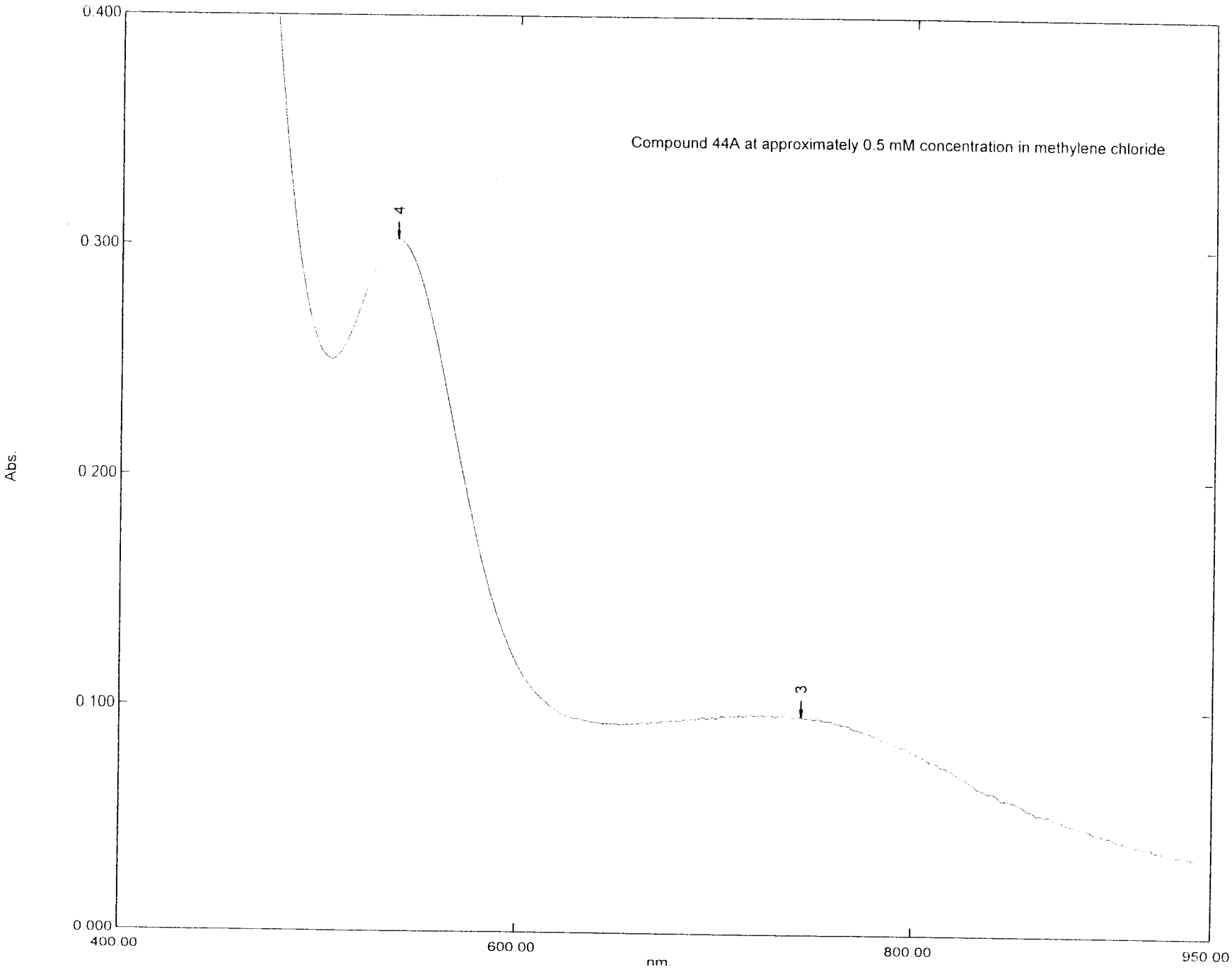
Compound 44A at approximately 0.5 mM concentration in methylene chloride
0.400
0.300
0.200
0.100
0.000
Abs.
400.00
600.00
800.00
950.00
nm.
4
3

Figure 22

IR spectrum of

$[(CO)_4Mo(\mu\text{-}PPh_2)_2Mo(CO)_3\ (\mu\text{-}PPh_2C{\equiv}CPPh_2)\ (CO)_3Mo(\mu\text{-}PPh_2)_2Mo(CO)_4]$

(E-3-B).

Figure 23

$^{31}P\ \{^{1}H\}$ NMR spectrum of

$[(CO)_4Mo(\mu\text{-}PPh_2)_2Mo(CO)_3\ (\mu\text{-}PPh_2C{\equiv}CPPh_2)\ (CO)_3Mo(\mu\text{-}PPh_2)_2Mo(CO)_4]$

(E-3-B).

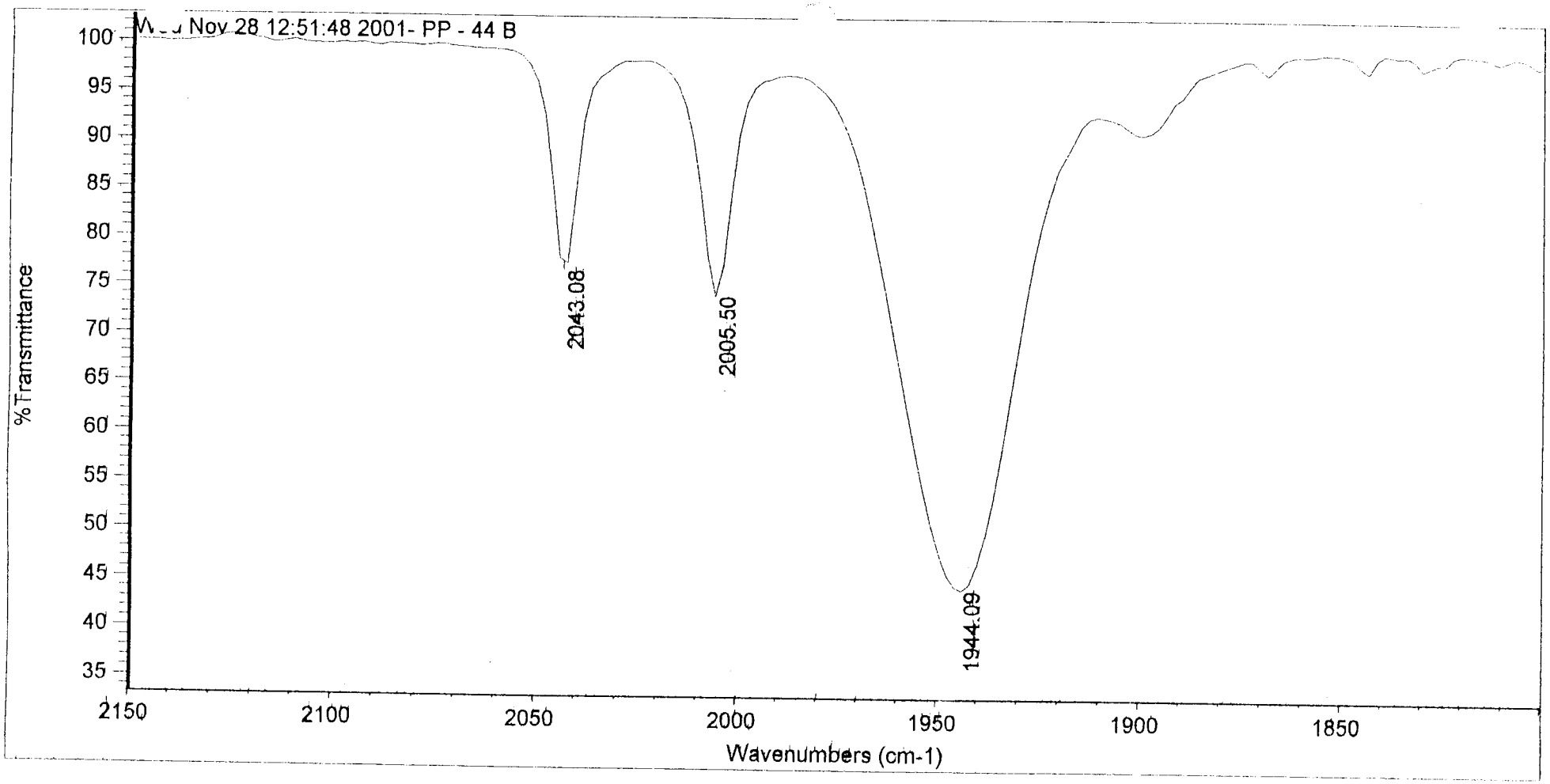

Wed Nov 28 12:58:47 2001
FIND PEAKS:

Spectrum:	Wed Nov 28 12:51:48 2001- PP - 44 B	
Region:	2150.00	1800.00
Absolute threshold:	98.186	
Sensitivity:	50	
Peak list:		

Position:	1944.09	Intensity:	44.310
Position:	2005.50	Intensity:	74.186
Position:	2043.08	Intensity:	76.793

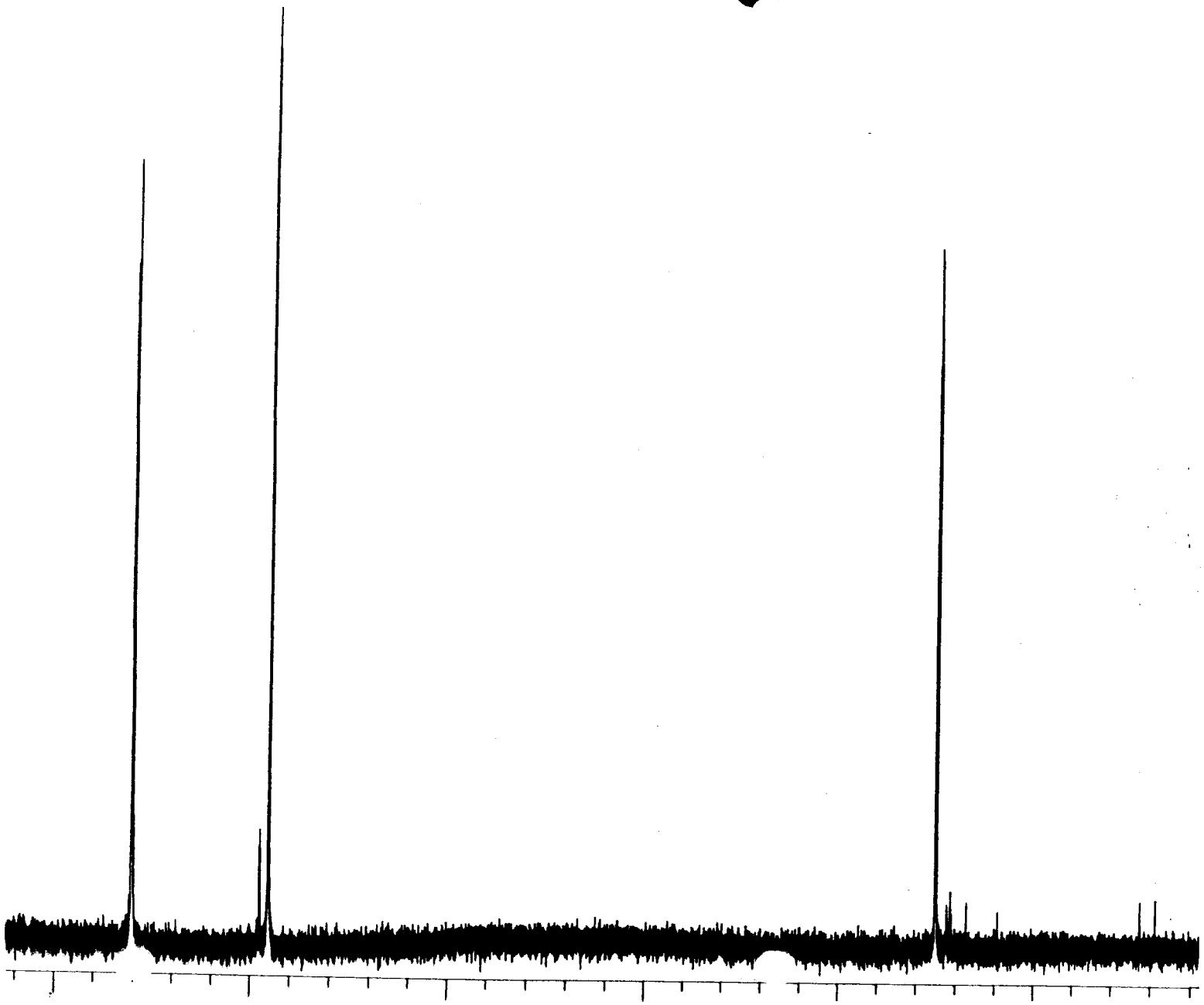

GE NMR
QE-300

EAK.232
11DEC97

PP-448
MO-MO-DPPA-MO-MO
~~12/11/01~~ 12/10/01

OPERATOR: EAK

ONE PULSE SEQUENCE

PULSE WIDTH = 7.00 USEC
= 36 DEGREE
ACQ. TIME = 442.37 MSEC
RECYCLE TIME = 1.88 SEC

NO. OF ACQS. = 11784
DATA SIZE = 65536
LINE BROADNG = .20 HZ
SPIN RATE = 19 RPS

OBSERVE:
FREQUENCY = 121.720872 MHZ
SPEC WIDTH = 37037 HZ
GAIN = 52 *1

DECOUPLER: STANDARD-64 MODULAT:
FREQUENCY = 4.000 PPM
POWER = 3040/ 3000
HIGH POWER ON
HIGH POWER OUTPUT = 63 DB

PLOT SCALE:
1851.85 HZ/CM
15.2139 PPM/CM
FROM 261.96
TO -42.30 PPM

EAK.232
12/10/01

PP-44B

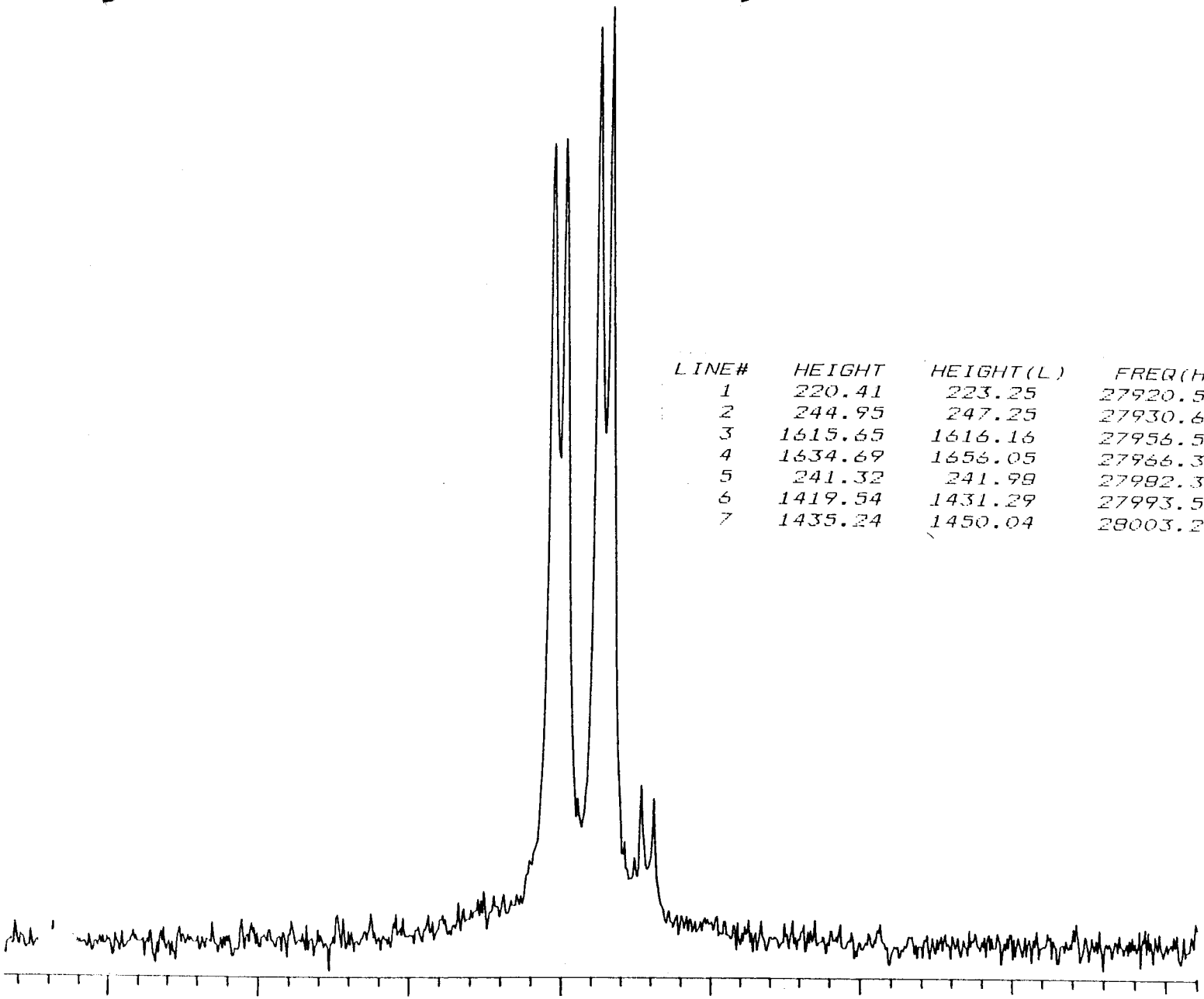

LINE#	HEIGHT	HEIGHT(L)	FREQ(HZ)	PPM
1	220.41	223.25	27920.52	229.381
2	244.95	247.25	27930.69	229.465
3	1615.65	1616.16	27956.56	229.677
4	1634.69	1656.05	27966.35	229.758
5	241.32	241.98	27982.36	229.889
6	1419.54	1431.29	27993.51	229.981
7	1435.24	1450.04	28003.23	230.061

EAK.232
12/10/01

PP-448

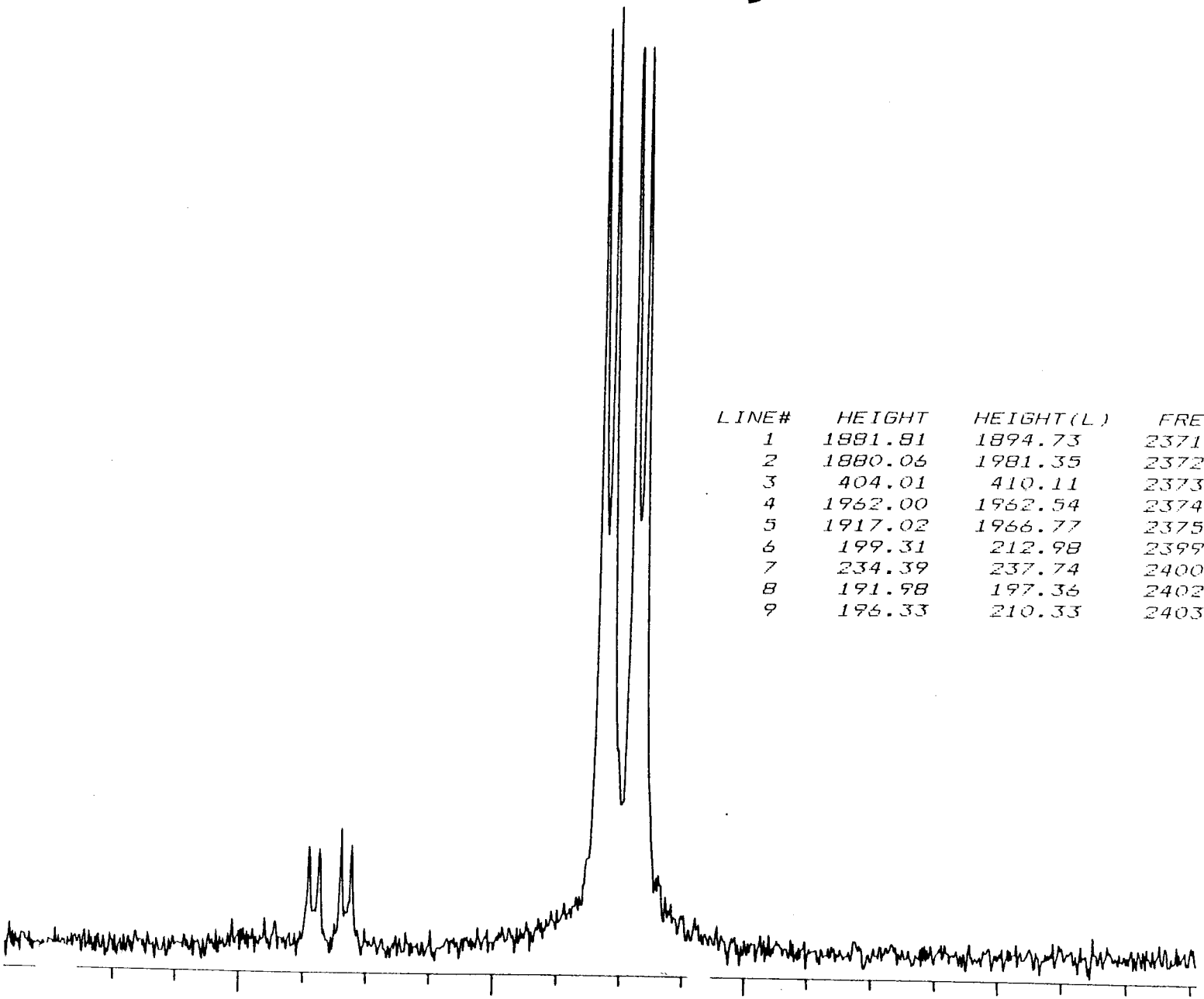

LINE#	HEIGHT	HEIGHT(L)	FREQ(HZ)	PPM
1	1881.81	1894.73	23713.23	194.816
2	1880.06	1981.35	23723.02	194.896
3	404.01	410.11	23737.68	195.017
4	1962.00	1962.54	23743.99	195.069
5	1917.02	1966.77	23753.75	195.149
6	199.31	212.98	23991.87	197.105
7	234.39	237.74	24001.81	197.187
8	191.98	197.36	24022.78	197.359
9	196.33	210.33	24032.90	197.442

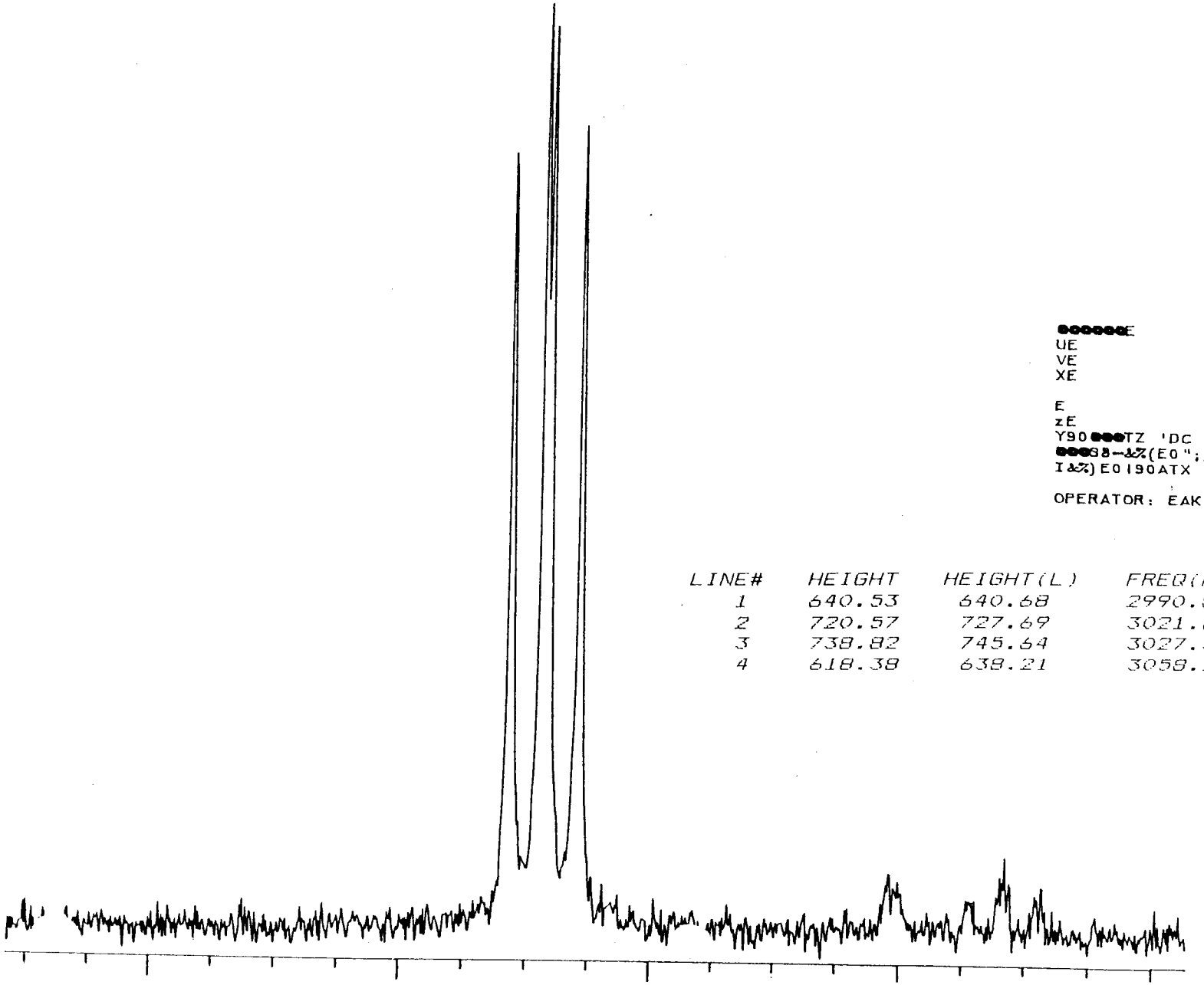

GE NMR
QE-300

EAK.232
11DEC97

PP-44B
(CO)4MO(PPH2)2MO(CO)3DI

[redacted]E
UE
VE
XE

E
zE
Y90[redacted]TZ 'DC
[redacted]8-&%(E0";.TA0$[redacted]"8(E
I&%)E0190ATX

OPERATOR: EAK

LINE#	HEIGHT	HEIGHT(L)	FREQ(HZ)	PPM
1	640.53	640.68	2990.83	24.371
2	720.57	727.69	3021.68	24.824
3	738.82	745.64	3027.34	24.871
4	618.38	638.21	3058.21	25.124

Figure 24

IR spectrum of $[(CO)_4Mo(\mu\text{-}PPh_2)_2Mo(CO)_3(\textit{trans}\text{-}PPh_2CH{=}CHPPh_2)$ (E-4-A).

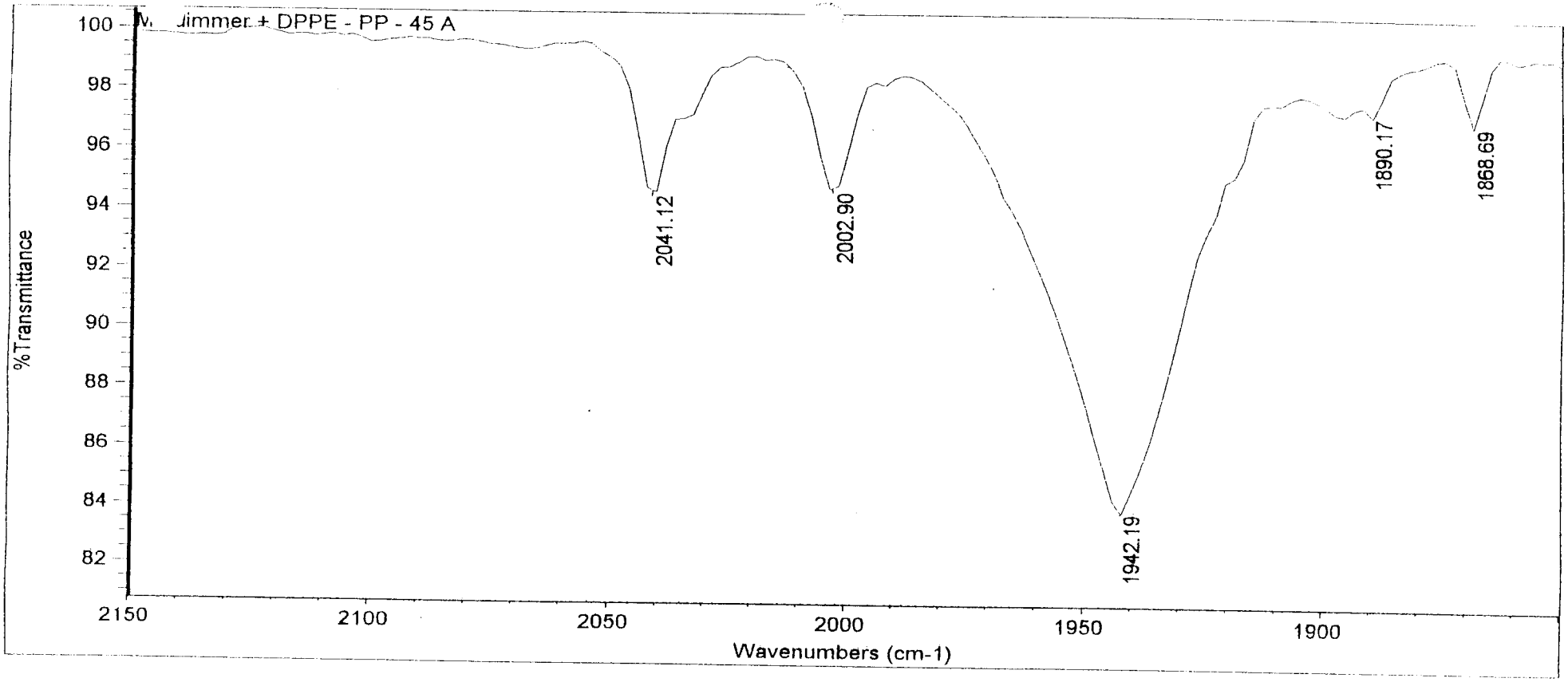

Tue Jan 08 22:15:31 2002
FIND PEAKS:

Spectrum: Mo dimmer + DPPE - PP - 45 A
Region: 2150.00 1850.00
Absolute threshold: 99.186
Sensitivity: 50
Peak list:

Position:	1942.19	Intensity:	83.915
Position:	2041.12	Intensity:	94.505
Position:	2002.90	Intensity:	94.676
Position:	1868.69	Intensity:	97.073
Position:	1890.17	Intensity:	97.344

Figure 25

$^{31}P\ \{^{1}H\}$ NMR spectrum of $(CO)_4Mo(\mu\text{-}PPh_2)_2Mo(CO)_3$(*trans*-$PPh_2CH{=}CHPPh_2$) (E-4-A).

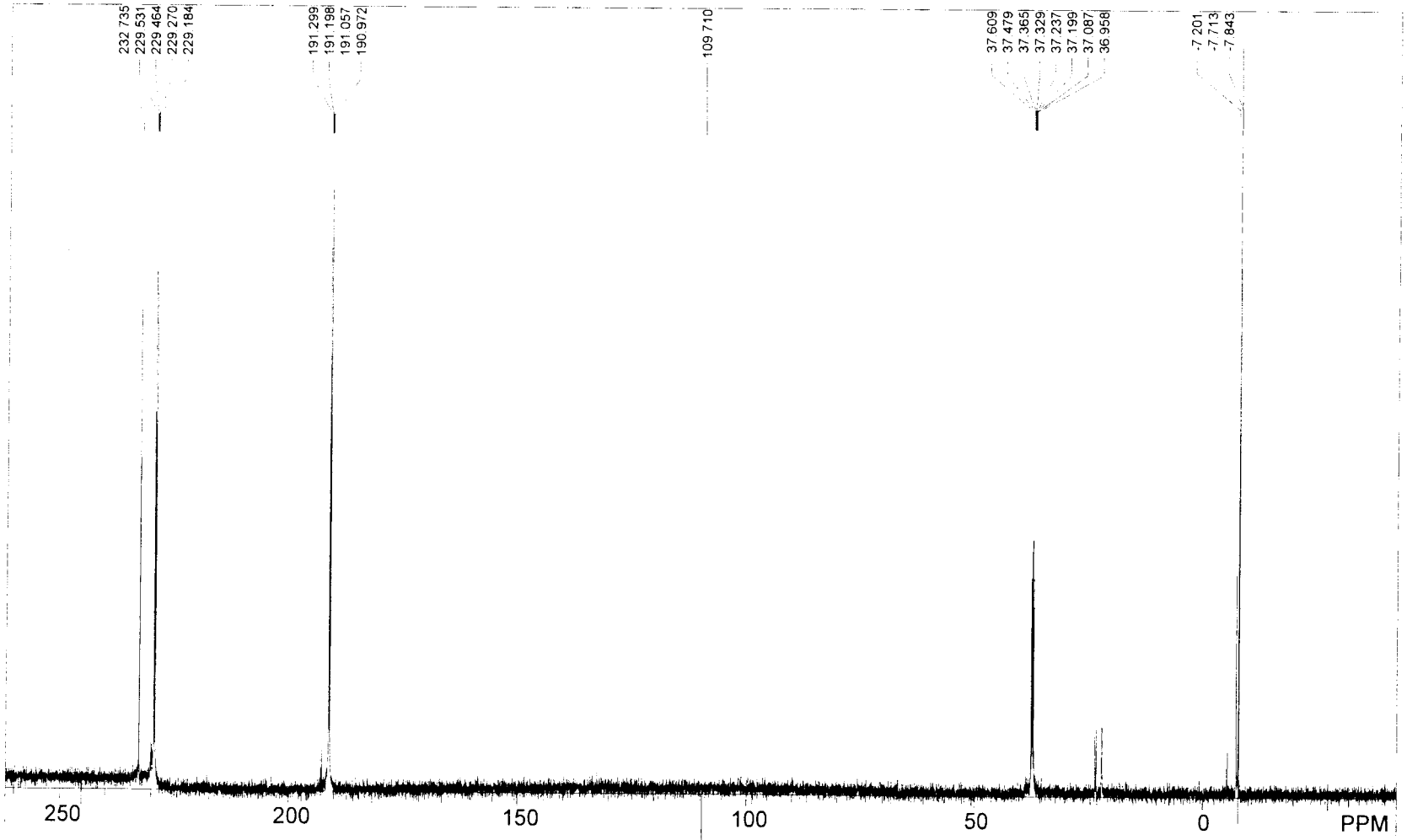

PP-45A[1/21/02

USER: EAK -- DATE: 22JAN1998

F1: 121.721	F2: 1.000	SW1: 37037		OF1: 13355.1		PTS1d: 16384
EX: 1PULSE		PW: 7.0 usec	PD: 1.0 sec	NA: 3092	LB: 0.0	WinNuts - $EAK.241

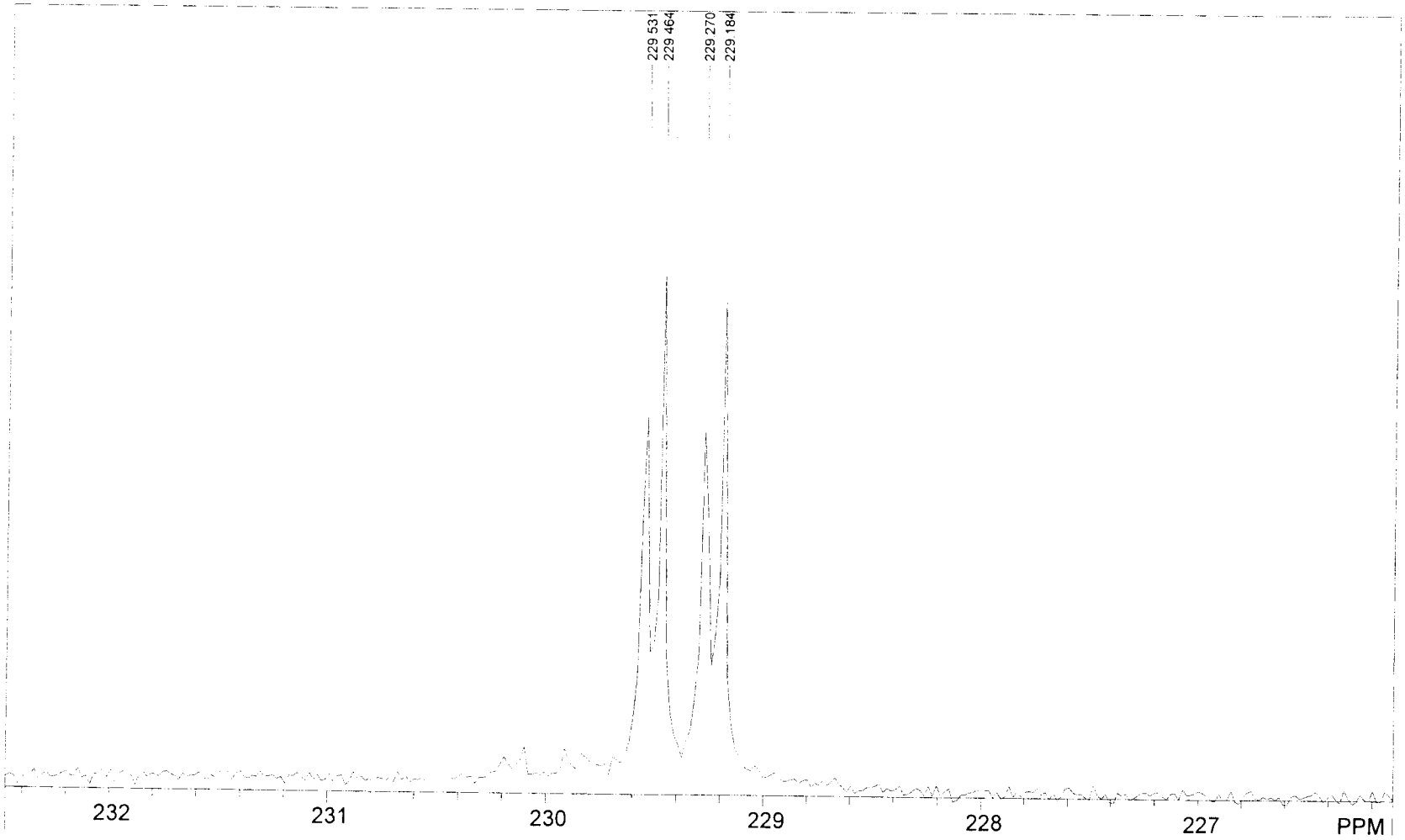

PP-45A[1/21/02

F1: 121.721	F2: 1.000	SW1: 37037		OF1: 13355.1		USER: EAK -- DATE: 22JAN1998
EX: 1PULSE		PW: 7.0 usec	PD: 1.0 sec	NA: 3092	LB: 0.0	PTS1d: 16384
						WinNuts - $EAK.241

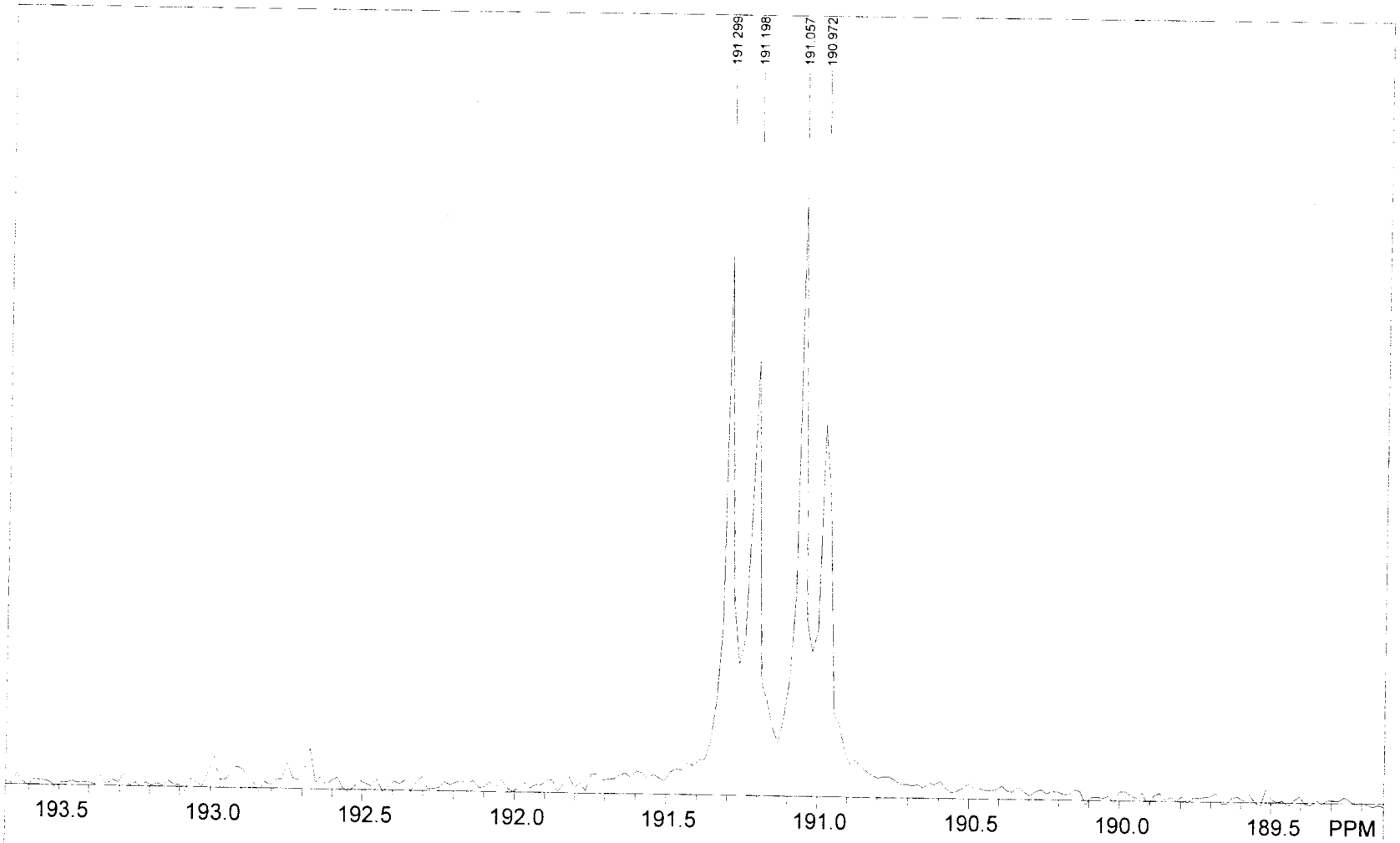

PP-45A[1/21/02

F1: 121.721	F2: 1.000	SW1: 37037		OF1: 13355.1		USER: EAK -- DATE: 22JAN1998
EX: 1PULSE		PW: 7.0 usec	PD: 1.0 sec	NA: 3092	LB: 0.0	PTS1d: 16384
						WinNuts - $EAK.241

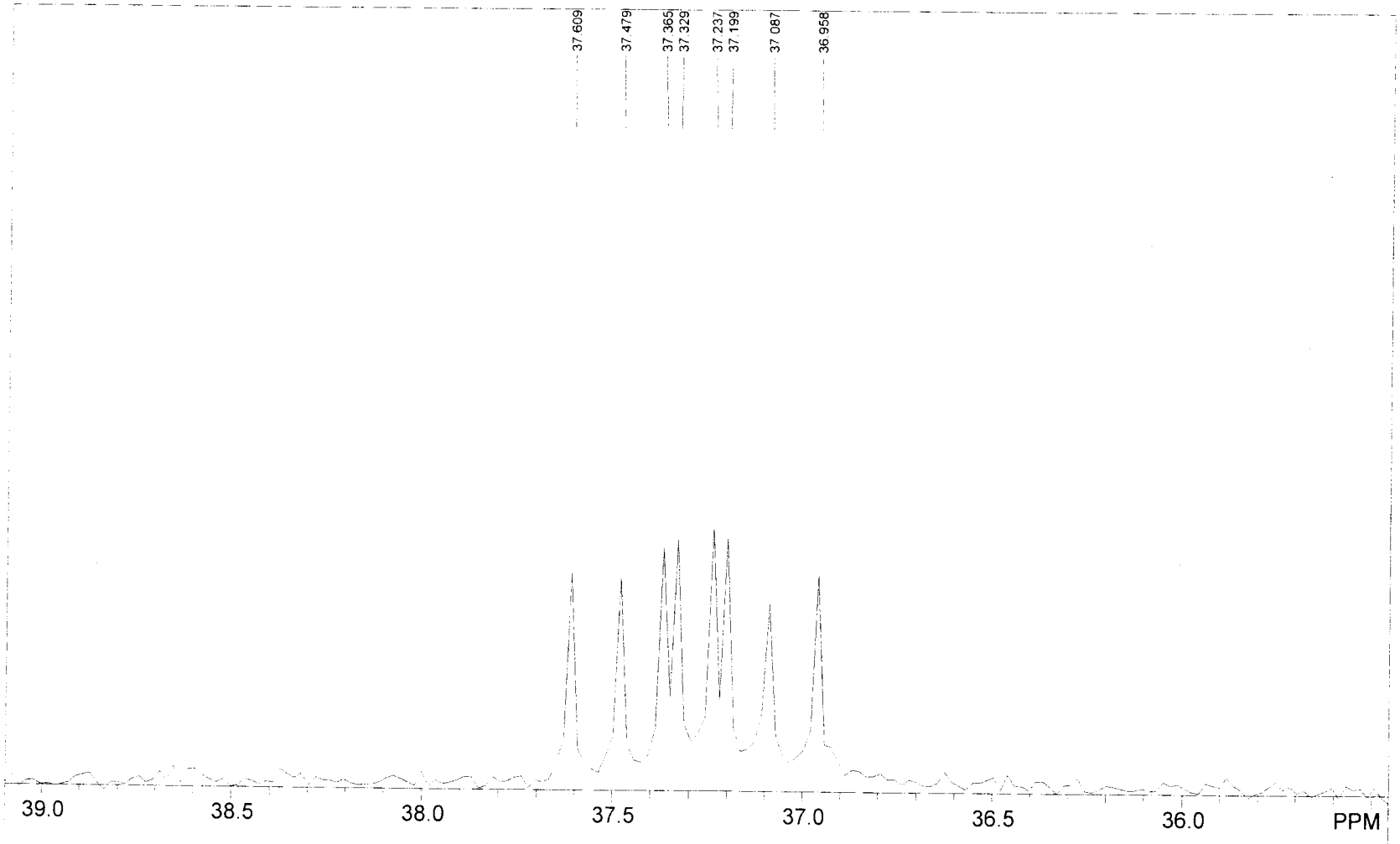

PP-45A[1/21/02

F1: 121.721	F2: 1.000	SW1: 37037		OF1: 13355.1		USER: EAK -- DATE: 22JAN1998
EX: 1PULSE		PW: 7.0 usec	PD: 1.0 sec	NA: 3092	LB: 0.0	PTS1d: 16384
						WinNuts - $EAK.241

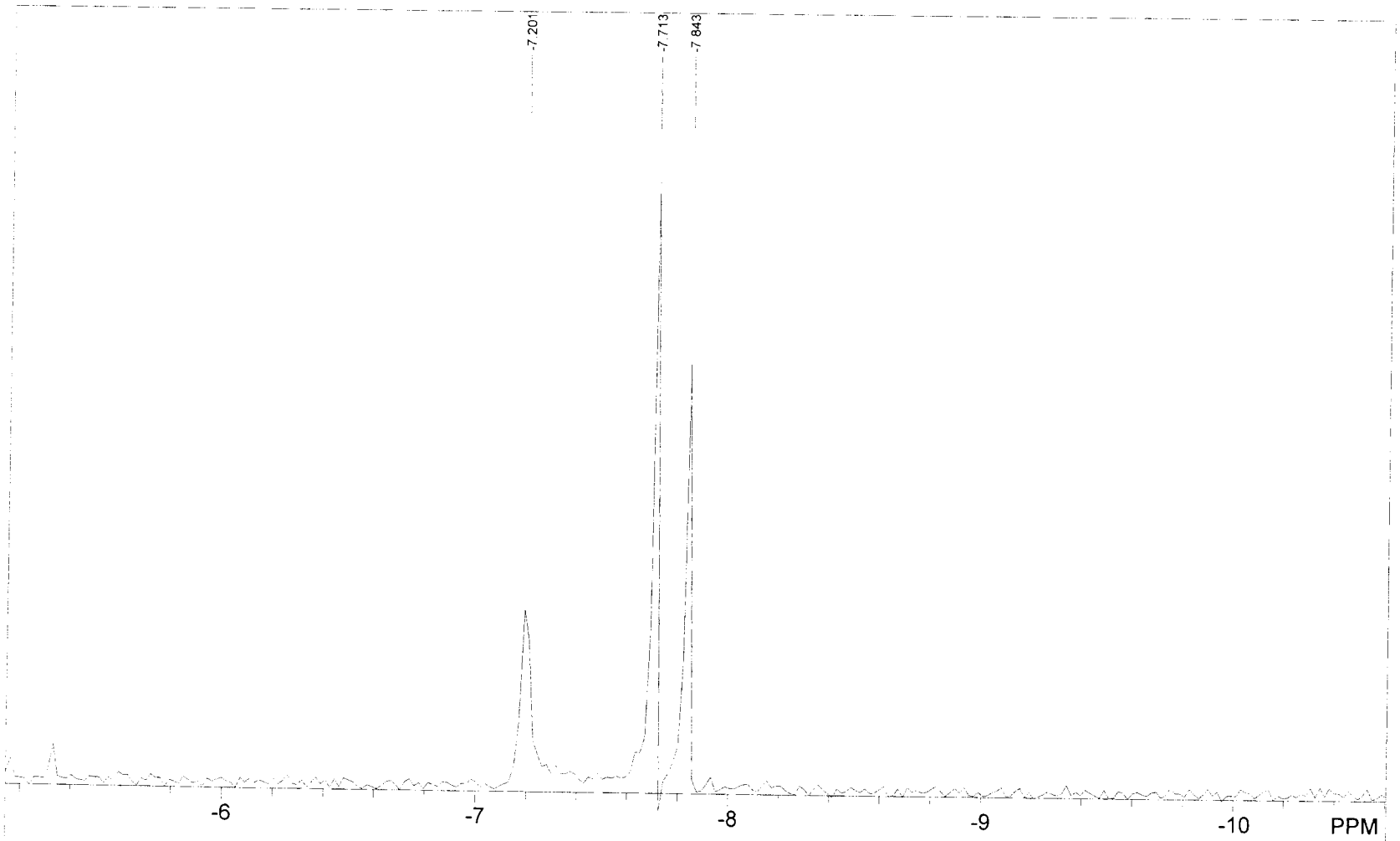

PP-45A[1/21/02

F1: 121.721	F2: 1.000	SW1: 37037		OF1: 13355.1		USER: EAK -- DATE: 22JAN1998
EX: 1PULSE		PW: 7.0 usec	PD: 1.0 sec	NA: 3092	LB: 0.0	PTS1d: 16384
						WinNuts - $EAK.241

Figure 26

$^{31}P\{^{1}H\}$ NMR spectrum of

$[(CO)_4Mo(\mu\text{-}PPh_2)_2Mo(CO)_3\text{-}(\mu\text{-}trans\text{-}PPh_2CH{=}CHPPh_2)(CO)_3Mo(\mu\text{-}PPh_2)_2Mo(CO)_4]$

(E-4-B).

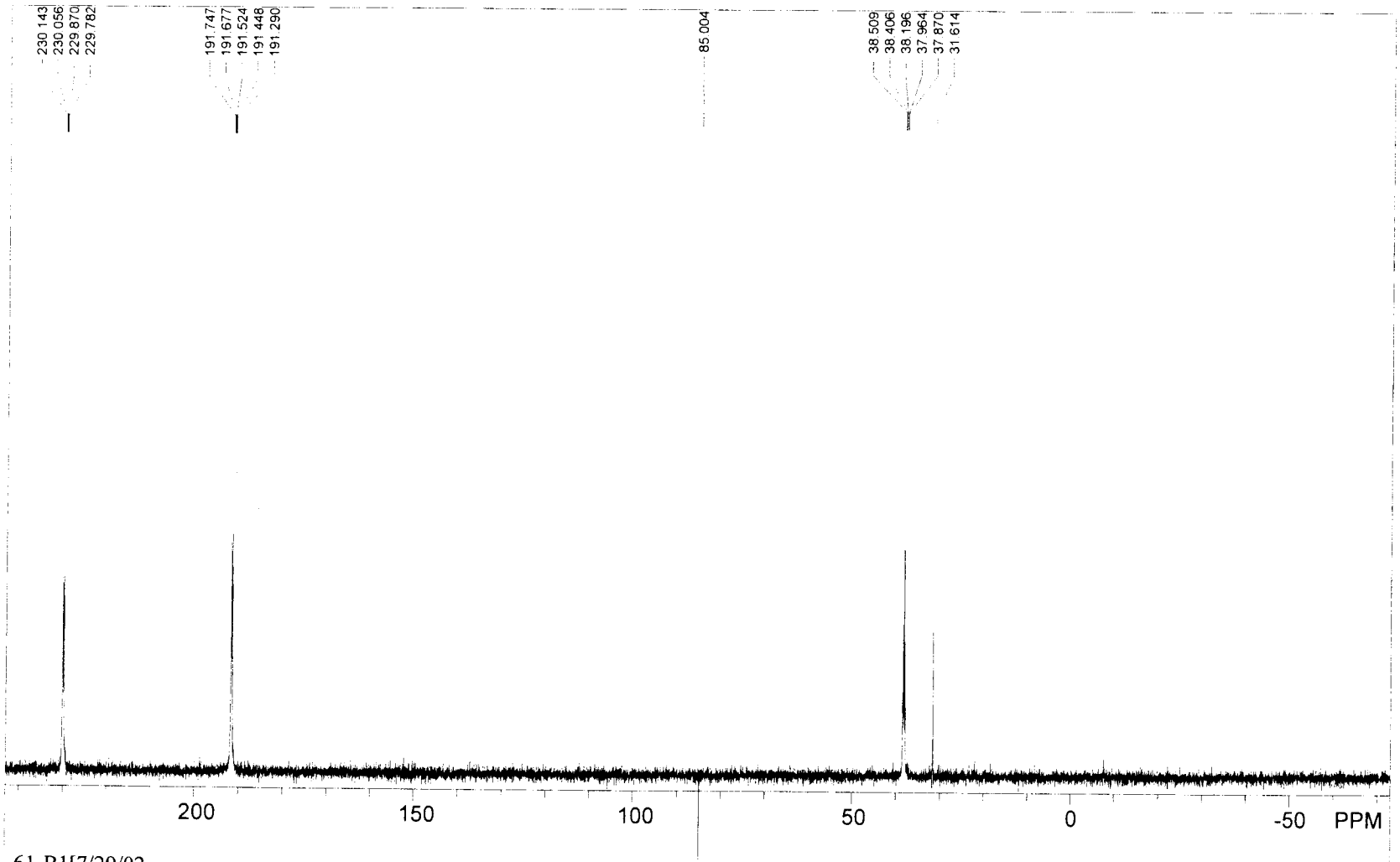

61-B1[7/29/02

USER: GAH -- DATE: 30JUL1997

F1: 121.718	SW1: 38462		OF1: 10347.8		PTS1d: 16384
EX: 1PULSE	PW: 7.0 usec	PD: 1.0 sec	NA: 147	LB: 0.0	WinNuts - $Gah.083

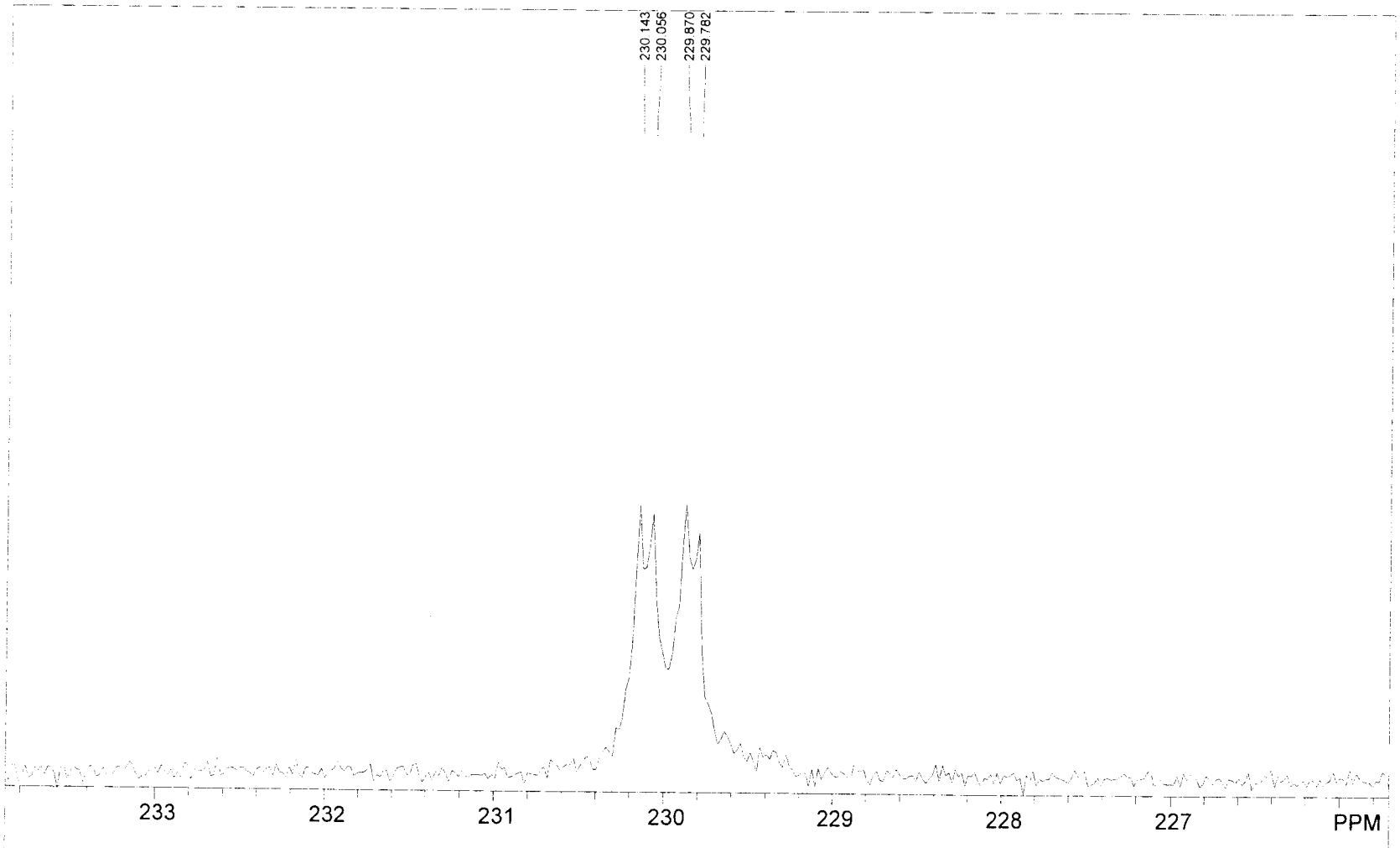

61-B1[7/29/02

F1: 121.718	SW1: 38462		OF1: 10347.8		USER: GAH -- DATE: 30JUL1997	
EX: 1PULSE	PW: 7.0 usec	PD: 1.0 sec	NA: 147	LB: 0.0	PTS1d: 16384	WinNuts - $Gah.083

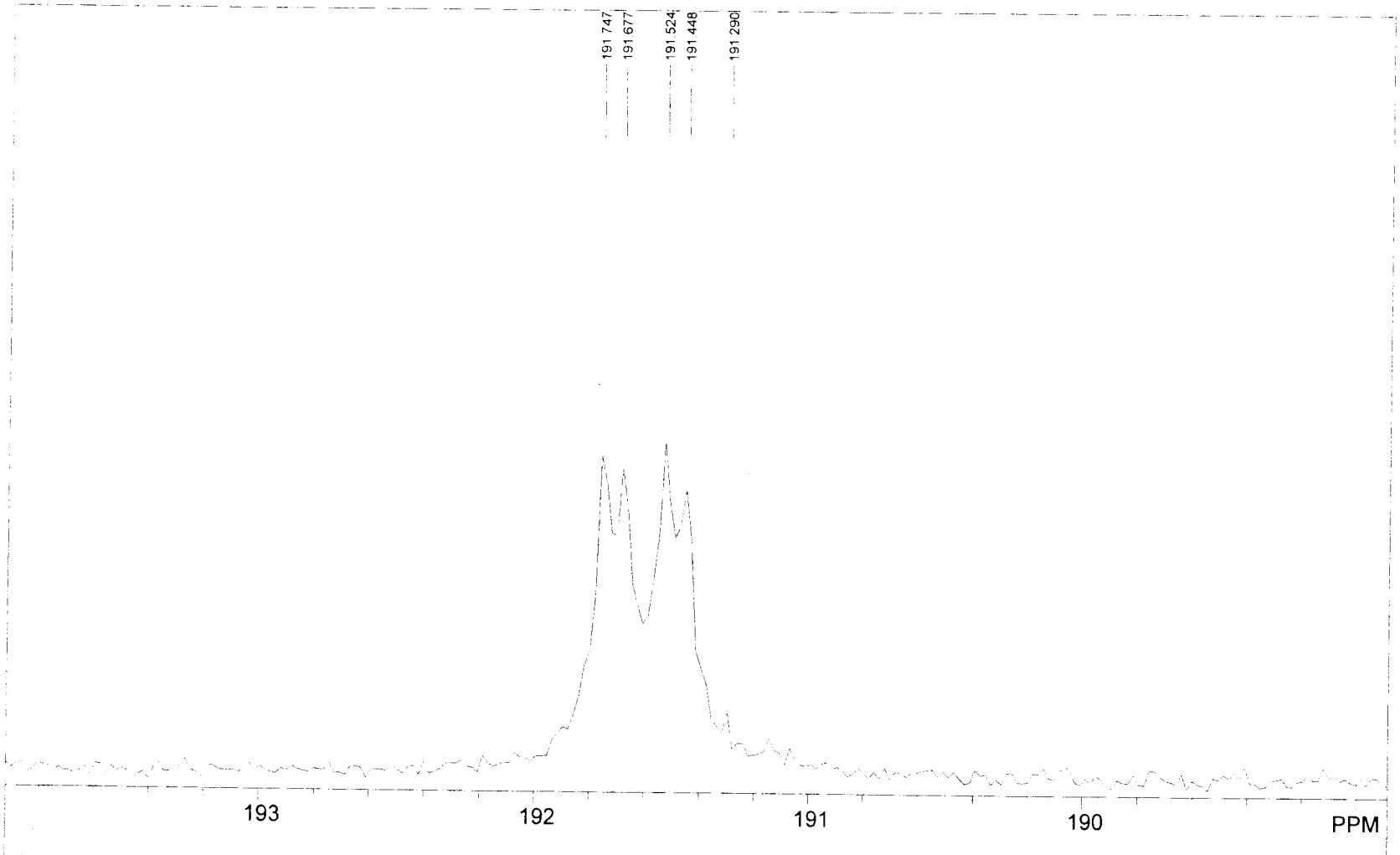

61-B1[7/29/02

USER: GAH -- DATE: 30JUL1997

F1: 121.718	SW1: 38462		OF1: 10347.8		PTS1d: 16384
EX: 1PULSE	PW: 7.0 usec	PD: 1.0 sec	NA: 147	LB: 0.0	WinNuts - $Gah.083

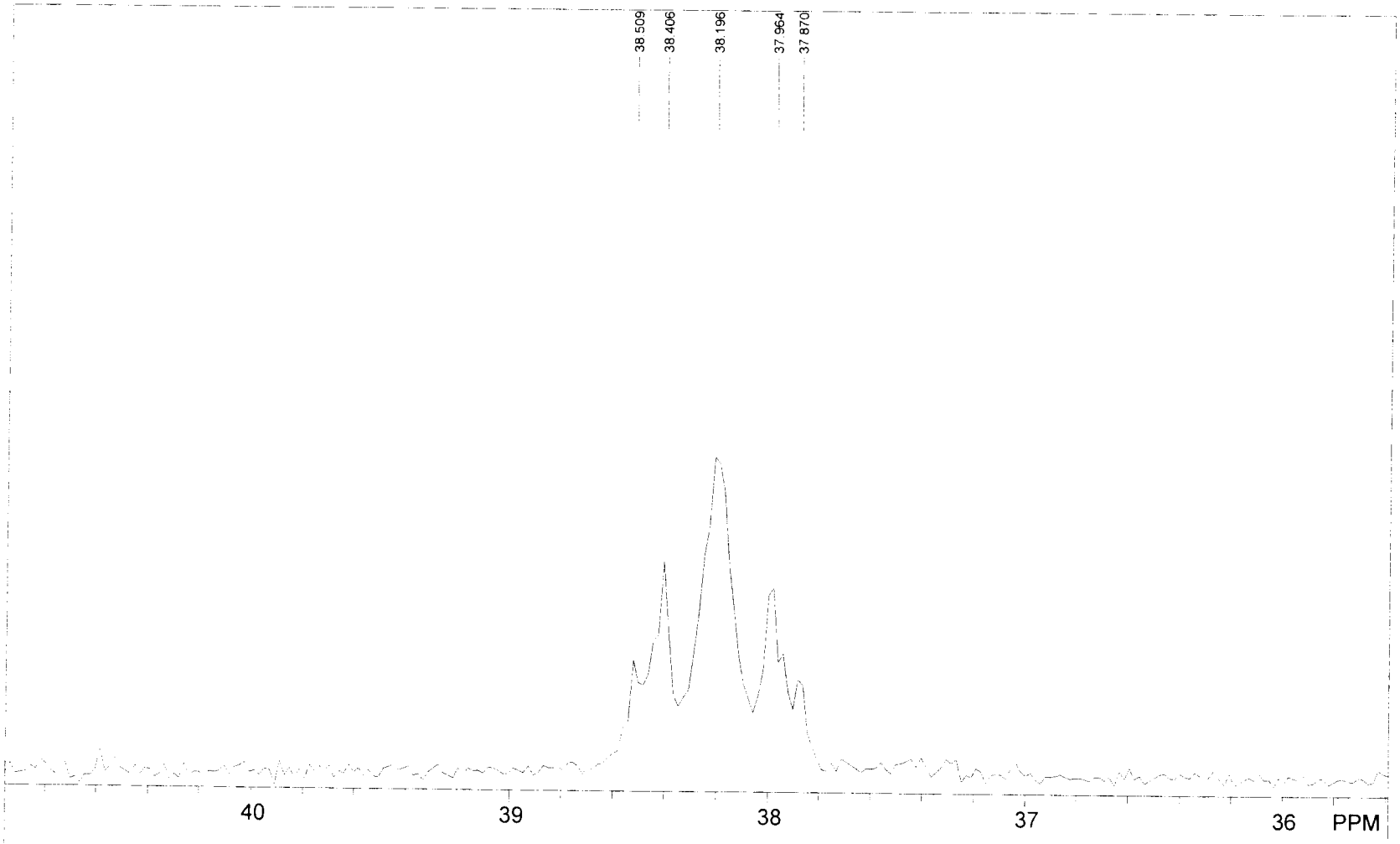

61-B1[7/29/02

USER: GAH -- DATE: 30JUL1997

F1: 121.718	SW1: 38462		OF1: 10347.8		PTS1d: 16384
EX: 1PULSE	PW: 7.0 usec	PD: 1.0 sec	NA: 147	LB: 0.0	WinNuts - $Gah.083

Figure 27

Simulated $^{31}P\ \{^{1}H\}$ NMR spectrum of $[(CO)_4Mo(\mu\text{-}PPh_2)_2Mo(CO)_3\text{-}(\mu\text{-}$ *trans*$\text{-}PPh_2CH{=}CHPPh_2)(CO)_3Mo(\mu\text{-}PPh_2)_2Mo(CO)_4]$

(E-4-B).

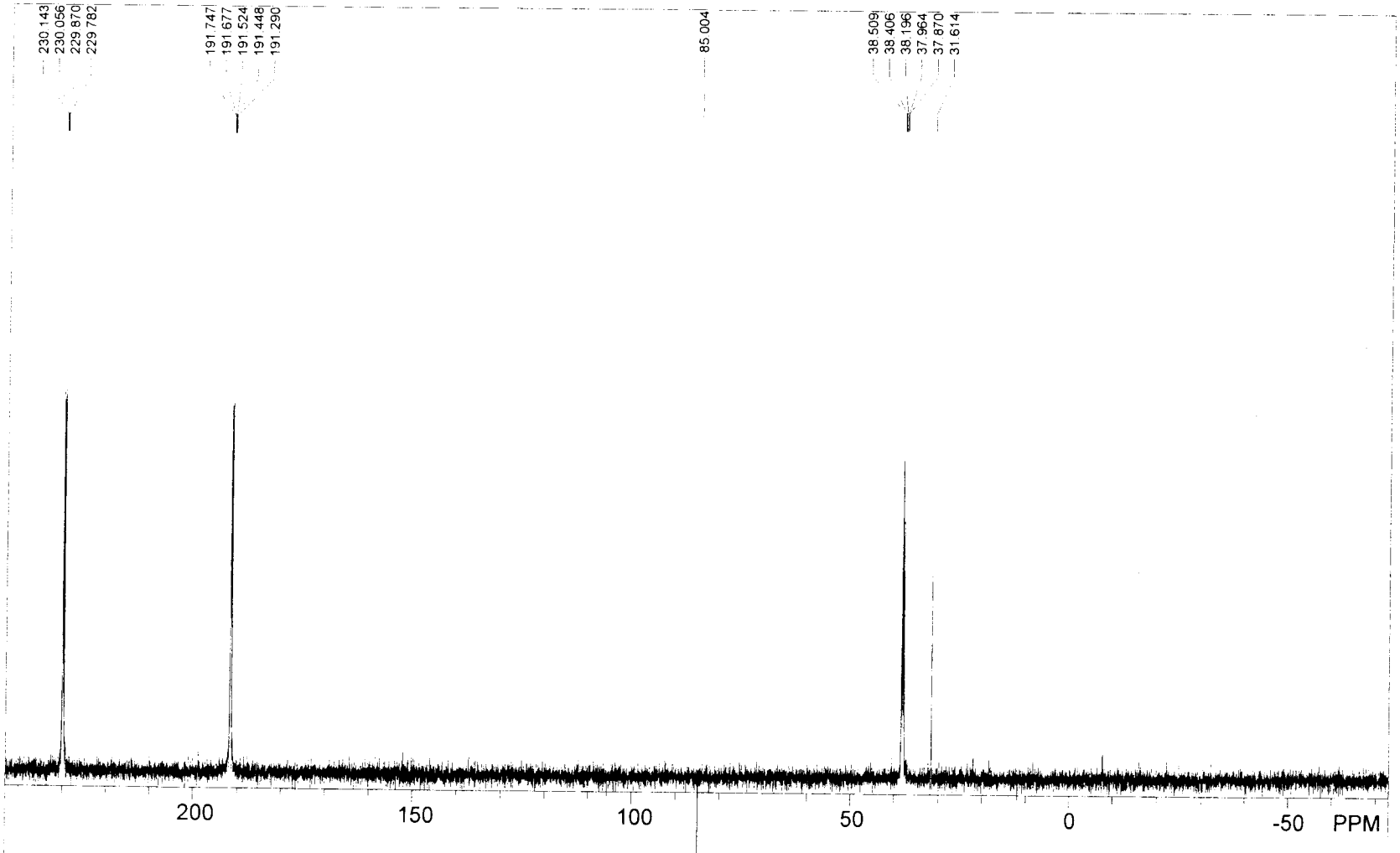

61-B1[7/29/02

F1: 121.718	SW1: 38462		OF1: 10347.8		USER: GAH -- DATE: 30JUL1997	
EX: 1PULSE	PW: 7.0 usec	PD: 1.0 sec	NA: 147	LB: 0.0	PTS1d: 16384	WinNuts - $Gah.083

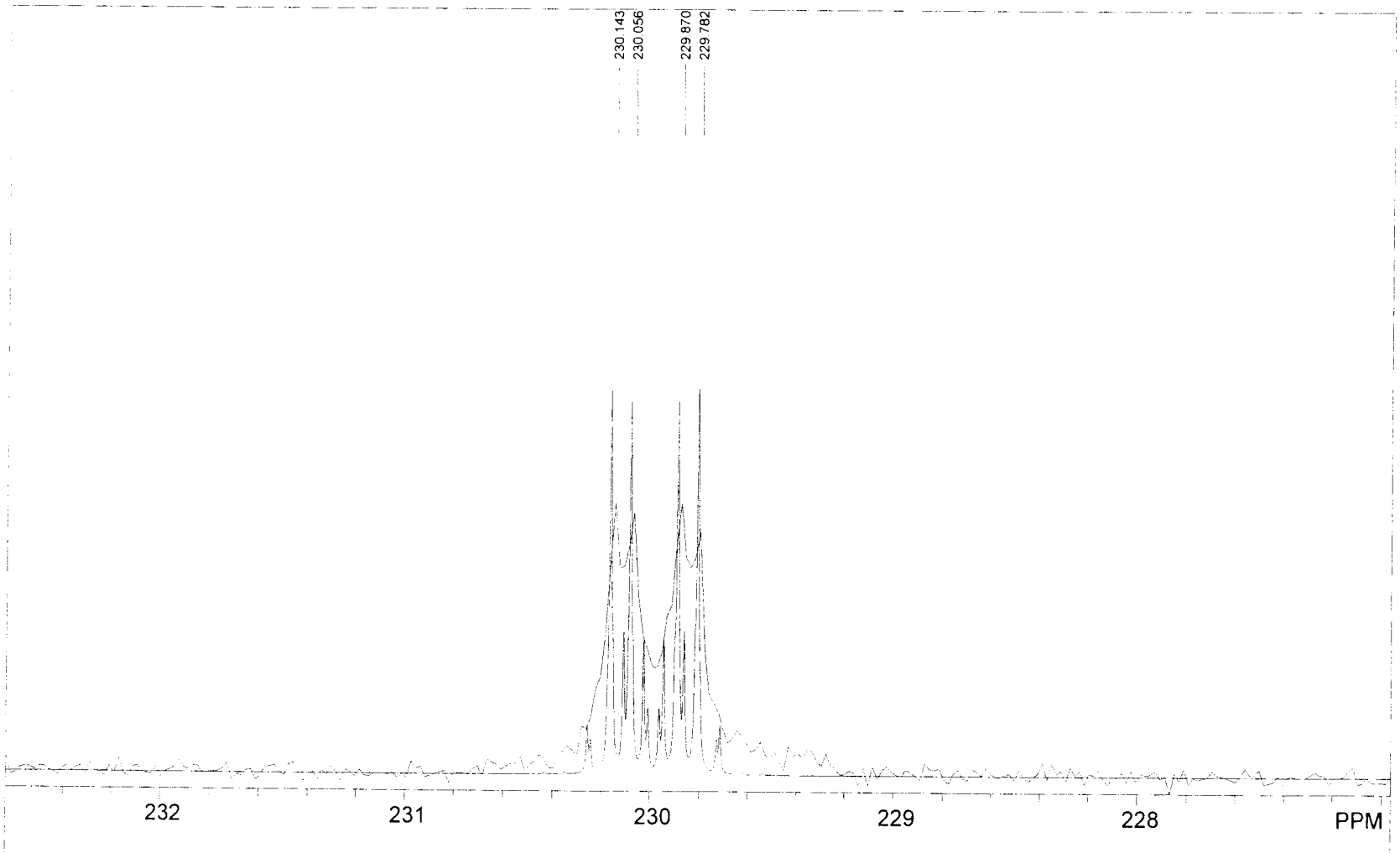

61-B1[7/29/02

USER: GAH -- DATE: 30JUL1997

F1: 121.718	SW1: 38462		OF1: 10347.8		PTS1d: 16384
EX: 1PULSE	PW: 7.0 usec	PD: 1.0 sec	NA: 147	LB: 0.0	WinNuts - $Gah.083

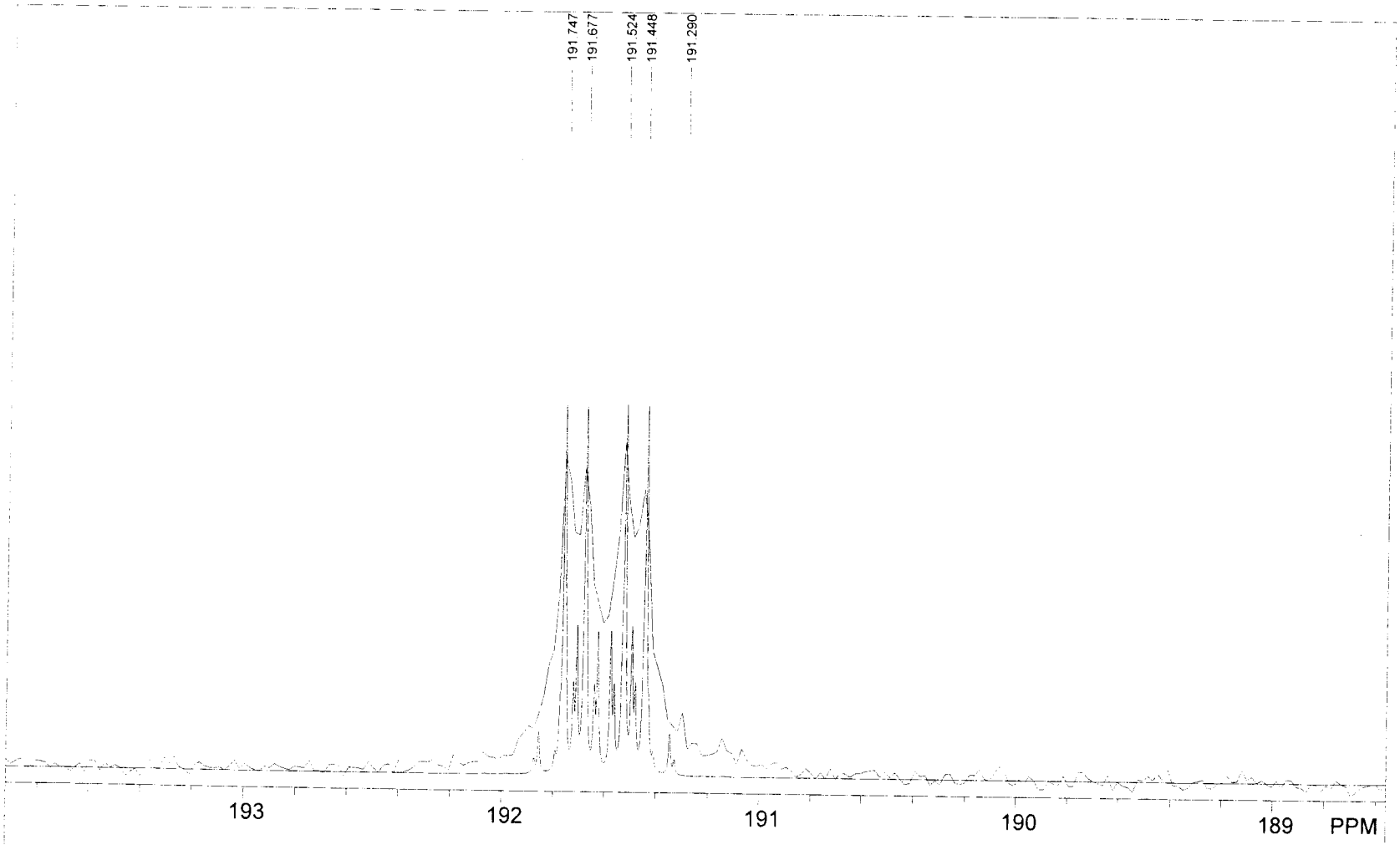

61-B1[7/29/02

F1: 121.718	SW1: 38462		OF1: 10347.8		USER: GAH -- DATE: 30JUL1997
EX: 1PULSE	PW: 7.0 usec	PD: 1.0 sec	NA: 147	LB: 0.0	PTS1d: 16384
					WinNuts - $Gah.083

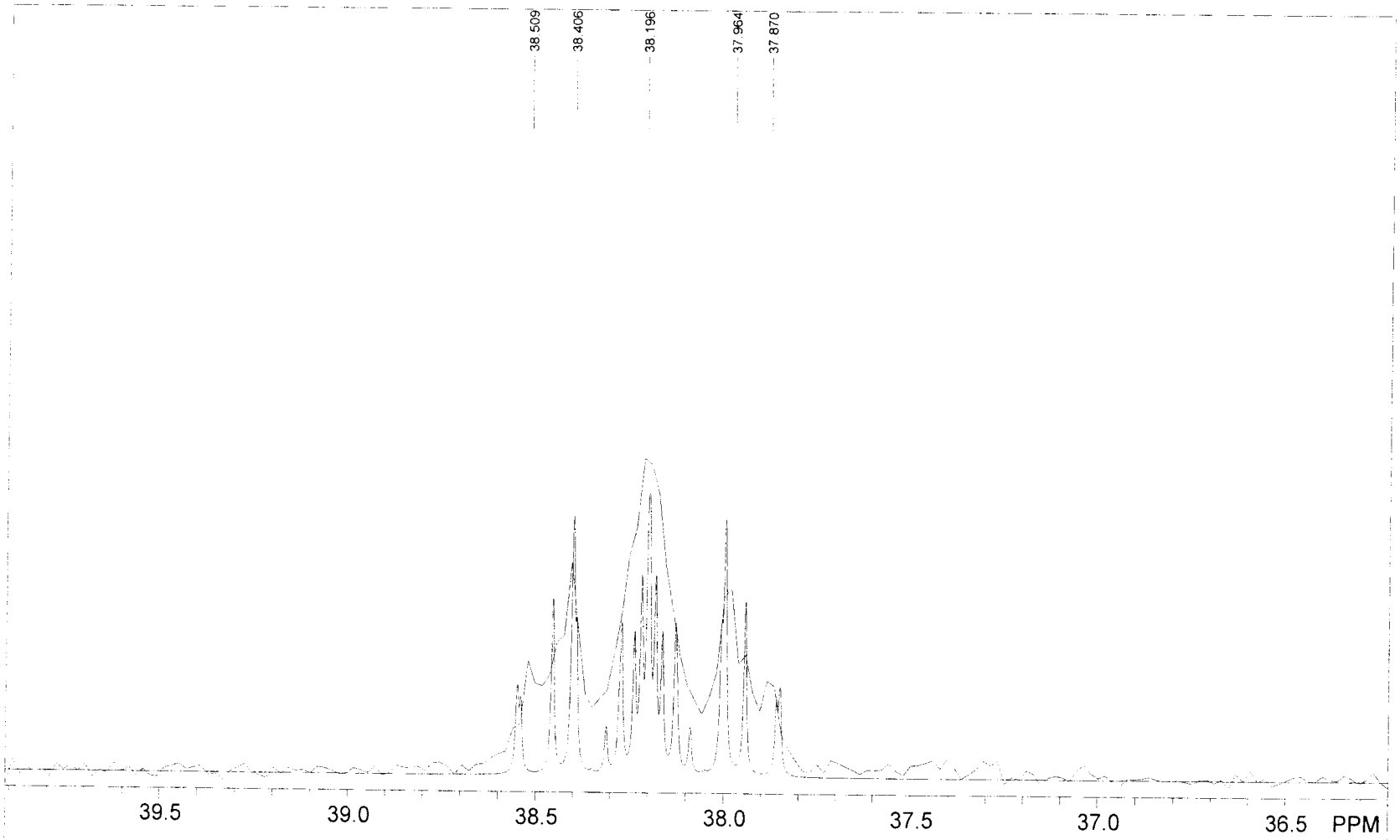

61-B1[7/29/02

F1: 121.718	SW1: 38462		OF1: 10347.8		USER: GAH -- DATE: 30JUL1997
EX: 1PULSE	PW: 7.0 usec	PD: 1.0 sec	NA: 147	LB: 0.0	PTS1d: 16384
					WinNuts - $Gah.083

Figure 28

UV/Vis spectrum of

[$(CO)_4Mo(\mu\text{-}PPh_2)_2Mo(CO)_3\text{-}(\mu\text{-}$*trans*$\text{-}PPh_2CH{=}CHPPh_2)(CO)_3Mo(\mu\text{-}PPh_2)_2Mo(CO)_4$]

(E-4-B).

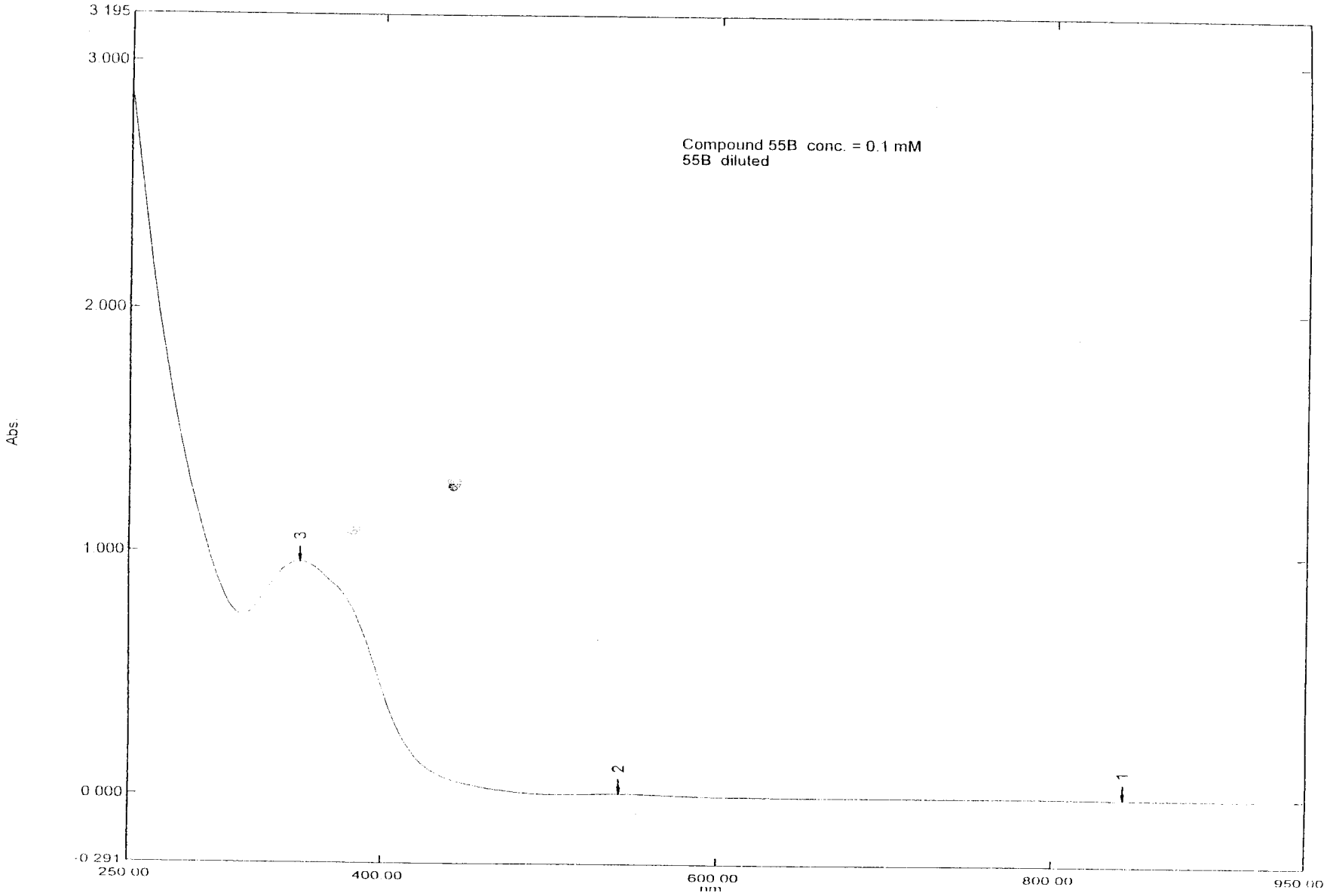
Compound 55B conc. = 0.1 mM
55B diluted
Abs.
3.195
3.000
2.000
1.000
0.000
-0.291
250.00
400.00
600.00
800.00
950.00
nm
1
2
3

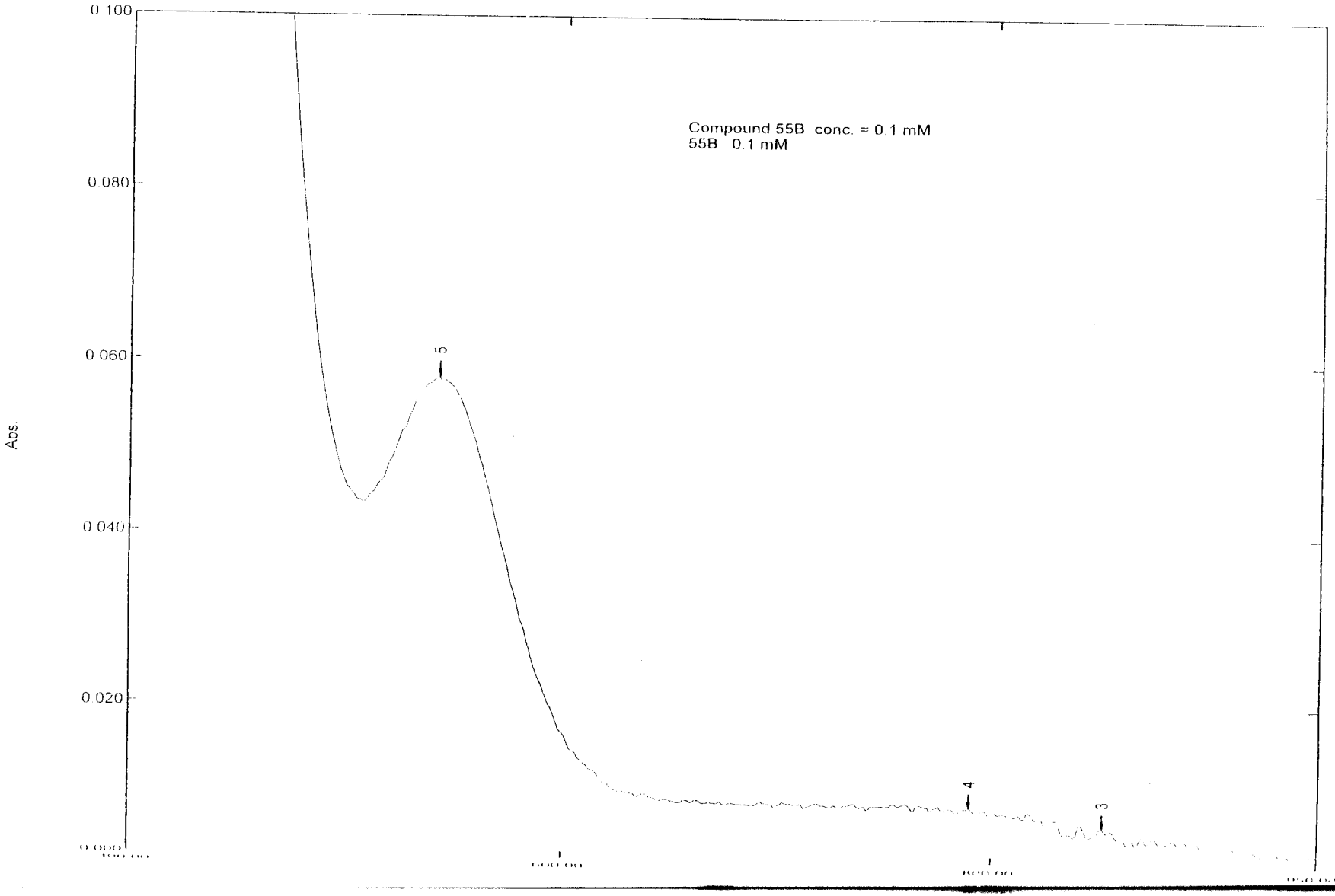
Compound 55B conc. = 0.1 mM
55B 0.1 mM
Abs.
0.100
0.080
0.060
0.040
0.020
0.000
5
4
3

Figure 29

UV/Vis spectrum of oxidation of

[$(CO)_4Mo(\mu\text{-}PPh_2)_2Mo(CO)_3\text{-}(\mu\text{-}$*trans*$\text{-}PPh_2CH{=}CHPPh_2)(CO)_3Mo(\mu\text{-}PPh_2)_2Mo(CO)_4$] (E-4-B) with AgCl.

Active Spectrum Graph Report

05/15/02 01:40:19 PM

Data Set: Storage 030058 PM - RawData - C:\WINDOWS\Desktop\Dr. McGuire\Pradeep\55B [1,1] after adding silver solid May 1 02.spc

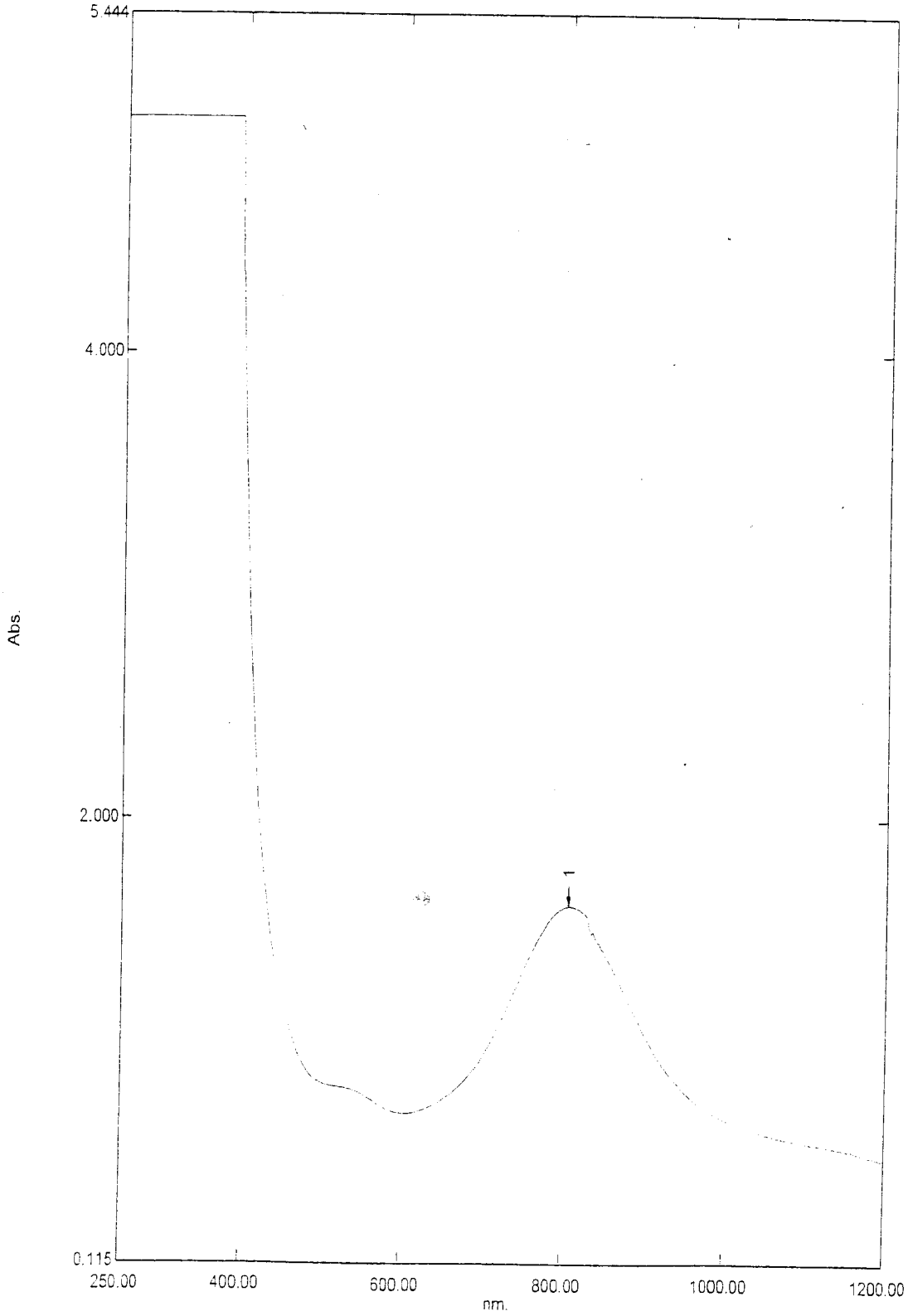

Active Spectrum Graph Report

06/05/02 12:17:27 PM

Data Set: Storage 030058 PM - RawData - C:\WINDOWS\Desktop\Dr. McGuire\Pradeep\55B [1,1] after adding silver solid May 1 02.spc

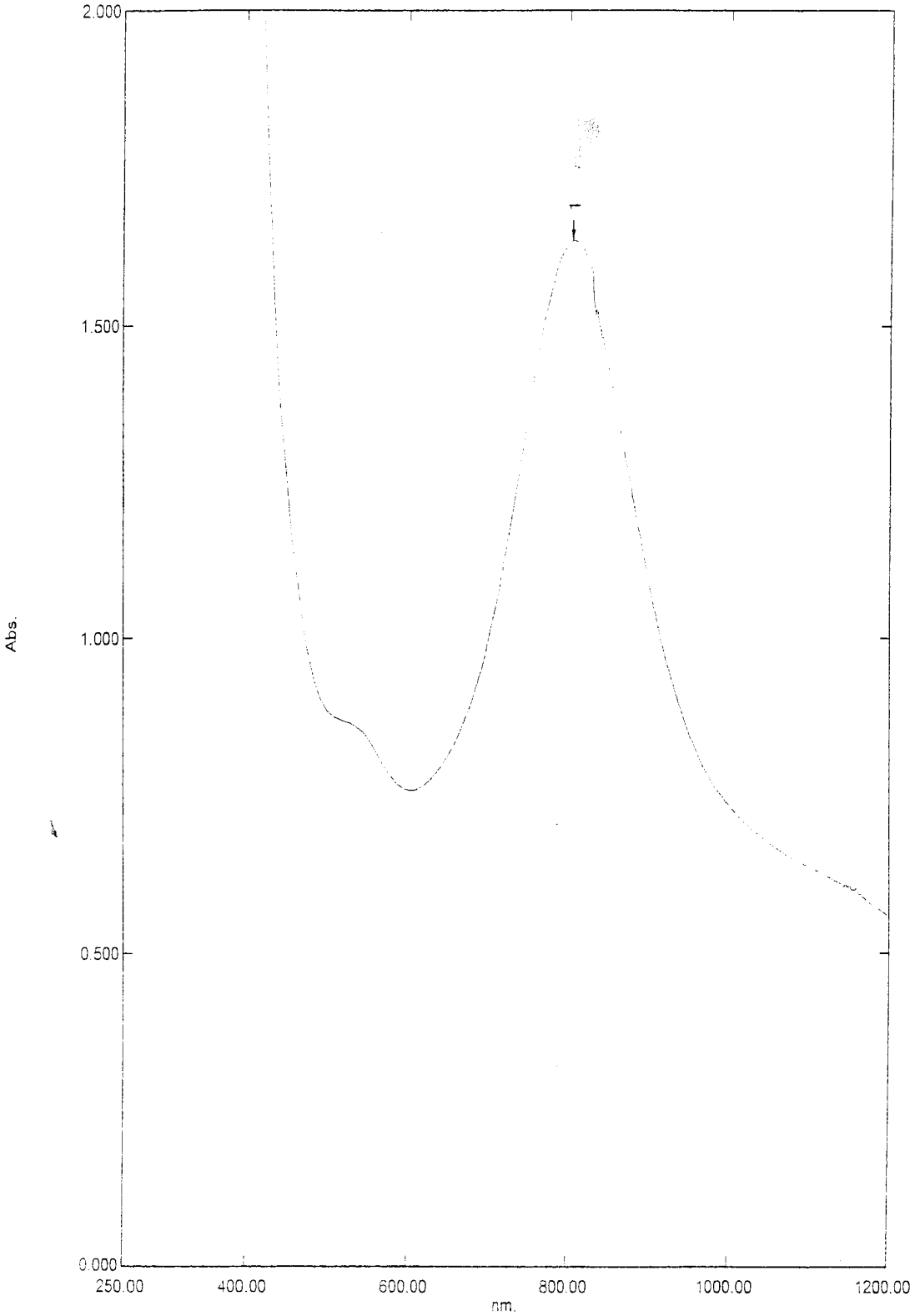

Figure 30

IR spectrum of the crude product of reaction E-5.

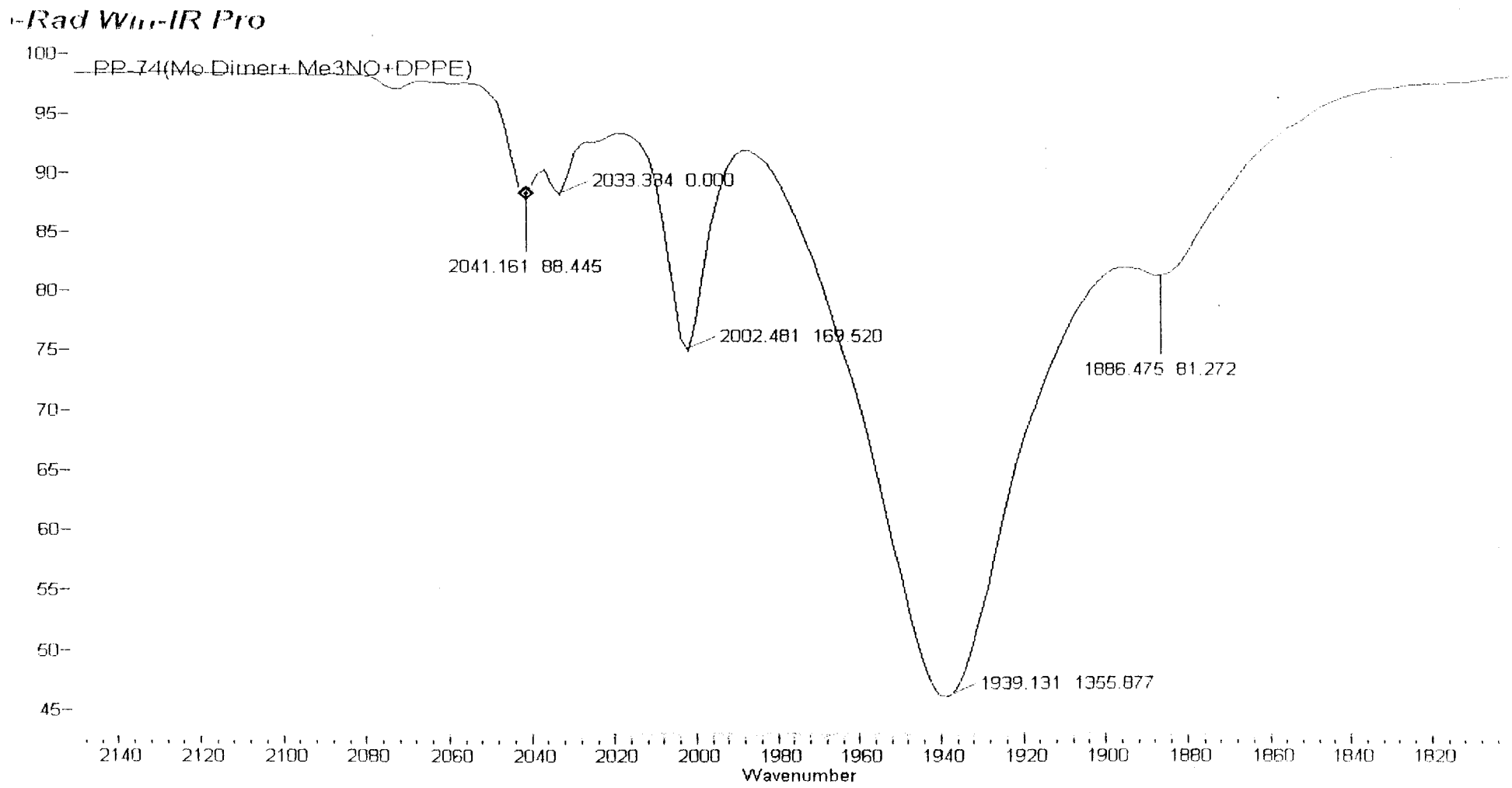
-Rad Win-IR Pro
PP-74(Mo Dimer+ Me3NO+DPPE)
2041.161 88.445
2033.384 0.000
2002.481 169.520
1939.131 1355.877
1886.475 81.272
100
95
90
85
80
75
70
65
60
55
50
45
2140
2120
2100
2080
2060
2040
2020
2000
1980
1960
1940
1920
1900
1880
1860
1840
1820
Wavenumber

Figure 31

A. **Voltammogram of $[(CO)_4W(\mu\text{-}PPh_2)_2W(CO)_3(PPh_2C{\equiv}CPPh_2)$ at 50 mV/sec.**

B. **Voltammogram of $[(CO)_4W(\mu\text{-}PPh_2)_2W(CO)_3(\mu\text{-}PPh_2C{\equiv}CPPh_2)$ at 100 mV/sec.**

A. Voltammogram of $(CO)_4W(\mu\text{-}PPh_2)_2W(CO)_3DPPA$ (D-4-A) at 50 mV/s

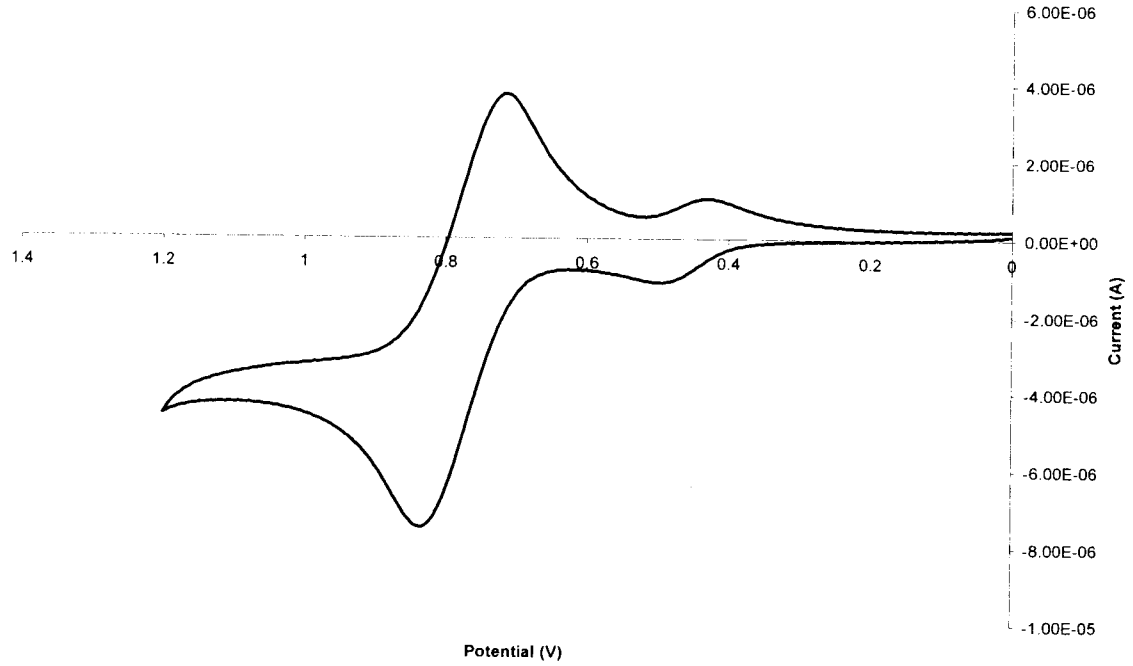

B. Voltammogram of $(CO)_4W(\mu\text{-}PPh_2)_2W(CO)_3DPPA$ (D-4-A) at 100 mV/s

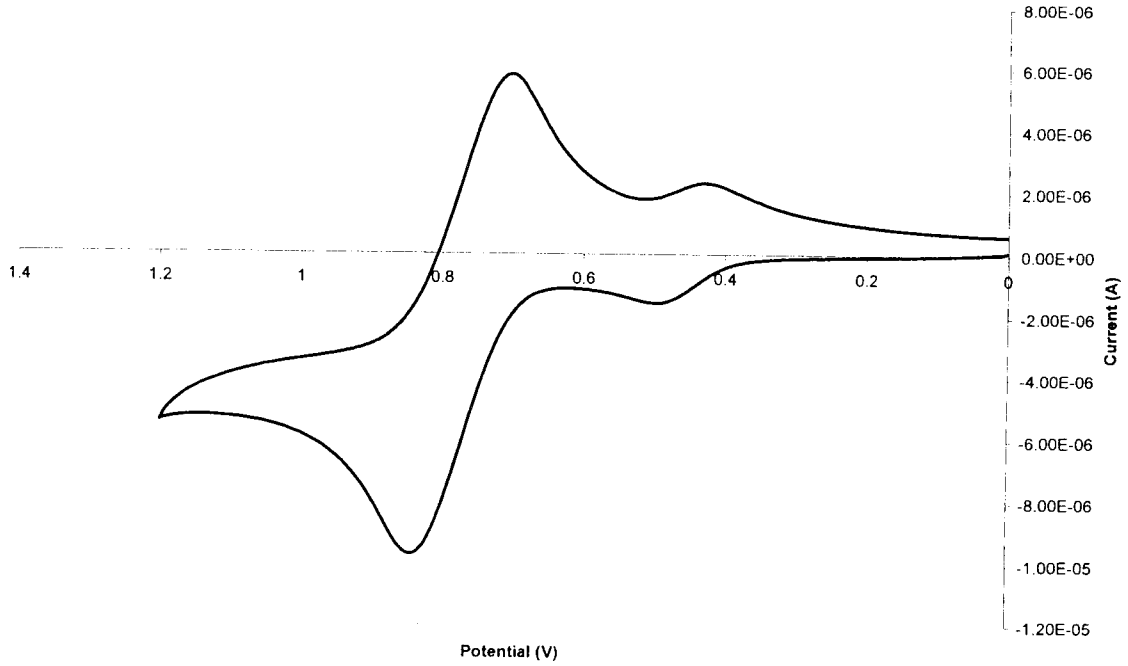

Figure 32

A. **Voltammogram of $[(CO)_4W(\mu\text{-}PPh_2)_2W(CO)_3(\mu\text{-}PPh_2C{\equiv}CPPh_2)(CO)_3W(\mu\text{-}PPh_2)_2W(CO)_4]$ at 50 mV/sec.**

B. **Voltammogram of $[(CO)_4W(\mu\text{-}PPh_2)_2W(CO)_3(\mu\text{-}PPh_2C{\equiv}CPPh_2)(CO)_3W(\mu\text{-}PPh_2)_2W(CO)_4]$ at 100 mV/sec.**

A. Voltammogram of $(CO)_4W(\mu\text{-}PPh_2)_2W(CO)_3(DPPA)(CO)_3W(\mu\text{-}PPh_2)W(CO)_4$ (D-4-B) at 50 mV/s

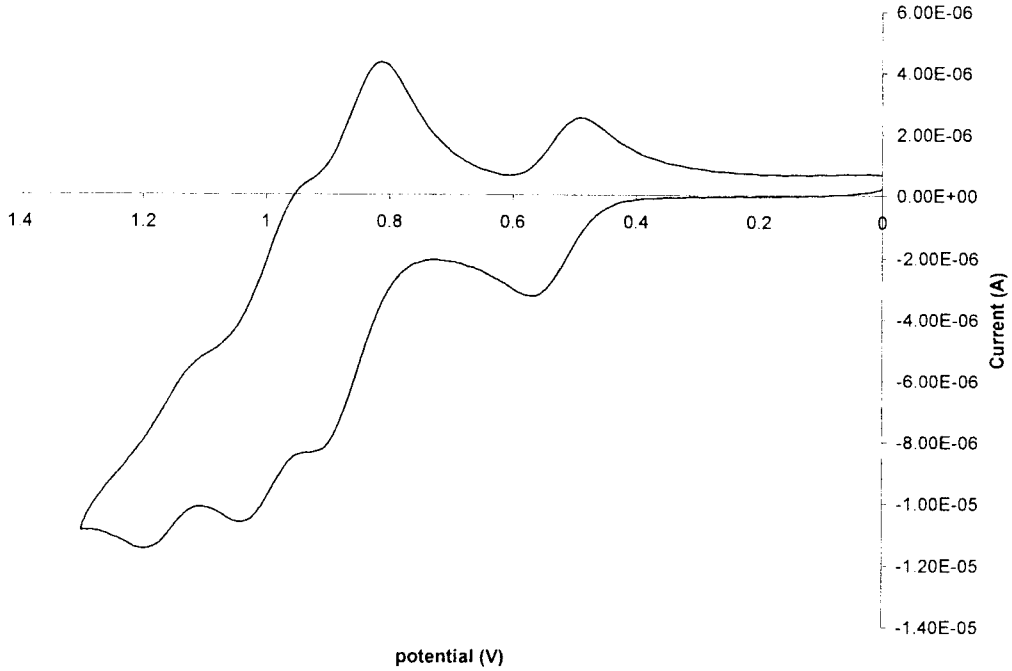

B. Voltammogram of $(CO)_4W(\mu\text{-}PPh_2)W(CO)_3(DPPA)(CO)_3W(\mu\text{-}PPh_2)W(CO)_4$ (D-4-B) at 100 mV/s

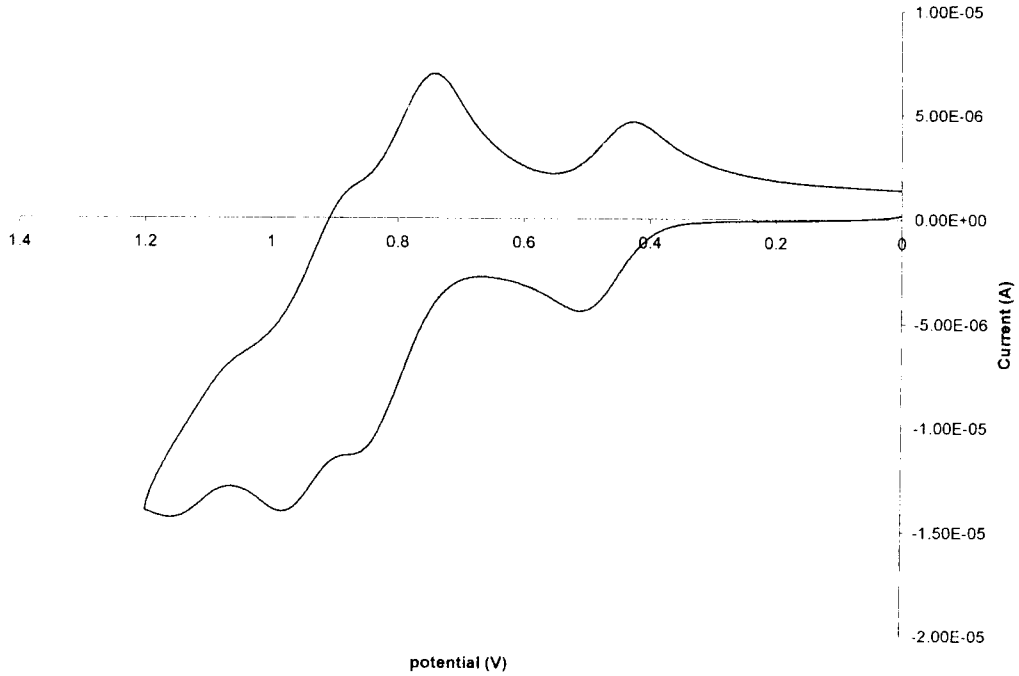

Figure 33

A. **Voltammogram of $[(CO)_4W(\mu\text{-}PPh_2)_2W(CO)_3$ (*trans*-$PPh_2CH{=}CHPPh_2$) at 50 mV/sec.**

B. **Voltammogram of $[(CO)_4W(\mu\text{-}PPh_2)_2W(CO)_3$(*trans*-$PPh_2CH{=}CHPPh_2$) at 100 mV/sec.**

A. Voltammogram of $(CO)_4W(\mu\text{-}PPh_2)_2W(CO)_3$(*trans* -DPPEthylene)(D-5-A) at 50 mV/s

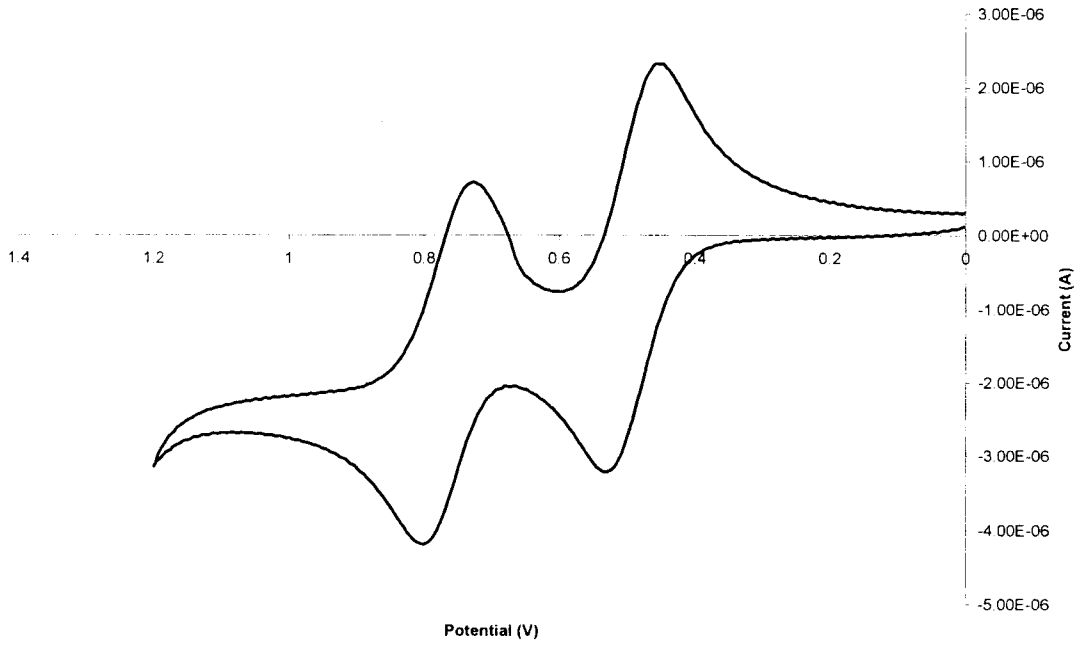

B. Voltammogram of $(CO)_4W(\mu\text{-}PPh_2)_2W(CO)_3$(*trans* -DPPEthylene) (D-5-A) at 100 mV/s

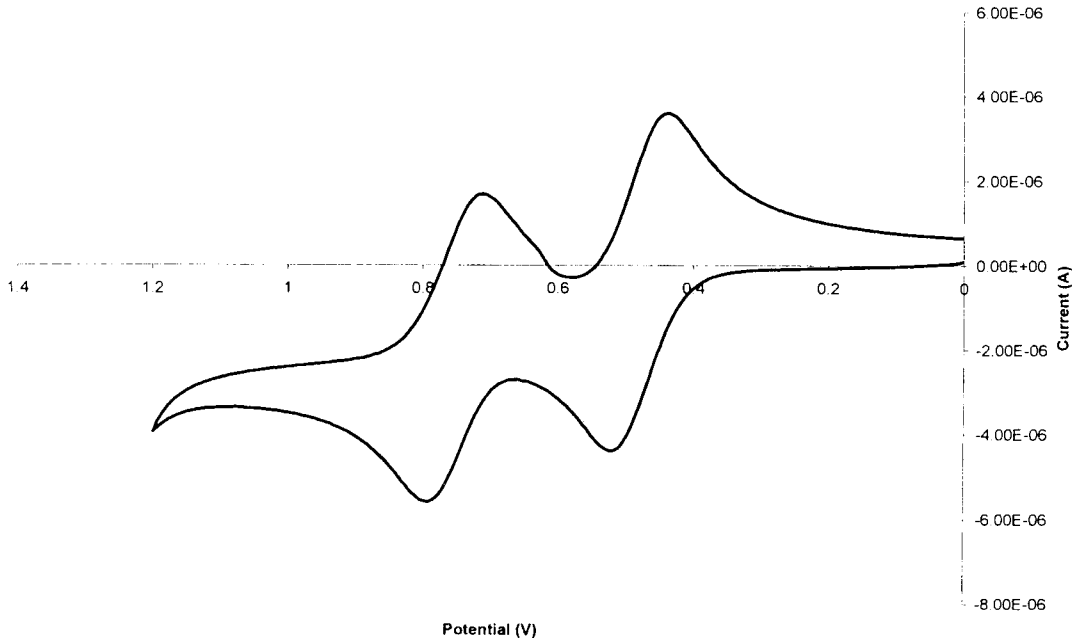

Figure 34

A. **Voltammogram of $[(CO)_4W(\mu\text{-}PPh_2)_2W(CO)_3$ (μ-*trans*-$PPh_2CH{=}CHPPh_2)(CO)_3W(\mu\text{-}PPh_2)_2W(CO)_4]$ at 50 mV/sec.**

B. **Voltammogram of $[(CO)_4W(\mu\text{-}PPh_2)_2W(CO)_3$ (μ-*trans*-$PPh_2CH{=}CHPPh_2)(CO)_3W(\mu\text{-}PPh_2)_2W(CO)_4]$ at 100 mV/sec.**

A. Voltammogram of $(CO)_4W(\mu\text{-}PPh_2)_2W(CO)_3$(*trans*-DPPEthylene)$(CO)_3W(\mu\text{-}PPh_2)_2W(CO)_4$ (D-5-B) at 50 mV/s

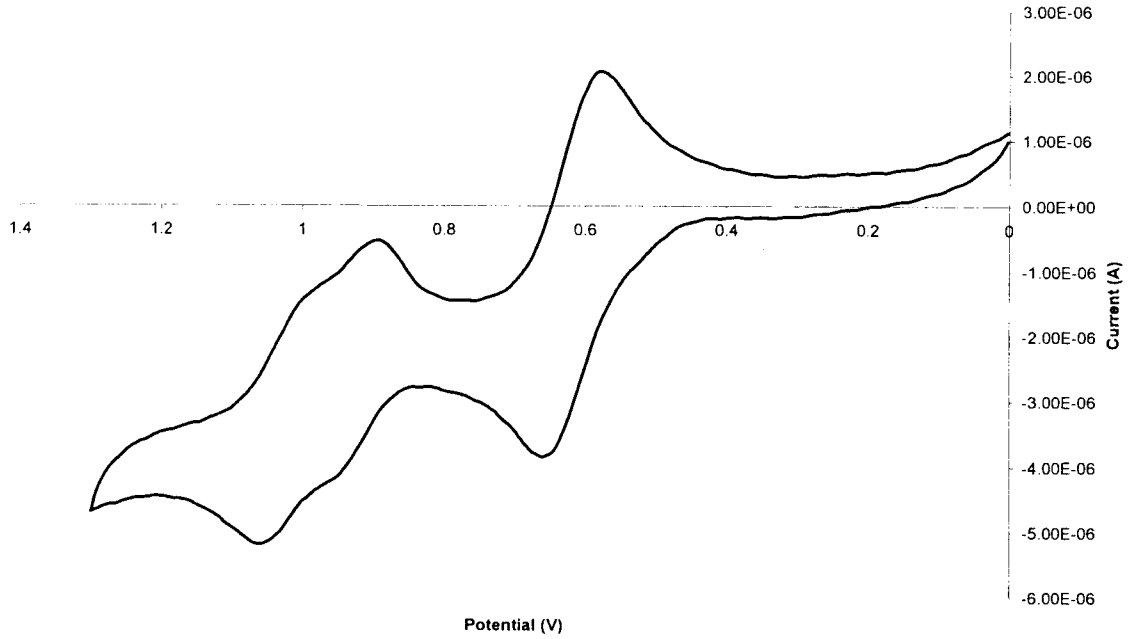

B. Voltammogram of $(CO)_4W(\mu\text{-}PPh_2)_2W(CO)_3$(*trans*-DPPEthylene)$(CO)_3W(\mu\text{-}PPh_2)_2W(CO)_4$ (D-5-B) at 100 mV/s

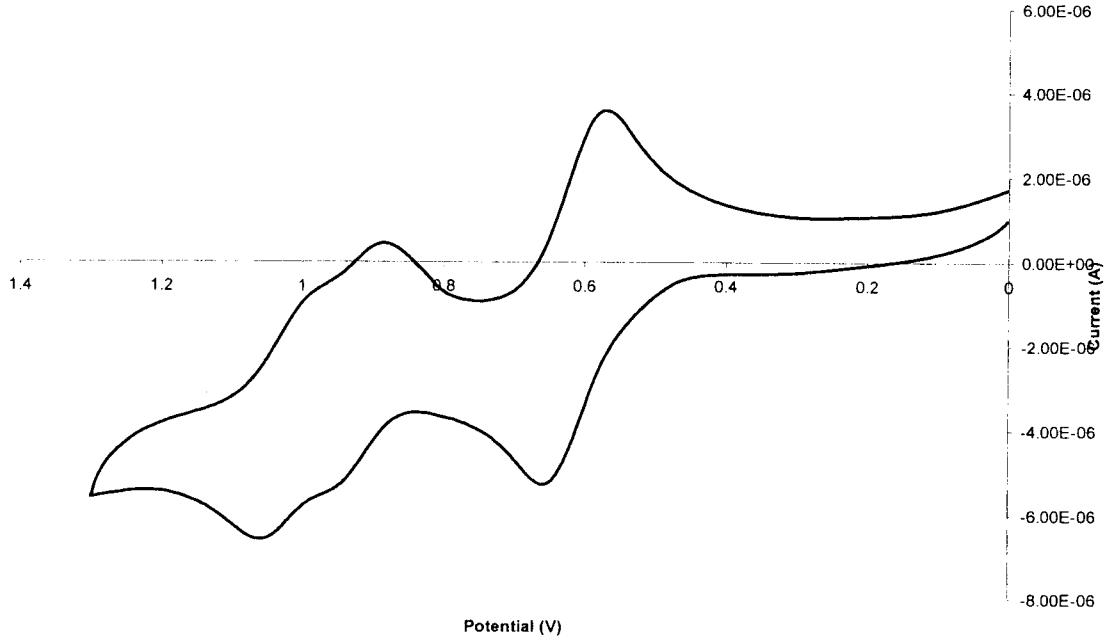

Figure 35

A. **Voltammogram of $[(CO)_4Mo(\mu\text{-}PPh_2)_2Mo(CO)_3(PPh_2C{\equiv}CPPh_2)$ at 50 mV/sec.**

B. **Voltammogram of $[(CO)_4W(\mu\text{-}PPh_2)_2W(CO)_3(Ph_2C{\equiv}CPPh_2)$ at 100 mV/sec.**

A. Voltammogroam of $(CO)_4Mo(\mu-PPh_2)_2Mo(CO)_3DPPA$ (E-3-A) at 50 mV/s

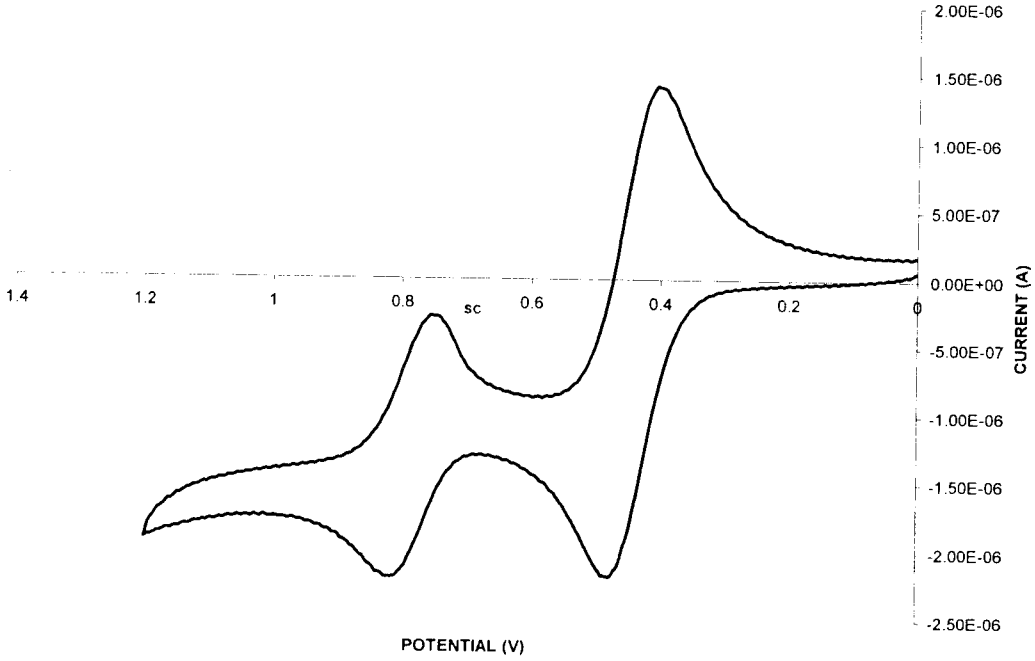

B. Voltammogram of $(CO)_4Mo(\mu-PPh_2)_2Mo(CO)_3DPPA$ (E-3-A) at 100 mV/s

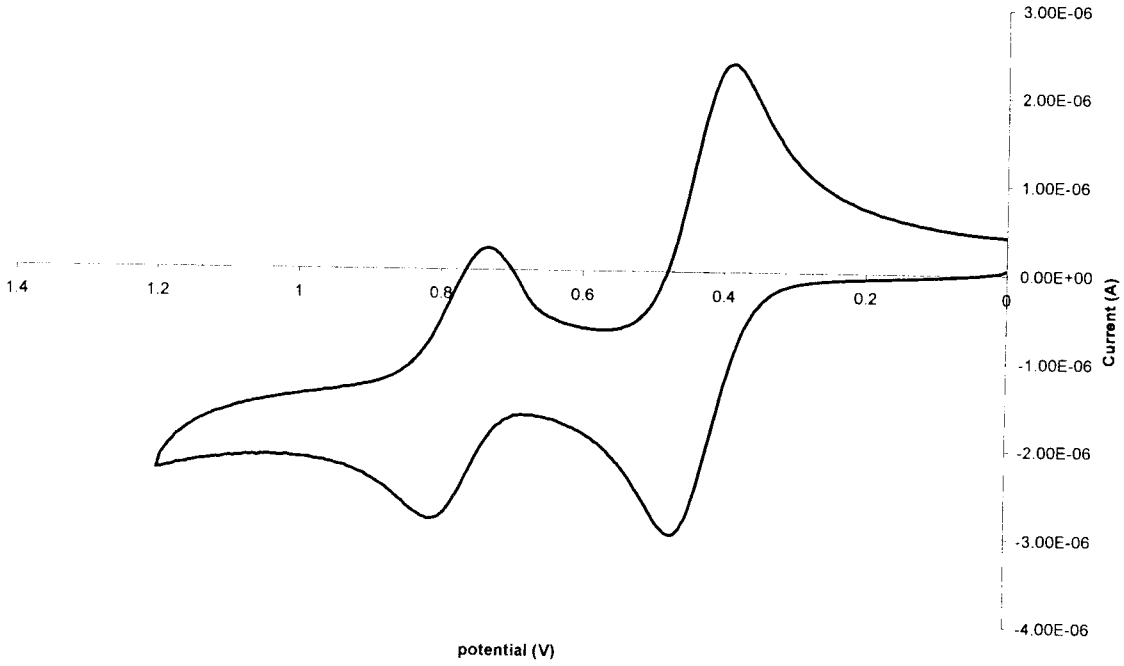

Figure 36

A. **Voltammogram of $[(CO)_4Mo(\mu\text{-}PPh_2)_2Mo(CO)_3(\mu\text{-}PPh_2C{\equiv}CPPh_2)(CO)_3Mo(\mu\text{-}PPh_2)_2Mo(CO)_4]$ at 50 mV/sec.**

B. **Voltammogram of $[(CO)_4Mo(\mu\text{-}PPh_2)_2Mo(CO)_3(\mu\text{-}PPh_2C{\equiv}CPPh_2)(CO)_3Mo(\mu\text{-}PPh_2)_2Mo(CO)_4]$ at 100 mV/sec.**

A. Voltammogram of $(CO)_4Mo(\mu\text{-}PPh_2)_2Mo(CO)_3DPPA(CO)_3Mo(\mu\text{-}PPh_2)_2Mo(CO)_4$ (E-3-B) at 50 mV/s

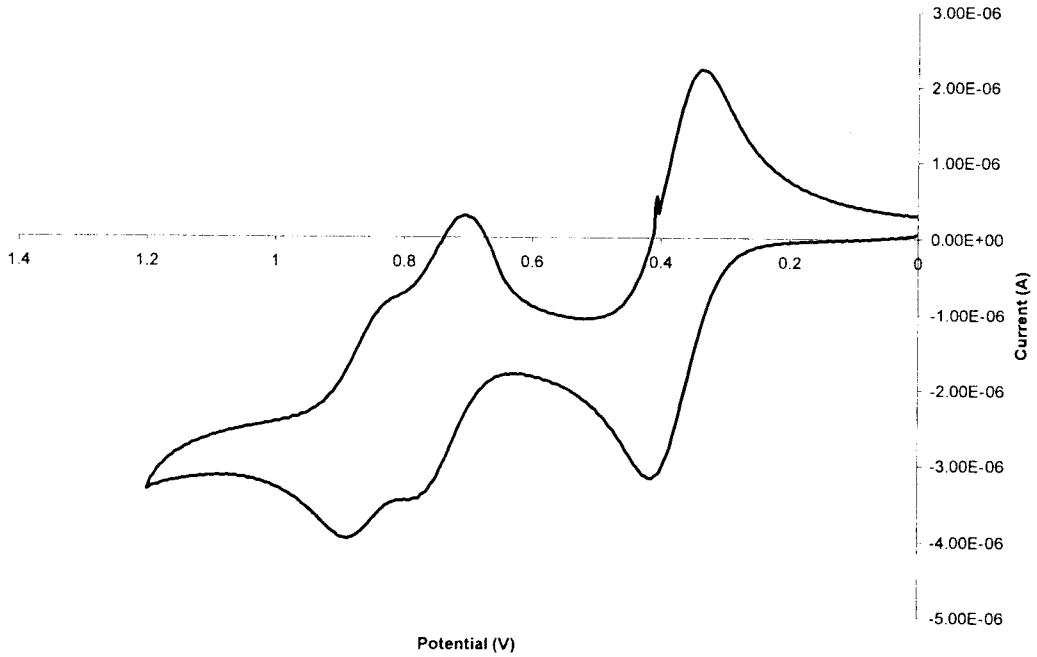

B. Voltammogram of $(CO)_4Mo(\mu\text{-}PPh_2)_2Mo(CO)_3DPPA(CO)_3Mo(\mu\text{-}PPh_2)_2Mo(CO)_4$ (E-3-B) at 100 mV/s

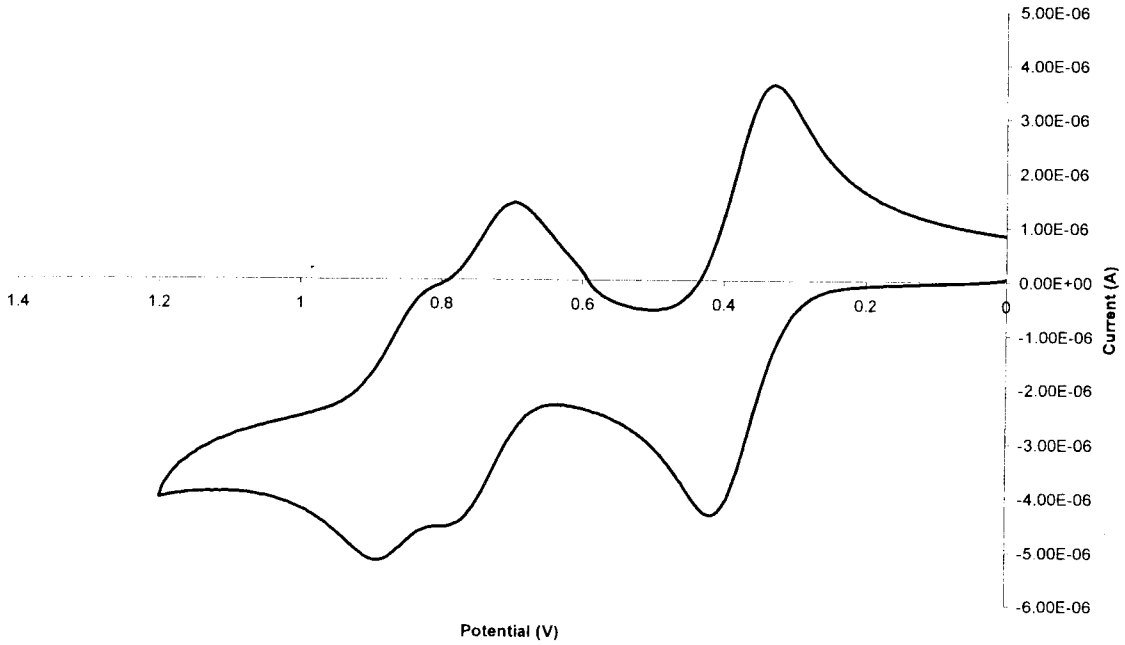

Figure 37

A. **Voltammogram of $[(CO)_4Mo(\mu\text{-}PPh_2)_2Mo(CO)_3$ (*trans*-$PPh_2CH{=}CHPPh_2$) at 50 mV/sec.**

B. **Voltammogram of $[(CO)_4Mo(\mu\text{-}PPh_2)_2Mo(CO)_3$ (*trans*-$PPh_2CH{=}CHPPh_2$) at 100 mV/sec.**

A. Voltammogram of $(CO)_4Mo(\mu\text{-}PPh_2)_2Mo(CO)_3$(trans-DPPEthylene) (E-4-A) at 50 mV/s

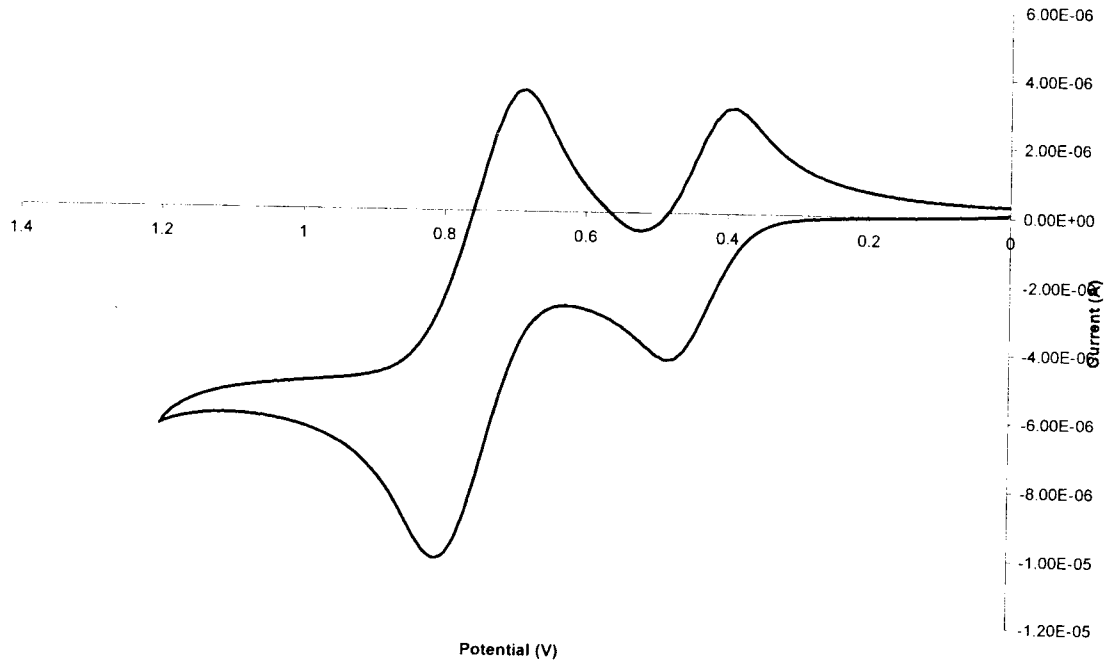

B. Voltammogram of $(CO)_4Mo(\mu\text{-}PPh_2)_2Mo(CO)_3$(trans-DPPEthylene) (E-4-A) at 100 mV/s

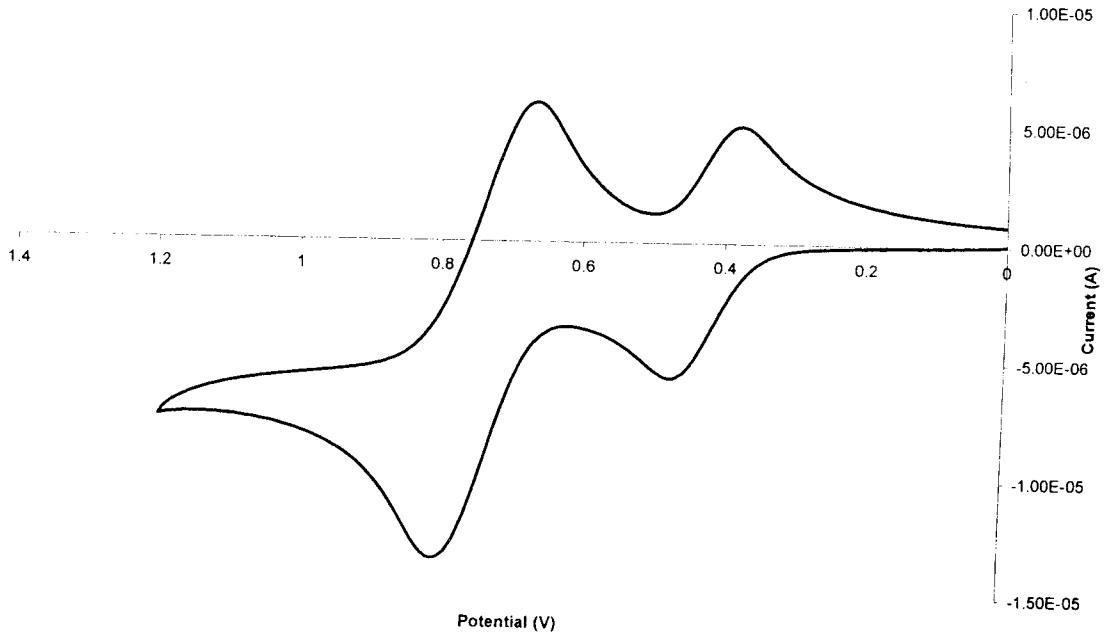

Figure 38

A. **Voltammogram of $[(CO)_4Mo(\mu\text{-}PPh_2)_2Mo(CO)_3$ (μ-*trans*-$PPh_2CH{=}CHPPh_2)(CO)_3Mo(\mu\text{-}PPh_2)_2Mo(CO)_4]$ at 50 mV/sec.**

B. **Voltammogram of $[(CO)_4Mo(\mu\text{-}PPh_2)_2Mo(CO)_3$ (μ-*trans*-$PPh_2CH{=}CHPPh_2)(CO)_3Mo(\mu\text{-}PPh_2)_2Mo\ (CO)_4]$ at 100 mV/sec.**

A. Voltammogram of $(CO)_4Mo(\mu\text{-}PPh_2)_2Mo(CO)_3$(*trans*- DPPEthylene)$(CO)_3Mo(\mu\text{-}PPh_2)_2Mo(CO)_4$ (E-4-B) at 50 mV/s

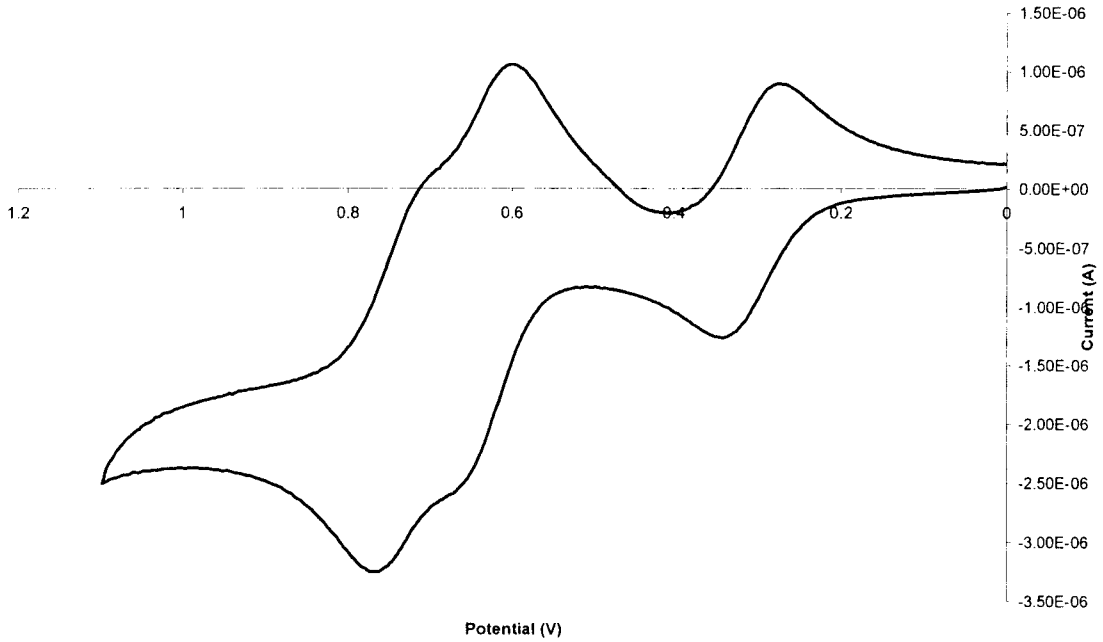

B. Voltammogram of $(CO)_4Mo(\mu\text{-}PPh_2)_2Mo(CO)_3$(*trans* -DPPEthylene$(CO)_3Mo(\mu\text{-}PPh_2)_2Mo(CO)_4$ (E-4-B) at 100 mV/s